THERMOPLASTIC COMPOSITE WIND TURBINE BLADES

VACUUM INFUSION TECHNOLOGY FOR ANIONIC POLYAMIDE-6 COMPOSITES

Proefschrift

ter verkrijging van de graad van doctor
aan de Technische Universiteit Delft,
op gezag van de Rector Magnificus prof.dr.ir. J.T. Fokkema,
voorzitter van het College voor Promoties,
in het openbaar te verdedigen op dinsdag 10 april 2007 om 10:00 uur

door

Kjelt VAN RIJSWIJK

ingenieur luchtvaart en ruimtevaart
geboren te Gouda.

Dit proefschrift is goedgekeurd door de promotoren:

Prof.ir. A. Beukers

Prof.dr. S.J. Picken

Toegevoegd promotor:

Dr.ir. H.E.N. Bersee

Samenstelling promotiecommissie:

Rector Magnificus, voorzitter

Prof.ir. A. Beukers, Technische Universiteit Delft, promotor

Prof.dr. S.J. Picken, Technische Universiteit Delft, promotor

Dr.ir. H.E.N. Bersee, Technische Universiteit Delft, toegevoegd promotor

Prof.dr.ir. G.A.M. van Kuik, Technische Universiteit Delft

Prof.dr. P. Hubert, McGill University, Montreal, Canada

Dr. V. Michaud, École Polytechnique Fédérale de Lausanne, Lausanne, Zwitserland

A.A. van Geenen, Brüggemann Chemical, Heilbronn, Duitsland

The research described in this thesis forms part of the project PhD@SEA, which is substantially funded under the BSIK-programme (BSIK03041) of the Dutch Government and supported by the consortium WE@SEA.

ISBN: 978-90-9021696-6

Cover design: K. van Rijswijk
Photography: D.P.N. Vlasveld and E.M. Baten

Printed at Haveka, The Netherlands

Opgedragen aan:

Opa Versluys

20 mei 1916 — 8 februari 2007

SUMMARY

Due to the increasing costs of fossil fuels and the improved efficiency of wind turbines in the last decade, wind energy has become increasingly cost-efficient and is well on its way of becoming a mainstream source of energy. To maintain a continuous reduction in costs it is necessary to increase the size of the turbines. For the blades a structural redesign is inevitable and an aircraft-wing-like design consisting of ribs, spars and skins made of thermoplastic composite parts is proposed. Unfortunately, state-of-the-art melt processing of thermoplastic composites requires heavy presses, which makes it impossible to produce large and thick structures like wind turbine blades.

As an alternative, this thesis describes the development of reactive processing of thermoplastic composites through vacuum infusion, which is a commonly used technique for manufacturing of thermoset composite wind turbine blades. An AP Nylon® casting resin with water-like viscosity is used to impregnate a stack of 'dry' glass fiber fabrics, after which *in situ* polymerization of the semi-crystalline anionic polyamide-6 (APA-6) matrix takes place within 30 minutes at temperatures around 180ºC. Using vacuum as driving force for impregnation and shaping allows manufacturing of composite parts of virtually infinite size and thickness. The research was conducted in the following three inter-related steps: (i) curing of APA-6, (ii) processing of unreinforced APA-6 panels, and (iii) vacuum infusion of APA-6 composites. On a parallel track, the necessary processing equipment and tooling was developed.

Curing of APA-6: To allow filling of large moulds with dense fiber fabrics, an activator-initiator combination was selected, which delays the onset of polymerization. Because curing takes place at temperatures below the crystallization point of the final APA-6 polymer, polymerization and crystallization occur simultaneously. As it affects the rates of polymerization and crystallization in an opposite manner, the temperature is the most important processing parameter and largely determines the properties of the final polymer.

Unreinforced APA-6: At the optimum processing temperature (taking both internal (exothermic cure) and external (the mould) heat sources into account), APA-6 obtains a morphology in which small crystals are connected by a well-developed high molecular weight network of slightly branched tie-molecules. Due to this unique morphology that can only be obtained through reactive processing, APA-6 has a significantly higher modulus and strength than melt processed polyamide-6 and is less affected by moisture absorption.

APA-6 composites: Processing of composites requires a higher mould temperature than processing of the neat resin (i) to compensate for the loss in exothermic heat production due to the added fibers and (ii) for the formation of chemical fiber-to-matrix bonds. The higher temperature and reduced mobility of the bonded polymer chains reduce the degree of crystallinity of the APA-6 matrix. The related reduction of shrinkage-induced voids is regarded as an advantage, whereas the reduction in modulus and the increased susceptibility to moisture absorption are a clear disadvantage. A compromise between optimizing the interfacial properties and optimizing the matrix seems inevitable.

The developed technology was successfully applied to infuse 2 to 25 mm thick thermoplastic composites with a fiber volume content of 50%. These APA-6 composites possess outstanding static properties and a promising resistance against fatigue, which is one of the main requirements for wind turbine blade composites. Additional advantages for application in wind energy are the low costs of the resin, the short infusion and curing time, and the fact that APA-6 can be recycled in various ways in an economically sound manner. Increasing the moisture resistance of APA-6 composites is mentioned as most important recommendation for further development.

SAMENVATTING

Door de sterke prijstoename van de fossiele brandstoffen en het efficiënter worden van wind turbines is het opwekken van elektriciteit uit wind in het laatste decennium alsmaar kosten effectiever geworden en mede daarom is wind energie hard op weg om een van onze voornaamste bronnen van elektriciteit te worden. Om de daling in opwekkingskosten van energie voort te zetten is het noodzakelijk om de turbines op te schalen en lijkt een structureel herontwerp van de turbine bladen onvermijdelijk. Een constructie gelijk een vliegtuigvleugel bestaande uit ribben, liggers en huidvelden gemaakt van thermoplastische composieten is een mogelijke oplossing. Helaas is het met de huidige stand van de techniek, welke gebruik maakt van zware persen om thermoplastische composieten via de smelt te verwerken, niet mogelijk om grote en dikke constructies zoals wind turbine bladen te maken.

Als een alternatief wordt in dit proefschrift het reactief verwerken van thermoplastische composieten beschreven middels een vacuüm injectie proces wat een veelgebruikte techniek is voor de productie van wind turbine bladen van thermohardende composieten. Na het impregneren van geweven glasvezels met een waterdunne giethars, genaamd AP-Nylon®, hardt deze op een temperatuur rond 180ºC binnen 30 minuten uit tot semi-kristallijn anionisch polyamide-6 (APA-6). Door vacuüm te gebruiken als drijvende kracht voor het impregneren en het vervormen kunnen thermoplastische composieten geproduceerd worden van nagenoeg elke grootte en dikte. Het onderzoek is uitgevoerd in de volgende drie aan elkaar gerelateerde stappen: (i) het uithardingsproces van APA-6, (ii) het produceren van oversterkte APA-6 panelen, en (iii) vacuüm injectie van APA-6 composieten. Tevens zijn in een parallel traject de nodige productie apparatuur en het mallen systeem ontwikkeld.

Het uithardingsproces van APA-6: Om het vullen van grote mallen met geweven glasvezels mogelijk te maken is een aktivator-initiator combinatie geselecteerd, welke het uithardingsproces uitstelt. Daar de hars uithardt op een temperatuur onder de kristallisatie temperatuur van het uiteindelijke polymeer, vinden polymerisatie en

kristallisatie tegelijkertijd plaats. Daar het beide processen sterk beïnvloedt, is de uithardingstemperatuur de belangrijkste productie parameter.

Onversterkt APA-6: Op de optimale proces temperatuur (rekening houdend met zowel interne (exotherme reactie) en uitwendige (de mal) warmtebronnen), verkrijgt APA-6 een morfologie bestaande uit kleine kristallen welke verbonden zijn door een dicht netwerk van licht vertakte polymeer ketens van hoog moleculair gewicht. Door deze unieke morfologie, welke alleen tot stand kan komen tijdens reactief verwerken, heeft APA-6 een significant hogere modulus en sterkte dan polyamide-6 welke via de smelt is verwerkt. Tevens is APA-6 minder gevoelig voor vochtopname.

APA-6 composieten: Het maken van composieten vereist een hogere mal temperatuur dan het maken van onversterkt APA-6 om (i) te compenseren voor de gereduceerde productie van exotherme warmte door het toevoegen van de vezels en (ii) voor het vormen van chemische verbindingen tussen de vezels en de matrix. De hogere temperatuur en de verminderde mobiliteit van de aan de vezels gebonden ketens resulteren in een reductie in kristalliniteit van de APA-6 matrix. De hieraan gerelateerde vermindering van krimpgerelateerde holtes kan gezien worden als een voordeel, de lagere modulus en de verhoogde gevoeligheid voor vochtopname zijn echter een duidelijk nadeel. Het is derhalve noodzakelijk om een compromis te sluiten tussen optimaliseren van de matrix en optimaliseren van de vezel-matrix hechting.

Composieten van 2 tot 25 mm dikte en een vezel volume gehalte van 50% zijn succesvol geïnjecteerd met de ontwikkelde technologie. Deze APA-6 composieten bezitten uitstekende statische eigenschappen en veelbelovende vermoeiings-eigenschappen, wat een van de voornaamste eisen is voor wind turbine blad materialen. De lage kosten van de giethars, de korte injectie en uithardingstijd, en het feit dat APA-6 economisch verantwoord gerecycled kan worden op verschillende manieren, worden gezien als additionele voordelen voor toepassing in wind energie. Het verhogen van de resistentie tegen vocht is de voornaamste aanbeveling voor verder onderzoek.

CONTENTS

CHAPTER 1

GENERAL INTRODUCTION: LARGE THERMOPLASTIC COMPOSITE WIND TURBINE BLADES

1.1 Introduction

The current technology trends in wind energy aim at developing dedicated offshore wind power systems. It is expected that these remotely deployed turbines will be equipped with rotor blades with a length in excess of 100 meters. Whether such large blades can be manufactured with the current structural design is doubtful and spar-rib-skin structures are suggested as alternative design. The re-introduction of ribs in blade technology will also be beneficial for installation of active load damping devices and health monitoring systems. Because current blade manufacturing technology based on thermoset composites is not suitable for producing spar-rib-skin assemblies in an economically sound manner, technology based on fully recyclable and weldable thermoplastic composites is proposed. The main drawback related to melt processing of thermoplastic composites is the limited size and thickness of the parts that can be obtained. Production of larger and thicker thermoplastic composite parts for wind turbine blades forms the main incentive for development of a reactive infusion process for thermoplastic composites at the Delft University of Technology, which forms the main topic of this thesis as is outlined in the final paragraph of this chapter.

1.2 Current trends in wind energy

Due to the increasing costs of fossil fuels and the increasing efficiency of wind turbines in the last decade, wind energy has become increasingly cost-efficient [1]. With the current growth rate of installed power (annual growth rate world wide: 25%), which forecasts that in 2020 12% of the global electricity will be produced by

wind turbines (23% by 2040), wind energy is well on its way of becoming one of our mainstream sources of energy. In order to keep up this high growth rate, the wind energy market is currently facing a transformation from onshore energy production to offshore installation of so-called wind farms. Remote deployment of a turbine in such a harsh environment makes operation and maintenance difficult and expensive, which brings up the need for dedicated offshore wind power systems.
In order to maintain a continuous reduction in costs per kWh (40% cost reduction compared to 2002 is envisaged in 2020 [2]), technological developments predominantly aim at increasing the (rated) power output per turbine (currently 3.5 MW, near future 6-10 [1]). In order to extract more power from the wind, such multi-MW size turbines require larger blades to increase the rotor swept area. Therefore, it is expected that the maximum blade length will increase from 65 m (2006) to over 100 m in the next decades [3]. Not being bound by noise pollution regulations and having to deal less with aesthetical issues, offshore turbines seem to be well suited for these super-sized blades. However, it is feared that soon the limit of the current blade technology is reached and that new and improved materials and more efficient blade designs are necessary to overcome what has truly become a technological challenge: manufacturing of large wind turbine blades [4, 5].

1.3 Large wind turbine blades at the Delft University of Technology

The interfaculty Delft University Wind Energy Research Institute (DUWIND [6]) has over 25 years of experience in wind turbine design, manufacturing and testing, and covers almost all aspects of modern wind turbine technology. DUWIND is one of the initiators of a program called WE@SEA, which involves public and private participation towards realizing the ambitious target of the Dutch government of having 6,000 Megawatt of wind power installed offshore by 2020. The central objective of this program is to develop a structural basis for long-term business development in The Netherlands, for the purpose of preparing, designing, constructing, operating, maintaining and, in due course, dismantling offshore wind power plants. The program comprises the entire chain of technological, economical and ecological activities.

Within the WE@SEA framework, a BSIK funded research project called PhD@SEA was started April 1st 2004 (BSIK03041). Research line 1 of this project deals with the challenge of manufacturing large wind turbine blades and was executed by one of DUWIND's participants: the disciplinary group Design and Production of Composite Structures (DPCS [7]) at the Faculty of Aerospace Engineering. DPCS concentrates on the development of new concepts for composite materials and structures preferably combined with novel production technologies in which material, structure and product are formed in one step. The philosophy followed is called 'think composites' and is based on 'pro-active or forward integration of design parameters'. Therefore, the research programs are organized in such a way that the development of knowledge on composites emphasizes the mutual relationship of the following subgroups, which form the so-called 'trinity essence': (i) development and design of composite materials, (ii) development and design of composite structures, and (iii) development of dedicated manufacturing techniques [8]. DPCS has already successfully introduced 'composite technology packages' in the aerospace and automotive industry and using the same philosophy, DPCS is currently working on the development of large wind turbine blades, see Figure 1.1.

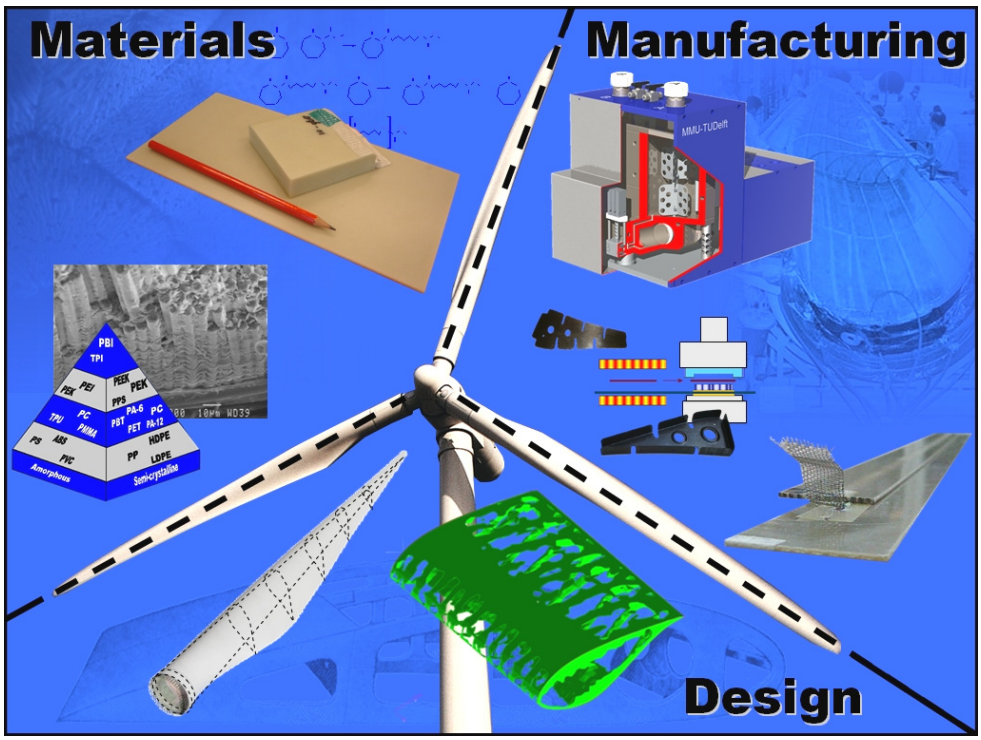

Fig. 1.1: Development of a complete technology package for thermoplastic composite wind turbine blades at DPCS.

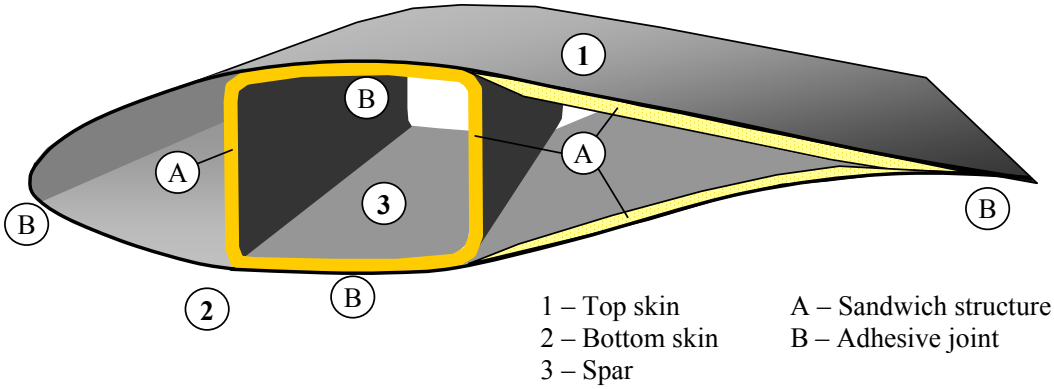

Fig. 1.2: Representative cross-section of a modern wind turbine blade.

1.4 Re-introducing ribs in blade structures

Figure 1.2 shows a representative cross-section of a modern wind turbine blade. A turbine blade commonly consists of three functional parts: the spar, the top skin and the bottom skin. The composite materials used generally consist of E-glass fiber fabrics (woven or unidirectional) in a thermoset matrix (epoxy, polyester or vinylester). After manufacturing the three individual parts separately they are bonded together with a structural adhesive.

The thickness of the blade and the thickness of sandwich skins contribute positively to the flexural stiffness of the blade and prevent local buckling. In general, longer blades are subjected to larger bending moments, which is predominantly caused by the tremendous increase in gravitational forces (proportional to the cube of the blade length: $\sim m^3$) and up to a lesser extent by the increase in aerodynamic loads (proportional to the square of the blade length: $\sim m^2$) [9]. To prevent longer blades from hitting the tower, the stiffness of the blades needs to be increased, which up till now has been accomplished by increasing the thickness of the blades and the skins without changing the structural design much. In this case, the stiffness increase is proportional to the area of the cross-section and therefore scales according to the square of the blade length ($\sim m^2$). From the square-cube law can be concluded that the current structural design becomes less efficient with increasing blade length and that at a certain point the limit of what is technically feasible will be reached [9]. An

additional drawback of the currently followed upscaling methodology, which increases both length and thickness of the blades, is the fact that from an aerodynamic point of view more slender blades with thinner airfoils are desired [4].
Although the introduction of high strength and stiffness carbon fibers will allow further upscaling of the blades using current blade technology [4, 10], a change in structural design forms a more elegant solution and is wider applicable. Therefore, a PhD study at the Delft University of Technology by S. Joncas on the structural design of large wind turbine blades was conducted parallel to the research that lead to the present thesis. The preliminary results from this study using topology optimization techniques already indicate that monolithic composite spar-rib-skin structures, which are commonly used in aircraft wings, could be best suited for large wind turbine blades, see Figure 1.3 [11]. Further refinement of this study is expected to reveal a blade structure, which resembles the ones shown in Figure 1.4 and 1.5 more closely. The same figures also show that the idea of wind turbine blades with a spar-rib-skin assembly is not entirely new.

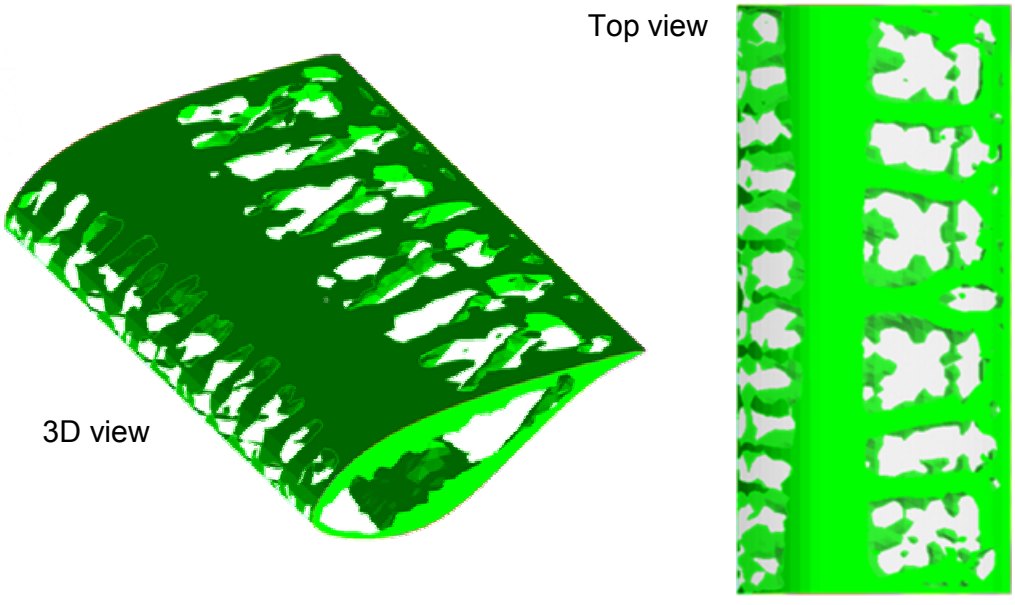

Fig. 1.3: Preliminary results of the topology optimization study of a blade section conducted by S. Joncas et al. using a density method [11].

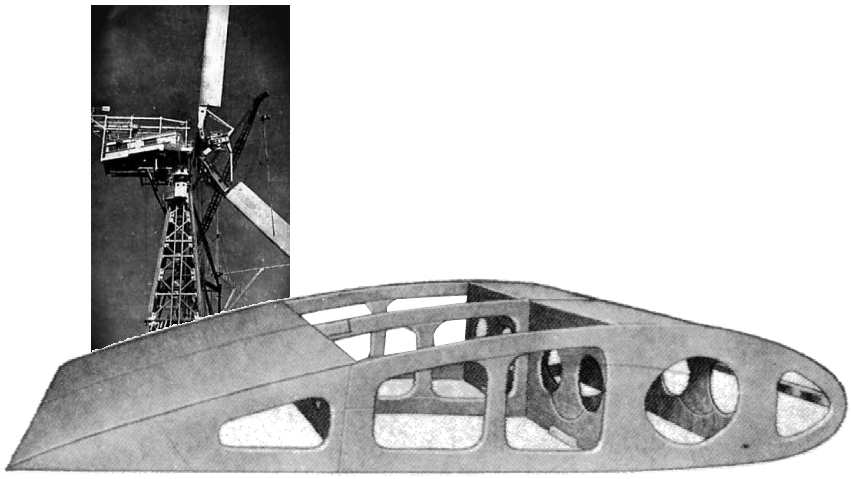

Fig. 1.4: Mock-up of an aluminum blade section (front) that was used in the 1.25 MW Smith-Putnam wind turbine in 1941 (back) [12].

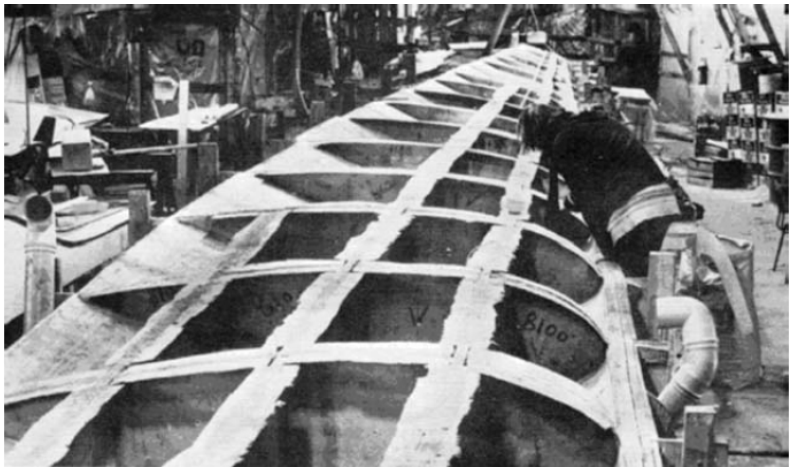

Fig. 1.5: Manufacturing of the thermoset composite skin-spar-web assembly of a Tvind wind turbine blade [5].

Additional benefits of ribs arise from developments, which aim at reducing the operation and maintenance costs of remotely deployed offshore turbines and increasing their operational life (currently 20 years, limited by the blades [5]). The latter not only focuses on increasing the fatigue resistance of the blade materials and structures [5], but also on equipping so-called 'smart blades' with active load damping devices like flaps, micro-tabs and other kinds of actuators [13, 14]. A reduction in

operation and maintenance costs is expected from the use of health monitoring systems. Smart blades that can signal when maintenance is necessary will ease maintenance logistics and reduce the number of scheduled yet unnecessary maintenance visits. Embedment of fiber optic sensors and piezoelectric actuators in composite structures are among the current research efforts [15, 16]. Ribs will not only be useful as attachment point for smart devices such as actuators and control surfaces, but will also provide the necessary load-path between these devices and the blade spar.

1.5 Thermoplastic composite wind turbine blades

Since joining of thermoset composites through structural bonding or mechanical fastening is tedious, labor intensive and time consuming [17], current blade manufacturing is based on the principle of minimizing the number of parts and joints. Commonly the skins and spar are manufactured as a single part by vacuum infusion or pre-pregging, which are joined afterwards by structural bonding. A spar-rib-skin structure, on the other hand, consists of a larger number of parts and will require more joining. It is consequently expected that with the current thermoset composite technology manufacturing of such blades will become too labor intensive and time consuming, and therefore most likely too expensive.

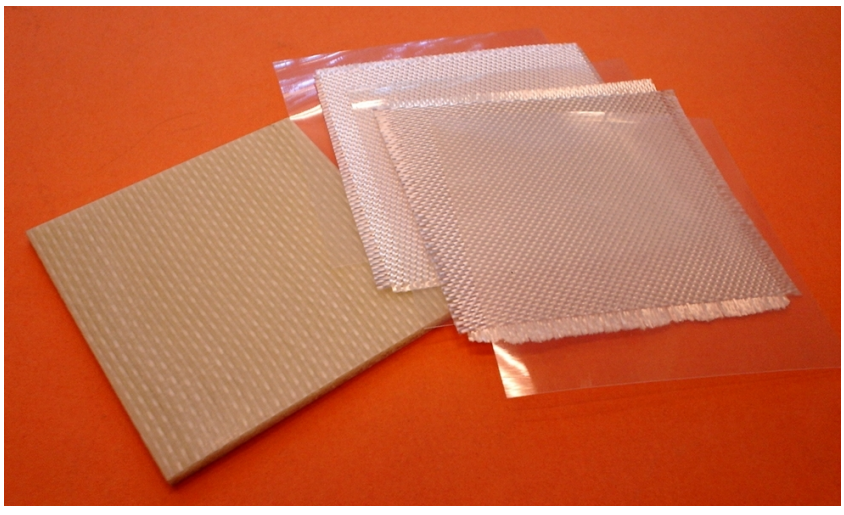

Fig. 1.6: Thermoplastic composite intermediate materials. Left: pre-consolidated laminate sheet material, right: a stack of alternating layers of polymer films and woven fiber reinforcement.

Thermoplastic composite technology, however, seems more suitable for producing spar-rib-skin assemblies. Thermoplastic composites with a fiber fabric reinforcement can be processed rapidly from intermediate materials (extruded polymer films or pre-consolidated laminate sheet material, see Figure 1.6) using a melting and solidification procedure [18] and do not require a time-consuming curing cycle like their thermoset counterparts [19]. A typical cycle time for manufacturing a thermoplastic part through rubber forming for instance (see Figure 1.7) is 5-8 minutes, whereas the curing time of a thermoset resin is in the order of hours. Afterwards, the various parts can be joined through welding in a matter of minutes: local heating and application of pressure causes the material at the interface of two parts to melt and fuse together, whereas in the subsequent cooling stage the weld is finalized. Depending on the method of heating, a distinction is made between resistance welding (see Figure 1.8 [17]), induction welding [20] and ultra-sonic welding. Rapid manufacturing of a large number of thermoplastic composite ribs, spars and skins through rubber forming, followed by assembly with resistance welding is already commercially applied for aeronautical parts, see Figure 1.9. In addition to the short cycle times that can be achieved with the abovementioned forming and joining processes, all related technology has the potential of becoming fully automated [21, 22], which is a paramount issue when realizing that an incredibly large number of wind turbine blades needs to be manufactured in the coming decades.

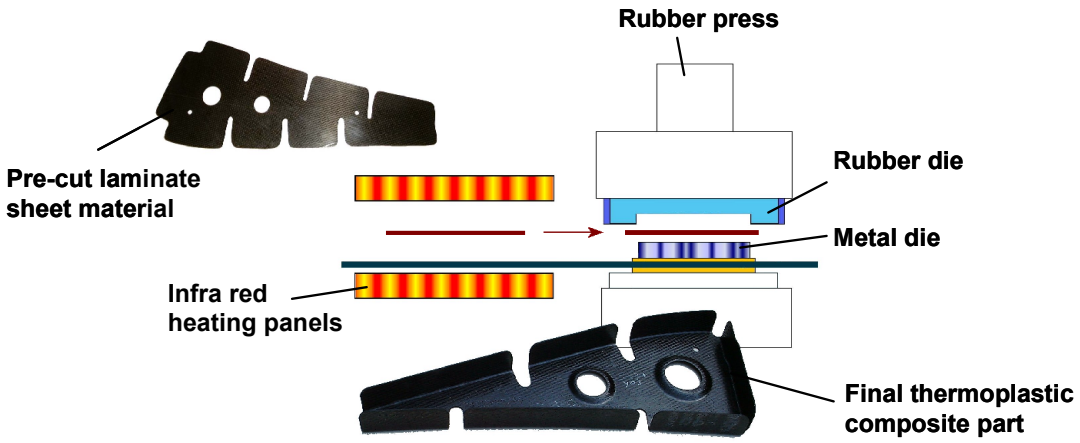

Fig. 1.7: Rubber forming of thermoplastic composite parts.

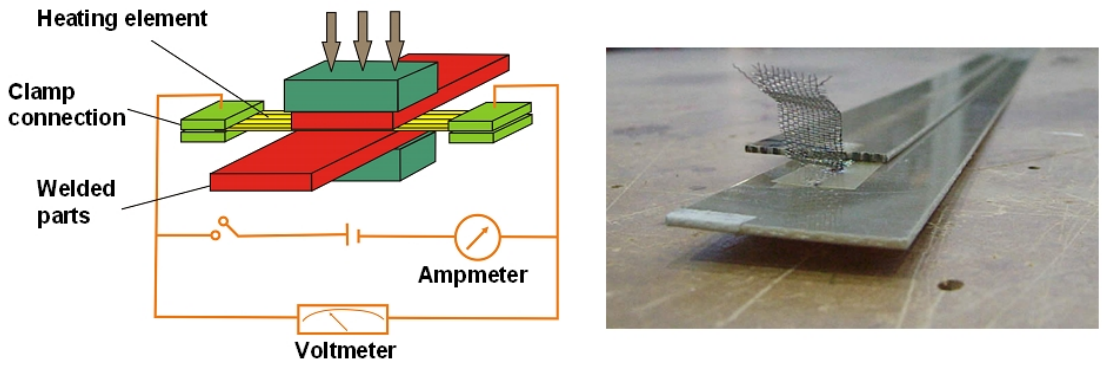

Fig. 1.8: Resistance welding of thermoplastic composites. Left: process schematics, right: welded parts.

Fig. 1.9: Airbus A350 inboard leading edge or 'J-Nose', manufactured by Stork Aerospace, The Netherlands.

Although according to the author this is the first time that thermoplastic composites are linked to wind turbine blades for specifically structural design reasons, the interest in these materials from blade manufacturers already existed for the past 10 to 15 years, for the following, more classic, reasons [5]: (i) due to their higher toughness, thermoplastic composites have better impact properties and do not turn brittle at low temperatures, (ii) the shelf life of the intermediate materials (films, semi-pregs, consolidated laminates) is unlimited, (iii) the absence of 'chemistry' during processing provides a clean and healthy processing environment, and (iv) the fact that thermoplastic composites can be melt-processed numerous times offers the possibility

of reusing the material in less demanding applications. This type of recycling goes beyond the aim of current research efforts, which deal with more efficient incineration procedures to reduce the amount of blade material that has to be deposited as slag [23] and the use of natural fibers as composite reinforcement [5]. Especially when using expensive carbon fibers, reuse of blade materials also offers substantial economic benefits [4].

Fig. 1.10: Thermoplastic composite blade parts manufactured at the Risø National Laboratory in Denmark. Left: cross-section made of glass/PP [24], right: small blade made of glass/PET [25].

Given the extensive list of potential advantages, the list of actual applications of thermoplastic composites is surprisingly short. In 1996, manufacturing of a melt-processed 3.2m long thermoplastic composite airfoil for wind turbine blades made of glass fiber reinforced polyethyleneteraphthalate (PET) was demonstrated by LM Glassfiber, Comfil and the Risø National Laboratory [25]. The same laboratory developed a process for manufacturing complete blades of glass fiber reinforced polypropylene (PP) in cooperation with Bonus Energy, which was demonstrated by building a 0.5m long blade section, see Figure 1.10 [24]. The fact that thermoplastic composites have so far found only limited application is caused by the following drawbacks:

- The use of heavy presses sets a limit to the achievable part thickness, size and level of integration that can be achieved with melt processing [18]. The current

maximum achievable part thickness is 5-10 mm, which clearly demonstrates the technological hurdle that needs to be taken in order to produce for instance a blade spar, which will requires a laminate thickness of up to 10 cm near the blade root.

- Despite the high toughness of the matrix, the fatigue performance of thermoplastic composites is often disappointingly low because of a poor fiber-to-matrix interface [26]. Whereas during its entire lifetime an aircraft is subjected to a number of cyclic loadings in the order of 10^6, for wind turbine blades this number increases to a mere 10^9, which clearly underlines fatigue resistance as one of the most important design drivers [9].
- Whereas thermoset composite blades can be manufactured directly from the uncured resin and the dry reinforcement, processing of continuous fiber reinforced thermoplastics requires the use of intermediate materials like extruded polymer films, semi-pregs or pre-consolidated laminates, which adds significantly to the material costs [5].
- Manufacturing of thermoplastic composites blades requires the introduction of new processing methods and expensive equipment [5].
- Melt processing is generally performed at temperatures in excess of 200ºC, which requires expensive temperature resistant tooling and leads to the introduction of thermal stresses, which degrade the material properties [5].

1.6 Vacuum infusion technology for thermoplastic composites

Application of thermoplastic composites in wind turbine blades seems more than promising and in order to overcome the previously mentioned drawbacks related to melt processing, the following idea was born at DPCS: use current blade manufacturing technologies for manufacturing of thermoplastic composites. In other words, combine processing technology of thermoset resins with the material properties of thermoplastics: vacuum infusion of thermoplastic composites.
In a common vacuum infusion process for thermoset composites [27], dry fiber fabrics are placed on a solid mould half, which defines the part geometry, see Figure 1.11. A flexible mould half or vacuum foil is applied together with a sealant tape to bag the fiber lay-up in an airtight manner. Subsequent application of vacuum compacts the bagged fibers and induces a resin flow from inlet to outlet. After

impregnating the fibers with a low viscosity monomer or prepolymer, *in situ* polymerization of the thermoset matrix (for instance polyester or epoxy) around the fibers takes place. Upon completion of the curing step, the product can be demolded, which results in a composite part with a smooth and well-defined surface on one side and a slightly rough and less defined surface on the other. Because of the *in situ* polymerization step this process is referred to as reactive processing.

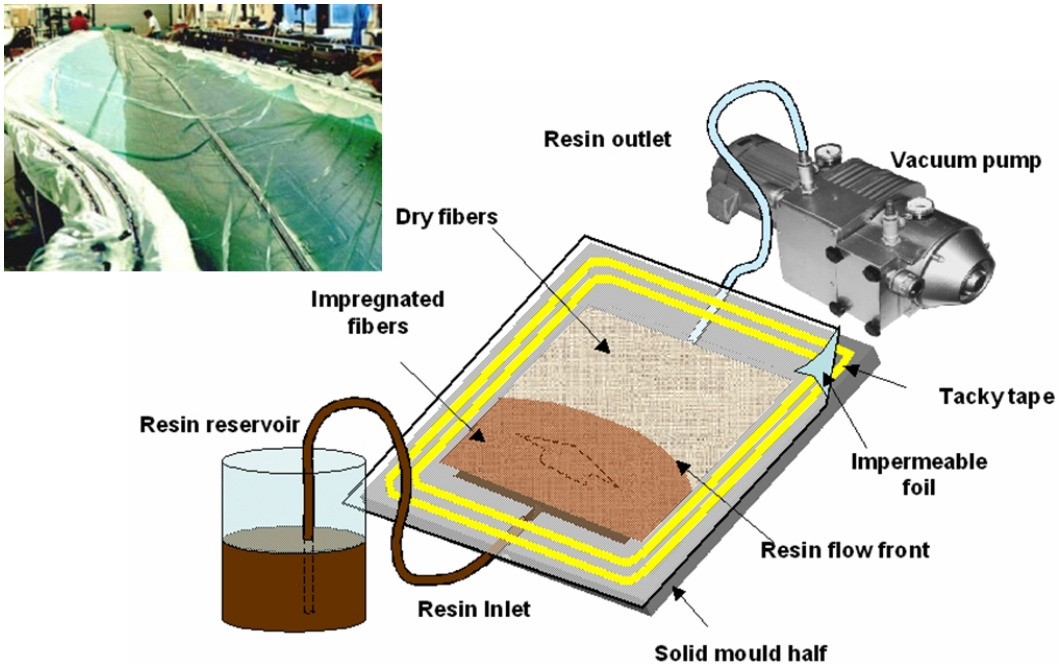

Fig. 1.11: Schematic representation of the vacuum infusion process. Insert: Vacuum infusion of a wind turbine blade skin.

Because of their high viscosity, thermoplastic polymers are not suitable for vacuum infusion and therefore reactive processing is proposed as an alternative: infusion of the fibers by a low viscosity monomer followed by *in situ* polymerization of the thermoplastic matrix. In addition to the advantages that thermoplastic materials already have to offer such as weldability and recyclability, reactive processing of thermoplastic composites yields the following benefits for manufacturing of thermoplastic composite wind turbine blades:

- Using vacuum as driving force for fiber impregnation no longer requires heavy presses, which makes it possible to manufacture thermoplastic composite blades or parts with a similar size and thickness as thermoset composite blades.
- *In situ* polymerization of the thermoplastic matrix around the fibers opens the door for establishing a chemical fiber-to-matrix interface at a level, which is not possible with melt processing. It is expected that this will tremendously increase the fatigue performance of thermoplastic composites.
- Omitting the need for expensive intermediate materials significantly reduces material costs, see Figure 3.6.
- Vacuum infusion is a commonly applied technology for the manufacturing of wind turbine blades and consequently does not require the introduction of completely new processing methods.

1.7 Research goals and structure of the thesis

1.7.1 Research goals

The research goals have been formulated as follows:

- To provide an overview of the current status of reactive processing of thermoplastic composites involving both materials and processing methods.
- To identify and further develop a suitable (see section 1.7.2) material-process combination for vacuum infusion of thermoplastic composite wind turbine blades, focusing primarily on the involved chemistry and material science aspects. Given the early stage of this research on new wind turbine blade materials and the long-term aspirations of the Delft University in this field, development of models that simulate for instance material behavior or the manufacturing process is regarded as a follow-up step and is consequently out of scope of the present thesis.

1.7.2 List of requirements

In order to determine whether a material-process combination is ‘suitable’ for manufacturing of wind turbine blades and for guiding the research in the proper direction, the following list of requirements is used throughout the thesis. The aim of

the envisaged infusion process is to manufacture thermoplastic composites suitable for thick and thin-walled wind turbine blade structures:

- with sufficiently high specific properties (stiffness and strength per unit weight);
- with sufficient resistance against fatigue (cyclic loading);
- that are able to withstand environmental exposure: high humidity and salinity levels and static temperatures ranging from -50 (arctic conditions) to 50ºC (desert conditions);
- with sufficient resistance against physical attack: UV radiation and the abrasive force of wind and sand;
- that are resistant against chemical attack against for instance oil and cleaning agents that are commonly used in the offshore industry;
- which have the potential of being cost-competitive over their entire life time with the current state-of-the-art within reasonable time;
- that should be suitable for an eco-designed wind turbine blade (minimum energy usage and waste during production, suitable for recycling).

1.7.3 Structure of the thesis

The structure of this thesis is as shown in Figure 1.12. A literature survey on the current status of reactive processing of thermoplastic composites is presented in Chapter 2, followed by a material trade off. The selected material anionic polyamide-6 (APA-6) is discussed in Chapter 3, whereas Chapter 4 deals with the equipment that was developed throughout the project. Curing of the APA-6 resin is discussed in Chapter 5 and the effect of various processing parameters on the neat resin properties in Chapter 6. By means of a comparison with melt processed polyamide-6 and polyamide-6 nano-composites, the potential for APA-6 as composite matrix is assessed in Chapter 7. Chapter 8 deals for the first time with the actual manufacturing of APA-6 composites and Chapter 9 focuses on the formation of fiber-to-matrix bonds. The static and dynamic properties of APA-6 composites are compared with a melt-processed PA-6 composite and a vacuum infused epoxy composite in Chapter 10. The effect of additives on APA-6 and APA-6 composites is explained in Chapter 11. Finally, conclusions and recommendations for future research are presented in Chapter 12.

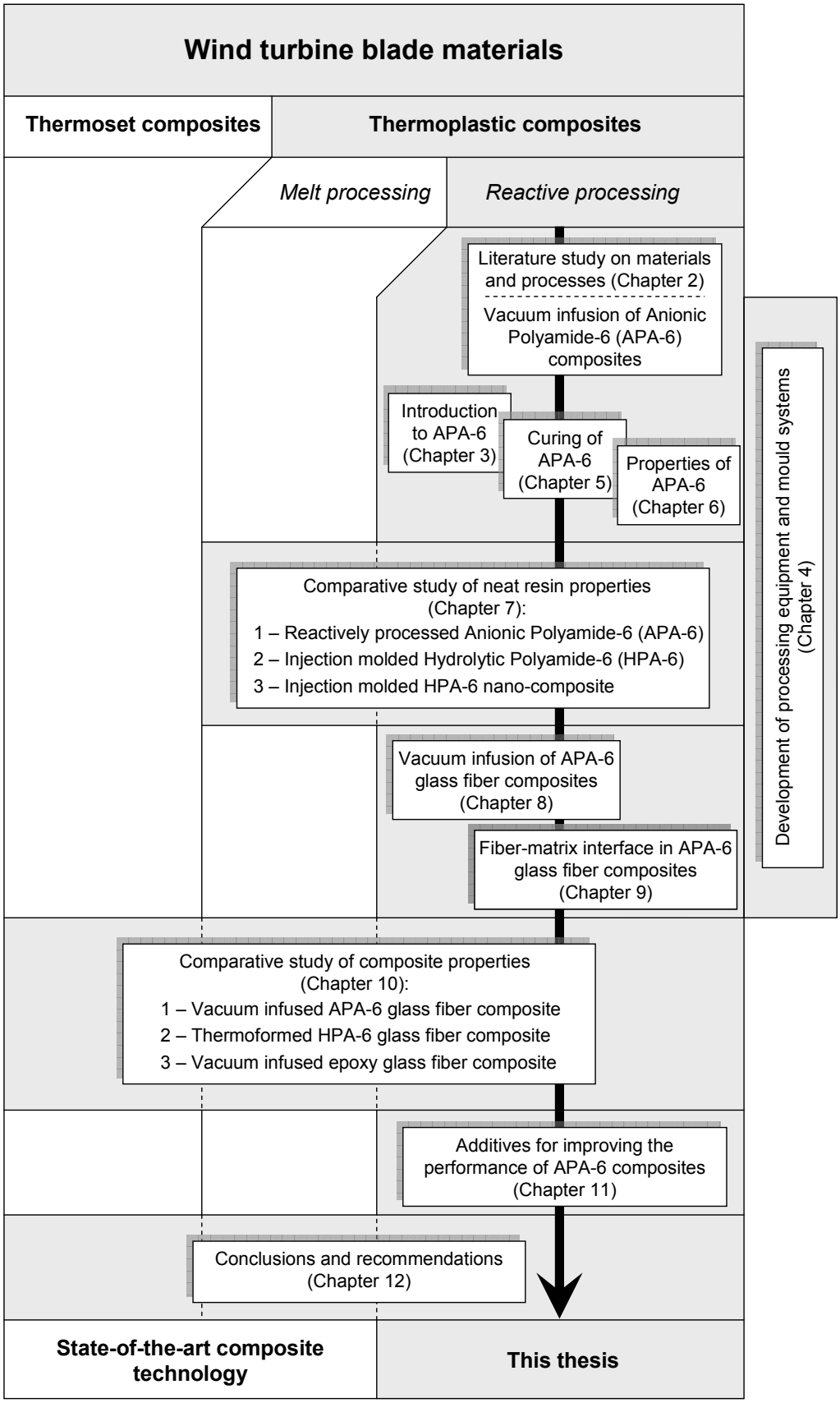

Fig. 1.12: Structure of this thesis.

CHAPTER 2

REACTIVE PROCESSING OF THERMOPLASTIC COMPOSITES: AN OVERVIEW OF THE LITERATURE

2.1 Introduction

In the previous chapter vacuum infusion of thermoplastic composites was identified as a potential solution for manufacturing of future wind turbine blades. This chapter depicts the current status of reactive processing of thermoplastic polymers by means of a literature study. First, the requirements are listed for a thermoplastic polymer in order to be suitable for reactive processing. Second, an overview of suitable polymers is given; a distinction is made between engineering and high-performance plastics. Finally, a resin material for further research is selected by means of a trade-off study. The various reactive processes that are mentioned in this chapter are described in paragraph 3.4.2.

2.2 Requirements for reactive processing of thermoplastic materials

For reactive processing of thermoplastic composites, the *in situ* polymerization of the matrix basically has to meet the following requirements: a high molecular weight linear polymer has to be formed at sufficiently high conversions without the generation of unwanted by-products. Suitable polymerization types are consequently narrowed down to addition polymerizations of mono- and difunctional species, of which vinyl polymerization and ring opening polymerization are most common.

2.2.1 Vinyl polymerization

Vinyl polymers are polymers made from vinyl monomers: small molecules containing carbon-carbon double bonds. During polymerization the double bonds are broken into single bonds, resulting in two free electrons. The free electrons are used to join monomer units to form a long chain of many thousands of carbon atoms containing only single bonds between atoms, see Figure 2.3.

2.2.2 Ring-opening polymerization

As the name already suggests, ring-opening polymerization (ROP) is based on a polymerization mechanism in which ring-shaped molecules (cyclics) are opened into linear monomers or oligomers and subsequently connected into high molecular weight polymers without generating by-products, see Figure 2.4. ROP initially received attention as clean alternative for polymerization routes that result in the generation of nasty by-products or require the use of large amounts of hazardous solvents. Production of polyetheretherketone (PEEK) and polyphenylenesulfide (PPS) for instance makes use of high-boiling solvents such as diphenyl sulfone and dichlorobenzene [28, 29], whereas toxic phosgene gas is used for interfacial phosgenation polymerization of polycarbonates [30]. The fact that a so-called ring-chain equilibrium exists, which can be shifted by temperature or the addition of cleverly selected catalysts not only offers the possibility for *in situ* polymerization but also for recycling through cyclo-depolymerization (CDP) [31].
In the following sections, suitable thermoplastic material systems for reactive processing are introduced.

2.3 Reactive processing of engineering plastics

Figure 2.1 shows the thermoplastics pyramid, which ranks the polymers according to cost, performance and production volume. At the base of the pyramid, commodity plastics can be found, which possess weak mechanical properties and poor temperature resistance, and which are produced in large volumes for household appliances and for instance interior parts for the automotive industry. The high-

performance plastics can be found one step above the engineering plastics at the center of the pyramid. Both plastics show a higher modulus, strength and temperature resistance than the commodity plastics. The expensive specialty plastics form the top of the pyramid and are manufactured in small volumes for only the most demanding applications in military aviation and spacecrafts. The pyramid also shows that thermoplastic polymers can be divided into amorphous and semi-crystalline materials. Whereas in amorphous polymers the molecules have no order or arrangement, in semi-crystalline polymers part of the polymer chains are neatly ordered in crystal structures [32].

It is assumed that for application in wind turbine blades the plastic, amorphous or semi-crystalline, should rank as engineering plastic or higher. Reactive processing of engineering plastics is discussed in this section, whereas suitable high-performance plastics are discussed in the next.

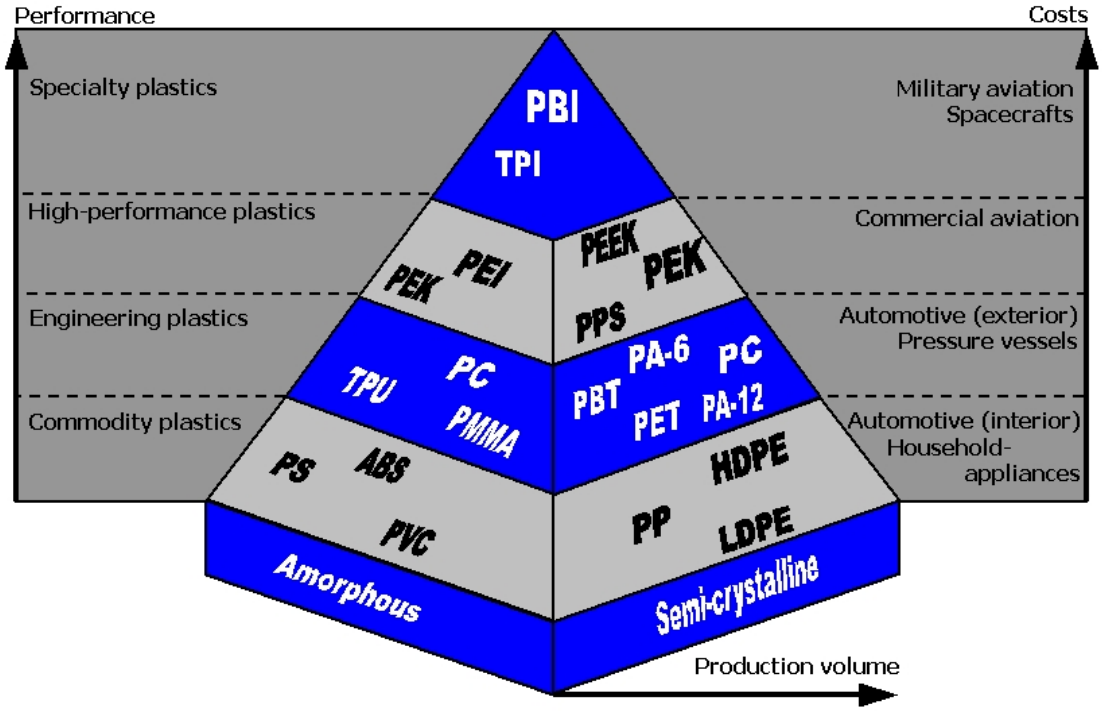

Fig. 2.1: Ranking pyramid of thermoplastic polymers.

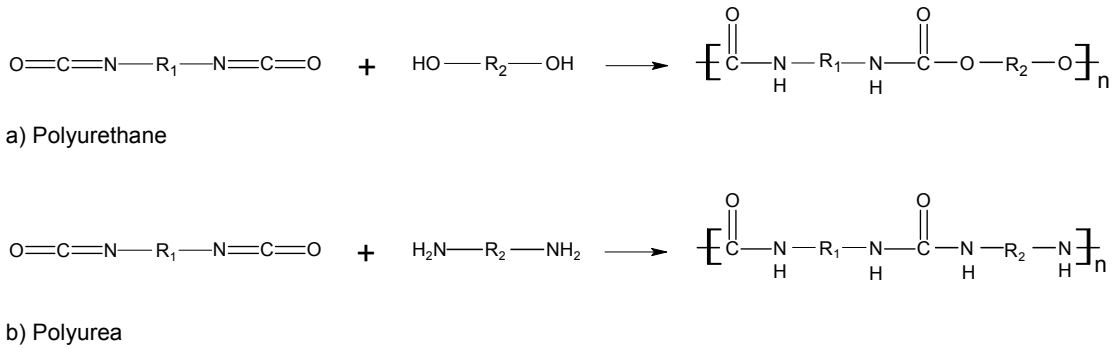

Fig. 2.2: Synthesis of polyurethane (a) and polyurea (b) [33].

2.3.1 Thermoplastic polyurethane (TPU)

Polyurethanes are among the most widely applied resin materials specifically developed for reactive processing [33]. Di-isocyanates react with di-ols in a matter of seconds when processed at around 60-80ºC, as is shown in Figure 2.2a. Sometimes, di-amines are used instead of di-ols to polymerize so-called polyureas, see Figure 2.2b. Most polyurethanes have a thermoset nature, although thermoplastic polyurethanes exist. These are however commonly sold as fully reacted granules or powder for melt processing. Dubé et al. [34], however, demonstrated the feasibility of Reactive Injection Pultrusion (RIP) of TPU composites based on the abovementioned chemistry. They pointed out that the high reactivity of the resin requires a fast responding process control system, since any deviation from ideal conditions can easily lead to a significant reduction in the final polymer properties.
Reactive processing of TPU based on a different type of chemistry was recently developed by Dow Chemicals (USA) and is currently applied by the Fulcrum Composites Company for the manufacturing of continuous fiber reinforced TPU pultrusion profiles [35, 36]. Whereas most polyurethanes are reactively processed from their monomers, Fulcrum TPU uses high molecular weight linear polymer as starting point and makes use of a depolymerization-repolymerization (DPRP) mechanism. Upon heating, depolymerization into lower weight fractions takes place, which results in a significant viscosity reduction. Subsequent cooling induces repolymerization and molecular weight rises again up to its starting value. A minimum viscosity of a few Pa·s is obtained at a processing temperature of 270ºC.

Although further heating reduces the viscosity into the mPa·s-range, the material loses its ability to repolymerize [37]. Recyclability of the Fulcrum resin through regrinding and injection molding without the loss of mechanical properties has been demonstrated [38].

2.3.2 Polymethylmetacrylate (PMMA)

Free radical vinyl polymerization of the methylmetacrylate monomer (MMA) into its polymer PMMA is usually conducted at temperatures in excess of 40ºC using peroxide initiators [39], see Figure 2.3. At lower temperatures the reaction time will soon exceed 16 hours, whereas at higher temperatures the danger exists that due to the exothermic nature (462.2 J heat is generated per gram material) the monomer will soon start to boil, resulting in voids in the final product. During polymerization the density increases from 0.9 g/cm^3 (monomer) to 1.2 g/cm^3 (polymer), and in order to reduce shrinkage, usually a pre-polymer (solution of PMMA in its monomer) is used. The melt viscosity of the pre-polymer is higher than that of the monomer (0.1 Pa·s at 50ºC), but is still low enough to cast (Plexiglas® or Lucite®) windows, which is the main application of this transparent but relatively brittle polymer. As far as composite processing is concerned, a monomer impregnation method of natural fibers [40] and a Reactive Injection Pultrusion process are mentioned in literature [41, 42]. In order to increase the reaction rate, which is necessary in a continuous process, the reaction temperature of the pre-polymer had to be increased to 160ºC, which is well above the glass transition temperature of the amorphous polymer.

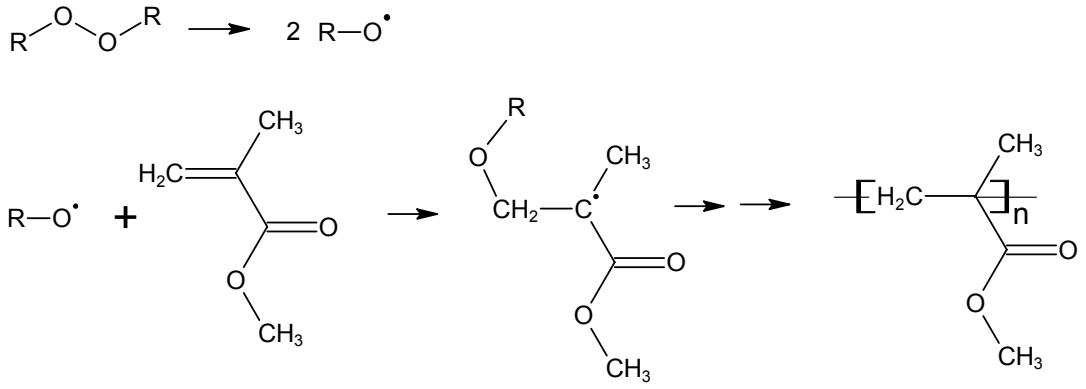

Fig. 2.3: Free radical vinyl polymerization of PMMA [39].

2.3.3 Polyamides

Anionic polymerization of lactams is the oldest and up to now the most developed way for reactive processing of thermoplastics through ring-opening polymerization (ROP). In the early 1940s, ROP of caprolactam into polyamide-6 (PA-6) was discovered and has been commercially exploited by for instance BASF, Bayer, DSM and Monsanto. Technology developed by DSM allows PA-6 to be fully depolymerized in a cost-effective way into caprolactam of virgin quality [43]. Anionic polymerization of laurolactam into PA-12 has recently gained interest due to the work conducted at EMS Chemie A.G. and the École Polytechnique Fédérale de Lausanne, both in Switzerland.

2.3.3.1 Polyamide-6 (PA-6)

Anionic ROP of ε-caprolactam (T_m = 69°C) into high molecular weight polyamide-6 (PA-6), see Figure 3.5, is a catalyzed reaction performed at 130-170°C [44]. Final conversions of up to 99.3 wt% can be obtained in 3 to 60 minutes, depending on the type and amount of activator and initiator added. Typical activators used are N-acyllactams, whereas metal caprolactamates are commonly used as initiator [45-51]. Usually two material batches are prepared, which after mixing start to polymerize: a monomer-activator batch and a monomer-initiator batch. Due to the anionic nature, the reaction is easily terminated by proton donating species, such as for instance moisture. Therefore, storage and processing have to be conducted in an absolutely moisture free environment. Since processing takes place below the polymer melting and crystallization point, polymerization and crystallization take place simultaneously, resulting in solid highly crystalline PA-6 [52-54]. The reaction is exothermic ($\Delta H_{polymerization}$ = -144 J/g [55], $\Delta H_{crystallization}$ = -190 J/g [56]), which leads to a significant temperature increase during curing. The complex kinetics of the anionic polymerization of caprolactam have been studied extensively, mainly focusing on the autocatalytic effect of the exothermic temperature rise [55, 57-64]. Numerous reactive processes have already been developed for unreinforced and reinforced PA-6 such as (rotational) casting [65-69], Reaction Injection Molding (RIM) [70-72], Reinforced Reaction Injection Molding (RRIM) [73, 74], Structural Reaction Injection Molding (SRIM) [75-77] and Reactive Injection Pultrusion (RIP) [78, 79]. In order to reduce mould shrinkage and to increase the toughness, a rubber-

modified block-copolymer called NyRIM® was developed by DSM and is currently traded under the name AP Nylon® by Brüggemann Chemical, Germany [80-84]. Due to the pre-polymer activator of NyRIM®, the viscosity is slightly higher (η = 60-90 mPa·s [81]) than of the unmodified resin (η = 10 mPa·s [85]). In addition to these rubber block copolymers also varieties with branches and cross-links have been investigated [86, 87]. Because in the present research PA-6 has been selected for development of vacuum infusion technology for thermoplastic composite wind turbine blades (see Section 2.5) at the Delft University of Technology, the following references have been added to complete this literature review [85, 88-92].

2.3.3.2 Polyamide-12 (PA-12)

Polyamide-12 is anionically polymerized from ω-laurolactam (T_m = 154ºC) using similar activators and initiators as discussed in the previous paragraph on PA-6, see Figure 2.4 [93]. In contrast to anionic PA-6, polymerization has to be conducted above the final polymer melting point (175ºC) to increase the polymerization rate and to avoid entrapment of growing chains inside rapidly forming crystals, which leads to a significant reduction in conversion [94]. As a consequence, when processing at 180-240ºC, an additional cooling step is required prior to demolding [10]. The melted monomer has an initial viscosity of 23 mPa·s [95] and has to be kept in nitrogen protective environment to prevent initiator deactivation. The reaction is slightly exothermic (53 J/g [94]) and total mould shrinkage is 8.3-9.6 % [96]. Reactive PA-12 is currently marketed by EMS Chemie A.G., Switzerland, who also developed a one pot activator-initiator solution called Grilonit® that can be stored indefinitely in inert atmosphere. This solution, which can also be used for anionic polymerization of PA-6, no longer requires pre-mixing of two separate material batches that slowly polymerize over time. Pultrusion [97] and SRIM-like processes [98-101] for PA-12 composites are currently being developed at the École Polytechnique Fédérale de Lausanne (EPFL), Switzerland, the National University of Ireland, Ireland and the Institut für Verbundwerkstoffe, Germany.

Caprolactam and laurolactam can be anionically copolymerized to tailor polymer properties. Material properties such as the strength and stiffness, glass transition and the melting point are in direct relation with the monomer ratios [102-104].

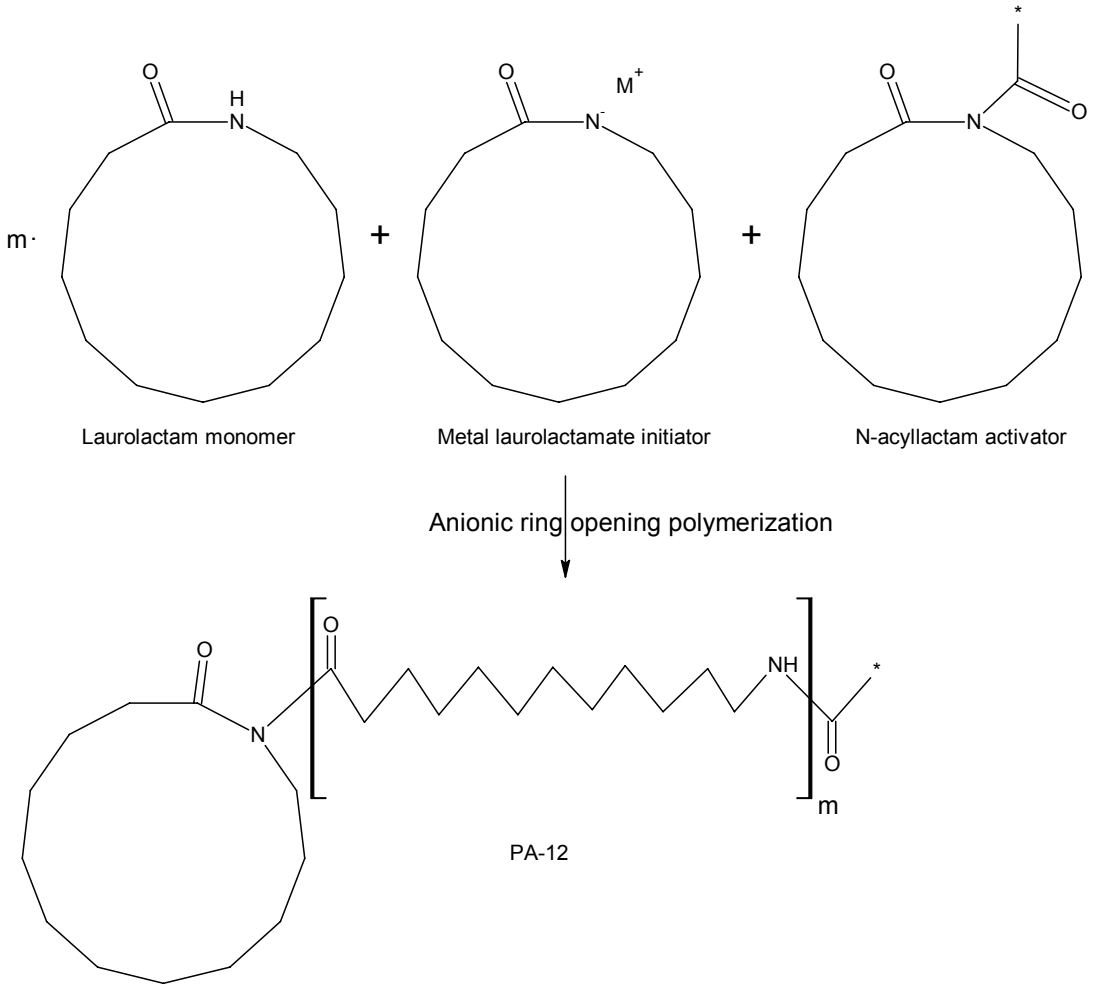

Fig. 2.4: Anionic ring opening polymerization of laurolactam into PA-12 [93].

2.3.4 Polyesters

Synthesis of macrocyclic polyesters and the ring-opening metathesis polymerization (ROMP) thereof was initially developed by D.J. Brunelle and his research group at the General Electrics Corporation, USA, in the late 1980s and early 1990s. Initially aiming at polycarbonates, see the next paragraph, reactive processing of both polyetheteraphthalate (PET) and polybutyleneteraphthalate (PBT) was developed. The latter is currently being marketed specifically for the production of composites under the name Cyclics® by the Cyclics Corporation, USA [105-107].

2.3.4.1 Polyethyleneteraphthalate (PET)

Macrocyclic oligomers can be obtained through cyclodepolymerization (CDP) of linear PET and subsequently repolymerized through ROMP into high Mw PET [108, 109]. Figure 2.5 shows polymerization of PET using a cyclic dimer (T_m = 225ºC). Up to 100 wt% conversion at 250-325ºC is obtained in several hours without a catalyst, whereas addition of a catalyst reduces the reaction time to 3-15 minutes at 225ºC. The initial melt viscosity of the cyclic precursors is 30 mPa·s [110, 111].

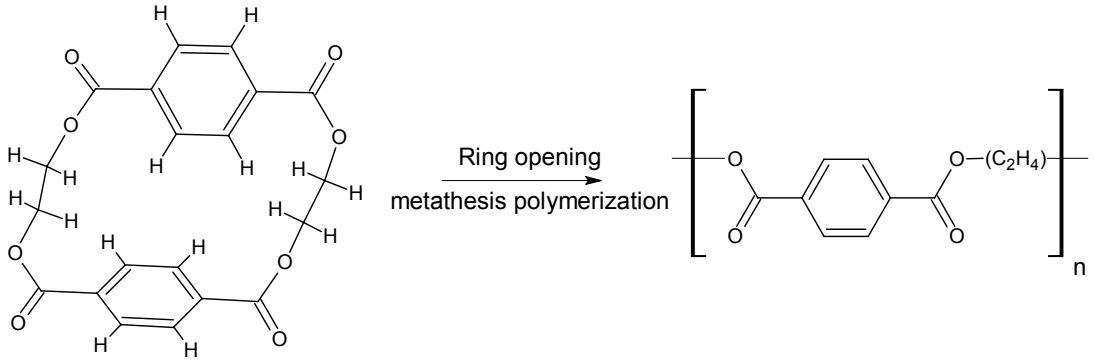

Fig. 2.5: Ring opening metathesis polymerization of PET [108, 109].

2.3.4.2 Polybutyleneteraphthalate (PBT)

Depolymerization of linear PBT yields a macrocyclic oligomer mixture, which can be repolymerized directly into solid high molecular weight (Mw = 445 000) semi-crystalline PBT at 180-200ºC by addition of a titanium initiator [112, 113], see Figure 2.6. The oligomer mixture has a melt viscosity of 150 mPa·s at 150ºC, which drops to 30 mPa·s at 190ºC. When processed at 190ºC in protective atmosphere, the viscosity reaches 1 Pa·s after approximately 5 minutes and final conversions of 95-99 wt% are obtained within 30 minutes [114]. Although polymerization itself is not exothermic, approximately 67 J/g of heat is generated in the subsequent crystallization phase. Final polymer properties strongly depend on the polymerization temperature. When isothermally polymerized below its melting point (T_m = 220-267ºC), the PBT obtained is highly crystalline and tends to become brittle (i.e. elongation at break = 1.8%), due to a phenomena called cold-crystallization [115]. A subsequent melting and cooling cycle brings back the more ductile behavior. Properties of initially

reactively processed PBT are largely unaffected after mechanical-thermal recycling (re-grinding followed by injection molding) [116]. In addition, PBT can be recycled chemically by depolymerization into the cyclic oligomers or all the way into its monomers dimethylterephthalate and butanediol [31]. RTM-like processes for manufacturing fiber reinforced PBT are developed at Delaware University (USA) and KU Leuven (Belgium) [115, 117-120]. Together with the Cyclics Corporation and Mitsubishi Heavy Industries, the National University of Ireland has started the development of Resin Film Infusion technology for the development of thermoplastic composite wind turbine blades [121, 122]. As this technology makes use of pre-impregnated fibers, using a one-component monomer-catalyst system, it is similar to the thermoset pre-pregging technology currently used by blade manufacturers [123].

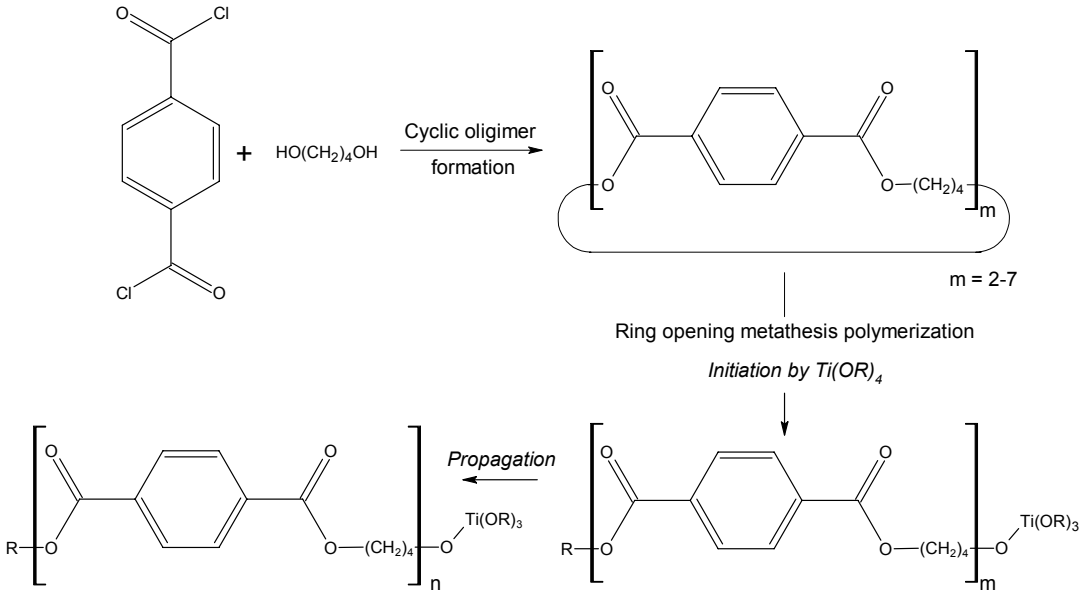

Fig. 2.6: Ring opening metathesis polymerization of PBT [112, 113].

2.3.4.3 Polycarbonate (PC)

Macrocyclic Bisphenol-A (T_m = 200-210ºC) can be polymerized into polycarbonate through ROMP conducted at 240-280ºC using anionic initiators [124], see Figure 2.7. When polymerized at 250ºC in protective atmosphere, the initial viscosity of the macrocyclic melt is 1 Pa·s and in 2-5 minutes high molecular weight PC is obtained (Mw = 300 000) with conversions of over 99 wt% [125]. The reaction is entropy

driven, which means that no exothermic heat is generated during polymerization. ROMP of macrocyclics consisting of Bisphenol-A and hydroquinone at 300ºC results in a solvent resistant PC, which in contrast to the amorphous grade used in melt processing can be obtained in either amorphous or semi-crystalline form [30, 126]. Other versions reported in literature are cross-linked [127] and copolymerized PCs [128]. Salem et al. successfully produced glass fiber reinforced PC composites through reactive processing, although an additional consolidation step in a hot-press was necessary to reduce the void content [129].

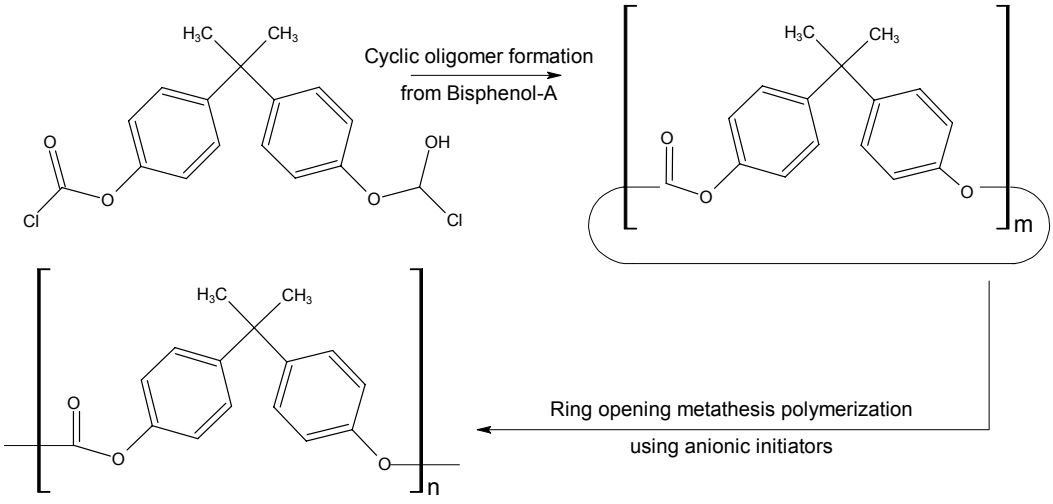

Fig. 2.7: Ring opening metathesis polymerization of polycarbonates [124].

2.4 Reactive processing of high-performance plastics

After the successes of reactive processing of engineering plastics such as PU, PMMA and PA-6, several attempts were made to develop similar technology for processing of high performance plastics, mainly focusing on ROP of polyarylethers. Initial results, however, brought complications to light, which were directly related to the inherent properties of high-performance plastics, which make them so interesting in the first place: an extremely stiff polymer backbone combined with outstanding chemical resistance and thermal properties. Whereas the relatively flexible engineering plastics

are easily converted into cyclic precursors of only a single or a few monomer units, a much larger number of monomer units is required to form so-called macrocyclic precursors of the more rigid high-performance plastics. The higher molecular weight of the cyclic precursors brings up the following problems:

- Synthesis of the cyclic precursors has to be conducted in high-dilution or pseudo-high-dilution conditions, which is explained by the fact that just before ring closure the ends of the relatively long polymer chains are rather far apart from each other. In case the solid concentration during synthesis is too high, it is more likely that a chain will react with a neighboring chain rather than having its two ends react together to form a cycle. Synthesis therefore requires a lot of solvent and leads to relatively low yields [31].
- The macrocyclic precursors obtained are often an oligomer mixture, rather than a substance consisting of single sized rings, which is related to matters discussed in the previous point. Various oligomers might differ in properties such as melting points, solubility in the other oligomers within the same mixture or even in being amorphous of crystalline [130, 131]. These differences complicate synthesis and further processing.
- In order to obtain high conversions, polymerization has to be conducted at high temperatures for two reasons: (i) the processing temperature has to exceed the melting point of all oligomers, and (ii) the viscosity of the growing polymer chains has to be kept low enough to induce sufficient chain mobility. Unfortunately, at temperatures ranging from 300 to 400ºC side reactions like cross-linking are unavoidable, which strongly reduce the polymer performance [131].

Recent advances in cyclics technology are (i) the use of monomer units containing *meta* and *ortho* rather than *para* linkages, see Figure 2.8, in order to produce macrocyclics with a lower molecular weight (at a slight reduction of thermal stability of their equivalent polymer) and (ii) isolation of specific oligomers with a low melting point or an amorphous character in order to reduce the required polymerization temperature [130]. In the next paragraphs an overview of reactive processing equivalents of common high performance plastics is given.

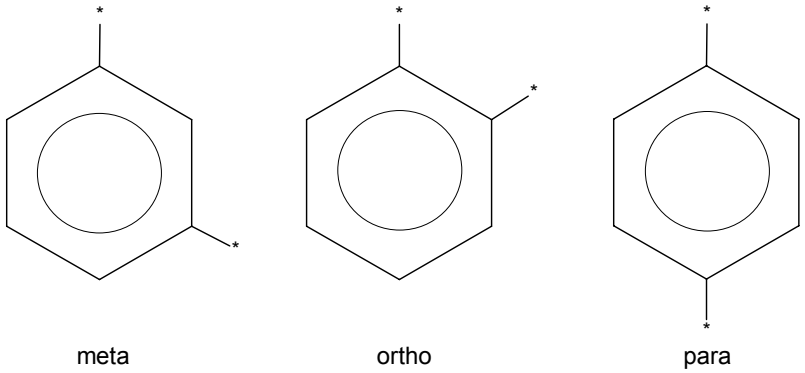

Fig. 2.8: Meta, ortho and para linkages.

2.4.1 Polyetheretherketone (PEEK)

Literature mentions synthesis of 45-60-90 membered macrocyclics from 4,4-difluorobenzophenone and hydroquinone in pseudo-high-dilution conditions at a yield of 60%, which polymerized at 350ºC in 5 minutes using Caesium fluoride as initiator [132], see Figure 2.9. Another source reports synthesis of cyclic 2-mers, 3-mers and 4-mers, but fails to discuss ring opening polymerization [29].

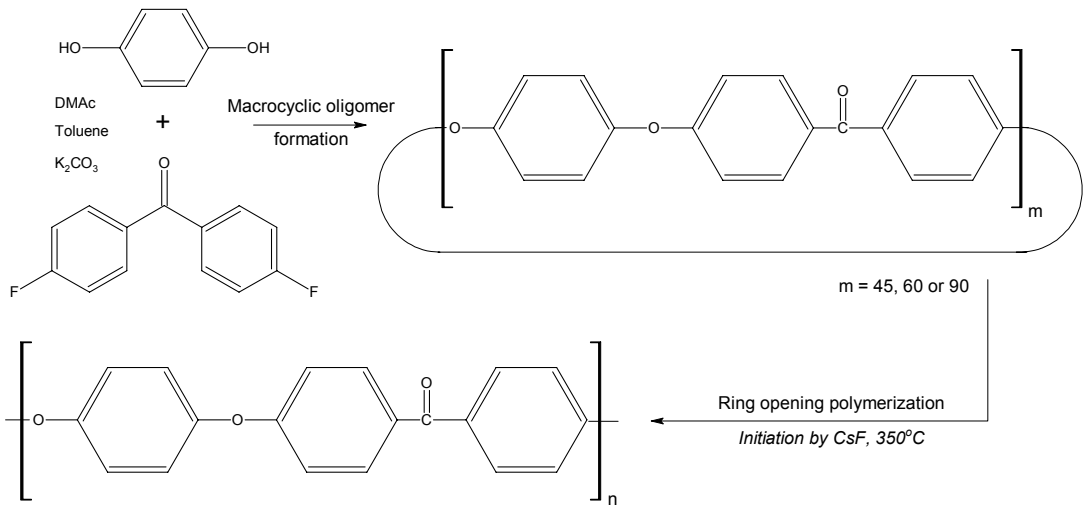

Fig. 2.9: Reactive processing route of PEEK [132].

2.4.2 Polyetherketone (PEK)

According to Jiang et al. [133-135], macrocyclic oligomers for polyetherketones (PEK) were produced at a yield of 54%. These cyclics (T_g of 127ºC) formed a clear melt at 280ºC and could subsequently be polymerized for 1 hour at the same temperature up till a conversion of 93.5 wt%. The resulting linear polymer is slightly branched and has a T_g of 216ºC, which is slightly lower than commercially produced PEK (T_g = 228ºC) due to the presence of oligomers that failed to polymerize. Ring opening polymerization at 390ºC for 30 minutes of a cyclic PEK dimer into an amorphous polymer (T_g = 162ºC) was reported by the same authors [136].
The potential of reactive processing of high performance thermoplastics is clearly demonstrated by the work conducted at McGill University, Canada [137, 138]. It was shown that macrocyclic PEK containing a 1,2-dibenzoylbenzene moiety, see Figure 2.10, has a stable melt viscosity (80 mPa·s at 330ºC) and could be polymerized at 340ºC in 30 minutes after addition of a nucleophilic initiator.
Baxter et al. managed to polymerize cyclic PEK in 30 minutes at 300ºC using a Caesium fluoride initiator into a semi-crystalline polymer (T_g = 168ºC, T_m = 302ºC) [130]. In addition, they showed that instead of using macrocyclics specifically synthesized for ring opening polymerization, one could also use the cyclic oligomer byproduct that is generated during production of commercial PEK-390 and polymerize these in 25 minutes at 385ºC [139].

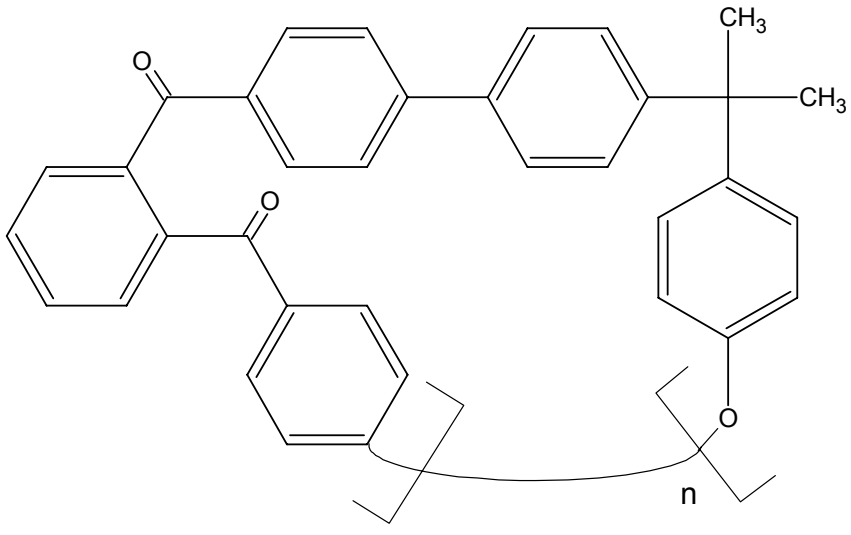

Fig. 2.10: Macrocyclic precursor for PEK [137].

2.4.3 Polyethersulfon (PES)

ROP of PES cyclic precursors, conducted at 300ºC for 2 hours, is shown in Figure 2.11 [140]. Different types of poly arylene sulfone cyclics are discussed in [141, 142].

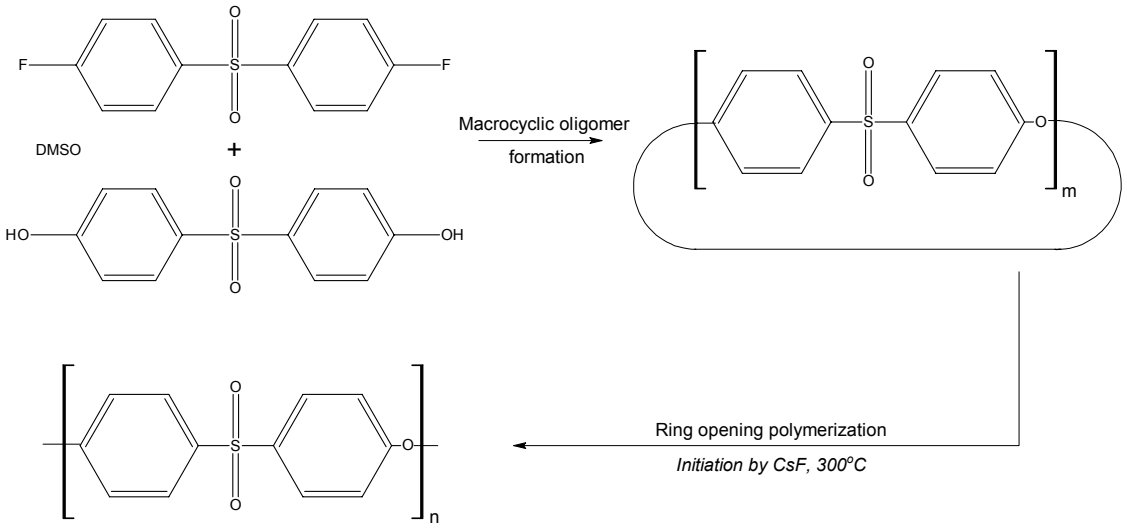

Fig. 2.11: Reactive processing route of PES [140].

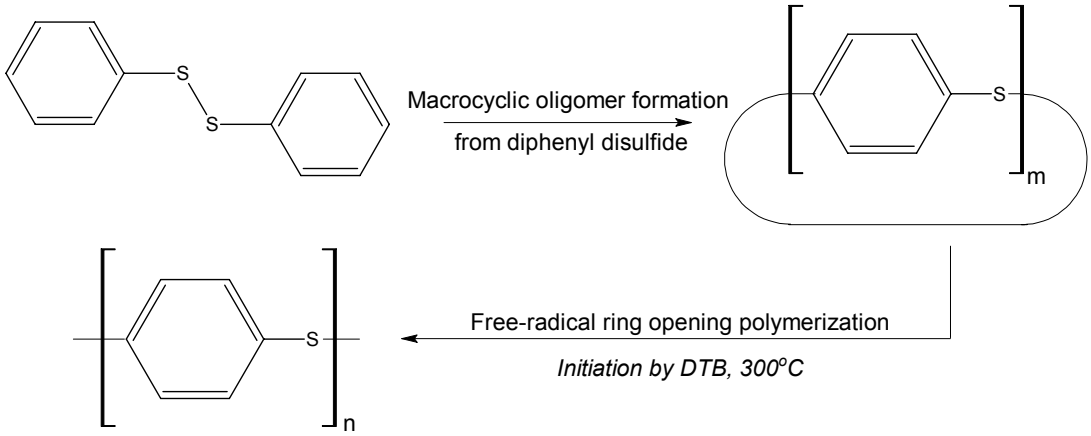

Fig. 2.12: Reactive processing route of PPS [143].

2.4.4 Polyphenylenesulfide (PPS)

Melt polymerization of cyclic PPS pentamer and hexamer at 300ºC under Nitrogen environment is discussed in [143], see Figure 2.12. The resulting high molecular weight polymer is highly crystalline and has a melting point of 277ºC, which is comparable to that of commercial grades PPS (T_m = 285ºC). An alternative method for preparing the same cyclic PPS precursor is discussed in [144].

2.4.5 Polyethylenenaphthalate (PEN)

According to [145], a PEN (polyethylenenaphthalate) macrocyclic oligomer mixture with a melting point of 250-285ºC was prepared at a 57% yield. In 25 minutes ROP was conducted in the presence of a peroxide initiator at 295-300ºC, see Figure 2.13. The final polymer (T_m = 261ºC) suffered from impurities present in the cyclic oligomer mixture and initiator residue.

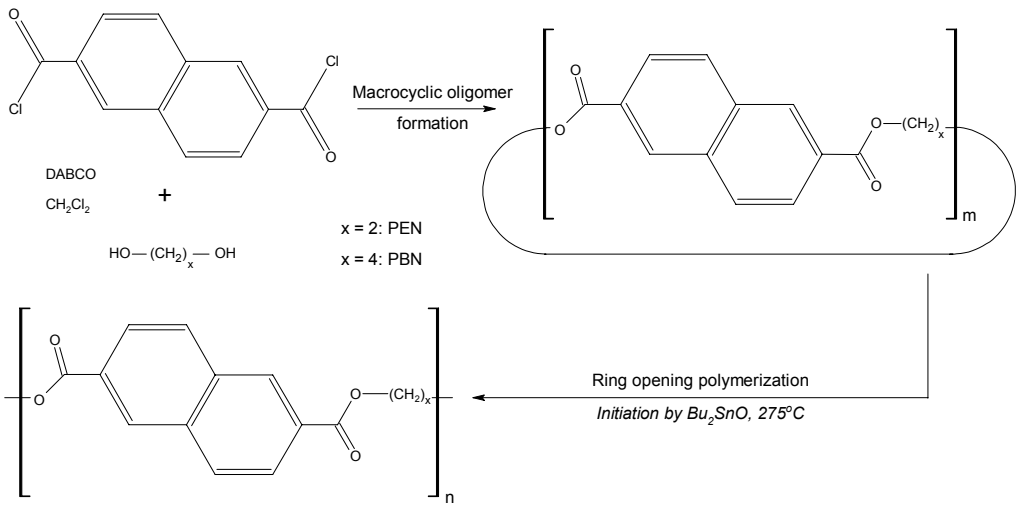

2.13: Reactive processing route for PEN and PBN [145].

2.4.6 Polybuthylenenaphthalate (PBN)

PBN (polybuthylenenaphthalete) macrcocylic precursors containing various size oligomers (T_m = 150-220ºC) were prepared at a 75% yield. ROP was subsequently

conducted in the presence of a tinoxide catalyst at 275ºC and was completed in 15 minutes, see Figure 2.13. The linear low molecular weight impurities in the cyclic oligomer mixture strongly affected the final polymer properties [145].

2.5 Material selection for further research

In this section a suitable reactive thermoplastic material is selected for manufacturing of composite wind turbine blades through vacuum infusion. The following requirements have been taken into consideration:

- Resin viscosity:
  The vacuum infusion process limits the maximum viscosity of the resin to 1 Pa·s in order to infuse the dense fiber lay up. This limit is not determined by the laws of physics, but is a value used in practice in order to infuse large composite parts in sufficiently short times. Although for small parts with a proper infusion strategy a slightly higher viscosity can be allowed, for large wind turbine blades this is certainly not advisable. Figure 2.14 shows that in addition to the commonly used thermoset resins, thermoplastic monomers meet this requirement. As mentioned before, however, reactive processing of ETPU and PMMA commonly involves a pre-polymerization step, during which the viscosity becomes too high for vacuum infusion. Of the reactive thermoplastic oligomers, only PEK seems a feasible material system.

- Availability:
  Development of a manufacturing process and detailed characterization of composite materials requires, from a research and development perspective, a relatively large amount of materials. Consequently, the matrix material should be sufficiently available and not just in lab scale quantities. Also scaling up of the process and the actual manufacturing of large wind turbine blades in near future would benefit from a matrix material, which is already commercially available at present, see Table 2.1.

- Material costs:

  In order to become a mainstream source of energy in the next decades, wind energy has to put continuous effort in reducing the costs per kWh produced electricity. A turbine blade consists for 30% (by weight) of matrix material, which makes the costs of the polymer an important economic factor. Forming the main ingredient of the resin systems, the monomer largely determines the resin costs. Based on production volumes, one can imagine that it is beneficial for the resin costs if the monomer for reactive processing is the same as the one that is used for the production of the equivalent polymer used in melt processing. Whereas for both polyamides this is the case, CBT and Fulcrum make use of a specifically for reactive processing developed monomer.

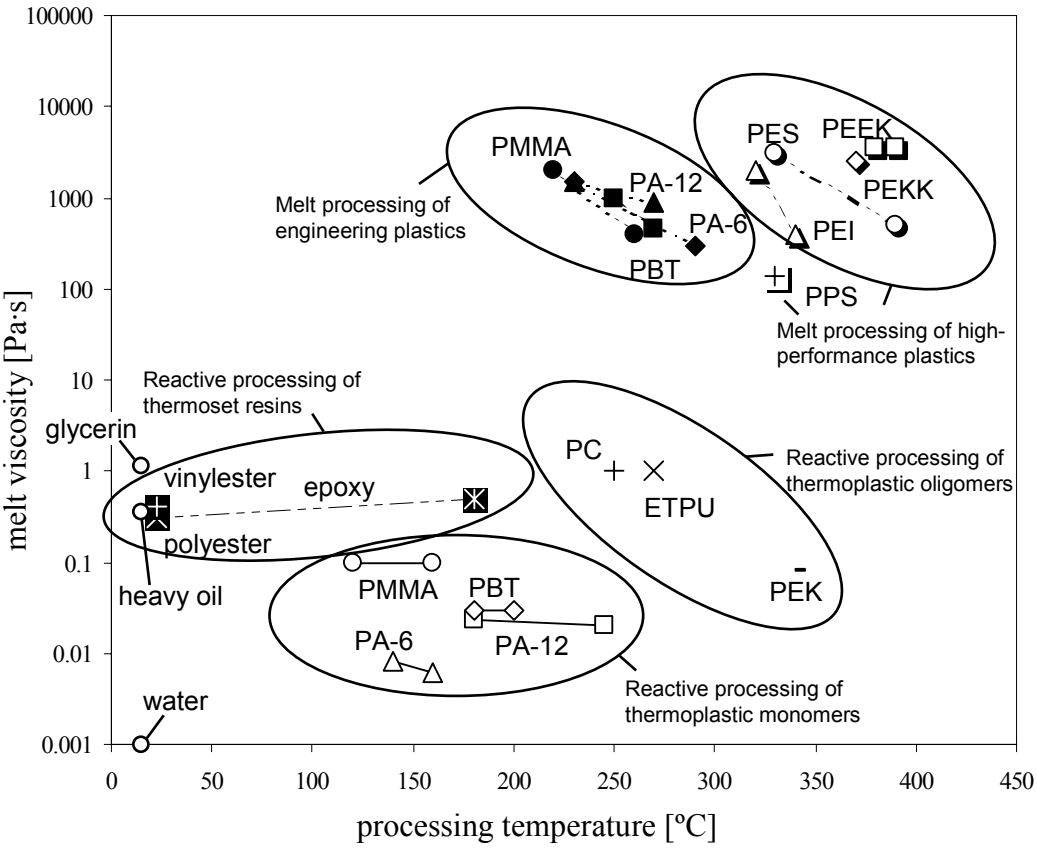

Fig. 2.14: Melt viscosities and processing temperatures of various matrix materials for both reactive and melt processing. The viscosity at room temperature of three common liquids (water, heavy oil and glycerin) has been added for comparison.

Table 2.1: Commercially available reactive thermoplastic precursors.

Polymer	Trade Name	Company
PA-6	AP Nylon	Brüggemann Chemical, Germany (2003 - …)
	NyRIM	DSM Fibre Intermediates, The Netherlands (… - 2003)
PA-12	APLC12	EMS Chemie, Switzerland
PBT	CBT	Cyclics Corp., USA
TPU	Fulcrum	Fulcrum Composites, USA

Table 2.2: Material trade-off (with the exception of PEK, high-performance plastics have been left out of the table for clarity).

Requirement	TPU	PMMA	PA-6	PA-12	PET	PBT	PC	PEK
Viscosity < 1Pa·s	X	X	√	√	√	√	X	√
Availability	√	√	√	√	X	√	X	X
Costs	X	√	√	√	X	X	X	X

√ - advantage
X - disadvantage

Table 2.2 shows that only the precursors for polyamides meet all the abovementioned requirements. PA-6 has been selected over PA-12 as the material of choice for further research for the following reasons:

- Performance/cost ratio:
  PA-6 has a higher Young's modulus (3 vs. 1.5 GPa) and tensile strength (81 vs. 55 MPa) compared to PA-12, and because PA-12 is produced in much lower quantities, the laurolactam monomer is more expensive than the caprolactam monomer [146]. As a consequence, PA-6 has a higher performance/cost ratio than PA-12.

- Available knowledge:
  Anionic PA-6 has been researched extensively as casting resin and for (R)RIM purposes. Scientific literature is abundant as well as the availability of compatible additives (nucleating agents, UV protecting agents, fire retardants, etc.) and processing agents (release agent), which could make the step towards composite

manufacturing easier. Also, at the start of the project, contacts with the technology center for reactive processing of PA-6 (DSM Fibre Intermediates) already existed and the fact that this center is located nearby in Geleen (The Netherlands) facilitated communication and the dissemination of knowledge. When in a later stage of the project the center was moved to Germany (Brüggemann Chemical, Heilbronn), the high-level of cooperation was maintained.

- Processing temperature:
  PA-6 has one of the lowest processing temperatures of all known reactively processable thermoplastics, see Table 2.3 and Figure 2.14. Additional costs of tooling and energy will therefore remain as little as possible, as well as the introduction of thermal stresses. Table 2.3 also confirms that reactive processing in general result in a reduction in processing temperature compared to melt processing of the same polymer.

Table 2.3: Comparison of processing temperatures for melt- and reactive processing for some common thermoplastic matrix materials.

Thermoplastic matrix	Processing temperature [ºC]		Temperature reduction [ºC] (reactive vs. melt processing)
	Melt processing	Reactive processing	
PA-6	230-290	140-160	70-150
PA-12	230-270	180-245	0-90
PBT	250-270	180-200	50-90
PMMA	220-260	120-160	60-140
PC	265-360	250	15-110
PET	265-325	250-325	0-15
PES	330-390	300	30-90
PPS	330	300	30
PEEK	380-390	350	30-40

2.6 Conclusions

- An overview of suitable thermoplastic material systems for reactive processing was given ranging from commercially available engineering plastics to high-performance plastics that are still in the pioneering stage.

- Based on polymer properties, viscosity, availability and material costs, polyamide-6 was selected for development of vacuum infusion technology for manufacturing of wind turbine blades. The availability of ample knowledge and the relatively low processing temperature of this material are mentioned as additional benefits.
- It is confirmed that reactive processing in general result in a reduction in processing temperature compared to melt processing of the same polymer.

CHAPTER 3

PROPERTIES AND PROCESSING OF POLYAMIDE-6

3.1 Introduction

This chapter starts with an introduction on polyamide (PA) engineering plastics including chemistry, crystal morphology and basic material properties. Next, focusing on polyamide-6 (PA-6), both melt and reactive processing is discussed. It will be demonstrated that especially for manufacturing of composites, reactive processing offers potential advantages.

3.2 Polyamide engineering plastics

Polyamides are commonly used engineering plastics in the automotive, household and textile industry because of their formidable mechanical properties, excellent resistance against abrasion and chemicals, ease of processing and good price/performance ratio [146]. Parts are manufactured from both the neat polymer as well as from polyamide-based composites with for instance a particle or fiber reinforcement.

3.2.1 Chemical characterization

Polyamides are characterized by the chemical "amide" group in the polymer backbone, see Figure 3.1 [147]. The chemical abbreviation for polyamide is PA, but also the trade name Nylon is commonly used. Polyamides with a single classification digit are polymerized using one type of monomer, which are called lactams: PA-4 is polymerized from butanelactam (also called 2-pyrrolidinone), PA-6 from caprolactam and PA-12 from laurolactam, see Figure 3.1 and 3.2. Polyamides with a double digit classification, like PA-4,6, originate from two different monomers, usually a di-amine

and a di-acid. The first classification digit represents the number of C-atoms in the di-amine, whereas the number of C-atoms in the di-acid determines the second digit.

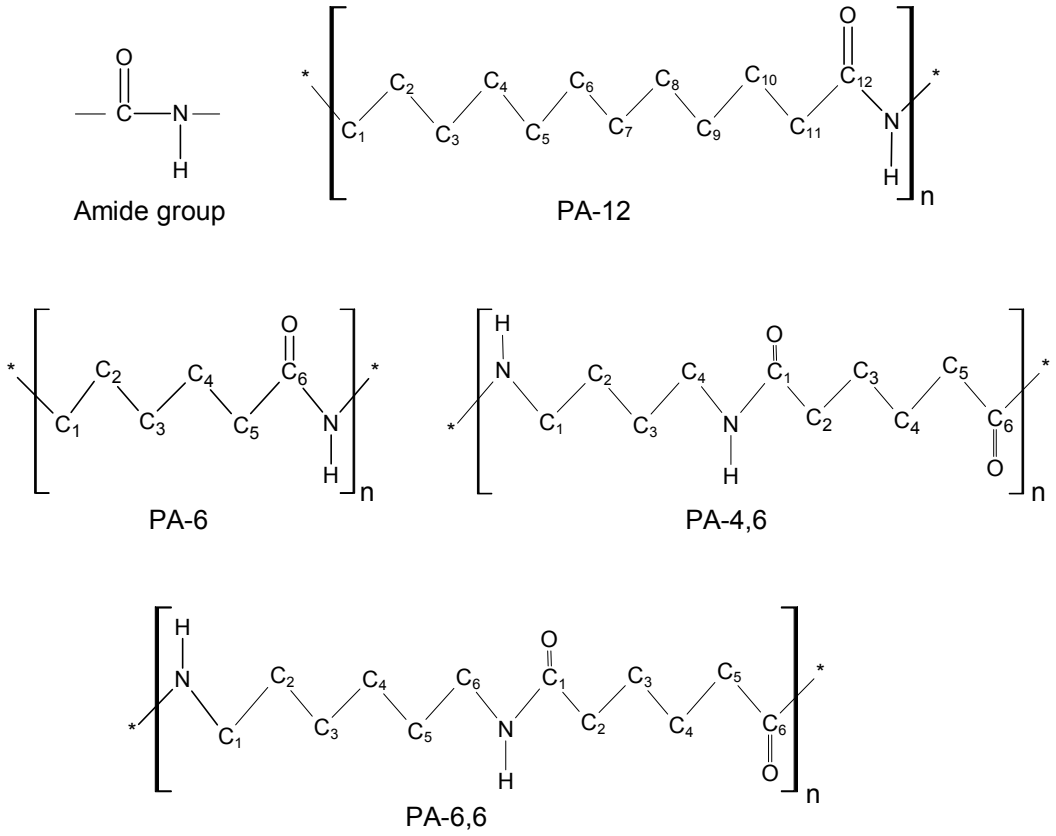

Fig. 3.1: Characterization of polyamides.

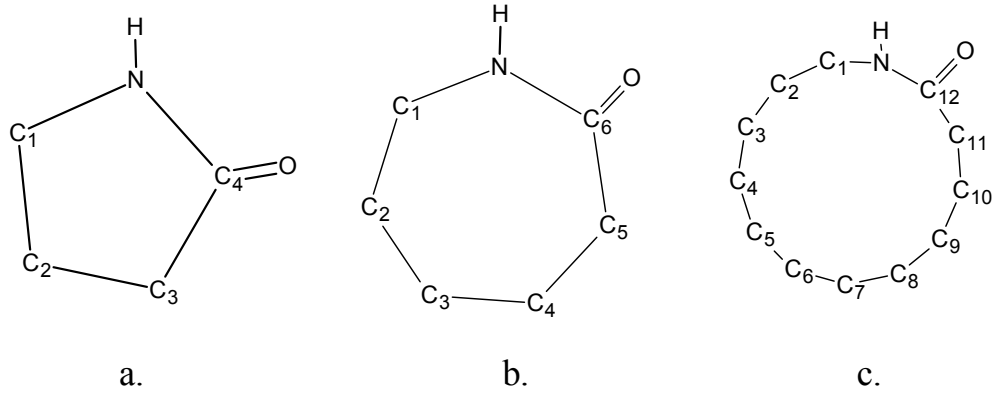

Fig. 3.2: Lactams: a. butanelactam, b. caprolactam, and c. laurolactam.

3.2.2 Crystal formation

Commonly, polyamide parts are manufactured through melt processing: after melting the polymer, the highly viscous polymer melt is shaped into the desired part geometry, which is frozen in the subsequent cooling step. Typical melt processes for manufacturing plastic and composite parts are extrusion, film blowing, vacuum forming, injection molding, pultrusion and rubber pressing [146].
When being cooled down sufficiently below the polymer melting point, amide groups can form hydrogen bonds with amide groups in the same polymer chain or in adjacent molecules, causing the polymer chains to align themselves in crystal structures, see Figure 3.3. The temperature at which the thermal motion of the polyamide chains is sufficiently low in order to be stacked into crystals by the attracting Van der Waals forces is called the crystallization temperature (T_c). Crystallization starts with the formation of so-called nucleation points. Crystals grow by reeling in polymer chains, which are subsequently stacked around the nuclei. Figure 3.3 shows that chain entanglements prevent that all polymer chains form crystals, which results in a two-phase structure with crystalline and amorphous regions [32]. At various length-scales the morphology of semi-crystalline polymers is commonly described using the terms ‘switchboards’ and ‘spherulites’, see Figure 3.3.

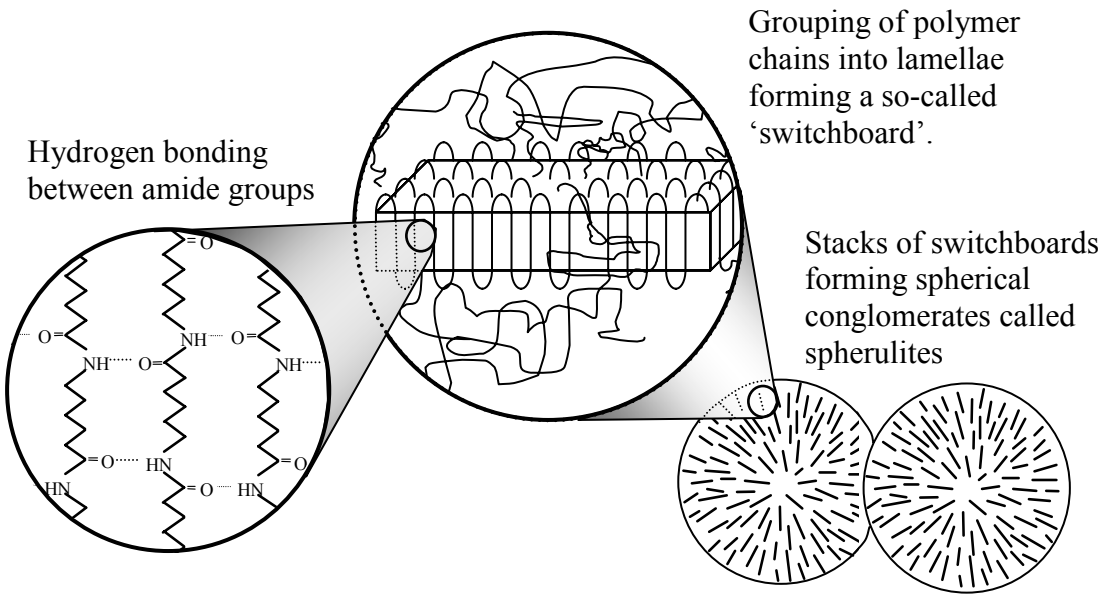

Fig. 3.3: The crystal morphology of polyamides.

Semi-crystalline polymers have two transition temperatures: the glass transition temperature (T_g) and the melting point (T_m). Below T_g the polymer chains in both the amorphous and crystalline phase are immobile. Above T_g only the chains in the amorphous phase are mobile and crossing the T_g is commonly accompanied by a drop in modulus and strength. Above the melting point the polymer turns into a highly viscous liquid, which has no significant load carrying capabilities. For most structural applications it is desired to get a high degree of crystallinity in order to obtain a polymer with high strength and modulus, and high resistance against chemicals and abrasion [74].

The rate of crystallization and the final crystal morphology are determined by the number of nucleated crystals, the magnitude of the inter-chain forces and the mobility of the polymer chains. The crystallization process can be influenced by the temperature at which the crystallization process takes place. With decreasing temperature [32, 148]:

- The number of nucleation points increases. Consequently, at equal degree of crystallinity, PA-6 crystallized at a lower temperature yields a smaller crystal size.
- The attracting Van der Waals forces become relatively stronger due to the lower thermal motion of the polymer chains.
- Reeling in of the polymer chains from the amorphous phase becomes increasingly difficult due to the lower thermal motion and related reduction in chain mobility.

Additional factors that influence the rate and degree of crystallization mainly have an effect on the chain mobility [32, 148]:

- A higher molecular weight increases the number of entanglements in the amorphous phase and consequently result in both a lower rate and degree of crystallization.
- Branch-points and cross-links not only reduce the chain mobility, consequently reducing both rate and degree of crystallization, but also cause distortions in the formed crystals when being reeled in.
- The presence of a solvent reduces chain interactions when the polymer is reeled in and consequently increases both rate and degree of crystallization.
- Reducing the cooling rate keeps the polymer chains mobile for a longer period, consequently extending the time to form crystals.

When processing conditions are insufficient to reach a high degree of crystallinity during melt processing, commonly taken measures are:

- Keeping the melt processed polymer at a steady temperature in between its glass transition and crystallization temperatures. This so-called annealing can take place in the mould or after demolding in for instance an oven. During annealing not only the degree of crystallinity increases, but also imperfections are removed from the crystal structure.
- A nucleation agent can be compounded into the polymer prior to melt processing. Nucleation of a larger number of crystals increases the rate of crystallization.

3.2.3 Effect of moisture absorption

Amide groups can also form hydrogen bonds with water. Although the chains in the crystalline phase are too densely packed for water to penetrate, the amorphous phase is capable of absorbing a significant amount of water. Absorbed water causes the polymer to swell and reduces the glass transition temperature, which causes a significant drop in modulus and strength depending on the application temperature. The higher the number of amide groups in the polymer chain (a lower methylene:amide ratio), the more the polyamide is prone to water absorption, see Table 3.1 [146].

Table 3.1: Effect of amide-concentration on the properties of various polyamides [146].

Property	PA-4	PA-6	PA-12
Methylene:amide ratio	3	5	11
Melting point [ºC]	260	223	180
Density [g/cm^3]	1.18	1.13-1.15	1.01-1.02
Equilibrium moisture content at 100% RH	28	9.5	2.0
Glass transition temperature [ºC]:	-	65	58
100% RH	-	-22	42
Flexural strength [MPa]:	-	113	56
50% RH	-	40	40
Flexural modulus [GPa]:	-	2.7	1.4
50% RH	-	1.0	1.0

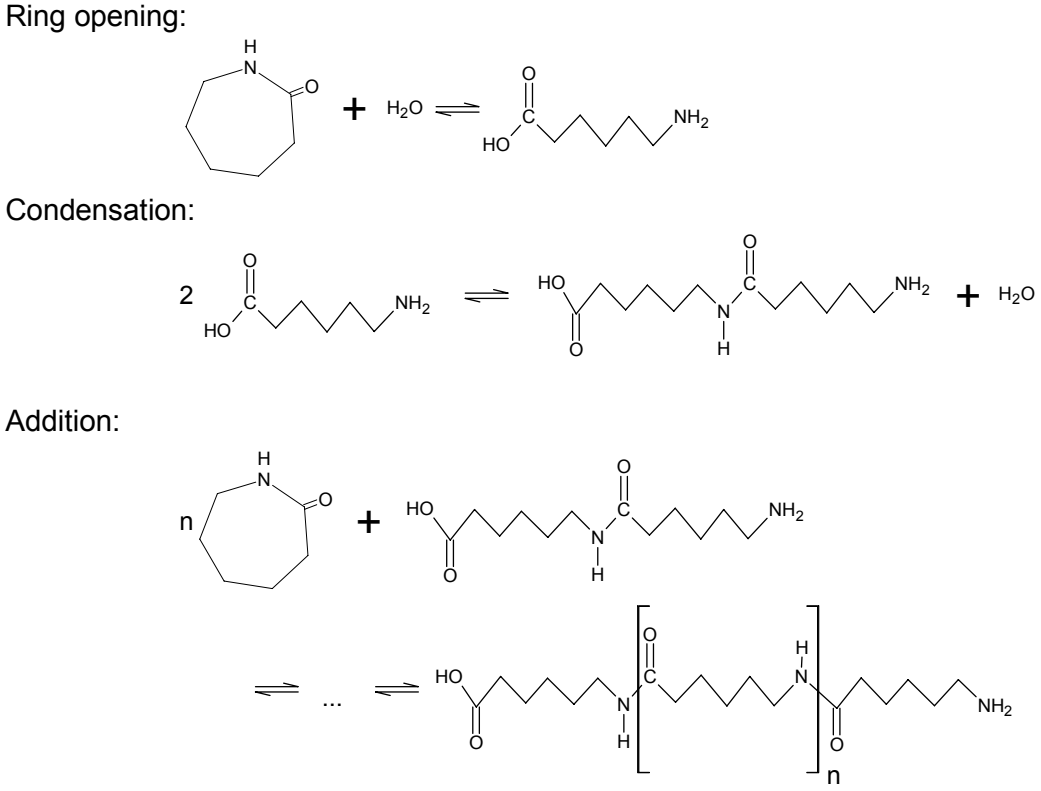

Fig. 3.4: Hydrolytic polymerization of PA-6.

3.3 Processing of polyamide-6

Together with PA-6,6, PA-6 is the most widely applied polyamide. The most common way of producing PA-6 (composite) parts is through melt processing of hydrolytic polymerized caprolactam. The alternative method of reactive processing via anionic polymerization of caprolactam, however, forms the focus of the current thesis. Both methods are briefly discussed next.

3.3.1 Melt processing of hydrolytic PA-6

Hydrolytic polymerization of caprolactam (Figure 3.4) is performed together with a small amount of water at around 270°C for 10 to 20 hours, after which the polymer is

purified at 100°C by water. Alternatively, purification can be performed by vacuum treatment at elevated temperatures (290°C) while being subjected to high shear forces in extruder-like equipment [146].

3.3.2 Reactive processing of anionic PA-6

Anionic polymerization of caprolactam is performed at 130-170°C and is completed within 3 to 60 minutes, depending on the reaction temperature and the catalyst formulation [44]. Since polymerization of the water-like caprolactam melt takes place below the polymer melting and crystallization point (T_c=185°C [146]), solid highly crystalline PA-6 is formed, which makes anionic polymerization perfectly suitable for manufacturing parts directly from the monomer via casting [65], reaction injection molding (RIM [70]) and rotational molding [66].
Due to the integration of the polymerization and part forming steps, the purification step has to be omitted. As a consequence, a small amount of monomer and catalyst traces stay behind in the final part. Due to the fact that after polymerization the material is not subjected to melt processing, the molecular weight of reactively processed PA-6 parts is significantly higher than of melt processed parts [149]. In the next paragraph, anionic ring-opening polymerization of caprolactam is discussed in more detail.

3.3.3 Anionic Ring-Opening Polymerization of Caprolactam

As the name already suggests, the anionic polymerization of caprolactam is initiated by negatively charged particles or anions, which open the ring-shaped caprolactam molecules and subsequently connect them into high molecular weight polymer chains [46, 47], see Figure 3.5. Commonly, caprolactam anions are used, which cause the caprolactam ring to open after which both particles connect to form an acyllactam. Subsequent deprotonation of a second caprolactam monomer regenerates the anion. These steps are repeated until all monomer is consumed and a high molecular weight polymer chain is obtained.

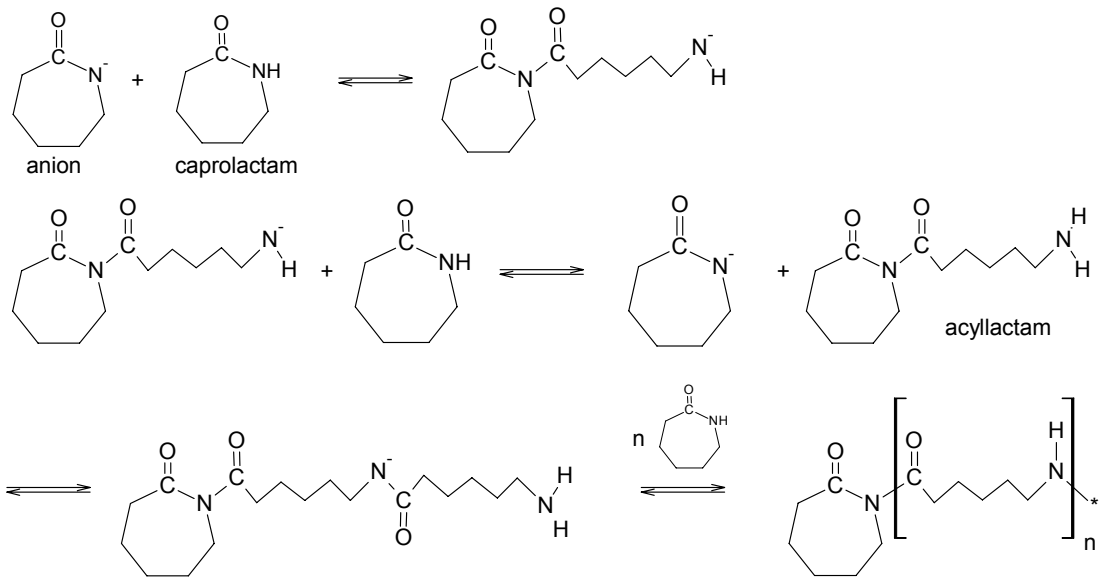

Fig. 3.5: Anionic ring-opening polymerization of caprolactam.

The reaction between caprolactam and the anion involves a high activation energy. As a consequence, the reaction has to be performed at temperatures in excess of 250°C [150], and even than the reaction rate is slow. The subsequent reaction of the acyllactam and the anion, however, involves a low activation energy and, therefore, it is common practice to already add acyllactams (or carbamoyllactams, see Figure 4.1) before the start of the reaction to bring down the required reaction temperature to 130-180°C. In this case, opening of the acyllactam rings by the anionic initiator forms the first step of the polymerization reaction, after which chain growth and continuous regeneration of the anions occur as is shown in Figure 3.5.

In addition to mono-functional activators also di- and multi-functional species are used to tailor the final polymer properties by controlling not only the molecular weight but also the degree of branching [45, 87]. In addition to using a multi-functional activator, branching can also be caused by side-reactions such as Claisen condensation [46]. Other side reactions include termination, oligomer formation [151, 152] and chain scission [86]. The occurrence of side reactions increases at higher activator content and higher reaction temperatures, and commonly takes place when monomer depletion at the end of the reaction makes interaction with the abundance of polymer chains more likely.

Whereas during melt processing it is sufficient to obtain a high degree of crystallinity in order to get a polymer with desirable properties for structural application, the additional requirement for reactive processing is to obtain a high degree of conversion. Unreacted caprolactam reduces the chain interactions in the amorphous phase of PA-6 in a similar way as water molecules do, consequently decreasing the strength and modulus of the polymer [150]. In order to obtain the required polymer properties, it is essential to balance the rate of polymerization and crystallization, which will be discussed in more detail in Chapters 5 and 6. It will be shown that balancing not only involves the mould temperature, but also the resin formulation, the part geometry and the amount and type of fiber reinforcement.
Although desirable, 100 wt% conversion of caprolactam into PA-6 cannot be achieved due to the existence of a monomer-polymer or ring-chain equilibrium. This temperature dependent equilibrium results in a certain amount of monomer always to be present in the polymer bulk, which can vary with temperature as long as reactive species (such as anions) remain active. At low temperatures the equilibrium shifts to the polymer side, which enables PA-6 to be used for structural applications. On the other hand, the shift towards the monomer side at elevated temperatures makes recycling of PA-6 back into its monomer possible [43].

3.4 Processing of fiber reinforced PA-6 composites

This paragraph gives a brief overview of processing of PA-6 composites with short, woven or continuous fiber reinforcement. Similar as in the previous paragraphs a distinction is made between melt and reactive processing.

3.4.1 Melt processing of PA-6 composites

Although the melting point of PA-6 is only 223ºC [146], for composite processing it is often necessary to increase the temperature to 270-280ºC in order to reduce the viscosity of the polymer melt sufficiently for the forming process. Because it is impossible to impregnate the fibers and form the composite part in a single processing step when using polymer granules in combination with the fiber reinforcement, intermediate materials like extruded films, co-mingled fabrics and consolidated

laminate sheet material are commonly used, see Figure 1.6. The complete manufacturing process for melt processing of polyamide-6 composites is schematically shown in Figure 3.6. The following melt processes have found worldwide application:

- Injection molding of PA-6 with randomly orientated short fibers [153].
- Compression molding of glass matt thermoplastic materials (GMTs [154]) with longer fibers and less random orientation.
- Fabric reinforced PA-6 by rubber forming [18], see Figure 1.7.
- Pultrusion of profiles with unidirectional continuous fibers [155].

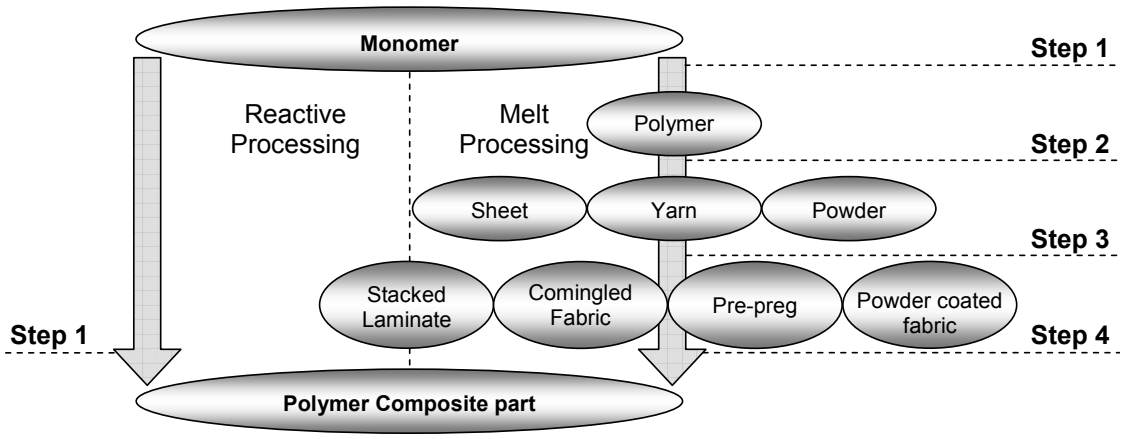

Fig. 3.6: Manufacturing steps from monomer to polymer composite part: melt vs. reactive processing.

3.4.2 Reactive processing of PA-6 composites

During reactive processing the fibers are impregnated with the reactive mixture, which subsequently polymerizes around the fibers. For the preparation of the caprolactam mixture commonly two heated tanks are used for melting and mixing a monomer-initiator and a monomer-activator solution. In both tanks a nitrogen protective environment prevents deactivation and oxidation of the reactive species.

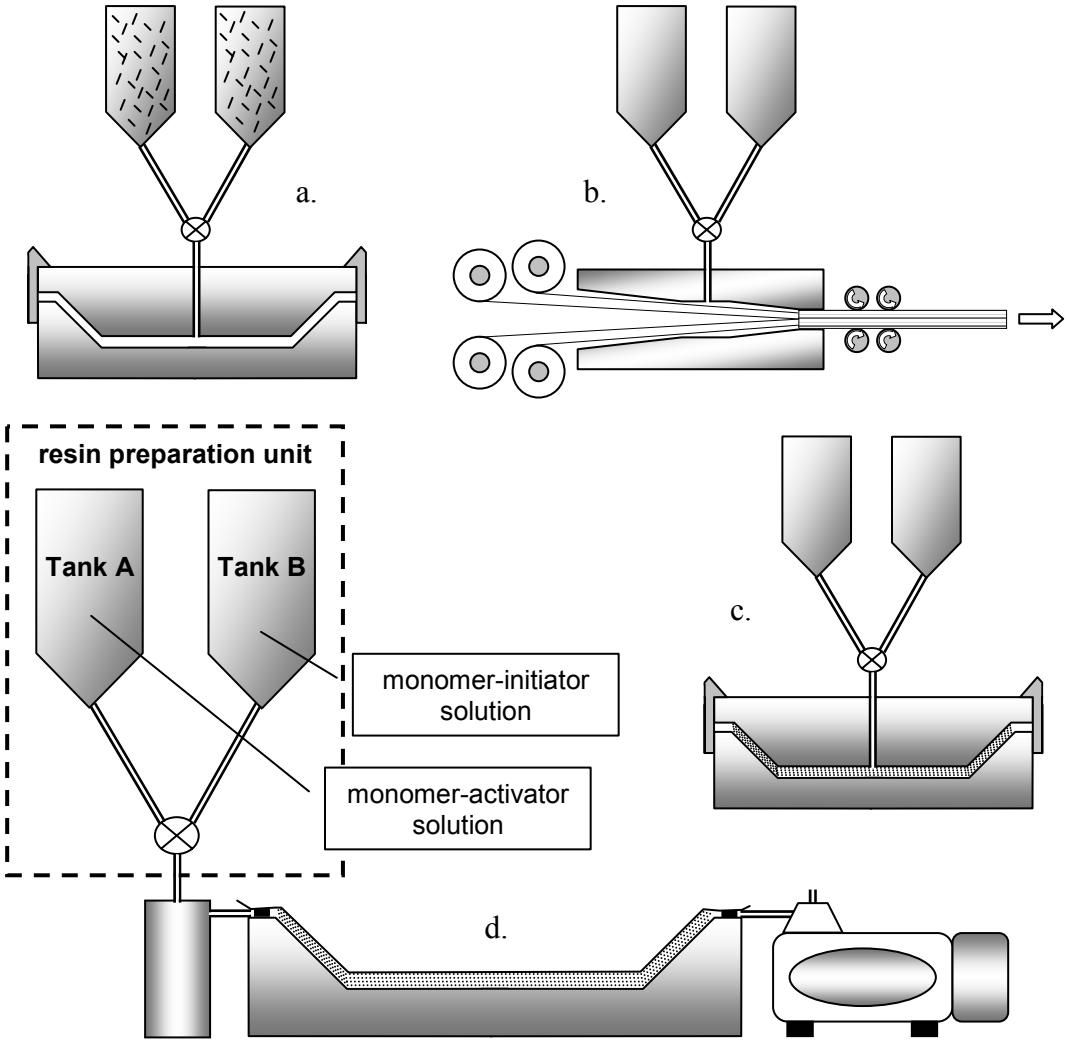

Fig. 3.7: Schematic representations of reactive processes for manufacturing of polyamide-6 composites: a. RRIM, b. reactive pultrusion, c. SRIM, and d. vacuum infusion.

The following reactive processes for manufacturing of PA-6 composites are presented in Figure 3.7:

- Reinforced reaction injection molding (RRIM): short fibers or particles are mixed with the caprolactam mixture before being injected into the mould. This way a medium size composite is obtained with a low content of a randomly distributed reinforcement [73, 74].

- Structural reaction injection molding (SRIM): the monomer mixture is infused under high pressure into a mould with pre-placed fiber swirl mat. The process results in small to medium size composites with a high reinforcement content with a random orientation [75-77].
- Vacuum infusion: the monomer mixture is infused by applying vacuum to a mould with pre-placed fabric reinforcement (woven or unidirectional). The process results in medium to large composites with a large amount of strongly orientated continuous fibers.
- Reactive pultrusion: the reinforcing fibers are impregnated by the monomer in a resin bath before being pulled through a die. The process is ideally suitable for manufacturing of profiles with a continuous cross-section and a high loading of fully oriented fibers [78, 79].

Whereas RRIM forms the mainstay of reactive processing of PA-6 composites, SRIM and reactive pultrusion are relatively new, as is vacuum infusion, of which the development is discussed in the present thesis.

The following benefits of reactive processing for manufacturing of composites are identified. The required temperatures for reactive processing are approximately 100-150°C lower than for melt processing, see Table 2.3. Due the low viscosity of the monomer melt (η = 10 mPa·s [85]), fiber impregnation requires relatively low pressures, which reduces the costs of equipment and tooling. Moreover, Figure 3.5 shows that manufacturing of composites directly from the caprolactam monomer significantly reduces the number of (cost adding) processing steps.

3.5 Conclusions

- Polyamides are semi-crystalline engineering plastics with excellent thermal and mechanical properties.
- The processing temperature has a large influence on the crystal morphology of the polymer.
- Due to the hydrophilic nature of the characteristic amide groups, polyamides are prone to water absorption, which reduces the glass transition temperature and the mechanical properties.

- Through melt processing parts can be manufactured from purified PA-6, which is hydrolytically polymerized. Melt processing of PA-6 composites often requires (cost adding) intermediate materials.
- With reactive processing, parts can be directly manufactured from the caprolactam monomer through anionic polymerization, which requires an activator and an initiator.
- Always some unreacted monomer is present in anionically polymerized parts, which is caused by the temperature dependent polymer-monomer equilibrium and the fact that purification after reactive processing is not possible.
- Anionic polymerization results in high molecular weight PA-6.
- Vacuum infusion will form a valuable addition to the currently existing reactive processes for PA-6 composites such as RRIM, SRIM and reactive pultrusion.

CHAPTER 4

DEVELOPMENT OF VACUUM INFUSION EQUIPMENT FOR MANUFACTURING OF ANIONIC POLYAMIDE-6 COMPOSITES

4.1 Introduction

This chapter discusses the manufacturing equipment and the various moulds that were used throughout the research. A proto-type setup is described first, which was directly derived from the traditional vacuum infusion process using thermoset resins, see Section 1.6. Initial manufacturing tests revealed that vacuum infusion of thermoplastic composites involves more than a 1-on-1 substitution of a thermoset resin by the anionic polyamide-6 casting resin. It will be made clear that both the infusion setup and the anionic polyamide-6 resin itself require modification, and that it is of paramount importance to use a chemically compatible fiber reinforcement. Whereas modifications to the resin material are discussed in Chapter 5 and the effect of the addition of fibers in Chapter 8, alterations to the infusion equipment are discussed in the remainder of this chapter.

4.2 Proto-type infusion equipment: the adapted thermoset infusion process

After a brief description of the initial infusion experiments, the process is evaluated and development of more dedicated processing equipment is discussed next.

4.2.1 Material and process description

In the first infusion tests, a commercial grade anionic polyamide-6 (APA-6) casting resin was used. In addition to caprolactam (DSM Fiber Intermediates, The

Netherlands), the formulation contained 0.6 mol% activator (hexamethylene-1,6-dicarbamoylcaprolactam, HDCL, 2 mol/kg concentration in caprolactam, "Brüggolen C20", Brüggemann Chemical, Germany) and 0.6 mol% initiator (sodium caprolactamate, NaCL, 1.4 mol/kg concentration in caprolactam, "Brüggolen C10", Brüggemann Chemical, Germany). The chemical structure of each material, as well as the polymerization scheme is presented in Figure 4.1. Calculation of the resin formulation is treated in Appendix I.

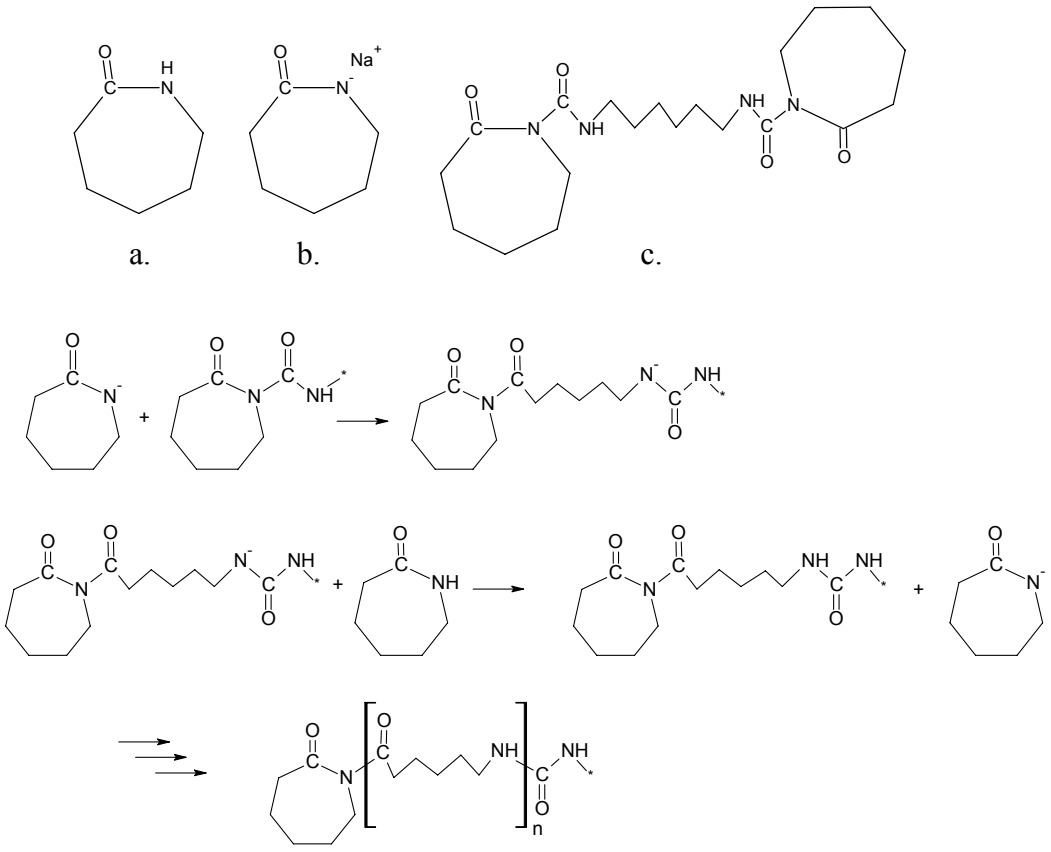

Fig. 4.1: Anionic polymerization of ε-caprolactam (a) into polyamide-6, using sodium caprolactamate as initiator (b) and hexamethylene-1,6-dicarbamoylcaprolactam as activator (c).

For the initial tests, the traditional infusion process for thermoset composites described in Chapter 1 was adapted for infusing APA-6. First, suitable processing consumables (vacuum foils, resin tubes, etc.) were selected: (i) they need to be

resistant to the high processing temperature of APA-6 (T_{max}=200ºC), (ii) upon contact they should not terminate or negatively influence the anionic polymerization of caprolactam, and (iii) they should not dissolve in the highly alkaline caprolactam melt. Initially, an acid-free silicon paste was applied as sealant for bagging the fibers using a polyimide film (Upilex®, UBE, Japan) and silicon rubber tubes (Rubber b.v., The Netherlands), see Figure 4.2. Later on, the silicon paste, which took long to cure, was replaced by a temperature resistant tacky tape (SM-5142, Schnee-Morehead, USA). Table 4.1 shows all the consumables that were tested.

8-harness satin weave E-glass fabrics (SS 0303 050 000, 300 gram/m^2) were kindly supplied by Ten Cate Advanced Composites (Nijverdal, The Netherlands). The bagged fibers (15 x 20 cm, 8 layers) were put in a convection oven at 150ºC, which was placed in a fume hood, see Figure 4.2. Whereas thermoset resins can be mixed in atmospheric conditions, the reactivity of the caprolactamate initiator decreases rapidly upon contact with moisture and oxygen from the air. To prevent this, the activator and initiator solutions in caprolactam were made separately in two closed test tubes (heated at 110ºC in an oil bath) with protective nitrogen atmosphere. Prior to infusion, the contents of both test tubes were mixed in a heated 3-neck flask, also with nitrogen environment. A silicon tube connected the 3-neck flask with the bagged fibers through a hole in the oven. Through the same hole, the outlet tube was connected to a membrane pump.

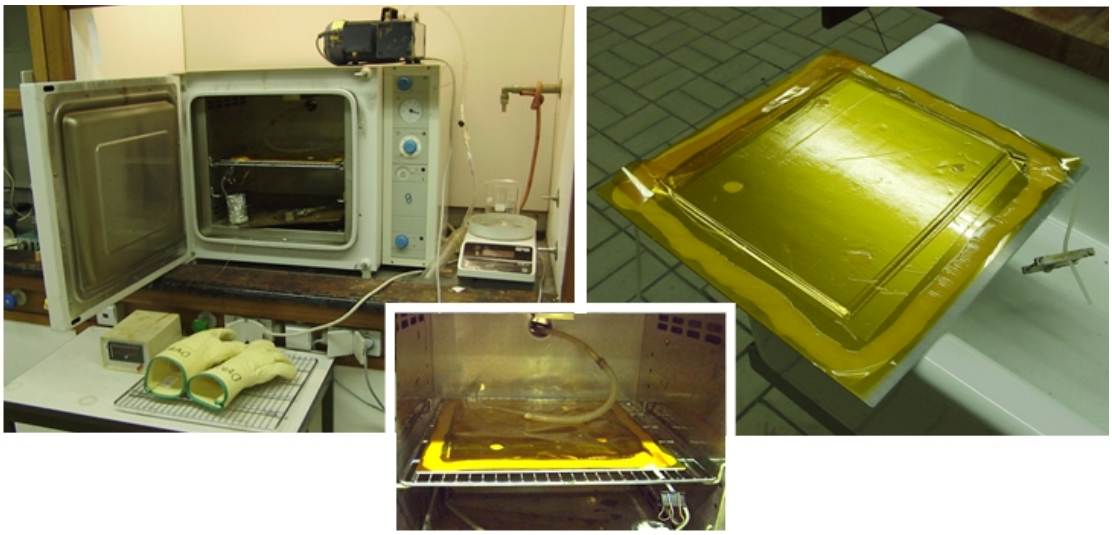

Fig. 4.2: Left and center: proto-type equipment, right: bagged fibers.

Table 4.1: Overview of tested processing consumables.

Consumable	Manufacturer/Supplier	Comment
Resin tubes		
Polyvinylchloride (PVC)	Rubber b.v., The Netherlands	Plasticizes at high temperatures and inhibits polymerization
Silicon rubber	Rubber b.v., The Netherlands	Compatible
Vacuum films		
Polyamide-6 (Capran® 980)	Honeywell, USA	Dissolves in caprolactam
Polyamide-6 (Capran® 988)	Honeywell, USA	Dissolves in caprolactam
Aluminum foil	-	Too brittle for bagging purposes
Polyetherimide (PEI, Ultem® 1000)	GE Plastics, The Netherlands	Dissolves in caprolactam
Polyphenylenesulphide (PPS, Fortron® 0214)	Ticona, Germany	Too brittle for bagging purposes
Polyimide (Upilex®-R)	UBE, Japan	Compatible
Fluorinatedethylenepropylene (FEP, A-4000)	Airtech, USA	Too vulnerable for bagging purposes
Halohydrocarbon polymer release film (E-3760)	Richmond Aircraft Products, USA	Dissolves in caprolactam
Halar ECTFE Fluoropolymer release film	Aerovac Systems Ltd., UK	Dissolves in caprolactam
Sealants		
Silicon sealant (acid free)	Bison International, The Netherlands	Compatible but takes long to cure
Terostat-81 sealant tape	Teroson, Germany	Plasticizes at high temperatures
SM-5142 sealant tape	Schnee-Morehead Inc., USA	Compatible
SM-5127 sealant tape	Schnee-Morehead Inc., USA	Not tacky at room temperature
GS43MR sealant tape	General Sealant Inc., USA	Compatible
Tape		
Flashtape 2 (silicon)	Aerovac Systems Ltd., UK	Compatible
Kapton tape (5413)	3M, USA	Compatible
Peelply		
Polyamide (Stitch Ply A)	Airtech, USA	Compatible but APA-6 is too tough to be peeled off
Flow meshes		
Polyethylene (N-1024)	Newbury, UK	Inhibits polymerization
Polyethylene (OM-70)	Diatex, France	Inhibits polymerization
Polypropylene (Breatherflow-60)	Airtech, USA	Softens above 170ºC

Despite the water-like viscosity, the infusion (220 mbar) through the dense fibers was slow and as a consequence, the residence time of the resin in the unheated tube between the 3-neck flask and the oven was long. The temperature of the mixture soon dropped below the melting point of caprolactam (T_m = 69ºC) and upon solidification the resin flow stopped. To overcome this problem, the entire inlet tube was placed inside the oven together with a beaker (without protective atmosphere), which replaced the 3-neck flask.

Temperature monitoring with a thermocouple inside the laminate showed that during infusion the heated fibers (150ºC) were cooled down by the reactive mixture (110ºC). The oven was not powerful enough to increase the temperature back to150ºC before polymerization initiated. As a consequence, the polymerization temperature was too low and an APA-6 matrix was obtained with a cheese-like texture as is explained in more detail in Chapter 6. Although raising the temperature of the oven and the resin components prior to infusion improved the texture of the matrix, the reaction rate increased at the same time, which prevented full impregnation of the fibers, see Figure 4.3. Reducing the infusion pressure to 10 mbar increased the infusion speed, but resulted in a 'void-rich' composite due to boiling of the caprolactam monomer, see Figure 4.4 and Section 6.5.1.

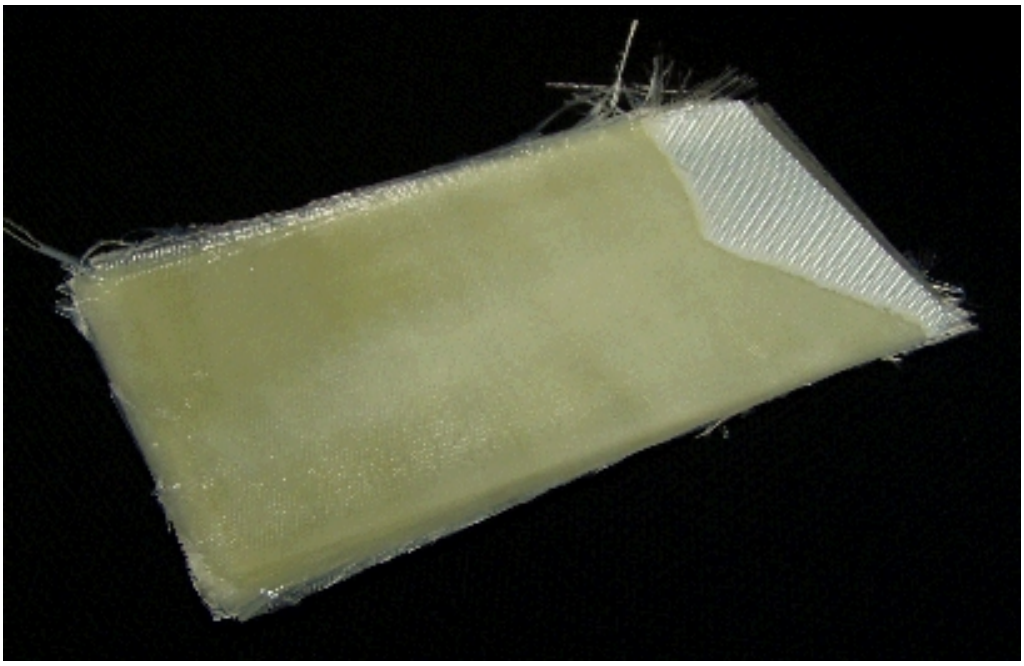

Fig. 4.3: Partially infused APA-6 composite.

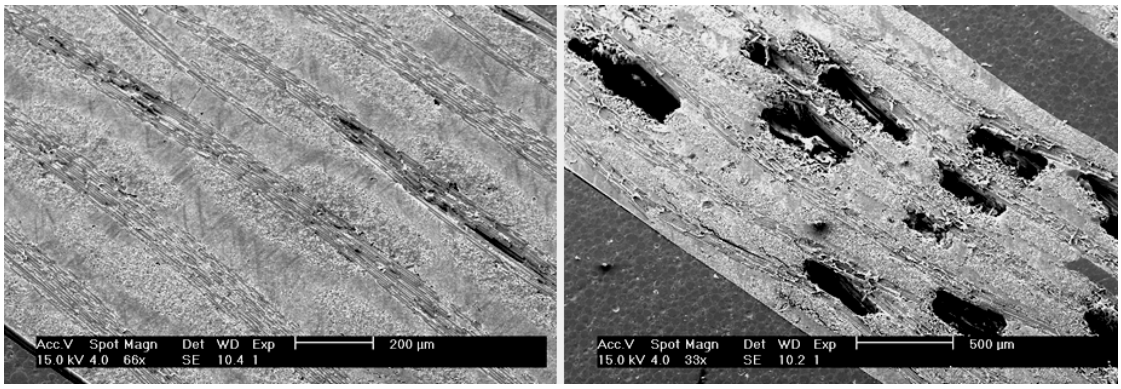

Fig. 4.4: 'Void-free' composite infused at 200 mbar (left) and a 'void-rich' composite infused at 10 mbar (right).

A final remark is made regarding the chemical compatibility of the fiber reinforcement and the APA-6 resin. Glass fibers are usually coated with a sizing, which protects against abrasive and corrosive damage, enhances further composite processing and improves the fiber-to-matrix bond due to so-called coupling agents. Coupling agents are di-functional molecules, which are capable of bonding with the fiber surface with one of their reactive groups, whereas the second group can interact with the polymer matrix either reactive or due to a good polymer matrix compatibility e.g. via hydrogen bonding. Such interaction should lead to bond formation with the matrix without (in the case of reactive processing) negatively influencing the polymerization reaction. At the start of this project, glass fabrics with an APA-6 compatible coupling agent were not known and therefore a variety of coupling agents was tested. Proof-of-concept for vacuum infused APA-6 composites was the primary goal of this assessment, which basically means that a coupling agent had to be found that causes no visible disturbance of the polymerization and that the actual formation of a fiber-to-matrix bond was not verified. The results of this assessment are presented in Table 4.2. The concept was finally proven using glass fabrics with an aminosilane coupling agent, see Figure 8.1. A detailed discussion on fiber-matrix interactions, including bond formation, is provided in Chapter 8 and Chapter 9.

Table 4.2: The compatibility of various coupling agents.

Coupling agent	Commercial name	Test result
Aminosilane	A1100, DS AMEO	No visible disturbance of the polymerization
Chromium(III)methacrylate	Volan A03	Inhibits polymerization
Epoxy	-	Brown coloration in flow direction
Ureidosilane	DS 2201	No visible disturbance of the polymerization

4.2.2 Material and process evaluation

The conclusions of the initial infusion tests form the basis for the development of more dedicated infusion equipment for processing of APA-6 composites and also the incentive for research described in the remaining chapters. The recommendations are split up into material related and equipment related issues.

Materials:

- Anionic polymerization of caprolactam with HDCL activator and NaCL initiator is a fast curing formulation, which is suitable for rapid processes like casting [65] and reaction injection molding (RIM) [70]. Vacuum infusion is a process with a long mould filling time, which requires a resin with a much lower reaction rate. Development of anionic polyamide-6 resin formulations specifically designed for vacuum infusion of composites is discussed in Chapter 5, whereas the resulting polymer properties are discussed in Chapter 6.
- It was found out that some of the fiber sizings terminated the anionic polymerization of caprolactam. In order to obtain a composite for structural applications, not only termination of the reaction has to be prevented, also a strong fiber-to-matrix interphase has to be obtained. The interaction between the fibers and the anionic polymerization of caprolactam is discussed in more detail in Chapters 8 and 9.

Equipment:

- Mixing of the small amounts of reactive components by hand for only a single infusion reduces both accuracy and reproducibility. Batch processing is expected to improve results and ease of operation significantly. In order to prevent

degradation of the prepared material batch it is necessary to introduce a nitrogen protective atmosphere, which was not possible with the small beaker used.

- Degassing the mixture prior to infusion, which is common practice for processing of thermoset resins, is impossible with the current setup. Degassing is expected to reduce the void contents of both the neat polymer and the composites. An accurate pressure control system for degassing and infusion without causing the resin to boil is therefore required.
- The convection oven is not powerful enough to heat up the infused fibers in a controlled manner. Also the need to open the door to add resin in the beaker and to start the infusion causes strong temperature fluctuations. A more powerful and accurate heating system is required and cold spots in the set-up need to be avoided to prevent solidification of caprolactam.

4.3 Dedicated infusion equipment

The equipment described in this section was used throughout the research and development was supported by Bronk Industrial b.v. (Waalre, The Netherlands) and DSM Fiber Intermediates (Geleen, The Netherlands).

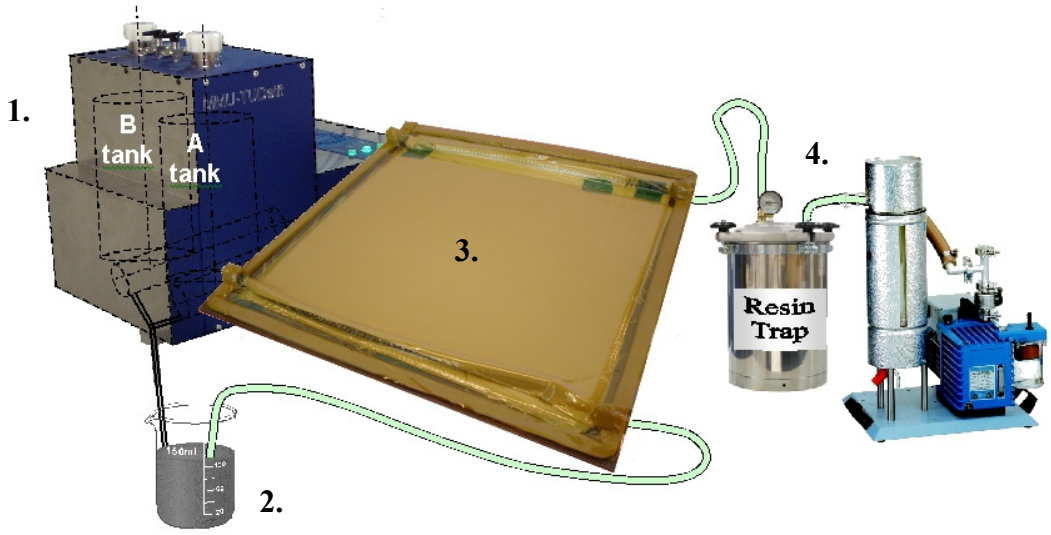

Fig. 4.5: Processing schematics: (1) mixing/dispensing machine, (2) resin buffer, (3) mould and heating system, and (4) pressure control system.

4.3.1. Processing equipment

The infusion setup basically consist of a mixing/dispensing machine for the APA-6 resin components, a resin buffer, a mould heating system and a pressure control system, see Figure 4.5.

Mixing/dispensing machine

For the preparation of material batches, and subsequent mixing and dispensing of the resin, a Mini Mixing Unit (MMU) was purchased from Bronk Industrial b.v. (Waalre, The Netherlands), see Figure 4.6 and 4.7.

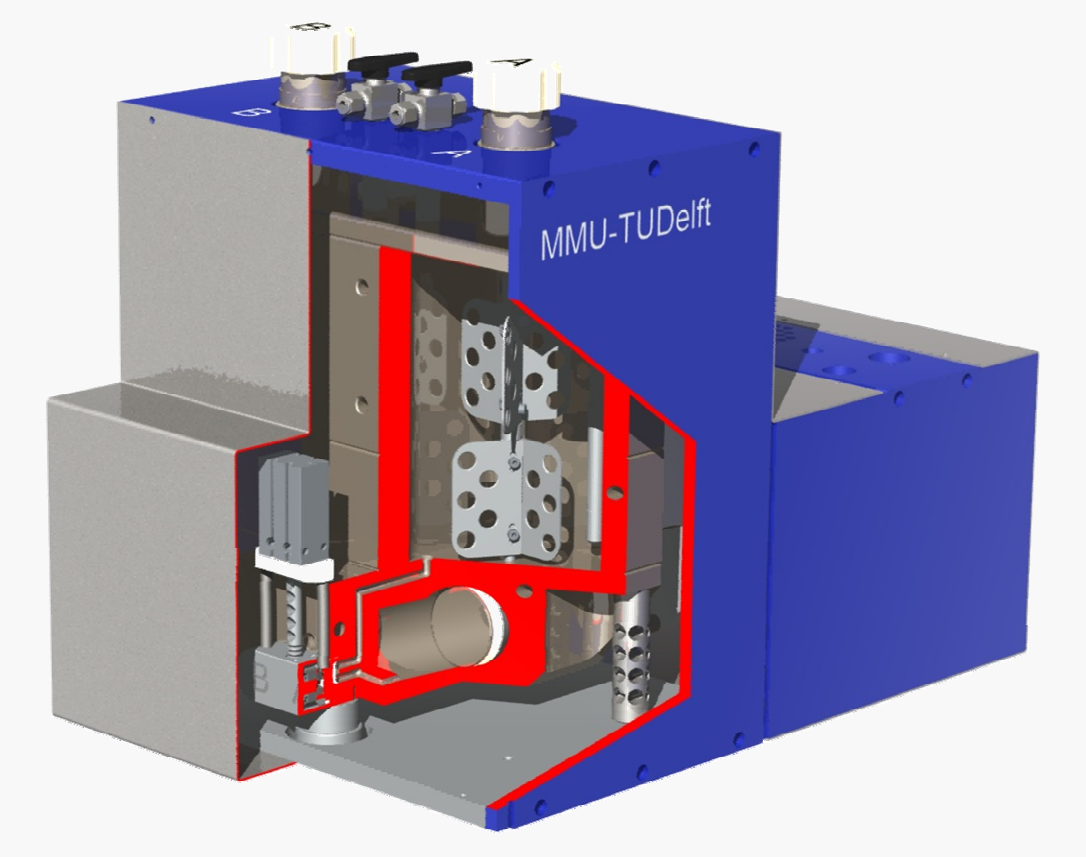

Fig. 4.6: Cross-sectional view of the Mini Mixing Unit (MMU-TUDelft).

The "MMU-TUDelft" features, see Figure 4.7:

- A modular anodized aluminum structure with Viton® rubber seals that can withstand the alkaline nature of the caprolactam melt up to high temperatures.

- Two 2.2 liter tanks for preparation of an activator-caprolactam and an initiator-caprolactam solution (1). The contents in each tank can be heated up to 200ºC and mixed by a pneumatic stirrer (2).
- 3-way valves are mounted on each tank to degas the contents and to apply a nitrogen protective cover (3).
- Two piston pumps to dispense the two material feeds with an accuracy of ± 1 gram at a maximum pressure of 8 bar (4). The shot volume is variable between 50 and 650 cm^3 and although the dispensing ratio of the two pistons is variable, only a ratio of 1:1 was used throughout the research. A pneumatic valve system (5) either dispenses the material flows or recirculates them back into the tanks in order to further homogenize the material feeds
- An impingement mixing head or heated static mixer for external mixing of the two material flows after dispensing can be attached to the dispensing nozzle at the bottom of the machine (6).
- An external control unit with touch screen to control mixing, recirculation and dispensing.

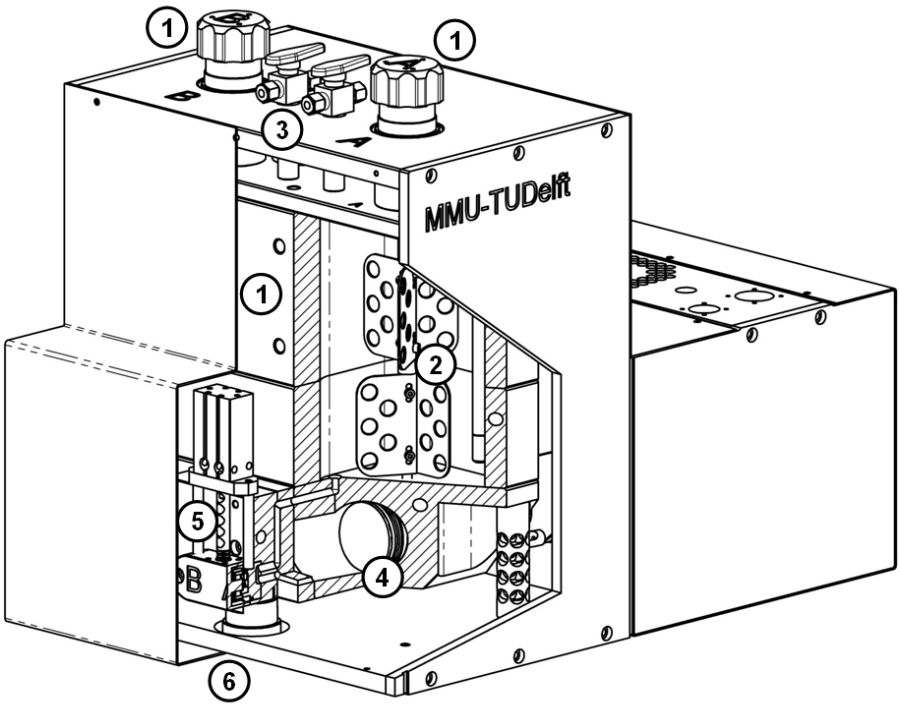

Fig. 4.7: Features of the Mini Mixing Unit (MMU-TUDelft).

Resin buffer

Because the MMU dispenses resin at an overpressure, whereas mould filling requires underpressure, it is necessary to separate the MMU from the mould by a resin buffer, see Figure 4.8. The buffer consists of a reusable 400 ml glass beaker equipped with a custom-made Teflon cover and nitrogen connection, which was placed in a heated oil bath at 110ºC. This temperature was selected since it is high enough to prevent solidification of caprolactam, while still being low enough to prevent polymerization to initiate. A silicon tube at ambient temperature connected the reservoir to the static mixer of the MMU, whereas a heated silicon tube (110ºC) made the connection with the mould. In a later stage of the research, the glass beaker was replaced by a Woulff bottle in an electrically heated aluminum fixture, to allow for additional degassing of the reactive mixture after dispensing, see Figure 4.8.

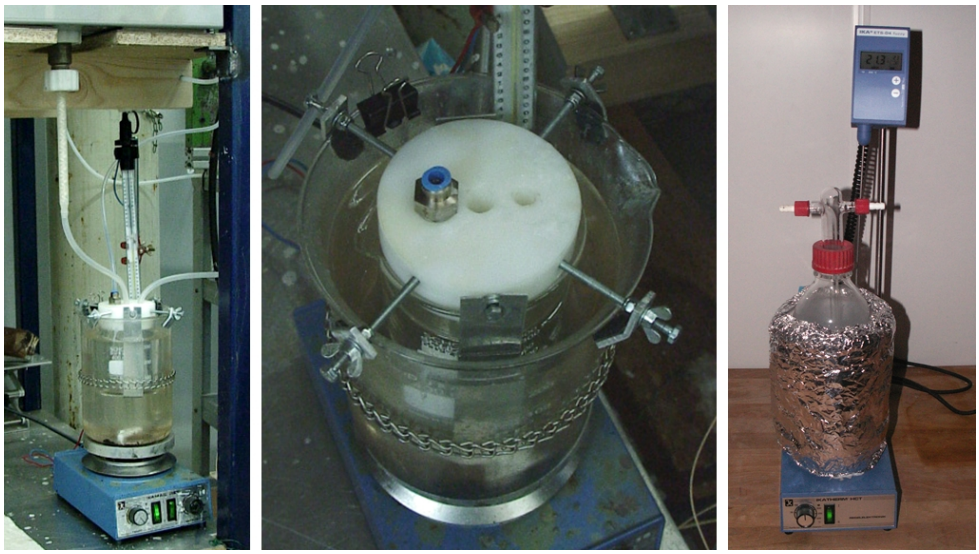

Fig. 4.8: Resin buffers. Left and center: oil-heated glass beaker, right: electrically-heated Woulff bottle.

Pressure system

Two vacuum pumps were used for degassing the tanks of the MMU and for infusing the moulds. Liquid caprolactam and caprolactam vapor was prevented to enter the pumps by using both a resin trap and a cold trap. Both pumps were equipped with a control system to accurately measure and set the pressure.

Heating system

A pneumatic press with two flat steel plates was used to clamp various moulds, see Figure 4.9. Each steel plate was equipped with six evenly distributed heating elements (Watlow Firerod, 230V, 1 kW) for fast heating in an accurate and homogenous manner. The press was vertically placed for bottom-to-top infusion of the moulds, which allows entrapped air and other gaseous substances to exit the moulds against the gravity.

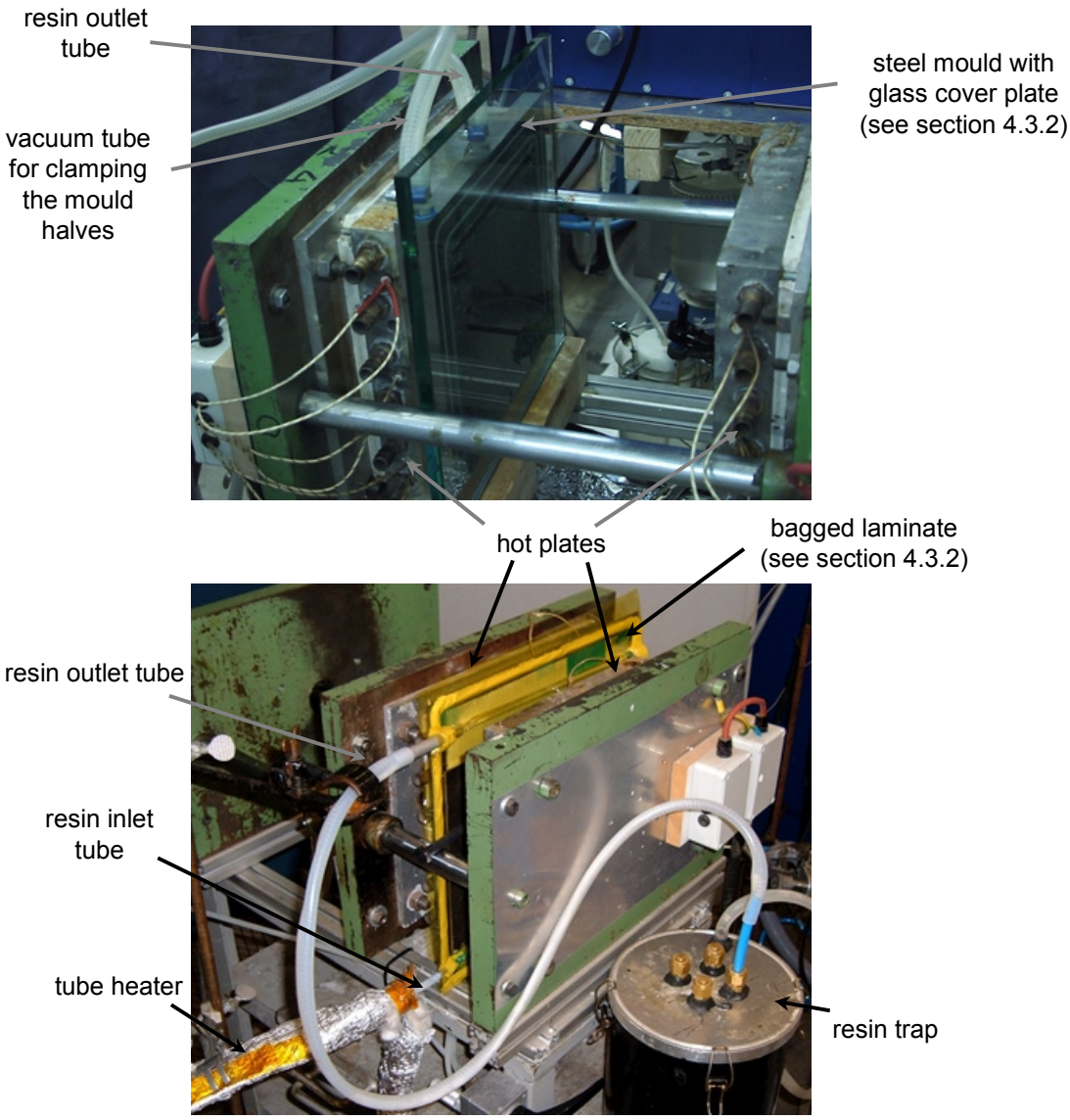

Fig. 4.9: Vertically placed hot press, which was used for heating the various moulds. Top: heated mould for infusing neat APA-6 panels, bottom: heated fiber lay-up.

4.3.2 Mould systems

Various moulds were designed for manufacturing and analysis purposes of both the neat resin and composites.

Neat resin infusion mould

To infuse neat polymer panels, a mould with a 2 mm thick square cavity (20 x 15 cm) and flat cover plate was used, see Figure 4.10. Steel was used instead of aluminum to prevent scratching of the surface during demolding and cleaning. A double O-ring sealing allowed clamping of the mould by applying vacuum. To maintain control over the pressure in the cavity during polymerization, it has to be prevented that resin enters the outlet tube, where it cools down and solidifies, hence cutting of the mould cavity from the pumps. To prevent resin to enter the outlet tube, a buffer cavity was machined in the mould near the outlet to slow down the infusion, hence giving ample time to stop the resin flow before it is able to exit the mould. For every infusion pressure, the infusion time to reach the buffer cavity was determined visually by replacing the steel cover plate by a hardened glass one (see Figure 4.9 on the top). The initial design proved demolding to be difficult and in the redesign the position of the inlet and outlet channels were changed and given a conical shape. Also, the size of the cavity was increased (45x34 cm) and the thickness could be set to either 2 or 10 mm, depending on the type of cover plate used.

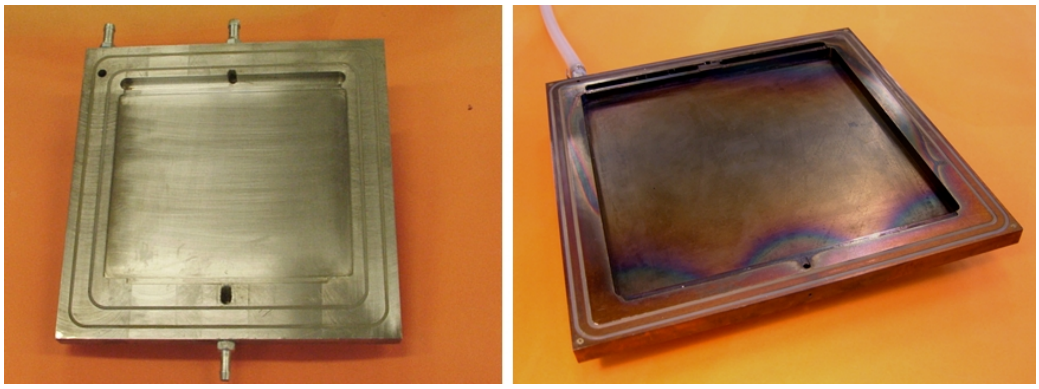

Fig. 4.10: Infusion moulds for neat APA-6 panels. Left: original design, right: improved design for easier demolding.

Composite infusion mould

Fibers were vacuum bagged using the same consumables as described in Section 4.2.1. In order to achieve a line infusion rather than a point infusion, the inlet and outlet tubes were connected to metal springs, which were placed inside the mould alongside the positioned fibers, see Figure 4.11. To prevent crushing of the springs by the pneumatic press, care was taken to position the springs outside the area of the flat steel plates. Although the figure shows that a highly permeable glass fabric is used to connect the metal springs with the fiber lay-up, in a later stage of the research this connection was made by simply extending one of the glass layers of the actual lay-up. Note that glass fabric had to be used as the available flow meshes were not compatible with the APA-6 resin, see Table 4.1. A second reason for separating the springs from the lay-up is to prevent that resin is drawn out of the infused fibers due to shrinkage of the resin in the metal spring near the outlet. To maintain control over both the infusion rate and the fiber compaction with the vacuum pumps, spacers were used to prevent full closure of the mould, which would otherwise lead to maximum compaction, see Figure 4.12. For the sake of heat transfer, the flat plates were allowed to just touch the bagged fibers. Figure 4.9 shows the bagged fiber lay-up between the heated plates.

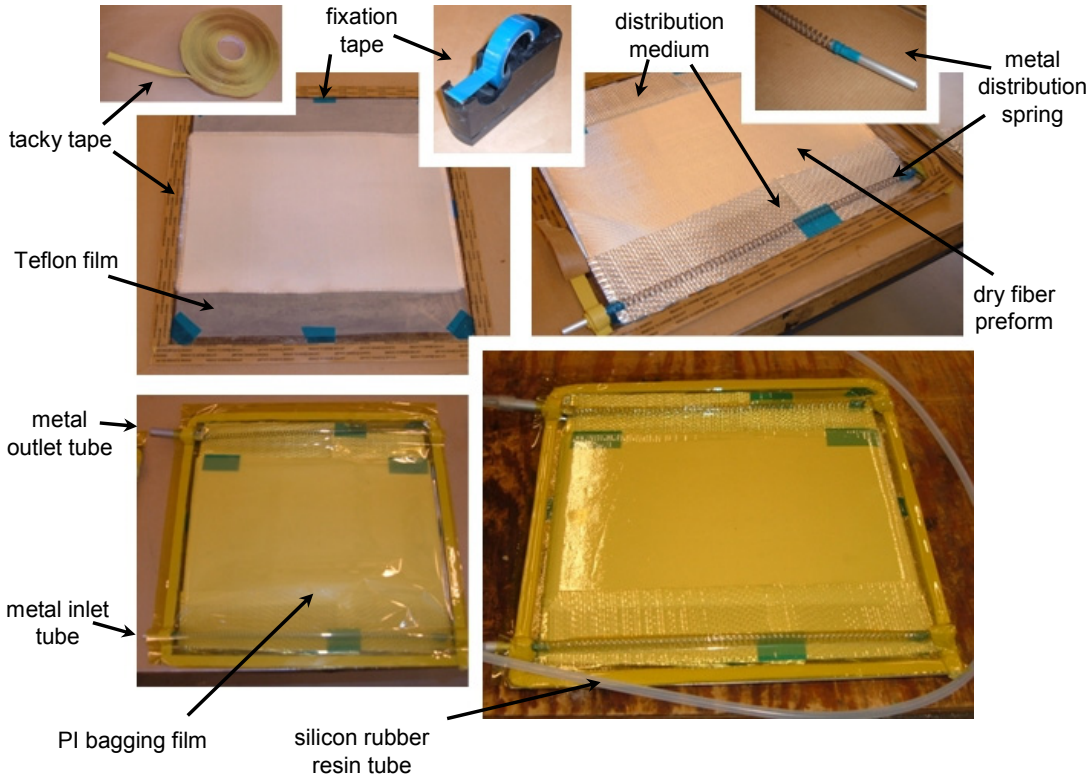

Fig. 4.11: Fiber bagging procedure for vacuum infusion of APA-6 composites.

Visco-measure mould

To measure the viscosity increase during the reaction, a casting mould consisting of two aluminum halves was used with a 500 cm^3 cavity, thermal isolating lid and nitrogen connection, see Figure 4.13. A Bohlin rotating viscosity meter was used to measure the viscosity of the polymerizing mixture in the mould cavity through a hole in the lid. The housing of the meter, which contains all the electronic parts, was cooled by a continuous flow of compressed air.

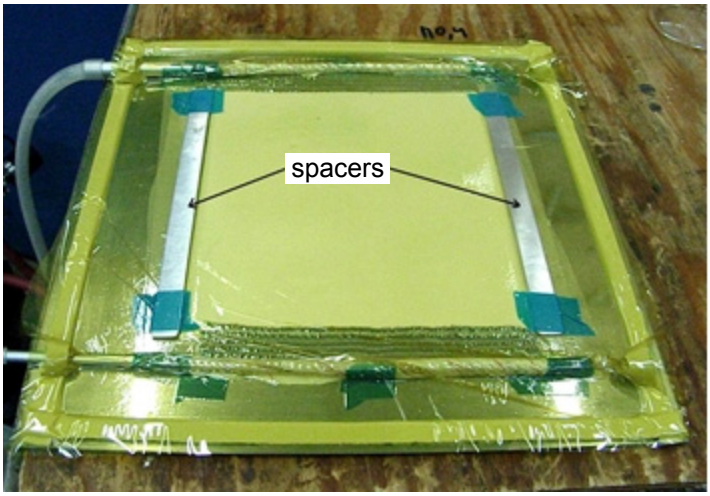

Fig. 4.12: Bagged fiber lay-up with spacers.

Fig. 4.13: The visco-meter mould with the Bohlin rotating viscosity meter.

4.4 Conclusions

- Initial manufacturing tests revealed that vacuum infusion of thermoplastic composites involves more than a 1-on-1 substitution of a thermoset resin by the anionic polyamide-6 casting resin: both the infusion setup and the anionic polyamide-6 resin itself require modification.
- Dedicated infusion equipment for manufacturing of APA-6 composites consisting of the MMU mixing/dispensing machine for the APA-6 resin components, a resin buffer, a mould heating system and a pressure control system were described.

- The various moulds used throughout the research were discussed and an overview was given of suitable processing consumables like vacuum foils, sealants and resin tubes.
- It was shown that it is of paramount importance to use glass fibers with a compatible sizing.

CHAPTER 5

ANIONIC POLYMERIZATION OF CAPROLACTAM: CONTROLLING THE REACTION RATE

5.1 Introduction

The initial infusion experiments described in Section 4.2 revealed that the current reaction rate of the anionic polyamide-6 (APA-6) casting resin is too high and therefore severely limits the size of the composite parts that can be infused. This chapter describes the available tools to influence the reaction rate and their side effects on the polymer properties. First, the role of the activator and the initiator in each individual step of the reaction (dissociation, complex formation and polymerization) is discussed followed by the effect of the temperature. The rate of polymerization is not constant but increases in time due to so-called temperature-induced and crystallization-induced autocatalytic effects. It is argued that due to the simultaneous occurrence of polymerization and crystallization it is not feasible to control the reaction rate during the polymerization step in an attempt to match the envisaged infusion process as this has a too large effect on the final polymer properties. Instead, it is demonstrated that clever selection of an activator-initiator combination results in an APA-6 resin with a long initiation time, which is perfectly suitable for vacuum infusion of composites.

5.2 Experimental

5.2.1 Materials

Anionic polymerization grade caprolactam (CL, AP-Caprolactam) was used in this study as it has a low moisture content (<100 ppm). The monomer was stored at 50 °C under dry atmospheric conditions to keep it dry without causing the monomer flakes

to fuse together due to sublimation and recrystallization. Two types of activators were used in this study, as shown in Figure 5.1. The first is monofunctional N-acetylcaprolactam (N-ACL, 100%, "Activator0") and the second is difunctional hexamethylene-1,6-dicarbamoylcaprolactam (HDCL, 2 mol/kg concentration in caprolactam, "Brüggolen C20"). The former was stored as liquid in glass jars, whereas the latter was stored as granules in sealed polyethylene lined aluminum drums. As initiator, both sodium caprolactamate (NaCL, 1 mol/kg concentration in caprolactam, "Brüggolen C10") and caprolactam magnesium bromide (MgBrCL, 1.4 mol/kg concentration in caprolactam, "Brüggolen C1") were used in this study, see Figure 5.1. Both were stored as flakes in sealed polyethylene lined aluminum drums. All reactants were kindly supplied by Brüggemann Chemical, Germany. Calculation of the resin formulation is treated in Appendix I.

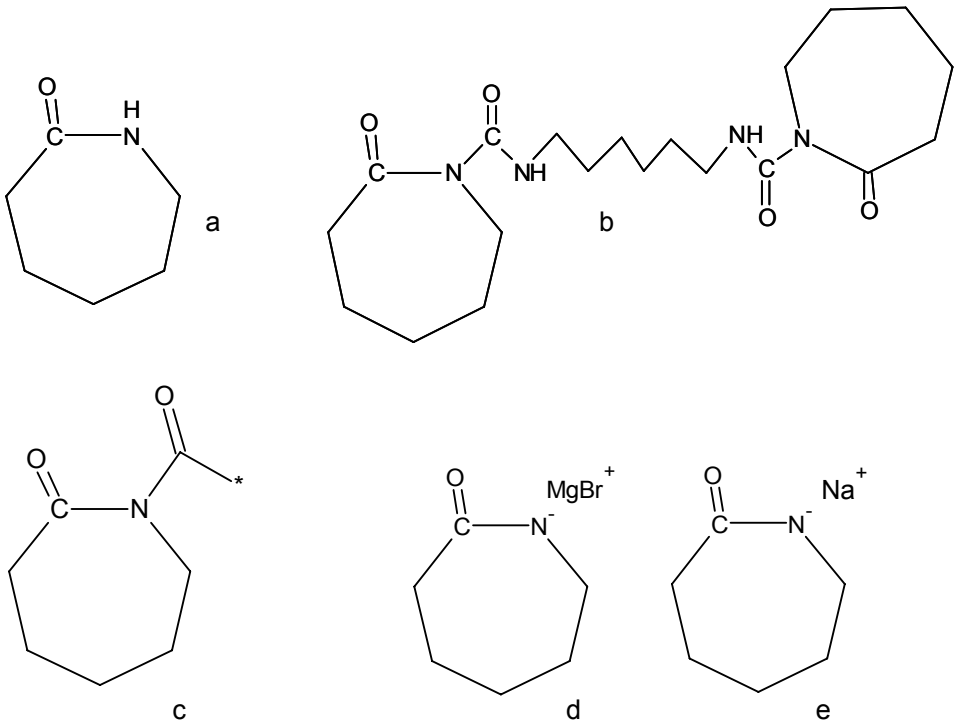

Fig. 5.1: Chemical structure of (a) caprolactam, (b) hexamethylene-1,6-dicarbamoylcaprolactam, (c) N-acetylcaprolactam, (d) caprolactam magnesium bromide, and (e) sodium caprolactamate.

5.2.2 Processing methods

A special designed lab-scale mixing unit (Mini Mixing Unit "MMU-TU Delft", Bronk Industrial b.v., The Netherlands) was used to prepare two liquid material formulations at 110°C under a nitrogen atmosphere: a monomer/activator-solution in tank A and a monomer/initiator-solution in tank B, see Section 4.3.1. After degassing (15 minutes at 100 mbar), the two material feeds were mixed in a heated static mixer (110°C, 1:1 ratio) and dispensed into heated test tubes that were used as casting mould. Rubber stoppers were used to prevent uptake of moisture and oxygen from the air.

5.2.3 Analysis methods

Degree of conversion (DOC)

The degree of conversion (DOC) of cast APA-6 samples was determined for various polymerization temperatures using test tubes as casting moulds. Polymerized samples were chopped into thin flakes (t < 0.5 mm), weighed (m_{tot}) and refluxed overnight in demineralized water. After drying, samples were weighed again (m_{pol}). Whereas the monomer caprolactam dissolves easily in water, the polyamide-6 does not and the degree of conversion was determined according to Equation 5.1. To obtain conversion-time relations, polymerization was terminated at various stages by quenching the sample containing test tubes in ice water.

$$DOC = \frac{m_{pol}}{m_{tot}} \cdot 100\% \tag{5.1}$$

It has to be noted that together with the residual monomer water-soluble low molecular weight PA-6 oligomers are also washed out of the sample [151]. Although, as a consequence, the abovementioned method cannot be used to calculate the exact degree of conversion, it can determine the fraction of the polymer with load carrying capabilities, which is in fact more useful in the present research.

Differential Scanning Calorimetry (DSC)

A Perkin Elmer Differential Scanning Calorimeter (DSC-7) was used to measure the degree of crystallinity (X_c) and melting point (T_m) of the various samples of

approximately 5 mg, which were dried overnight at 50°C in a vacuum oven. During testing, each sample was first held for 2 minutes at 25°C before being heated to 230°C at 10°C/min. Finally, X_c was calculated and corrected for the degree of conversion (DOC) according to Equation 5.2.

$$X_c = \frac{\Delta H_m}{\Delta H_{100}} \cdot \frac{1}{DOC/100} 100\% \qquad (5.2)$$

in which ΔH_{100} is the melting enthalpy of fully crystalline PA-6: ΔH_{100} = 190 J/g [56].

Wide Angle X-Ray Scattering (WAXS)

In situ wide angle X-ray scattering (WAXS) measurements were taken in a Bruker D8 Discover diffractometer with a 2D (1024x1024) detector using a 10 cm sample-to-detector distance and incident Cu radiation of 1.54 Å. The beam cross-section used was of 0.5 mm. A capillary was filled with a reactive mixture and placed inside a special cell holder consisting of a carbon tube containing a hole allowing for the passage of the x-ray beam. The carbon tube was heated with an external power supply coupled to a thermo-couple allowing for temperature control. The temperature of the setup was raised from ambient to 150ºC in less than a minute. Sequential acquisition of scattering frames was launched immediately after the capillary achieved 150ºC and a series of scattering spectra was recorded, each taking 120 seconds to complete.

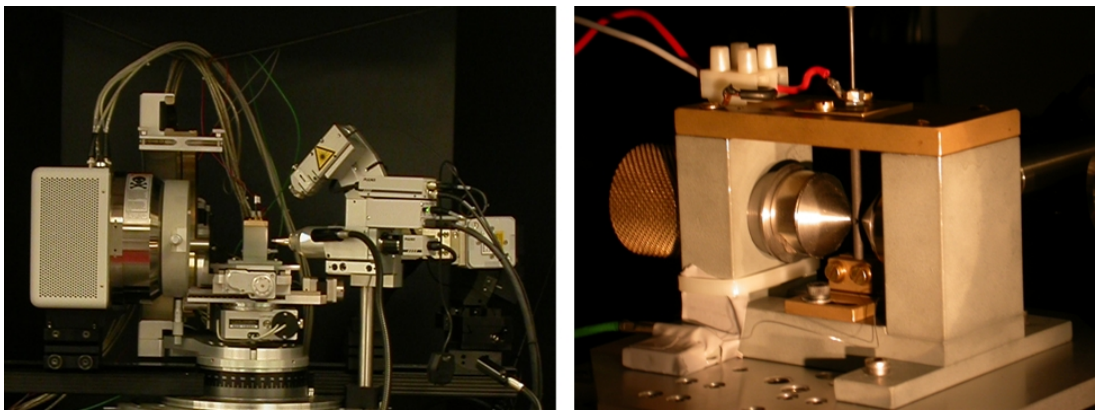

Fig. 5.2: Bruker D8 Discover diffractometer (left) and the carbon cell holder (right).

A typical 2D WAXS spectrum of fully crystalline APA-6, polymerized at 150ºC, is presented in Figure 5.3. The spectrum clearly shows two rings, which are associated with α-phase crystals [146]: α_1: 2θ = 20 (200 crystal plane) and α_1: 2θ = 24.5 (020 crystal plane). The black spot in the center of the spectrum is caused by the beam stop, which protect the detector from direct radiation.

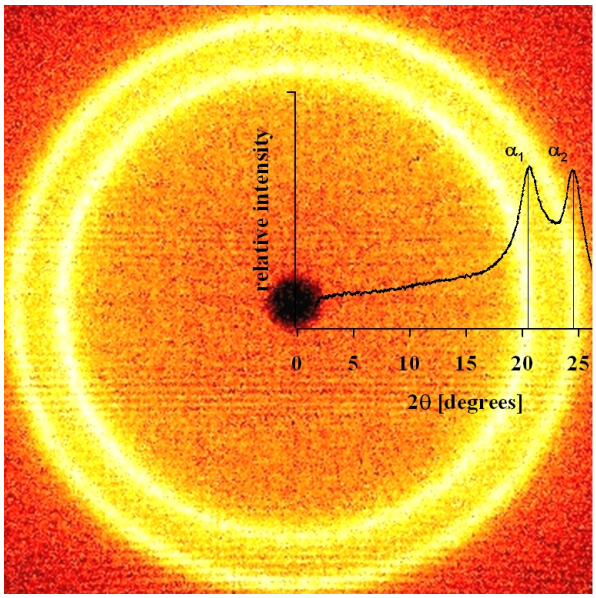

Fig. 5.3: Typical WAXS spectrum of APA-6 polymerized at 150ºC.

5.3 The effect of initiator and activator on the reaction rate

This section breaks down the curing reaction of APA-6 into its elementary steps: (i) dissociation, (ii) complex formation and (iii) polymerization. For each step the effect of the type of activator, the type of initiator, and the added amount of these reactive species is discussed.

5.3.1 Dissociation of the initiator

The first reaction step is the generation of anions (negatively charged species) by dissociation of the initiator, which is commonly a metal caprolactamate, see Figure

5.4. The degree of dissociation is determined by the dissociation parameter K_d. The rate of dissociation, and therefore the activity of the initiator, decreases with increasing size of the cation due to a decreasing ionization potential and restricted mobility [150]. Table 5.1 lists the dissociation constant (K_d) for various metal caprolactamates in caprolactam, with a higher K_d resulting in a higher rate of dissociation and consequently a lower processing-related pot life.

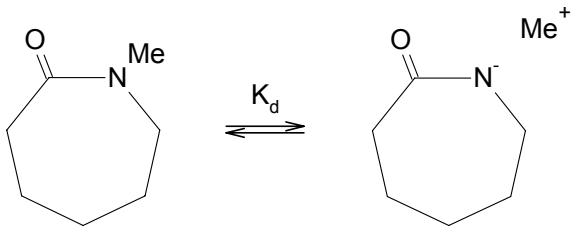

Fig. 5.4: Generation of anions due to dissociation of a metal caprolactamate initiator.

Table 5.1: Dissociation constants for various initiators [156].

Initiator	Dissociation constant [mole/l] at 150°C
Magnesiumbromide caprolactamate	$5.5 \cdot 10^{-3}$
Sodium caprolactamate	$6.7 \cdot 10^{-5}$
Potassium caprolactamate	$8.5 \cdot 10^{-5}$
Calcium di-caprolactamate	$7.9 \cdot 10^{-7}$
Magnesium di-caprolactamate	$1.0 \cdot 10^{-7}$
Aluminum tri-caprolactamate	$<10^{-7}$

5.3.2 Complex formation between the activator and the metal cation of the initiator

After dissociation, it is possible that the reactive end-group of the activator forms a complex with the metal cation (positively charged species) of the initiator. Upon complex formation, the metal cations are removed from the dissociation equilibrium shown in Figure 5.4, which makes generation of additional caprolactam anions possible. Therefore, complex formation increases the reaction rate. Whether or not a complex can be formed and the rate at which anions are generated due to complex

formation depends on both the geometry and the electric forces of the activator and the metal cation of the initiator [59, 63].

Figure 5.5 shows the conversion in time for four activator-initiator combinations (with respect to caprolactam: 0.6 mol% activator and 0.6mol% initiator) processed at 150ºC. Table 5.2 shows whether or not a complex is formed. It can be seen that for the two combinations that lead to complex formation, (N-ACL – MgBrCL) and (HDCL – NaCL), the reaction and the conversion increase exponentially in time. In case no complex is formed between the activator and the cation of the initiator, (N-ACL – NaCL), the reaction is slower and the conversion increase is more linear in time. In the case of the hexamethylene-1,6-dicarbamoylcaprolactam (HDCL) activator in combination with the MgBrCL initiator initially no complex is formed, which explains the slow linear conversion increase at the beginning of the reaction. However, after a single monomer addition, the carbamoylcaprolactam group is replaced by an acetylcaprolactam group, see Figure 5.6. Since this newly formed group is able to form a complex with the initiator, the reaction rate increases after 18 minutes.

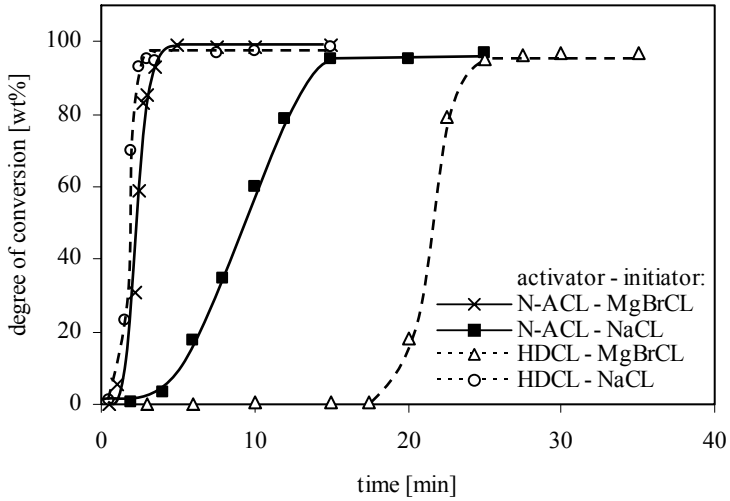

Fig. 5.5: Conversion-time relations for four activator-initiator combinations (0.6 mol% activator, 0.6mol% initiator) polymerized at an initial mould temperature of 150ºC.

Table 5.2: Ability of four activator-initiator combinations to form a complex [150, 157, 158].

		Activator	
Initiator		**N-acetylcaprolactam N-ACL**	**Hexamethylene-1,6-dicarbamoylcaprolactam HDCL**
Sodium caprolactamate	**NaCL**	No complex	Complex
Caprolactam magnesiumbromide	**MgBrCL**	Complex	Initially no complex

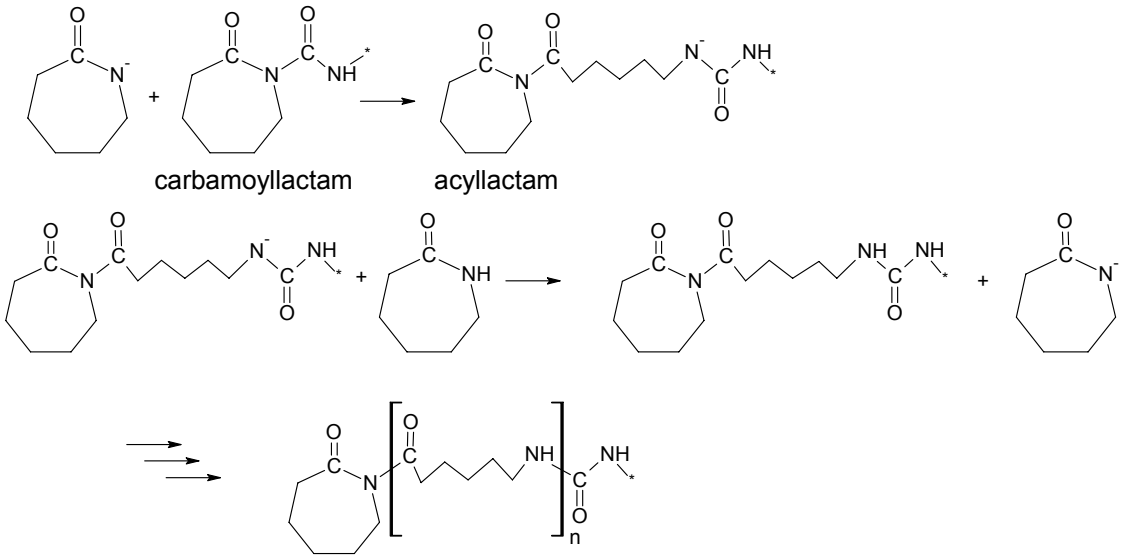

Fig. 5.6: Anionic polymerization of polyamide-6, using caprolactam magnesium bromide as initiator and hexamethylene-1,6-dicarbamoylcaprolactam as activator.

5.3.3 Polymerization of polyamide-6 through the anions

After dissociation and complex formation the polymer chains start growing rapidly in the subsequent polymerization step, see Figure 5.6. After every monomer addition, an anion is regenerated, which causes the polymerization to continue until all caprolactam is consumed to equilibrium. When increasing the concentration of the

initiator, more anions are set free and more complexes can be formed, and as a consequence, the monomer is consumed more rapidly, see Figure 5.7. Increasing the amount of activator increases the amount of initiation points for chain growth. As a consequence, the required time to consume all monomer up to the equilibrium conversion level decreases, see Figure 5.7, whereas the average molecular weight (Mw) will go down [46, 47, 61, 159]. The latter is accompanied by a decrease in toughness and (when adding extreme concentrations) in a reduction in both melting point (T_m) and glass transition temperature (T_g) [32].

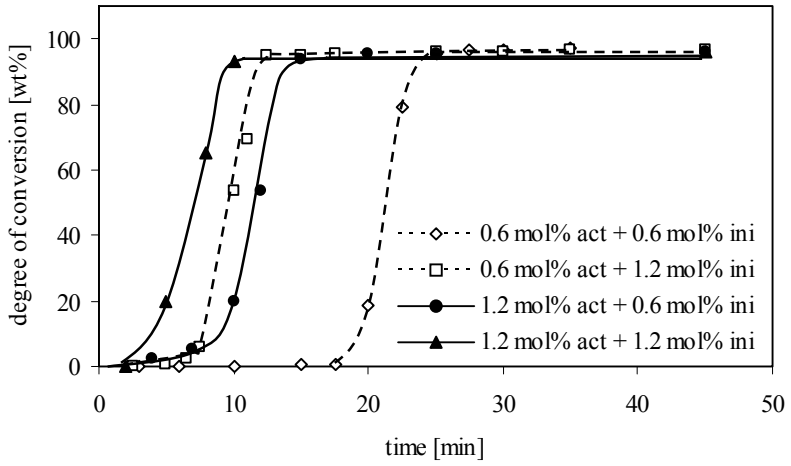

Fig. 5.7: Effect of the amount of activator (HDCL) and initiator (MgBrCL) on the reaction rate. (T_{mould} = 150°C).

An additional effect of adding more initiator is that the final degree of conversion is reduced as is shown in Figure 5.8. This is caused by the fact that with every initiator molecule a cation is introduced (see Figure 5.4), of which the positive charge needs to be compensated for by a caprolactam anion throughout the reaction. Therefore, to compensate for these cations not all caprolactam polymerizes, which limits the maximum obtainable degree of conversion. As a result, a conversion of 100 wt% is not achievable. Based on the weight of the caprolactam part of the initiator that is added to the resin a theoretical maximum conversion can be derived as is shown in Figure 5.8. Increasing the activator concentration also increases the amount of low molecular weight oligomers in the final polymer [151]. Being water soluble, these oligomers reduce the degree of conversion as measured by the previously described

method. Figure 5.8 indeed shows that at equal initiator concentration, the experimentally determined conversion reduces with increasing activator concentration.

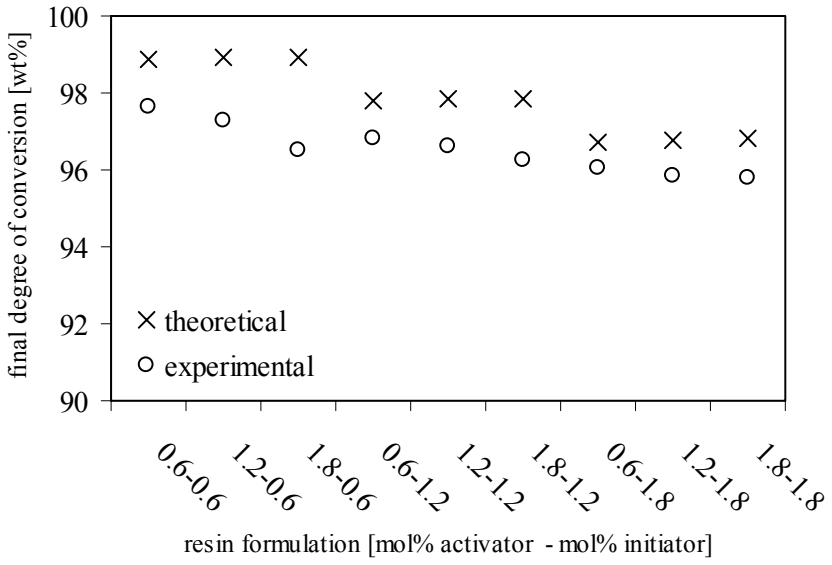

Fig. 5.8: Final degree of conversion for various concentrations of activator (HDCL) and initiator (MgBrCL), polymerized at a starting temperature of 140ºC.

5.4 The effect of the temperature on the reaction rate

The polymerization of caprolactam is not isothermal and due to its exothermic nature (ΔH_{pol} = -144 J/g [55]) the encountered temperature rise during polymerization is significant as can be seen in Figure 5.9. As a consequence, it is impractical to use the temperature during polymerization as a controllable research parameter and instead the initial temperature of the mould is used as such. The results obtained at different mould temperatures can be compared with each other as long as the same mould is used throughout the experiments. Caprolactam that is polymerized in a different mould (mould material, cavity size, etc.) will be exposed to a different thermal history, even if the initial mould temperature is the same. Such a variation not only has an effect on the rate of polymerization but also on the polymer properties as is explained in Chapter 6.

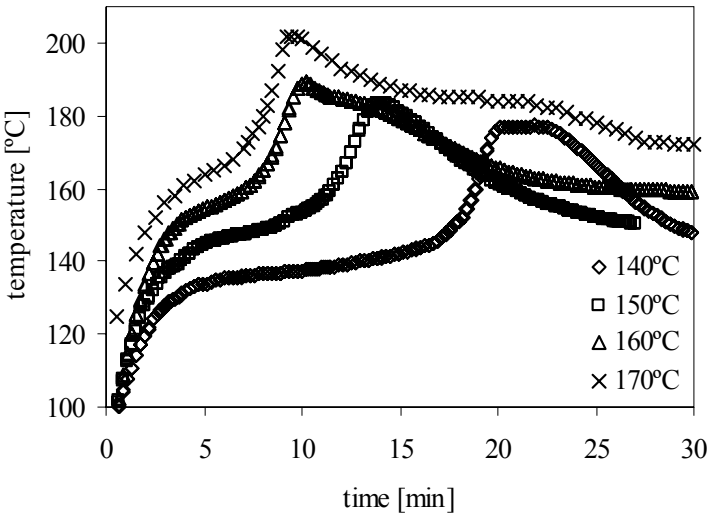

Fig. 5.9: Temperature progression during casting for various initial mould temperatures measured by inserting a thermocouple in the center of the test tubes.

In general, a higher initial mould temperature increases the reaction rate, see Figure 5.10, which is caused by the higher thermal motion of the molecules and the fact that the dissociation constants of the metal caprolactamates, and hence their activity, increase with increasing temperature [160].

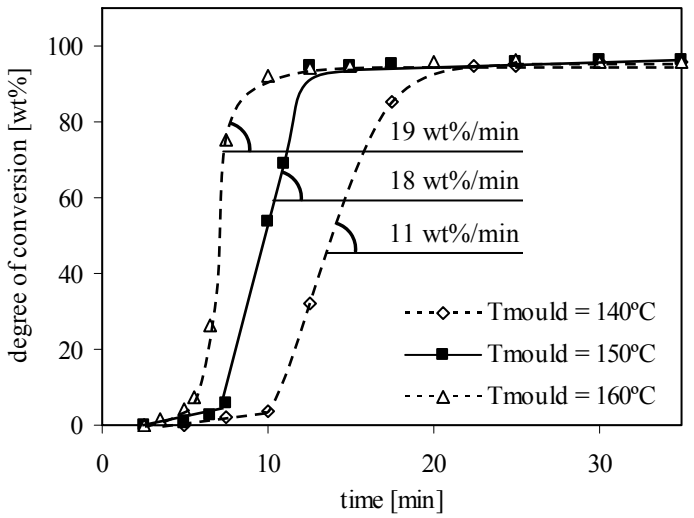

Fig. 5.10: Effect of the starting temperature on the conversion (1.2mol% HDCL – 0.6mol% MgBrCL). The reaction rate [wt%/min] can be determined from the slope of the graphs.

5.5 The autocatalytic nature of the polymerization

The polymerization rate (or rate of conversion) is not constant as can be seen in Figure 5.10. After a slow start, the polymerization rate keeps increasing until the rising viscosity and monomer depletion near the end of the reaction slow it down again. The self-accelerating or autocatalytic effect at the start of the polymerization step is related to the exothermic nature of the polymerization and the simultaneous occurrence of crystallization, which is explained next.

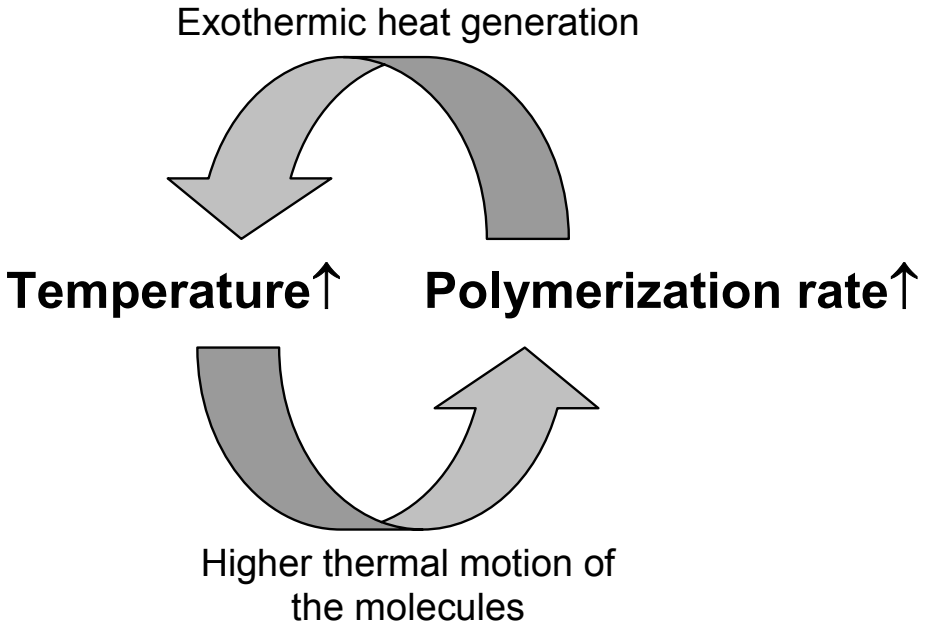

Fig. 5.11: The exothermic autocatalytic effect.

5.5.1 The exothermic autocatalytic effect

The exothermic autocatalytic effect is best described by the loop in Figure 5.11: a rise in temperature initiates polymerization, which due to its exothermic nature further increases the temperature, which again causes a further increase in the rate of polymerization, etc. The relation between the exothermic nature and the self-accelerating behavior of the polymerization has already been extensively described in

literature and various kinetic models have been derived [55, 57-59, 61, 63]. None of these models, however, takes the complex relation of polymerization, crystallization and the processing temperature into account, see Section 5.5.2, and although the existing kinetic equations can be used to fit the conversion data presented in this thesis, they are of little practical use as the derived fitting parameters are no longer valid when a different mould is used or when for instance fibers are added to the reactive mixture. Although the development of an accurate kinetic model is beneficial for further development of APA-6 technology, it is impossible with the existing analysis methods to simultaneously measure the conversion, crystallinity and temperature. Development of a curing model for APA-6 is consequently regarded as out-of-scope of the current thesis, but it is emphasized to address this matter in future research.

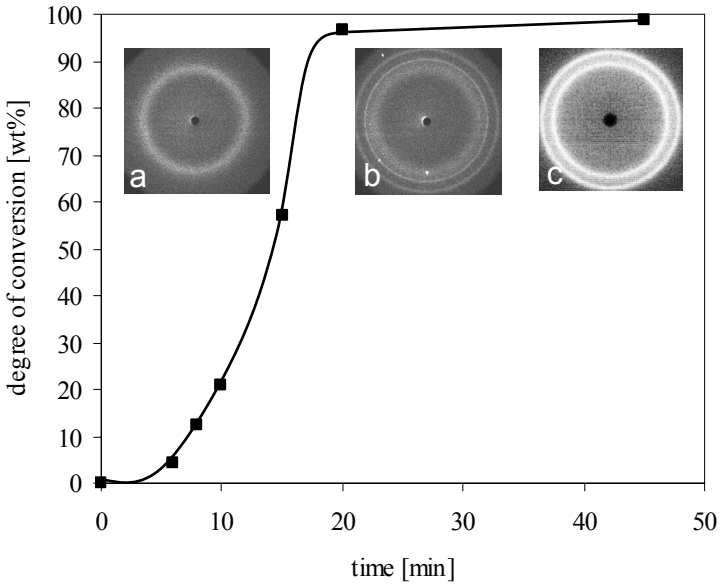

Fig. 5.12: Progress of conversion at an initial mould temperature of 150ºC. Inserts: WAXS scattering spectra; a – initial spectra without crystals, b – onset of crystallization, c – fully developed crystal morphology.

5.5.2 The crystallization-induced autocatalytic effect

Because processing of APA-6 takes place below the crystallization temperature of PA-6, polymerization and crystal formation occur simultaneously. This is

demonstrated by the fact that next to temperature peaks (see Figure 5.9) a second peak or shoulder is visible, which is caused by the exothermic crystallization process (ΔH_{cryst} = -190 J/g [56]). The simultaneous occurrence of both processes was also confirmed by *in situ* WAXS measurement of crystal growth, see inserts a-c in Figure 5.12: initially, no crystals exist in the caprolactam melt and therefore an isotropic scattering spectrum is obtained. After a while, the onset of crystal formation is shown by the appearance of faint rings at high scattering angles in the spectrum, which in this case relate to the α-phase crystals of polyamide-6. As the degree of crystallinity increases the rings gain in intensity.

Due to its exothermic nature, crystallization contributes to the previously described exothermic autocatalytic effect, but not as much as the polymerization process. Although the crystallization process is slightly more exothermic, -190 J/g vs. –144 J/g, the degree of polymerization reaches almost 100%, whereas in contrast the maximum degree of crystallization is only about 50% (equilibrium). As a consequence, the amount of heat generated per gram APA-6 by the formation of crystals is effectively only 95 J (50% of 190). Finally, whereas the rising temperature accelerates the polymerization, crystallization is slowed down, which limits the accelerating effect. Furthermore, if the temperature increases sufficiently to melt the crystals, a decelerating effect is encountered. This self-braking mechanism has important consequences for manufacturing of thick composites as it prevents the occurrence of excessive core temperatures. The continued exothermic temperature rise during cure of thermoset resins on the other hand can lead to extensive core degradation, which forces blade manufacturers for instance to resort to slow curing resin systems and long curing cycles.

There may be a second contribution of the crystallization to the self-acceleration effect, the crystallization-induced autocatalytic effect as is illustrated in Figure 5.13. During the crystallization process polymer chains are reeled in to form crystals and impurities such as monomer, anions and reactive chain-ends are expelled from the crystals into the amorphous region of the polymer. Lacking reactive species, polymerization cannot take place inside the crystals (the non-reactive material volume) and only occurs in the amorphous region (the reactive material volume). Absence of termination reactions and continuous regeneration of anions cause the number of reactive species in the total material volume to remain constant. As

crystallization reduces the amorphous phase, the concentration of reactive species in the reactive volume increases, which has an accelerating effect on the polymerization. When the polymerization rate is too low (or the rate of crystallization too high), the danger exists that reactive species cannot escape the rapidly growing crystals in time and are consequently confined, see Figure 6.17. This will not only reduce the contribution of crystal growth to the autocatalytic effect, but will also have a negative effect on the polymer properties as is discussed in more detail in the next chapter.

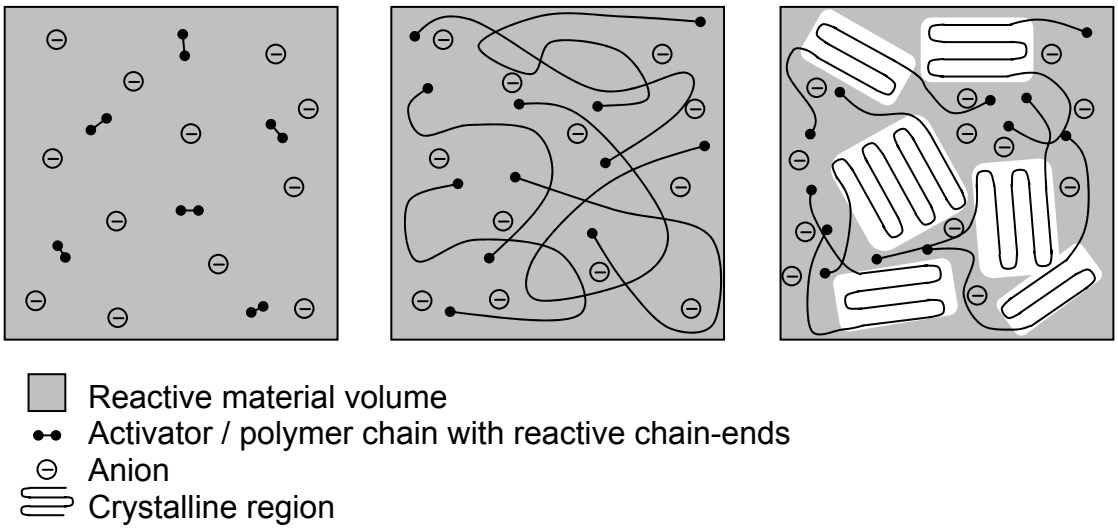

Fig. 5.13: The crystallization-induced autocatalytic effect.

5.6 Controlling the reaction rate

In the previous paragraphs, the following parameters for controlling the polymerization rate have been discussed: type and amount of activator, type and amount of initiator, the ability of activator and initiator to form a complex, and the temperature. It was discussed that these parameters can be easily used to increase the reaction rate, although side effects such as a reduction in conversion and molecular weight have to be taken into account. Reducing the reaction rate, however, is more difficult given the autocatalytic nature of the polymerization and because confinement of reactive species, which is caused by a too low polymerization rate, has to be prevented. It is concluded here (and discussed more deeply in the next chapter) that

due to the simultaneous occurrence of polymerization and crystallization, it is of paramount importance to give priority to controlling the rate of polymerization in such way that a well-developed polymer morphology is obtained. This implies that controlling the reaction rate to match a certain processing method cannot take place during the polymerization step as is described in Section 5.3.3, but should be accomplished in the earlier dissociation and complex formation steps. Figure 5.5 shows that this indeed is possible:

- The fast reacting system makes use of an activator and an initiator, which can directly form a complex. The resulting reaction profile is well suited for rapid processes that are characterized by short mould filling times such as casting or reaction injection molding (RIM).
- The slow reacting system uses an activator-initiator combination, which initially will not form a complex. As a result, at the start of the reaction the concentration of anions is low and it takes rather long before the actual polymerization initiates. Therefore, this system is well suited for the vacuum infusion process, which is characterized by relatively long mould filling times. Due to the fact that after a single monomer addition complex formation becomes possible, the reaction rate during polymerization increases rapidly and confinement of reactive species is consequently prevented.

5.7 Conclusions

- In order to reduce the reaction rate to make the APA-6 resin suitable for vacuum infusion, the effect of the temperature, type of activator, the type of initiator, and the added amount of these reactive species on the reaction rate during the various steps of the anionic polymerization of caprolactam (dissociation, complex formation and polymerization) was discussed.
- It was explained that reducing the reaction rate during the polymerization step is not only difficult due to the exothermic and crystallization-induced autocatalytic nature of the reaction, but that also the potential danger exists of confinement of reactive species, which strongly degrades the final polymer properties.

- The self-braking mechanism that is incorporated in the exothermic cure of APA-6 has important consequences for manufacturing of thick composites as it will prevent the occurrence of excessive core temperatures.
- Specifically for the vacuum infusion process an activator-initiator combination was selected, which prolongs the initial dissociation and complex formation steps sufficiently to allow for long mould filling times. In the subsequent polymerization step the reaction rate increases again, which prevents confinement of reactive species and consequently results in a highly crystalline polymer with a high conversion.

CHAPTER 6

THE INFLUENCE OF VARIOUS PROCESSING PARAMETERS ON THE PROPERTIES OF NEAT ANIONIC POLYAMIDE-6

6.1 Introduction

In Chapter 5, an activator-initiator combination specifically suitable for vacuum infusion of anionic polyamide-6 (APA-6) composites was identified. In this chapter, the effect of processing parameters like temperature, demolding time and pressure on the physical and mechanical properties of the neat polymer is discussed.

6.2 Experimental

6.2.1 Materials

The caprolactam monomer, hexamethylene-1,6-dicarbamoylcaprolactam activator (HDCL) and caprolactam magnesium bromide initiator (MgBrCL) are described in Section 5.2.1.

6.2.2. Processing methods

The APA-6 resin material was prepared in the mini mixing unit (MMU) as described in Section 5.2.2. After degassing the tanks of the MMU (15 minutes at 100 mbar), the reactive mixture was dispensed in the resin buffer (110°C, nitrogen protective atmosphere, see Figure 4.8) and subsequently infused at 900 mbar in a stainless steel mould to produce neat polymer panels, see Figure 4.10.

6.2.3. Analysis methods

Dilute solution viscosimetry

The viscosity average molar mass (M_v) was determined by dilute solution viscometry using a Micro-Ubbelohde Capillary II. Dried polymer samples from which all residual monomer had been extracted by refluxing overnight in demineralized water were dissolved in aqueous H_2SO_4 (40%) to obtain clear solutions. A single-point measurement at a concentration of 0.5 g/dl was used to obtain an approximation of M_v for each sample according to the method discussed in [161]. First, the inherent viscosity (η_{inh}) was calculated from the flow times (averaged over three measurements) of the solutions according to Equation 6.1.

$$\eta_{inh} = \frac{\ln\left(\frac{t}{t_0}\right)}{c} \tag{6.1}$$

In which t is the flow time for the polymer solution, t_0 the flow time of the pure solvent and c the concentration of the polymer solution. In a single-point measurement it is assumed that the inherent viscosity equals the intrinsic viscosity (η_{int}). Due to this simplification, the actual M_v is slightly higher than the one measured. M_v can be calculated from η_{int} by using the Mark-Houwink Equation [32], see Equation 6.2.

$$\eta_{\text{int}} = K' M_v^{\,a} \tag{6.2}$$

Here *K'* and *a* are the Mark-Houwink constants which have a specific value for each polymer-solvent combination. In this particular case: $K' = 5.92 \cdot 10^{-4}$ dl/g and $a = 0.69$ [162]. Although these constants were originally obtained for hydrolytically polymerized PA-6, Biernacki et al. demonstrated that values for anionic PA-6 are similar [163].

Degree of conversion (DOC)

The degree of conversion of the polymer samples was determined according to the method described in Section 5.2.3.

Differential Scanning Calorimetry (DSC)

The degree of crystallinity and the melting point of polymer samples were determined according to the method described in Section 5.2.3.

Density measurements

For each panel, the density of a single dogbone shaped specimen was determined by displacement according to the ISO 1183 standard using a Mettler AG204 DeltaRange® microbalance. Prior to testing, all specimens were dried in a vacuum oven at 50 mbar and 70°C for at least 85 hours.

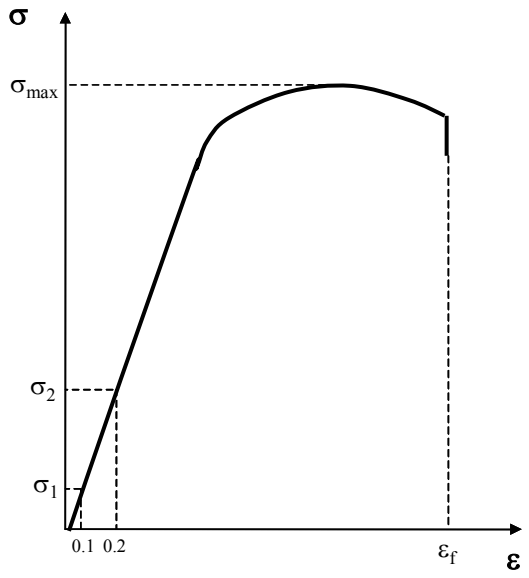

Fig. 6.1: Typical stress-strain curve showing the material parameters acquired from the tensile test.

Tensile testing

Tensile tests were performed on a Zwick 1455 universal testing machine equipped with a 10kN force cell according to ISO 527-2, using dogbone shaped specimens (type 1b, 5 of each sample), which were machined from the infused panels. Once clamped, a load was applied at a rate of 5 mm/min up to a strain of 0.3 % and subsequently released to get a slip-free grip on the sample without inducing plastic deformation. This procedure was repeated twice, but this time to calculate the

Young's modulus from the slope of the stress-strain curve between 0.1 and 0.2% strain, see Figure 6.1. Finally, a full test (up to a maximum strain of 50%, limited by the size of the climate chamber) was conducted to obtain values for the maximum strength (σ_{max}, also called ultimate strenght) and strain at failure (ε_f).

Microscopy

For optical microscopy, a Leica DMLM system with CCD camera and Qwin color software was used.

6.3 The effect of the mould temperature on the properties of APA-6

Polymerization and crystallization are both strongly influenced by temperature. Their simultaneous occurrence during reactive processing of APA-6, as was explained in the previous chapters, makes the polymerization temperature the most important processing parameter. This influence already becomes clear from visual inspection of infused polymer plates, as is demonstrated in Figure 6.2. Whereas at high polymerization temperatures a homogeneous translucent polymer is obtained, at low temperatures a pattern of white (opaque) stains is obtained. This paragraph discusses the effect of the mould temperature on both physical and mechanical properties of APA-6.

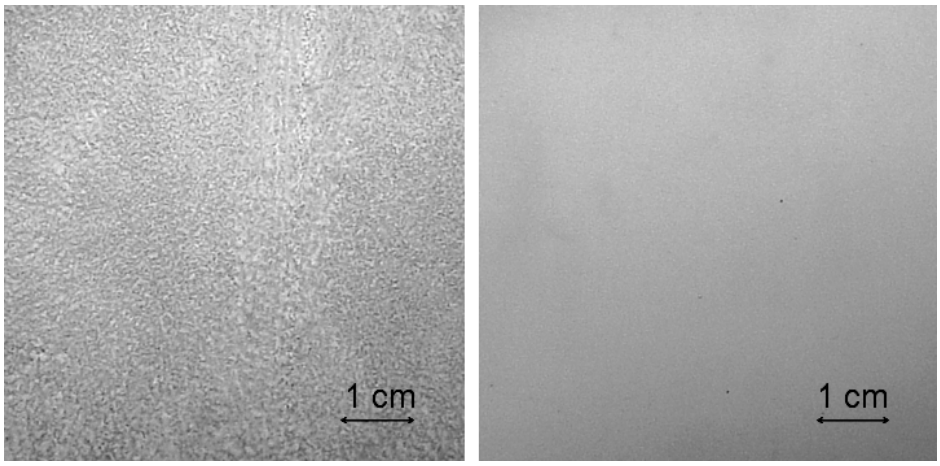

Fig. 6.2: Contrast-enhanced photos of vacuum infused APA-6 plates polymerized at different temperatures. Left: Surface representative for 140°C. Right: Surface representative for 150 – 170°C.

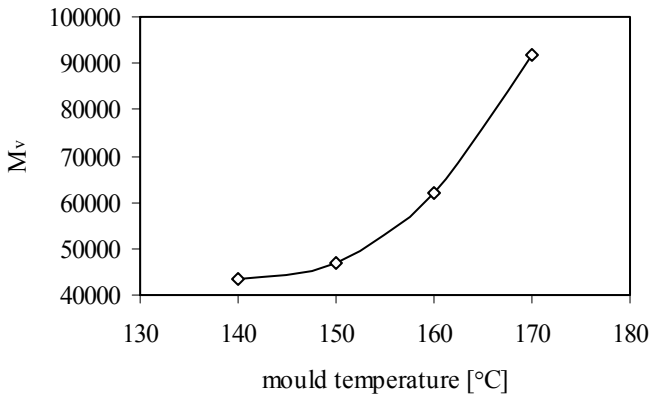

Fig. 6.3: Viscosity average molar mass for various polymerization temperatures.

6.3.1 Effect of the mould temperature on the molar mass

In Figure 6.3 the viscosity average molar mass (M_v) of the infused polymer plates is given for various mould temperatures. It can be seen that with increasing temperature the M_v increases rapidly. This increase is explained by the occurrence of various types of branching reactions, which are discussed next.

Low-temperature branching

The carbamoylcaprolactam activator used in this research is made by blocking a di-isocyanate with caprolactam rings. These blocked isocyanates are not temperature stable and above their de-blocking temperature, carbamoylcaprolactam follows a so-called de-blocking equilibrium according which it continuously changes from a blocked configuration into a de-blocked configuration and visa versa, see step 1 in Figure 6.4 [164]. Whereas in the blocked configuration the activator can induce chain growth, the free isocyanate groups of the de-blocked configuration can react with amide groups of a neighboring chain to form a branch-point. Although these types of reactions occur for both mono- and di-functional carbamoylcaprolactam activators, the effect of a branch point is more severe with di-functional activators due to the fact that all chain-ends remain active after branching and continue to polymerize.
Once chain growth has been initiated by the addition of a single monomer, the carbamoyl group has changed into an acyllactam group that is unable to form an isocyanate and which is therefore no longer capable of branching, see Figure 5.6. For branching to occur according to this mechanism, it has to take place before a single

monomer reacts with the activator. As a consequence, this type of branching takes place at low conversions and because at this early stage of the reaction the exothermic temperature rise is yet to start, the mechanisms is referred to as 'low-temperature branching', see also Figure 6.10. From the fact that hexamethylene-1,6-dicarbamoylcaprolactam has a de-blocking temperature of 160ºC [164], one can deduct that low temperature branching is indeed the cause for the large increase in molecular weight at this temperature as is shown in Figure 6.3.

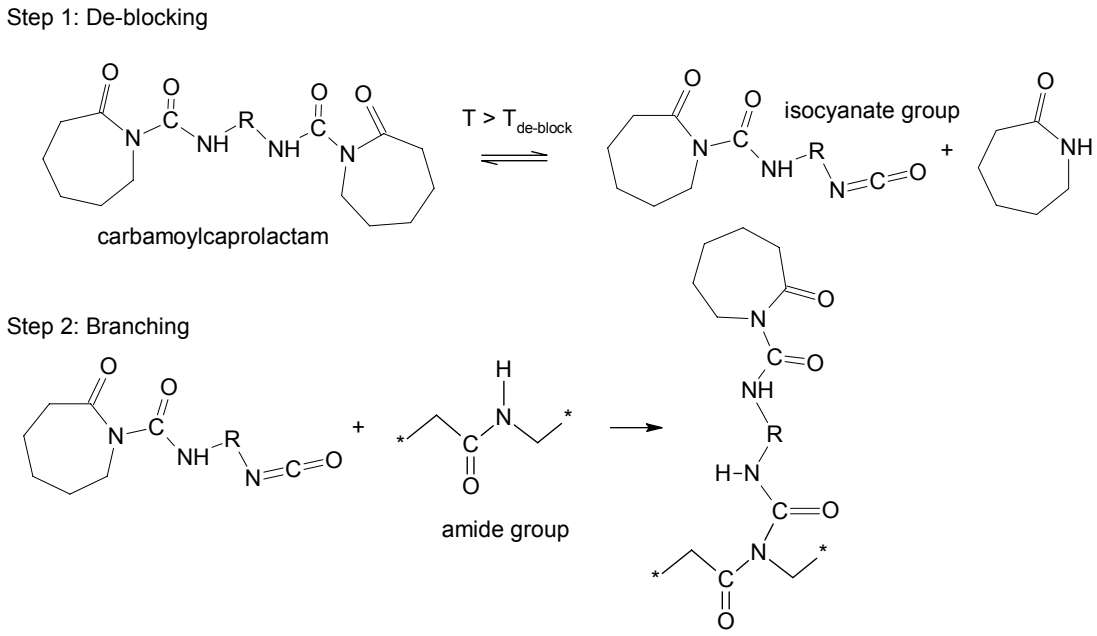

Fig. 6.4: Reaction scheme for low-temperature branching during anionic polymerization of ε-caprolactam when using a di-functional blocked isocyanate activator.

Although Ricco et al. [49] reported that for hexamethylene-1,6-dicarbamoylcaprolactam the rate of branching is only significant at polymerization temperatures exceeding 180°C, one has to keep in mind that in that particular research a much faster activator-initiator combination was used together with a slightly lower activator concentration. The increase in M_v in the present research clearly indicates that with a higher activator concentration (higher chance of a branching reaction taking place) and the use of a slower activator-initiator combination (longer time during which branching can take place) branching already takes place at lower

temperatures. The dependence of the degree of branching on the activator concentration and the reaction rate has also been reported in literature [50].

High-temperature branching

Towards the end of the reaction, monomer depletion makes interaction of reactive chain ends with the abundance of polymer chains more likely. Due to the exothermic temperature rise high-temperature branching reactions like Claisen condensation and transamidation occur [48-50, 61, 150]. Figure 5.9 shows that a higher mould temperature is accompanied by a higher peak temperature and consequently leads to more extensive high temperature branching, which is in agreement with the increase in molecular weight as shown in Figure 6.3.

6.3.2 Effect of the mould temperature on the degree of conversion

In Figure 6.5, the final degree of conversion of the infused polymer plates is presented for various polymerization temperatures for demolding times of 30 minutes (instant demolding) and 45 minutes (cooled with 40ºC/hr to 80ºC prior to demolding). An approximate conversion of 97 wt% is found on average for both polymerization times, which is relatively low compared to the equilibrium conversions found by Kohan [146], given the fact that extrapolated data would predict a final conversion in the order of 99 wt% as is shown in the same figure. It has to be kept in mind, however, that Kohan performed his measurements on purified hydrolytically polymerized PA-6. In the current case, no purification has taken place and residual initiator (initial concentration 1.2 mol%) decreases the conversion by 2.21 wt%, see Figure 6.5. When taking this into account, the correlation with data from Kohan becomes clear. This implies that the equilibrium conversion obtained at the various polymerization temperatures is frozen when the panels are rapidly cooled to room temperature after demolding. It is pointed out that the small discrepancy between the experimental data and the for initiator residue corrected equilibrium data can be explained by the presence of oligomers, see Section 5.2.3, or a small mismatch in crystallinity. The effect of crystallinity on the conversion is explained in the next paragraph.
Kohan mentions two reasons for the decrease in conversion with increasing polymerization temperature. The first reason is the shift in the ring-chain equilibrium of the anionic ring opening polymerization reaction towards the monomer side. The

second reason is the decreasing degree of crystallinity (see Section 6.3.3), or more precisely, the increase of the amorphous phase: during crystallization the attracting forces between the folded polymer chains are so high that monomer is expelled from the crystals, provided that the rate of crystallization is low enough to allow diffusion of the monomer. The crystalline regions are therefore free of monomer, which basically implies that the ring-chain equilibrium mentioned earlier only exists in the amorphous region [165]. Due to the fact that crystalline regions have a 100 wt% conversion, the overall conversion of PA-6 decreases at lower crystallinity. The large drop in conversion that is found by Kohan at the polymer melting point illustrates this, because at that temperature the crystallinity is suddenly reduced to zero.

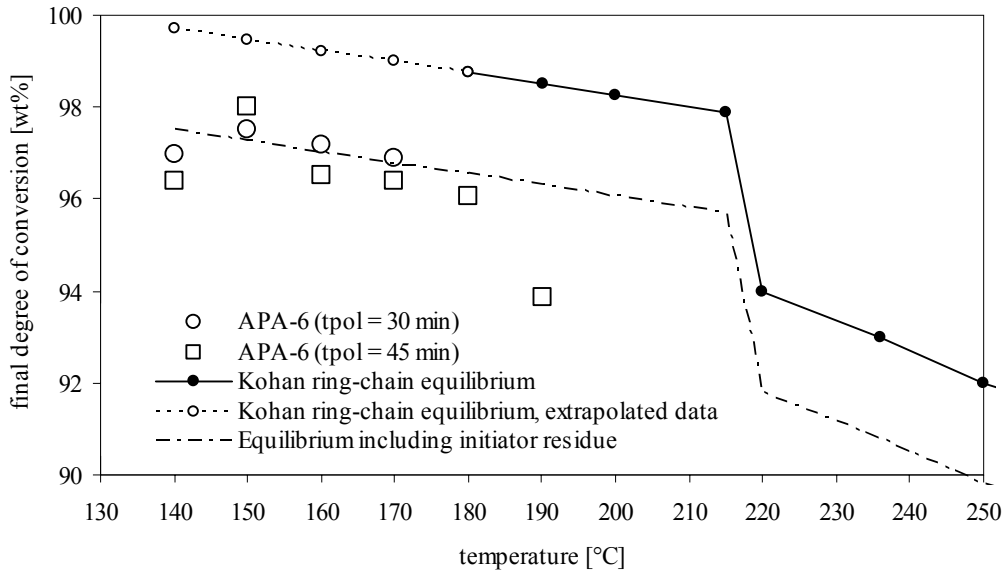

Fig. 6.5: Final degree of conversion of APA-6 for various mould temperatures and Kohan ring-chain equilibrium data [146].

At a polymerization temperature of 140°C the measured conversion no longer follows the trend discussed in the previous paragraph. It is believed that at 140°C the crystallization rate is so high that caprolactam can become trapped inside growing crystals before it can diffuse to an amorphous region where it can equilibrate with the polymer chains. Trapped or confined caprolactam not only reduces the measured conversion [166], but also causes the white coloration of the crystals as can be seen in Figure 6.2.

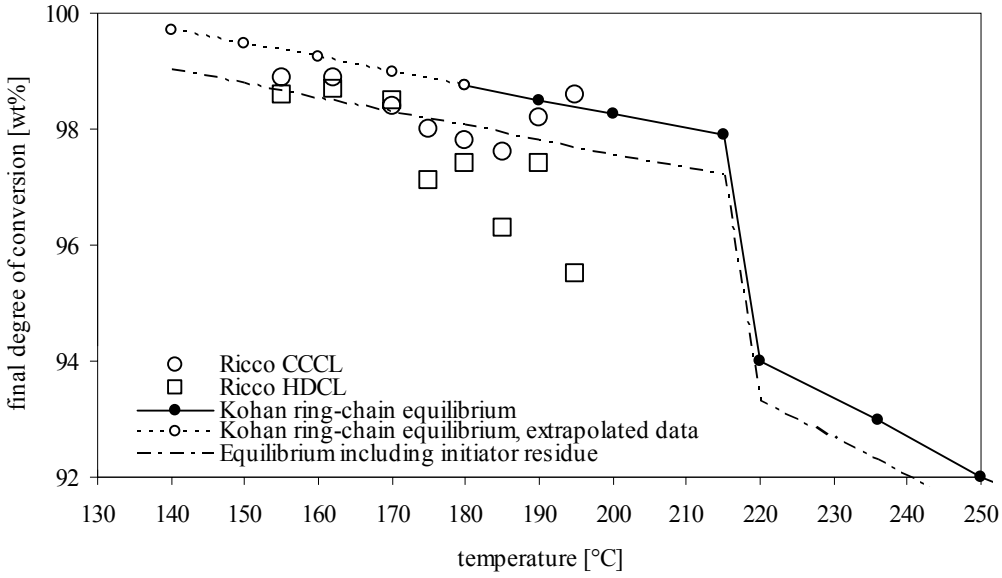

Fig. 6.6: Final degree of conversion data as obtained by Ricco et al. [49] and Kohan ring-chain equilibrium data [146].

Branching can also reduce the final degree of conversion, which can be explained in two ways. First, branching reduces the degree of crystallinity, see Section 6.3.3, and therefore indirectly reduces the conversion as explained previously. Second, with every branch-point made, the total number of reactive chain end-groups is reduced by one, see Figure 6.4. Ultimately, activator depletion can cause a reduction in the final conversion. Data of Ricco et al. is presented in Figure 6.6 to illustrate this [49]. The use of a lower concentration of a different initiator (0.6 mol% sodium caprolactamate) only results in an additional reduction in conversion of 0.7 wt% compared to Kohan's equilibrium data. It can be seen that for polymerization temperatures up to 170ºC the conversions for both the mono-functional (cyclohexylkcarbamoylcaprolactam, CCCL) and di-functional activator (hexamethylene-1,6-dicarbamoylcaprolactam, HDCL, the same activator as used in the present research) follow Kohan's equilibrium fairly accurately. At higher temperatures, branching occurs and consequently the obtained conversion drops below the equilibrium. Since branching is more apparent with a di-functional activator, the deviation from the equilibrium is obviously larger. The same deviation from the equilibrium is found in Figure 6.5 at 190ºC.

At temperatures above 190ºC, the obtained conversion using a mono-functional activator suddenly exceeds the equilibrium data. This is caused by the fact that at these high temperatures no crystallization takes place during polymerization. Only

when the temperature drops upon demolding crystals are formed. Due to the heat of crystallization (-16.3 kJ/mole [55]) the material is subjected to an overall lower cooling rate compared to when the crystallization has already taken place prior to demolding. As a consequence, the ring-chain equilibrium is not frozen but shifts to a value that corresponds to a lower temperature, which implies that the initiator remains active throughout the entire process.

6.3.3 Effect of the mould temperature on the degree of crystallinity

The degree of crystallinity gradually decreases with increasing mould temperature, as is shown by the DSC curves in Figure 6.7 and 6.8. The first explanation is that at higher temperatures the equilibrium degree of crystallinity is lower, which is caused by the higher thermal motion of the polymer chains. Similarly, the tendency to crystallize is lower at higher temperatures resulting in a longer time to achieve this equilibrium. The ultimately obtained crystallinity, just prior to demolding, is frozen in when the temperature rapidly drops below the glass transition temperature in the subsequent cooling phase. A second explanation is that branch points disturb the formation of crystals and therefore reduce the degree of crystallinity [53]. As proposed by Risch et al. in their research on cationically polymerized star-branched PA-6 [167], the majority of the bulky branch-points are not incorporated into the lamellar crystals but instead concentrate on their surface. A polymer chain can fold normally until a branch-point is reached. At that point a considerable disruption in the chain-folding pattern is required to incorporate the rest of the branches. It is generally recognized that such a disruption will lead to increased energy for folding and a reduced order at the lamellar surface. In addition, the lamellar thickness (l) increases at higher crystallization temperatures (T_c), see Equation 6.3 [32], which implies that the amount of branch-points per fold increases at higher processing temperatures, consequently enhancing their disturbing effect.

$$l = \frac{2\gamma_e T_m^0}{\Delta H_v \left(T_m^0 - T_c\right)} \tag{6.3}$$

in which γ_e is the fold surface energy of the lamellae, T_m^0 the melting point of a perfect crystal and ΔH_v the volumetric enthalpy of fusion.

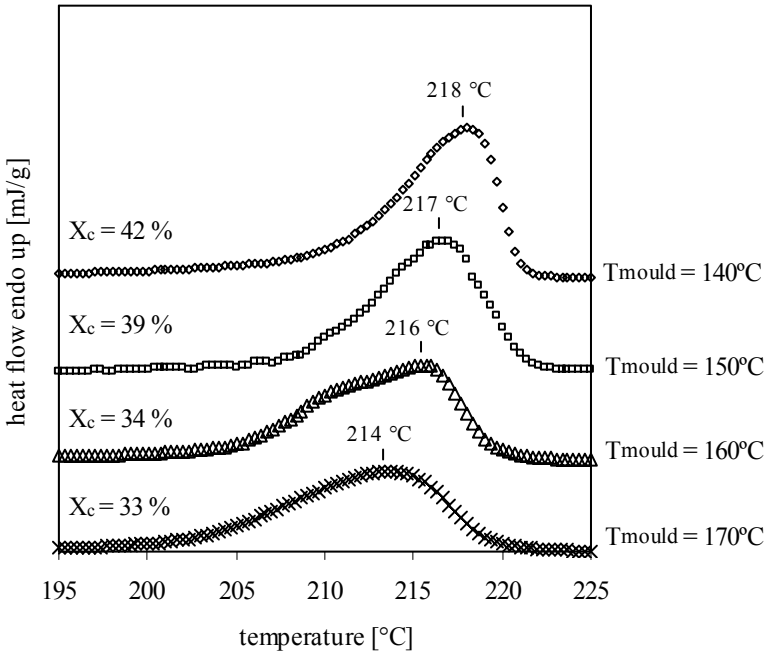

Fig. 6.7: Degree of crystallinity and polymer melting point for various mould temperatures for a demolding time of 30 minutes as measured by DSC (curves are shifted up for clarity).

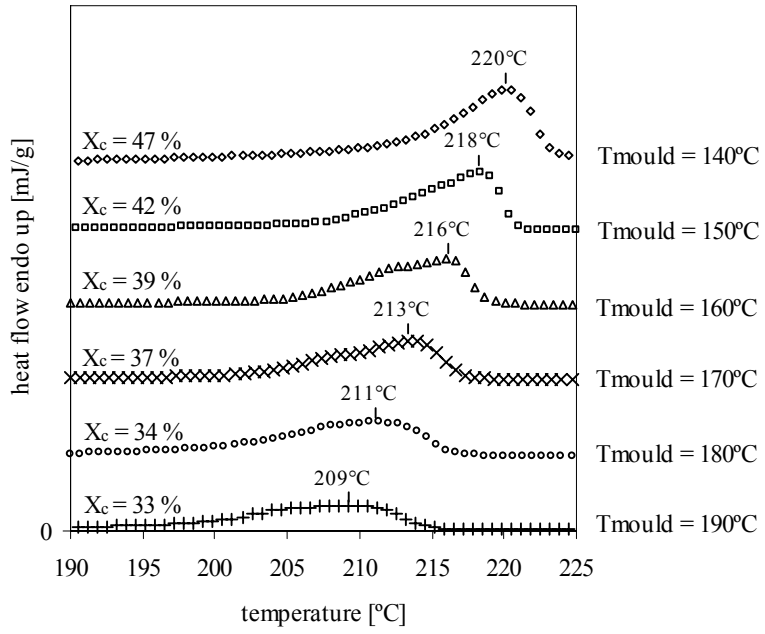

Fig. 6.8: Degree of crystallinity and polymer melting point for various mould temperatures for a demolding time of 45 minutes as measured by DSC (curves are shifted up for clarity).

To confirm the previously described effect of branch-points, the crystallinity at various mould temperatures is compared for resin formulations with different activator concentrations (1.2mol% HDCL vs. 0.6mol% HDCL), see Figure 6.9. Below the de-blocking temperature of the activator (160ºC), no branching occurs and the higher activator concentration results in a larger number of polymer chains and consequently a lower molecular weight. As was discussed in Section 3.2.2, a lower molecular weight leads to a higher degree of crystallinity. Above the de-blocking temperature, the higher activator concentration causes a significant increase in branch-points, which decreases the crystallinity as can be clearly seen.

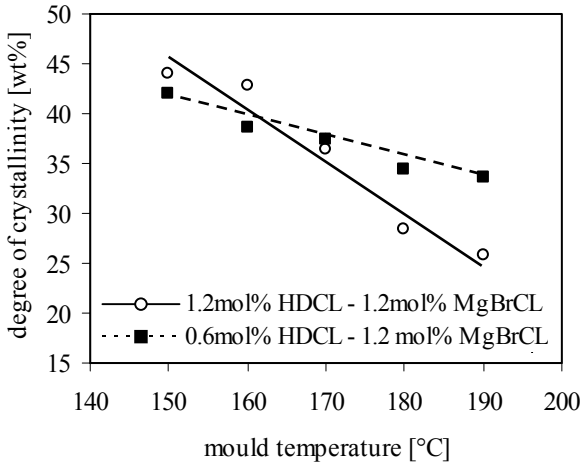

Fig. 6.9: Degree of crystallinity at various mould temperatures for two different activator concentrations.

6.3.4 Influence of the mould temperature on the polymer melting point

When increasing the mould temperature, a drop in polymer melting point of 4 to 11 degrees is observed, see Figure 6.7 and 6.8. Three possible explanations can be given:

1. First of all, residual caprolactam can reduce the polymer melting point. Ricco et al have reported melting point depressions between 3.5 and 5 degrees per wt% residual caprolactam [49]. In the present research similar gradients of 4.3 degrees per wt% (after 30 minutes polymerization time) and 3.5 (after 45 minutes) is found, which is in agreement with the previously reported values.
2. Secondly, the increasing number of crystal imperfections induced by the formation of branch-points, can cause a decrease in melting temperatures, simply

because less energy is required to break down a crystal [32]. According to Flory et al. [168], the melting point of the imperfections containing polymer (T_m) can be written as a function of the melting point of its perfect counterpart (T_m^0, which is 221ºC for PA-6, according to DSM) and the enthalpy of fusion per crystallizable repeating unit (ΔH_m), as is shown in Equation 6.4.

$$\frac{1}{T_m} = \frac{1}{T_m^0} - \frac{R}{\Delta H_m} \ln(1 - X_B) \tag{6.4}$$

In which R is the universal gas constant and X_B the mole fraction of imperfections such as chain-ends, branch-points and trapped monomer.

3. A third explanation for the reduction in melting point is the co-existence of two types of crystals, each formed in different stages of the crystallization process of APA-6, see Figure 6.10:

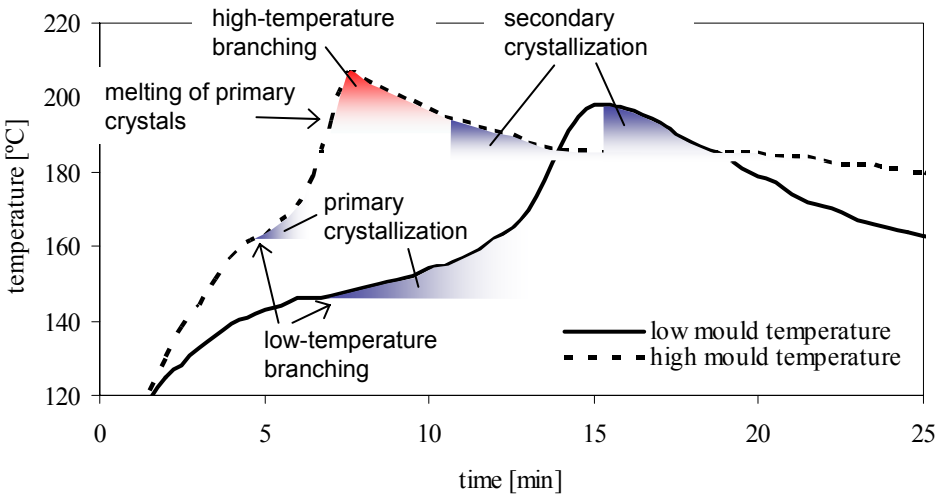

Fig. 6.10: Crystallization and branching.

- Primary crystallization takes place at the early stage of the reaction. As the reaction temperature increases, the rate of crystallization slows down until finally the exothermic temperature rise ends the primary crystallization phase.
- After the exothermic temperature peak has been reached, secondary crystallization initiates during subsequent cooling of the polymer.

The fact that at higher mould temperatures the DSC curves seem to be composed of two overlapping melting peaks forms evidence for this coexistence. Apparently, one of these crystal types has a lower melting point as is explained in the next paragraph.

Section 3.2.2 introduced various principles, which describe the link between the resistance encountered during the formation of crystals and the final crystal morphology. The same principles can be applied to explain the differences in morphology between crystals formed during primary and secondary crystallization.

- Secondary crystallization takes place at a higher temperature. The higher thermal motion of the molecules increases the resistance against crystal formation.
- The polymer chains have already reached a higher molecular weight before secondary crystallization initiates. A higher molecular weight increases the resistance against crystal formation.
- Caprolactam being a solvent for PA-6 reduces the resistance against crystallization. Because secondary crystallization takes place at higher conversions, more resistance is encountered.
- Whereas primary crystallization is only hindered by low-temperature branching, secondary crystallization encounters additional resistance due to high-temperature branching, see Section 6.3.1. When the temperature is such high that it causes the primary crystals to melt again, the effect of branching on secondary crystallization increases even further: (i) in the purely amorphous polymer extensive high-temperature cross-linking can take place, and (ii) secondary branching is now affected by both low- and high-temperature branches.

It can be concluded that the secondary crystallization process encounters more resistance, consequently introducing a larger number of crystal imperfections, which reduce the melting point. Literature reports that for APA-6 branching can cause a transition from crystals with an α-structure (T_m = 220°C) into crystals with a γ-structure (T_m = 214°C) [48, 49]. Although it seems obvious to correlate primary crystals to the α-structure and secondary crystals to the γ-structure, WAXS analysis showed no evidence about the existence of γ crystals. It is consequently assumed that APA-6 consists of two α-type crystals with different levels of perfection.

6.3.5 Influence of the mould temperature on the polymer density

Figure 6.11 shows the polymer density at various mould temperatures for demolding times of 30 and 45 minutes, as well as the thickness of the infused panels demolded after 30 minutes.

Between 150 and 170°C the density is in agreement with the measured degree of crystallinity, see Figure 6.7 and 6.8. The density of the crystalline phase (ρ_{cr} = 1.24 g/cm^3, α-phase) is higher than the density of the amorphous phase (ρ_{am} = 1.08 g/cm^3) and therefore a lower degree of crystallinity results in a polymer with a lower density. The fact that also the thickness is in agreement with the crystallinity demonstrates the orderly progression of polymerization and crystallization. The mould heats up the infused reactive mixture from the outside to the inside and hence polymerization proceeds in the same direction (despite the occurrence of convection flows). Crystallization follows instantly and the resulting shrinkage (9 % [50]) is initially compensated by the flow of low viscous caprolactam from elsewhere in the mould. As long as this flow of caprolactam can be maintained a void-free polymer results of which only the outer dimensions are affected by shrinkage.

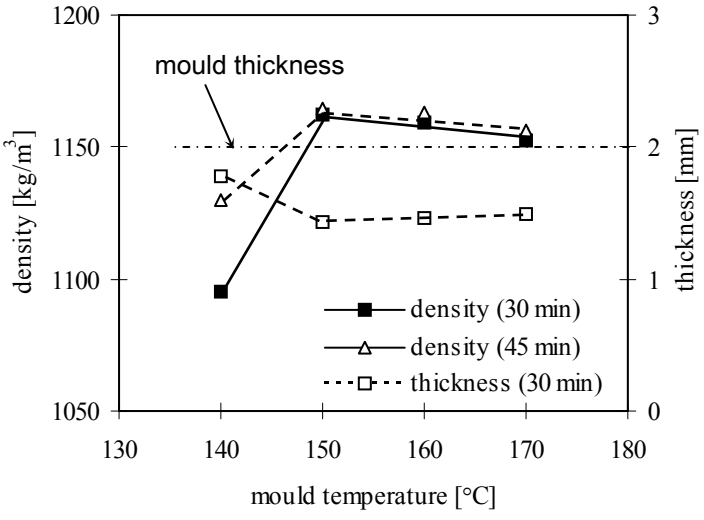

Fig. 6.11: Density and panel thickness at various mould temperatures for demolding times of 30 and 45 minutes. The mould thickness has been added as a reference.

At 140°C, however, the higher degree of crystallinity does not lead to an increase in density. It is assumed that at this temperature, the crystallization rate, and hence the shrinkage rate, is so high that the flow of liquid caprolactam inside the mould is not sufficient to keep up with the receding crystalline material. In this case, shrinkage does not affect the outer dimensions of the product, but instead introduces internal voids. Figure 6.11 indeed shows the reduced density at 140°C is accompanied by a higher thickness. This scenario for the generation of shrinkage induced voids is confirmed by examining a cross-section of the material, see Figure 6.12. Clearly, voids are present at the boundary layer between the more dense (dark) area of the polymer, which contains a high degree of rapidly formed caprolactam-infested crystals, and the less dense (light) areas, which polymerized from inflowing caprolactam.

When voids are generated, the internal pressure drops below the evaporation pressure of caprolactam, see Figure 6.18, consequently filling the voids with caprolactam vapor. This vapor no longer participates in the polymerization reaction and after removing the sample from the mould the caprolactam vapor cools down and precipitates on the inside of the void surface, which explains the reduction in the measured degree of conversion as shown in Figure 6.5.

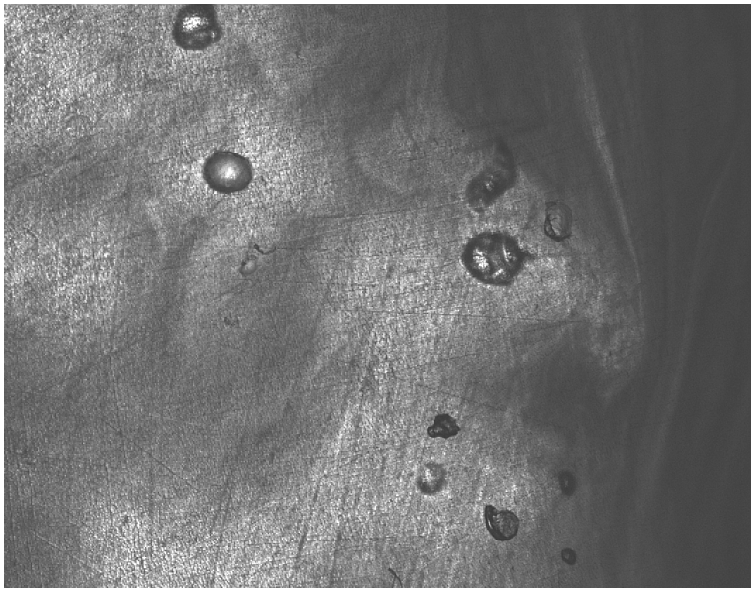

Fig. 6.12: Optical micrograph of the cross-section of APA-6 polymerized at 140°C.

6.3.6 Influence of the mould temperature on the tensile properties

The tensile properties of APA-6 manufactured at various mould temperatures are presented in Figures 6.13 to 6.15 for demolding times of 30 and 45 minutes.

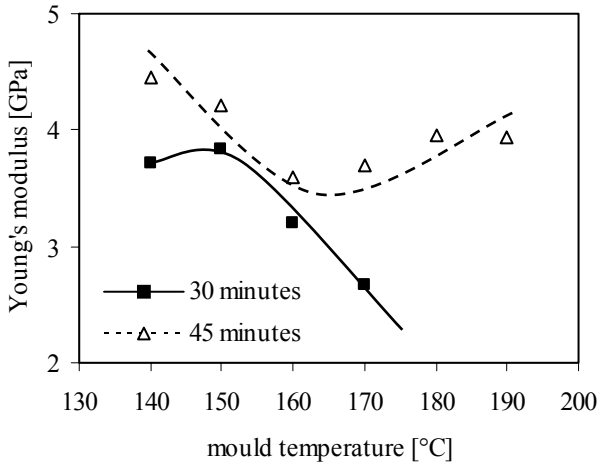

Fig. 6.13: Young's modulus at 23°C for various mould temperatures and for various polymerization times. Dry as molded properties.

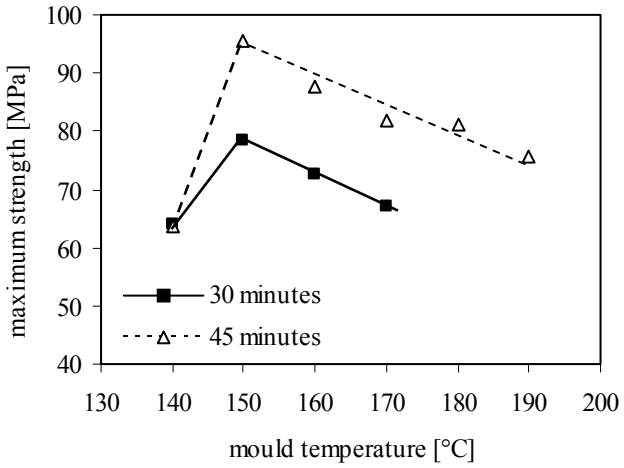

Fig. 6.14: Maximum strength at 23°C for various mould temperatures and for various polymerization times. Dry as molded properties.

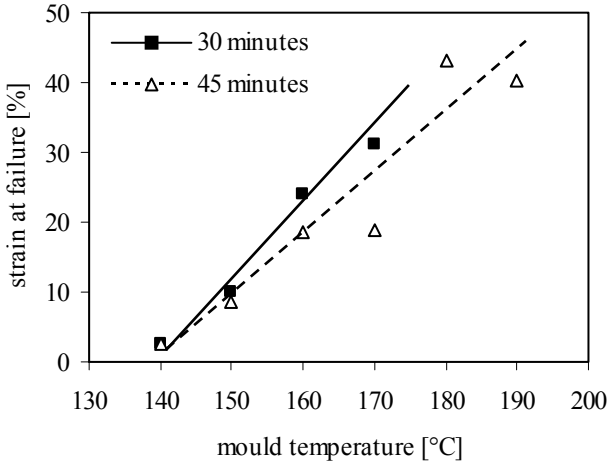

Fig. 6.15: Strain at failure at 23°C for various mould temperatures and for various polymerization times. Dry as molded properties.

Looking at Figure 6.13 and 6.14, it can be seen that for both demolding times a mould temperature of 150ºC leads to the highest strength and modulus, which is caused by the high degree of crystallinity and crystallinity (Figures 6.5, 6.7 and 6.8) and not so much by the degree of branching or the molecular weight, see Figure 6.3.

1. A high degree of conversion is necessary because residual caprolactam acts as a plasticizer: it prevents the formation of hydrogen bonds between polymer chains in the amorphous phase. As a consequence, chain interactions are reduced, which penalizes strength and modulus [150].
2. A high degree of crystallinity is required because chain interactions are maximized in this phase: chains are closely packed and a large number of hydrogen bonds are formed. Therefore, the larger the crystalline fraction the higher the strength and modulus of the entire polymer. However, the increase in crystallinity also decreases the ductility of the polymer, see Figure 6.15.

When decreasing the mould temperature from 150 to 140°C, the degree of crystallinity increases, but does not lead to the expected increase in strength and stiffness. As mentioned earlier, the high crystallization rate at 140°C results in a shrinkage-induced voids and a lower conversion, which reduce the structural integrity of the material. Consequently a brittle polymer is obtained as can be seen from the abrupt end of the stress-strain curve, see Figure 6.16.

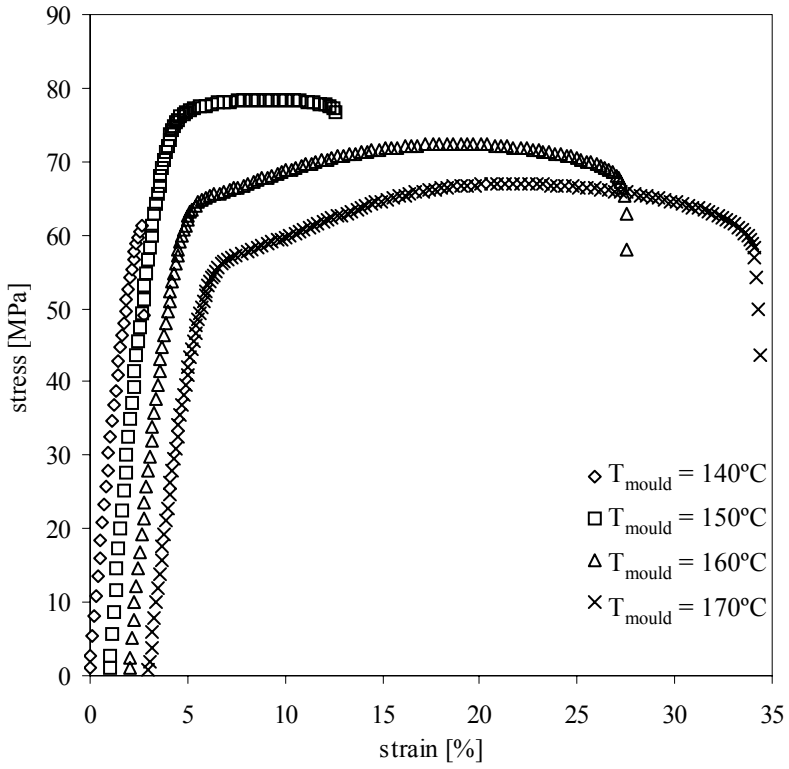

Fig. 6.16: Typical stress-strain curves at various polymerization temperatures for dry as molded (DAM) APA-6 demolded after 30 minutes (curves shifted to the right for clarity).

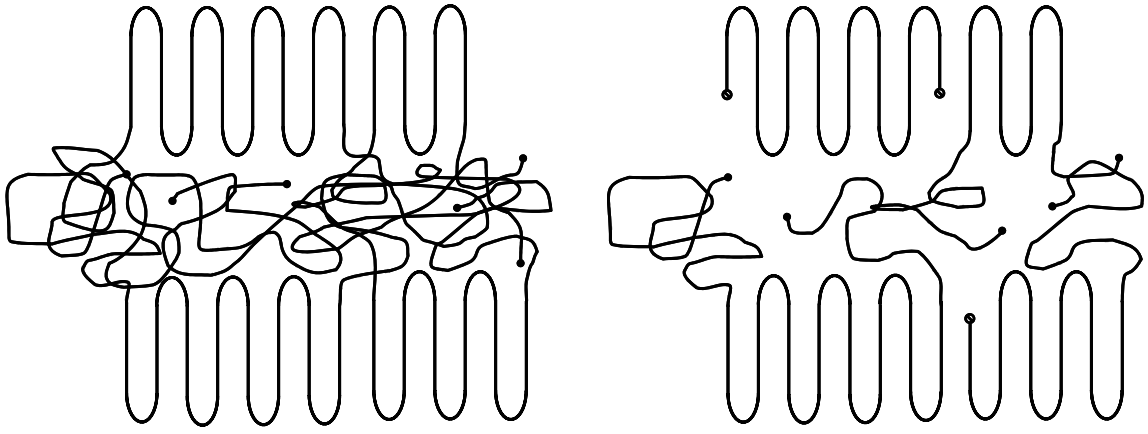

Fig. 6.17: The effect of entrapment of reactive chain-ends on the morphology of APA-6. Left: switchboard with fully developed morphology, right: switchboard with reduced structural integrity due to confinement of chain-ends.

Careful examination of the fracture surfaces showed that failure not always initiated at a void. Therefore, a second mechanism for the brittleness at 140°C is proposed. In addition to entrapment of caprolactam due to rapid crystallization, see Section 6.3.5, also reactive chain ends can get confined inside the crystals, hence abruptly ending chain growth and limiting interdiffusion of polymer chains between the amorphous and crystalline regions. The reduction in structural integrity caused by this second mechanism is schematically represented by means of a switchboard model in Figure 6.17.
The final remark is made that despite the continuous decrease in crystallinity and conversion at higher mould temperatures, the modulus starts increasing again above a mould temperature of 160°C, see Figure 6.13. As described in Section 6.3.1, above this temperature de-blocking of the HDCL activator causes the formation of branch-points, which apparently has a positive effect on the modulus. In Chapter 7 will be explained that the combination of a high degree of crystallinity and a slight degree of branching results in a unique polymer morphology, which results in extraordinary mechanical properties.

6.4 The influence of the demolding time on the properties of APA-6

Although after 30 minutes the maximum conversion plateau has already been reached for all polymerization temperatures, see Figure 5.10, the temperature inside the mould at that time, see Figure 5.9, is still close to the crystallization temperature. This implies that secondary crystallization can still continue, during which crystals can grow and imperfections are removed from the existing crystal morphology.
It can indeed be seen in Figures 6.7 and 6.8 that between 30 and 45 minutes the crystallinity increases, resulting also in a higher density (Figure 6.11), an increased modulus and strength (Figure 6.13 and 6.14), and a reduction in strain at failure (Figure 6.15). The degree of conversion (Figure 6.5) does not show a significant change between 30 and 45 minutes. The conclusion is drawn that, with respect to the influence of the demolding time on the properties, it is not the conversion that is the determining factor but the degree of crystallinity.

6.5 The influence of the processing pressure on the properties of APA-6

During three stages of the process the pressure plays an important role: (i) degassing of the resin prior to infusion, (ii) infusion of the mould, and (iii) curing of the resin. It will be demonstrated that the effect of degassing (or the absence thereof) on the void content is closely related to the pressure in the mould cavity during polymerization and therefore the effect of the pressure during both processing stages is discussed simultaneously. Whereas for composite manufacturing the infusion pressure is of paramount importance, its influence on the infusion of neat polymer panels is far less and as a consequence the infusion pressure is not further discussed.

6.5.1 Boiling-induced voids

The vapor pressure of a substance can be calculated using the Clausius-Clapeyron relation [169], see Equation 6.5.

$$\ln p_{vap} \approx \frac{\Delta H_{vap}}{R}\left(\frac{1}{T_b}-\frac{1}{T}\right)+11.5261 \qquad (6.5)$$

p_{vap} = vapor pressure [Pa]
T = temperature [K]
T_b = boiling point at one atmosphere (101325 Pa) = 540 K (Source: DSM)
ΔH_{vap} = molar evaporation enthalpy = 63713 $J \cdot mol^{-1}$ (Source: DSM)
R = gas constant = 8.3143 $J \cdot K^{-1} \cdot mol^{-1}$

Based on values provided by DSM and from literature [147], the vapor pressure of caprolactam is calculated for temperatures that are typically encountered during reactive processing of PA-6, see Figure 6.18. Assuming that 220°C is the absolute maximum temperature encountered during polymerization (including the exothermic temperature rise), one can deduct from Figure 6.18 that in order to prevent boiling of the resin the minimum processing pressure that can be used is 250 mbar.

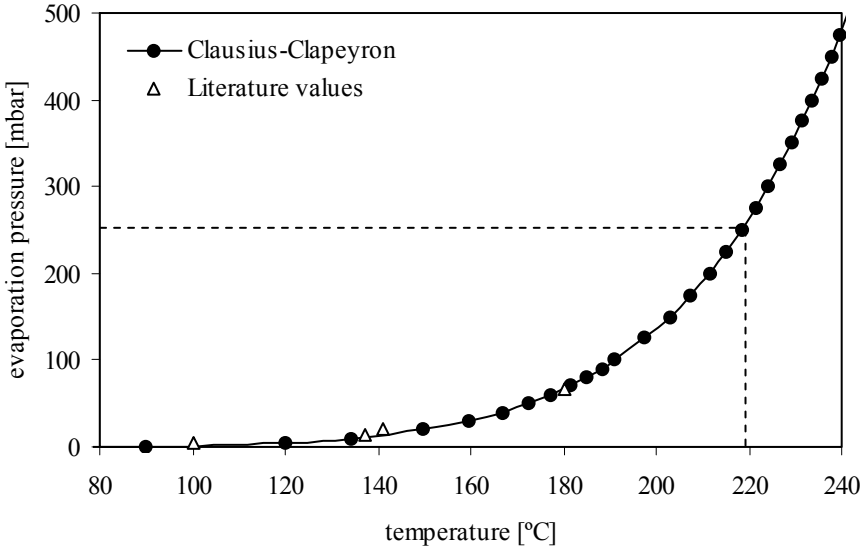

Fig. 6.18: Temperature vs. vapor pressure calculated according to the Clausius-Clapeyron equation.

6.5.2 Nitrogen-induced voids

It is well known that nitrogen (from the protective atmosphere in the MMU) can dissolve in lactams [100]. The solubility of a gas in a liquid is determined by the dimensionless solubility coefficient, δ [170], but can also be expressed in terms of Henry's coefficient, H, which has the dimension mole m^{-3} bar^{-1}, see Equation 6.6.

$$H = \frac{\delta}{RT} \tag{6.6}$$

in which R is the universal gas constant ($8.0978 \cdot 10^{-5}$ $m^3 \cdot bar \cdot mol^{-1} \cdot K^{-1}$) and T the absolute temperature. Using Henry's law, the concentration of the dissolved gas [C_g] at a certain temperature and pressure can be calculated, as is shown in Equation 6.6.

$$[C_g] = H \cdot p_g/\rho_g \tag{6.7}$$

in which p_g is the partial pressure of the gas in bar and ρ_g is the density of the liquid at temperature T in kg/m^{-3}. Both solubility and Henry's coefficients have been

determined experimentally by DSM for the case of dissolving nitrogen in caprolactam according to a method presented in reference [171]. The amount of dissolved nitrogen per kilogram caprolactam, calculated with Equation 6.7, for various temperatures and nitrogen pressures is presented in Figure 6.19.

Figure 6.19 shows that after melting the components in the MMU at 110ºC, the nitrogen blanket ($p \approx 1$ bar) results in 66 mg nitrogen dissolved per kilogram of caprolactam. After degassing at 100 mbar, the amount of dissolved nitrogen is reduced to 6.6 mg per kilogram. The following example treats infusion in a mould heated at 160ºC at a pressure of 500 mbar. Under these circumstances, only 43 mg of nitrogen can be dissolved per kilogram according to Figure 6.19. This implies that when a non-degassed mixture is infused, 23 mg nitrogen (66-43 = 23 mg) is released and exits the low viscosity mixture against gravity. Removal of nitrogen from the mould is hereafter called 'in-mould degassing'. When infusing a degassed mixture, no in-mould degassing takes place just after completing the infusion because the nitrogen concentration is already below 43 mg per kilogram. When polymerization initiates, the remaining nitrogen, which is not soluble in the polyamide-6 polymer, is released with increasing conversion.

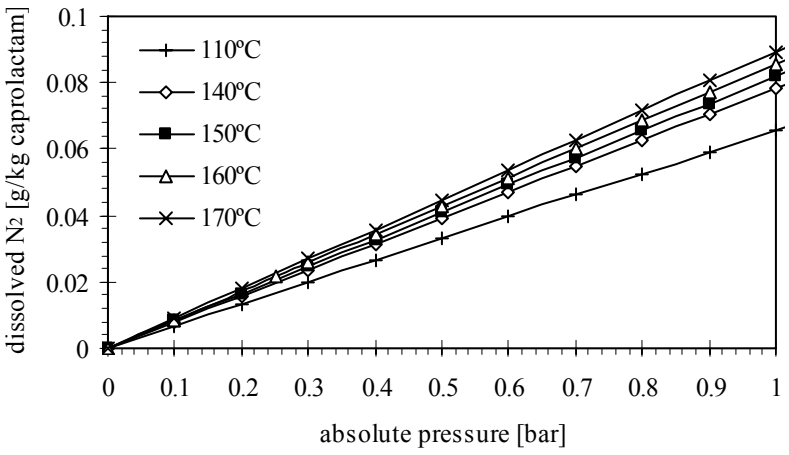

Fig. 6.19: Concentration of nitrogen in caprolactam for various temperatures and pressures.

The volume of nitrogen that is released just after infusion and during polymerization can be calculated using the ideal gas law, see Equation 6.8.

$$v = \frac{n \cdot R \cdot T}{p} \tag{6.8}$$

v = volume of the gas [m^3]

n = amount of gas [mole]

R = gas constant = 8.3143 [$J \cdot K^{-1} \cdot mol^{-1}$]

T = temperature of the gas [K]

p = pressure of the gas [Pa]

Using Equation 6.8, Figure 6.20 is constructed showing the volume of nitrogen that is released during various stages of the process in a heated mould at 160ºC at pressures ranging from 250 to 750 mbar. It can be seen that degassing significantly reduces the volume of nitrogen that is released just after infusion and during polymerization. For the degassed case, the amount of released nitrogen is independent of the polymerization pressure, which is explained by the fact that, although the volume of released nitrogen is larger at a lower pressure (Equation 6.8), a lower pressure also induces more in-mould degassing (Equation 6.7). Whether all nitrogen that is released during polymerization is able to exit the mould is uncertain: during polymerization, the viscosity rises rapidly and nitrogen bubbles can easily get trapped.

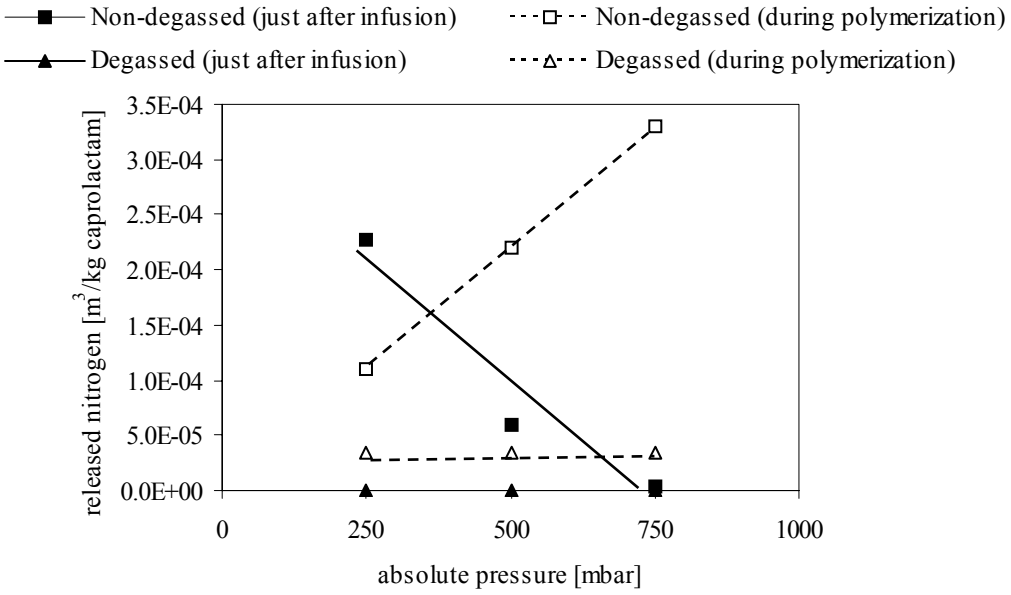

Fig. 6.20: Volume of nitrogen that is released during various stages of the process at a mould temperature of 160ºC.

To assess the effect of degassing, both degassed and non-degassed mixtures were infused in a mould at 160ºC and cured at pressures ranging from 250 to 750 mbar for 30 minutes. Table 6.1 shows the various material properties obtained.
Table 6.1 shows that although degassing does not seem to affect the degree of conversion significantly, an average 5 wt% decrease in crystallinity is obtained. Whereas this would normally lead to an increase in density and modulus, the fact that actually a decrease in density and an equal modulus is found, is caused by the presence of nitrogen-induced voids. Tensile failure of the non-degassed samples before reaching an actual peak value, see Figure 6.21, confirms this, given the fact that voids are a known source for premature mechanical failure. Why degassing reduces the degree of crystallinity is currently unknown: it is possible that the surfaces of nitrogen induced voids act as crystal nuclei or maybe local withdrawal of heat due to evaporation of caprolactam inside the voids results in cold spots that promote crystallization.

Table 6.1: Effect of degassing on APA-6 properties (T_{mould} = 160º).

Polymerization pressure [mbar]	**250**		**500**		**750**	
Degassing procedure*	**D**	**ND**	**D**	**ND**	**D**	**ND**
Degree of conversion [wt%]	96.3	96.4	96.7	96.4	97.2	96.7
Degree of crystallinity [wt%]	36	40	35	40	35	40
Melting point [°C]	216	218	216	218	216	217
Density [g/cm^3]	1.16	1.15	1.16	1.15	1.15	1.14
Tensile properties at 23°C, DAM**:						
Young's Modulus [GPa]	3.2	3.2	3.2	3.2	3.3	3.1
Maximum strength [MPa]	73	66	73	66	74	69
Strain at failure [%]	17	6	24	6	23	15

* D – Degassed, ND – Non-Degassed
** DAM – Dry As Molded

It can be concluded that degassing significantly reduces the volume of nitrogen-induced voids in the polymerized samples and consequently improves the mechanical properties. Once degassed, the polymerization pressure does not have much effect on the polymer properties (Table 6.1), which is in agreement with the previously calculated (equal) amounts of set-free nitrogen for various pressures, see Figure 6.20.

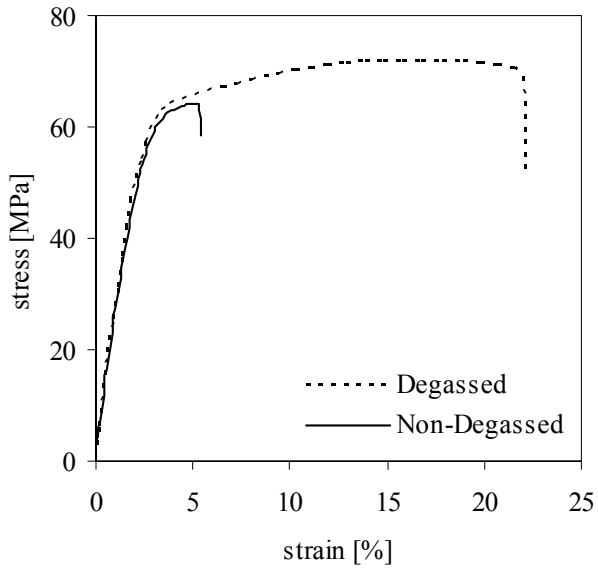

Fig. 6.21: Typical stress-strain curve for the degassed and non-degassed APA-6 polymer (T_{mould} = 160°C, p_{pol} = 500 mbar).

6.6 Conclusions

With respect to each of the key processing parameters, the following is summarized.

The mould temperature

- In general, an increase in mould temperature results in a higher degree of branching and a lower degree of crystallinity. A higher degree of branching is accompanied by a reduction in final conversion, a higher molecular weight and a depression in melting point.
- Branching at low temperatures is caused by de-blocking of the activator, whereas branching at high temperatures is related to monomer depletion.
- A clear difference in morphology exists between crystals formed before the exothermic temperature peak (primary crystallization) and crystals formed upon cooling after the exothermic temperature peak has been reached (secondary crystallization).
- As is the case with all semi-crystalline polymers, the Young's modulus and the maximum strength increase with increasing degree of crystallinity, whereas the elongation at break decreases.

- When at low mould temperatures the crystallization rate becomes too high, caprolactam and reactive chain ends are trapped inside the crystals, which causes the mechanical properties and the overall conversion to be reduced. Caprolactam-infested crystals can be clearly seen as white stains in such samples. A second consequence of the rapid crystallization is the generation of shrinkage-induced voids, which decreases both the density and the mechanical properties.
- The highest mechanical performance is obtained at an optimum temperature at which shrinkage-induced voids are still absent and where the highest amount of caprolactam-free crystals is formed. This optimum mould temperature is not simply a matter of setting the correct mould temperature, but also the heat caused by the exothermic nature of the reaction needs to be taken into account. Due to the latter contribution, the mould geometry, the used resin formulation, and even the type and amount of fibers added become important parameters.

The demolding time

- It was shown that the optimal demolding time is determined by the secondary crystallization process rather than by the polymerization.

The processing pressure

- To prevent boiling of the caprolactam, a minimum processing pressure of 250 mbar was determined.
- Regarding the pressure, it is concluded that, although degassing is essential for improvement of the mechanical properties, once degassed the pressure in the mould only has a marginal effect.

CHAPTER 7

THE POTENTIAL OF ANIONIC POLYAMDE-6 AS MATRIX MATERIAL FOR COMPOSITES: A COMPARATIVE STUDY

7.1 Introduction

In this chapter the potential of anionic polyamide-6 (APA-6) as matrix material for composites is assessed by comparing its mechanical and physical properties with an injection-molding grade PA-6 and an injection-molded PA-6 nanocomposite. These materials have been selected in order to compare APA-6 with traditional and state-of-the-art polyamide-6 technology. Being a semi-crystalline thermoplastic material that is prone to water absorption, both the effect of temperature and moisture absorption on the polymer properties is assessed. It will be demonstrated that differences in the crystal morphology, formed during either reactive or melt processing, have a distinct effect on the polymer performance.

7.2 Experimental

7.2.1 Materials and processing methods

The four polyamides that are compared in this chapter are:

- High crystalline APA-6 (X_c = 42 wt%): polymerized at a mould temperature of 150ºC and a pressure of 900 mbar for 45 minutes using 0.6 mol% HDCL activator and 1.2 mol% MgBrCL initiator. Reactive processing is described in Section 6.2.
- Low crystalline APA-6 (X_c = 37 wt%): polymerized at a mould temperature of 170ºC and a pressure of 900 mbar for 45 minutes using 0.6 mol% HDCL activator and 1.2 mol% MgBrCL initiator. Reactive processing is described in Section 6.2.

- Hydrolytic polyamide-6 (HPA-6): Akulon® K222D, low Mw injection-molding grade hydrolytically polymerized PA-6 from DSM, The Netherlands: M_n = 16000, M_w = 32000 g/mol, T_m = 220ºC. Processing of this material is extensively documented in literature [172].
- HPA-6 nanocomposite: Akulon® K222D nanocomposite, in house extruded nanocomposite containing 10 wt% Somasif® ME-100 clay platelets (Synthetic Mica®) from Co-op Chemicals, Japan. Injection-molding of this material is extensively documented in literature [172].

7.2.2 Analysis methods

Degree of conversion (DOC)

The degree of conversion of the polymer samples was determined according to the method described in Section 5.2.3.

Differential Scanning Calorimetry (DSC)

The degree of crystallinity and melting points of the polymer samples were determined according to the method described in Section 5.2.3.

Density measurements

The density of the polymers was determined according to the method described in Section 6.2.3.

Dynamic Mechanical Analysis (DMA)

A Perkin Elmer Dynamic Mechanical Analyzer 7e was used to measure the loss modulus of a single rectangular polymer sample (25 x 5 x 2 mm) in three-point bending at a frequency of 1Hz with amplitude control of 10 μm. The glass transition temperature (T_g) was determined from the peak in the loss modulus versus temperature curve. Glass transition temperatures were determined for samples, which had been conditioned prior to testing:

- Dry as molded (DAM) samples were dried in a vacuum oven at 50 mbar and 70°C for at least 85 hours before testing.

- Moist samples were conditioned, according to ISO 1110, in a climate chamber (Weiss SB11/300-40) at 70°C and 62% RH (relative humidity) until a constant weight was obtained as was measured using a Mettler AG204 DeltaRange® microbalance. According to the ISO 1110 standards, these conditions lead to equivalent moisture content as when conditioned at 23°C and 50% RH but in a shorter time period.
- Wet samples were conditioned by submersion in demineralized water at 70°C until an equilibrium weight was obtained.

Tensile testing

The tensile test performed according to ISO 527-2 is extensively described in Section 6.2.3. Tests were conducted on samples which had been conditioned similarly to those for the dynamic mechanical analysis described previously.

Water absorption curves

Dry rectangular samples of identical size (40 x 40 x 2 mm) of the same material were placed in a climate chamber with known temperature and humidity. At time t, a single sample was removed from the chamber and the weight (w_t) was determined on a Mettler AG204 DeltaRange® microbalance. Subsequently, the sample was dried for 4 days in a vacuum oven at 70°C prior to weighing (w_d) in order to get the moisture content. After removal of all samples, both weight increase (Δw) and moisture content (mc) curves were constructed using equation 7.1 and 7.2.

$$\Delta w_t = \left(\frac{w_t - w_0}{w_0} \right) \cdot 100\% \qquad (7.1)$$

$$mc_t = \left(\frac{w_t - w_d}{w_d} \right) \cdot 100\% \qquad (7.2)$$

7.3 Comparison of physical properties

Although being essentially the same polymer, the type of polymerization (anionic vs. hydrolytic) and type of processing (reactive vs. melt) results in differences in physical properties, see Table 7.1.

Table 7.1: Physical properties of various polyamides.

	APA-6 (T_{mould}=150ºC)	APA-6 (T_{mould}=170ºC)	HPA-6	HPA-6 nanocomposite
Degree of conversion [wt%]	98	96	100	100
Degree of crystallinity [wt%]	42	37	37	35
Melting point [ºC]	218	213	220	220
Density [g/cm^3]	1.17	1.16	1.12	1.18
Glass transition temp. [ºC]				
Dry as molded	65 (0)*	62 (0)	69 (0)	67 (0)
Conditioned at 70ºC, 62% RH	15 (2.4)	14 (2.9)	14 (2.9)	14 (2.7)
Conditioned at 70ºC, 100% RH	-23 (7.0)	-23 (8.2)	-24 (7.7)	-22 (7.4)

* Values between brackets represent the moisture content [wt%] after conditioning.

After hydrolytic polymerization, unreacted monomer and catalyst residues can be removed from the polymer particles in a subsequent purification step before further processing [146]. In contrast, after reactive processing, purification of large products is not an option. Table 7.1 indeed shows that the degree of conversion of HPA-6 is 100 wt%, whereas APA-6 contains approximately 2-4 wt% monomer.

Anionic polymerization at 170ºC leads to a similar degree of crystallinity as the melt processed HPA-6. This might not be a coincidence, given the fact that the circumstances for crystallization are more or less the same: when cooled down from the melt, crystallization initiates at around 185ºC [146]. Due to the exothermic nature of the reaction, the initial mould temperature of 170ºC is increased by 10 to 20ºC, see Figure 5.9, resulting in the same crystallization temperature for anionic polymerization. In addition, in both cases the polymer chains have already obtained a high molecular weight before they crystallize.

The glass transition temperature, as determined by DMA, is slightly lower for both anionic polymerized materials in dry conditions. This is caused by the fact that residual monomer reduces the amount of hydrogen bonds in the amorphous phase of the polymer in a similar way as water and, consequently, reduces the T_g. Therefore, the higher the conversion, the higher the glass transition temperature. When the materials are moisture conditioned, it is the accumulative effect of residual monomer and absorbed water that determines the amount of hydrogen bonds that are broken. It can be seen that when conditioned, the T_gs are more or less the same for all polyamides.

7.4 Comparison of mechanical properties: effect of temperature

Figures 7.1 to 7.3 show mechanical properties as a function of the environmental temperature. For all polyamides, the gradual reduction in strength and stiffness when crossing the glass transition temperature (62-69°C, see Table 7.1) can be seen.

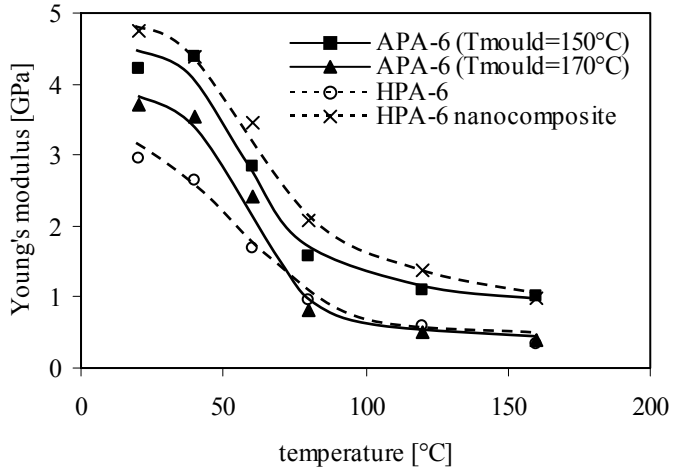

Fig. 7.1: Young's modulus at various temperatures (DAM).

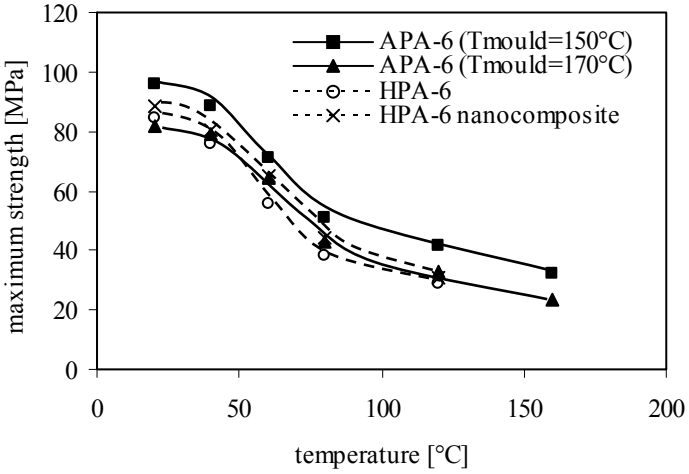

Fig. 7.2: Maximum strength at various temperatures (DAM).

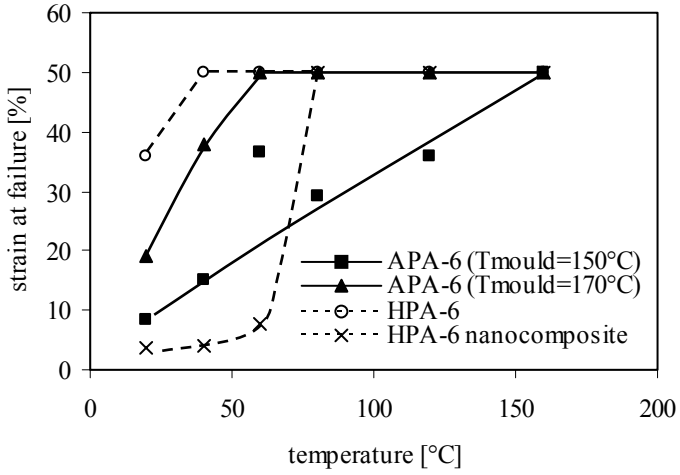

Fig. 7.3: Strain at failure at various temperatures (DAM). (Tests were stopped at a maximum of 50% strain, see paragraph 6.2.3).

As expected, the HPA-6 nanocomposite has the highest modulus. The reinforcing effect of the nano-particles is clear and is explained in [172]. Striking, however, is the performance of APA-6 polymerized at 150˚C: it has a higher maximum strength than the nanocomposite and an almost equal modulus, which is a direct consequence of its morphology as is explained in the next paragraph. Although the modulus and strength of injection molded HPA-6 correspond to typical values found in literature [146], they are by far the lowest, which demonstrates that the type of processing has apparently a strong impact on the mechanical properties of PA-6.

7.4.1 The extremely high modulus of APA-6

In this paragraph an explanation is given for the unusually high modulus of APA-6 using a so-called 'parallel model' as shown in equation 7.3, which shows that the modulus of semi-crystalline polymers can be calculated from the individual moduli of the amorphous and crystalline phase and their respective volume contents.

$$E_{pol} = V_{cr} \cdot E_{cr} + \left(1 - V_{cr}\right) \cdot E_{am} \tag{7.3}$$

in which E_{pol} is the modulus of the semi-crystalline polymer, V_{cr} the volume of the crystalline phase, E_{cr} the modulus of the crystalline phase and E_{am} the modulus of the amorphous phase. The volume of the crystalline phase can be calculated from the degree of crystallinity (X_c) according to equation 7.4, using the densities of the crystalline (ρ_{cr} = 1.24 g/cm^3) and amorphous phase (ρ_{am} = 1.08 g/cm^3).

$$V_{cr} = \frac{X_c / \rho_{cr}}{X_c / \rho_{cr} + (1 - X_c) / \rho_{am}} \tag{7.4}$$

Literature mentions that for melt processed polyamide-6 the modulus of the amorphous phase at room temperature is 2.2 GPa, whereas the crystalline phase has a modulus of 5.25 GPa [173]. The 'parallel model' used to calculate the modulus is commonly known to overestimate the measured values, as is the case for HPA-6, see Table 7.2. However, as the same table shows, the modulus of APA-6 is significantly underestimated. In the next paragraphs two explanations are proposed for the (unusually) high modulus of APA-6.

Table 7.2: Comparison of the calculated and measured Young's modulus for various polyamides.

	Crystal fraction		Young's Modulus [GPa]	
polyamide	**[wt%][1]**	**[v%][2]**	**Calculated[3]**	**Measured**
HPA-6	37	34	3.2	3.0
APA-6 (T_{mould} = 150ºC)	42	39	3.4	4.3
APA-6 (T_{mould} = 170ºC)	37	34	3.2	3.7

[1] measured by DSC
[2] calculated with equation 7.4
[3] calculated with equation 7.3

The first explanation for the extremely high modulus of APA-6 is based on the fact that APA-6 has a higher crystallinity than the value obtained by DSC. From the position of the measured moduli relative to the moduli of the crystalline and amorphous phase of PA-6, see Figure 7.4, one can deduct that the volume of the crystalline phase of APA-6 should be in the order of 69% and 49% when

manufactured at 150ºC and 170ºC respectively, which corresponds to crystallinities of 72% and 53% by weight. The crystallinities obtained by DSC are however significantly lower. A known source for errors when measuring the crystallinity with a DSC is the selection of a proper value for ΔH_{100}, the melting enthalpy of a 100% crystalline polymer (see Equation 5.2). This melting enthalpy is known to be dependent on the lamellar thickness or more precisely on the surface-to-volume ratio of the lamellae: thinner lamellae have a higher surface to volume ratio and have consequently a lower melting enthalpy [32]. Due to its lower processing temperature compared to HPA-6, APA-6 has thinner lamellae (see Equation 6.3), and consequently a lower ΔH_{100}. According to the method used, the crystallinity of APA-6 has indeed been underestimated, which makes the low lamellar thickness of APA-6 a valid explanation for its extremely high modulus.

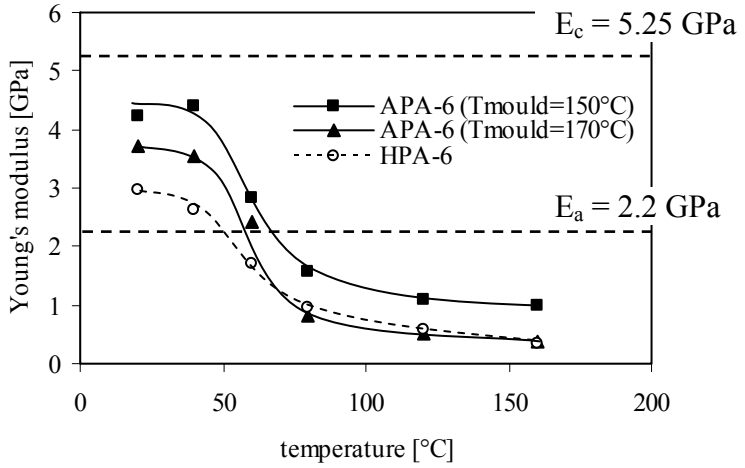

Fig. 7.4: Young's modulus of various polyamides in comparison with the modulus of their amorphous and crystalline regions.

The second explanation for the extremely high modulus of APA-6 is based on the fact that APA-6 has an amorphous phase with a higher modulus than HPA-6. From the high degree of crystallinity and the low lamellar thickness, one can derive that also the amorphous regions of APA-6 are thinner compared to HPA-6, see Figure 7.5. This figure also shows that at the crystalline-amorphous interface a region develops in which the orientation of the polymer chains gradually changes from a random orientation (amorphous bulk) into full alignment inside the crystals. The thickness of

this interface region is not dependent on the size of the amorphous and crystalline regions. However, in a polymer with smaller amorphous regions the interface region occupies a relatively larger volume, which increases the level of orientation and therefore the modulus of the amorphous region.

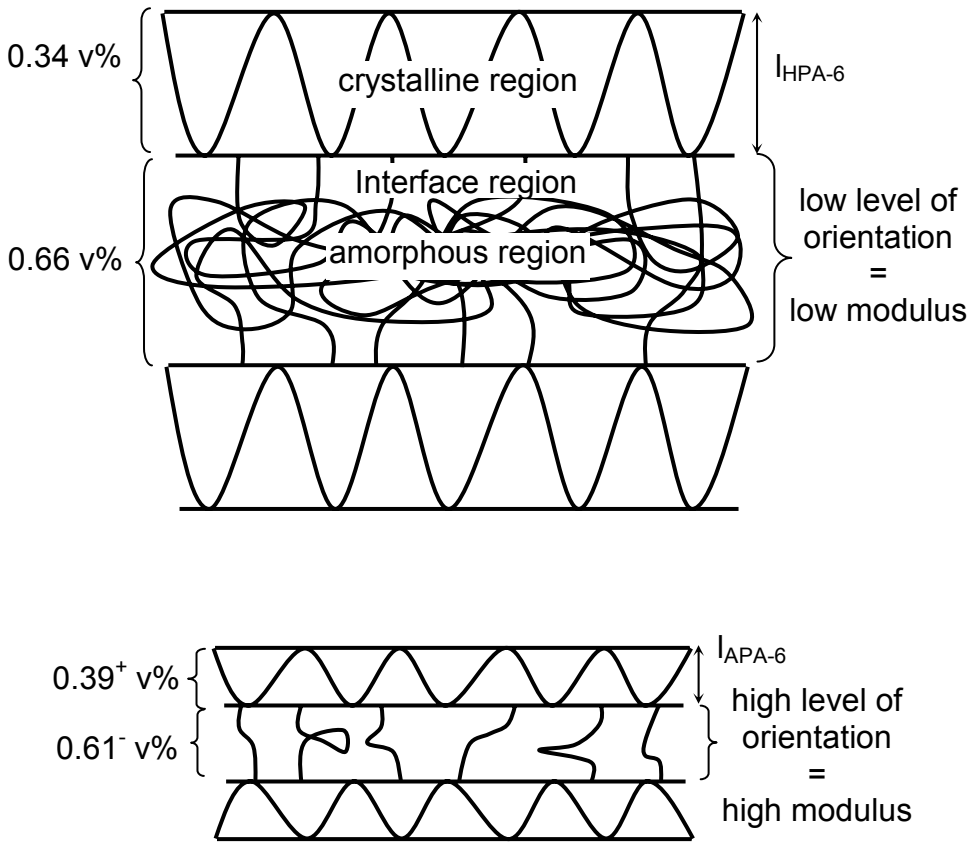

Fig. 7.5: Effect of the lamellar thickness and the degree of crystallinity on the modulus of the amorphous phase in HPA-6 (top) and APA-6 (bottom).

7.5 Influence of moisture conditioning on the polymer properties

First, the effect of moisture conditioning on the physical properties of APA-6 is discussed, as well as the effect of conditioning and subsequent drying. In the next paragraph, a comparison of the mechanical properties of the four polyamides at various moisture contents is made.

7.5.1 The effect of moisture conditioning on the properties of APA-6

The weight increase curve of APA-6 samples polymerized at 150 and 170°C is shown in Figure 7.6 for conditioning at 70°C-62%RH and 70°C-100%RH. The moisture content, obtained by subsequent drying of the same conditioned samples, is given in Figure 7.7.

As expected, since crystals are impenetrable for water, the APA-6 with the largest amorphous phase (T_{pol} = 170°C) absorbs the most moisture, see Figure 7.7. Figure 7.6 shows that when submersed in water the weight of the samples first increases, but that a decrease sets in after a while. Table 7.3 provides two explanations for this decrease:

1. Absorbed water molecules form strong hydrogen bridges with the amorphous polymer phase, consequently substituting residual caprolactam that forms a much weaker bond with the polymer chains. After being released, the monomer diffuses out of the polymer samples. This substitution occurs in a 1:1 molar ratio, but because the molecular weight of caprolactam is more than 6 times that of water the resulting weight decrease is significant: e.g. substitution of 1 wt% of unreacted caprolactam by water leads to a weight reduction of 0.84 wt%.
2. The absorbed water reduces the glass transition temperature, see Table 7.1, which makes the conditioning temperature of 70ºC high enough to induce continued crystallization. As a consequence, the crystalline phase not only grows but also increases its perfection, as becomes clear from the increasing melting point. The amorphous phase, which contains all the absorbed moisture, consequently decreases and water is forced out.

When conditioning at 62%RH for 500 hours, these effects are not encountered because (i) extraction of water-soluble caprolactam from the surface of the sample is not as easy as when it is submersed, and (ii) the amorphous phase only contains a small amount of water and the weight loss induced by continued crystallization is consequently very little.

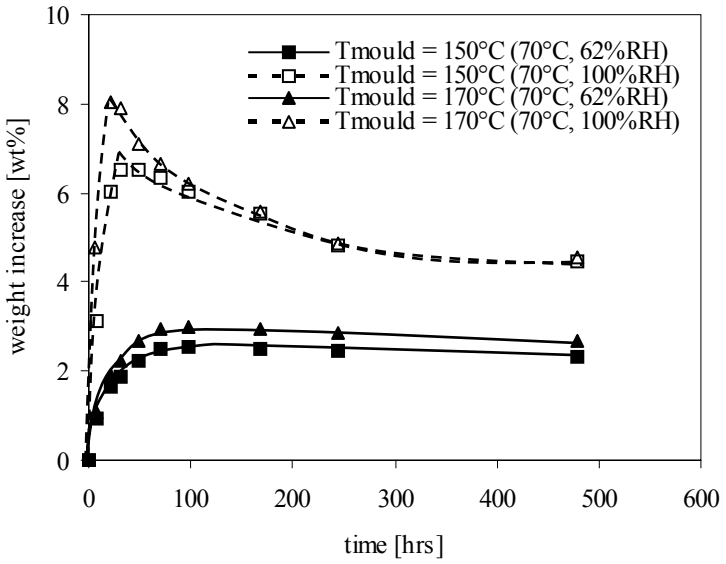

Fig. 7.6: Weight increase during conditioning of APA-6.

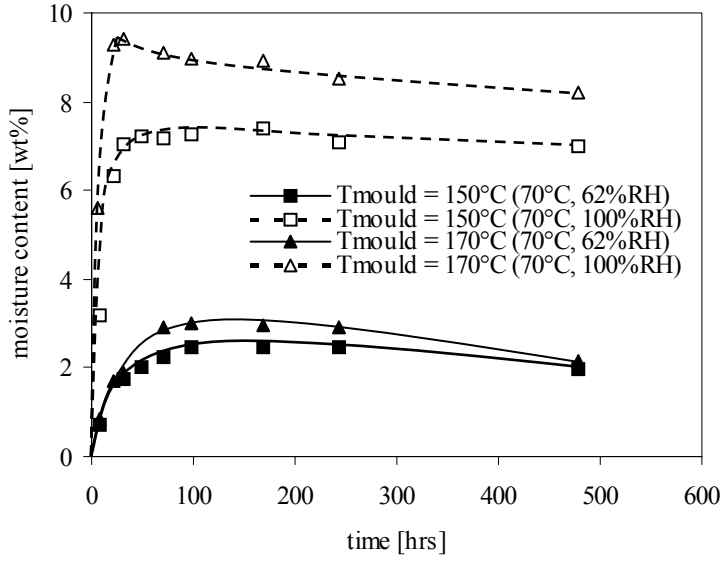

Fig. 7.7: Moisture content during conditioning of APA-6.

Table 7.3: APA-6 properties: before conditioning, and after conditioning for 500 hours and subsequent drying.

	APA-6 (T_{mould} = 150ºC)			APA-6 (T_{mould} = 170ºC)		
Degree of conversion [wt%]	2.0	2.0	0.3	3.6	3.4	0.8
Degree of crystallinity [wt%]	42	46	46	37	38	40
Melting point [ºC]	218	219	221	212	213	215
Density [g/cm^3]	1.16	1.16	1.16	1.16	1.16	1.15
Tensile properties:						
Young's modulus [GPa]	4.2	4.4	4.9	3.7	3.5	4.2
Maximum strength [MPa]	96	103	78	82	81	67
Strain at failure [%]	8.5	4.3	2.3	19	23	2.3
	Before conditioning (dry as molded)	Dried after conditioning at 70ºC-62%RH	Dried after conditioning at 70ºC-100%RH	Before conditioning (dry as molded)	Dried after conditioning at 70ºC-62%RH	Dried after conditioning at 70ºC-100%RH

Table 7.3 also shows the effect of absorption-desorption of water on the mechanical properties. After conditioning the samples, they were subsequently dried prior to tensile testing. It can be seen that conditioning at 70°C-62%RH during 500 hours affects the polymer properties only marginally. It is emphasized, however, that long term effects are still to be tested.

When conditioning at 70°C-100%RH, excessive crystallization, removal of caprolactam and the occurrence of surface cracks (visible for all polyamides tested in this study) cause a significant reduction in maximum strength and strain at failure. Given the fact that submersion at elevated temperatures is usually not an environment to which wind turbines are exposed, the encountered property reduction is therefore not detrimental for application of these materials.

7.5.2 Comparison of mechanical properties: effect of moisture

Figure 7.8, 7.9 and 7.10 show the tensile properties of all polyamides at various moisture contents. At first glance it seems that similar behavior is encountered as for

the dependence of mechanical properties on the temperature. The HPA-6 nanocomposite has the highest modulus for all moisture contents; APA-6 polymerized at 150ºC, however, comes close but has a higher strength. Whereas APA-6 polymerized at 170ºC has a higher modulus compared to HPA-6 in dry circumstances, their stiffness becomes equal when moisture conditioned. Again, this is related to the glass transition temperature: in dry conditions the T_g is higher than the testing temperature, whereas moisture absorption brings the T_g below the testing temperature (Table 7.1).

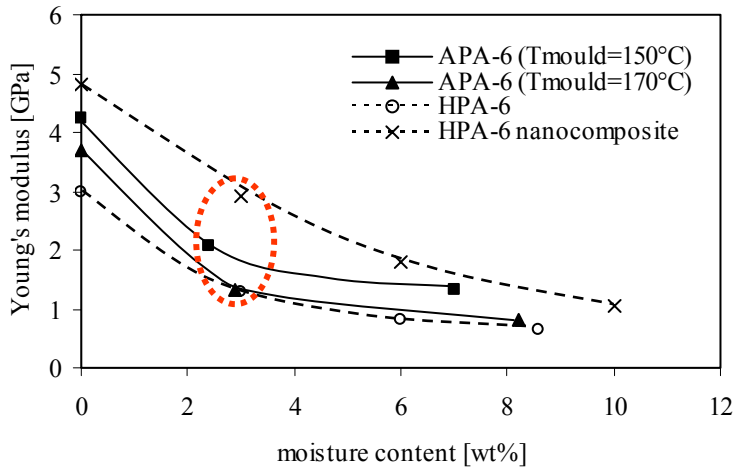

Fig. 7.8: Young's modulus at 23°C for various moisture contents.

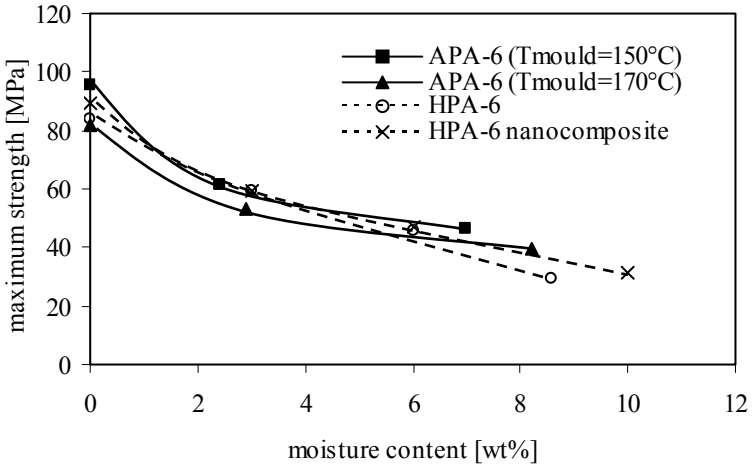

Fig. 7.9: Maximum strength at 23°C for various moisture contents.

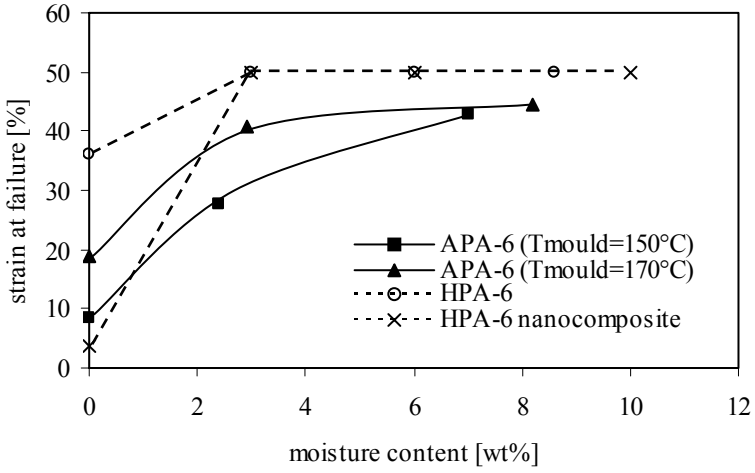

Fig. 7.10: Strain at failure at 23°C for various moisture contents. (Tests were stopped at a maximum of 50% strain, see paragraph 6.2.3).

Striking, however, is the fact that the encircled data-points in Figure 7.8 originate from samples that were all conditioned at 70°C-62%RH. It can be seen that the highly crystalline APA-6 absorbs less moisture and consequently, in the same environmental conditions, a much higher modulus (2.1 vs. 1.3 GPa) is obtained compared to HPA-6.

7.6 Conclusions

The mechanical properties of APA-6 were compared with injection molded neat HPA-6 and a HPA-6 nanocomposite:

- The HPA-6 nanocomposite has the highest modulus over the entire range of temperatures (20-160°C) and moisture contents (0-10 wt%) tested, see Table 7.4. However, highly crystalline APA-6 comes close and has the highest maximum strength due to its characteristic morphology consisting of thin lamellae and highly orientated amorphous regions. Outperforming HPA-6 in terms of modulus and maximum strength, highly crystalline APA-6 is expected to enhance the matrix dominated composite properties like compressive and flexural strength [174-176] in a similar way as is argued for HPA-6 nanocomposites [177], provided that a strong fiber-to-matrix interphase is obtained. APA-6 polymerized at 170°C performs equally as HPA-6.

Table 7.4: Relative property improvement of APA-6 and the HPA-6 nanocomposite compared to HPA-6 at various conditions.

		APA-6 (T_{mould}=150°C)	APA-6 (T_{mould}=170°C)	HPA-6 nanocomposite
23°C-DAM	Young's modulus	+ 41%	+ 23%	+ 60%
	Maximum strength	+ 14%	- 2%	+ 6%
23°C-50%RH*	Young's modulus	+ 59%	+ 1%	+ 125%
	Maximum strength	+ 4%	- 10%	+ 0%
80°C-DAM	Young's modulus	+ 65%	- 14%	+ 116%
	Maximum strength	+ 32%	+ 11%	+ 15%

* Conditioned at 70°C-62%RH

- Compared to the melt processed HPA-6, APA-6 polymerized at 150°C offers a higher modulus at similar temperature, or similar modulus at a higher temperature (40 to 80°C increase). Such an increase in maximum use temperature, related to the heat distortion temperature (HDT), can seriously expand the application field of PA-6 and PA-6 composites.
- For all polyamides, temperature and moisture absorption reduce the modulus and the strength and increase the maximum strain, which is directly related to the glass transition temperature. Whereas with increasing testing temperature at a certain moment the T_g of the dry polymer is exceeded, moisture absorption actually reduces the T_g at a certain point below the testing temperature. The effect of both is in essence however the same.
- The reduced strain at failure of APA-6 polymerized at 150ºC compared to both other polyamides (only 8.5% at 23ºC-DAM) is not a problem for application in composites given the fact that (i) the occurring strains are fiber dominated and are therefore typically less than 1% and (ii) the strain at failure of APA-6 is still significantly higher than of commonly used thermoset resins.
- Retention of mechanical properties of APA-6 after conditioning at 70ºC-62%RH for 500 hours and subsequent drying was demonstrated. Conditioning submersed in water at the same temperature, however, resulted in a brittle material with surface cracks as is common to most polyamides. Continued crystallization and removal of unreacted monomer cause this behavior. Given the fact that submersion at elevated temperatures is usually not an environment to which wind

turbines are exposed, the encountered property reduction is therefore not detrimental for application of APA-6.

CHAPTER 8

VACUUM INFUSED FABRIC REINFORCED ANIONIC POLYAMIDE-6 COMPOSITES

8.1 Introduction

Having pointed out the potential of anionic polyamide-6 (APA-6) as matrix material in Chapter 7, this chapter discusses for the first time the actual manufacturing of APA-6 composites by vacuum infusion. It will be shown that the presence of a large content of fibers in the mould strongly influences the cure of the APA-6 resin as described in Chapter 5 and 6. Section 8.3 deals with thermal interactions between the fibers and the APA-6 matrix, whereas deactivation of the initiator is discussed in Section 8.4. Finally, the effect of the dense fiber fabrics on various mass transport phenomena is explained in Section 8.5. Chemical bond formation between the APA-6 matrix and the glass fibers is explained in more detail in Chapter 9.

8.2 Experimental

8.2.1. Materials

The APA-6 resin material

The caprolactam monomer, hexamethylene-1,6-dicarbamoylcaprolactam activator (HDCL, Brüggolen C20) and caprolactam magnesium bromide initiator (MgBrCL, Brüggolen C1) are described in Section 5.2.1. A resin formulation containing 1.2mol% activator and 1.2mol% initiator relative to the amount of caprolactam was used, see Appendix I.

Glass fabrics

8-harness satin weave E-glass fabrics (SS 0303 050, weave style 7781, 300 gram/m^2, Ten Cate Advanced Composites, Nijverdal, The Netherlands) were used with and without a coupling agent (the sizing or surface finish), see Figure 8.1:

- Finish 8201 – Fabric without coupling agent (unsized fibers).
- Finish 8207 – Fabric with a propriety blend of aminosilane coupling agents (sized fibers).

For better understanding of the chemical interaction between the fibers and the matrix discussed further in this chapter, a short summary of the use of coupling agents is provided next.

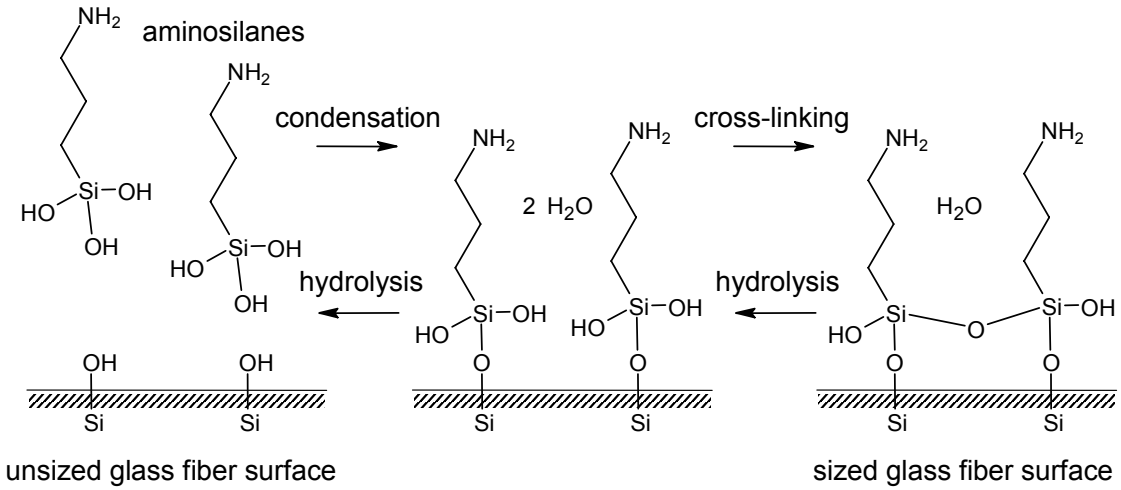

Fig. 8.1: Sizing of glass fibers with aminosilane coupling agents (simplified representation).

In order to improve the interface strength of polyamide glass fiber composites, organo-silicon coupling agents are commonly used [178]. These so-called silanes posses dual or multiple functionality, of which one bonds with the glass surface, see Figure 8.1, whereas the other interacts with the polymer matrix through either primary or secondary bonds. Fabrics with an aminosilane sizing were specifically selected for this research as they can form a strong chemical bond with the anionic polyamide-6

matrix, which is discussed in more detail in Chapter 9. Silanes are usually applied to glass fibers from an aqueous solution, which is called the sizing procedure. The water acts as wetting agent and causes condensation between siloxyl groups of the coupling agent and the glass surface. Condensation between neighboring silanes results in a (partially) cross-linked siloxane network. Figure 8.1 shows that after sizing the fiber surface is covered with a mixture of amino and siloxyl functional groups, of which the mixing ratio depends on the degree of cross-linking.
Although in reality the surface composition of sized glass fibers is more complex than is shown in Figure 8.1, the simplified representation is assumed to be sufficiently realistic enough for use in this thesis:

- Silane coupling agents are not the only ingredient of a fiber sizing, commonly other compounds are added such as for instance a film formers and anti-static agents, which protect the fibers during for instance subsequent weaving [179]. The fabrics used in this research are, however, sized after weaving and the previously mentioned sizing components have already been removed by the manufacturer prior to applying the aminosilanes and are therefore not taken into further consideration.
- Not all silanes form primary bonds with the glass surface and it is very likely that additional silanes react with the siloxyl groups of previously deposited coupling agents forming a multi-layer coating, whereas others remain in the vicinity of the fibers by secondary bonds only [178]. These additional silanes, however, do not chance the fact that after sizing the fiber surface is covered by a mixture of amino and siloxyl functional groups as shown in Figure 8.1.
- For specifically aminosilanes, the pH of the aqueous solution from which the coupling agents are applied determines whether the amino functional group points towards or away from the fiber surface [180, 181]. After subjecting the fabrics used in this research to a ninhydrin test, the purple coloration indicates that the amino groups point outward as shown in Figure 8.1.

8.2.2 Processing methods

The APA-6 resin material was prepared in the mini mixing unit (MMU) as described in Section 5.2.2. After dispensing the reactive mixture in the resin buffer (110°C,

nitrogen protective atmosphere, see Figure 4.8) degassing took place for 5 minutes at 10 mbar. Balanced and symmetrical laminates consisting of 12 plies (25 x 30 cm) of glass fabrics (vacuum bagged and heated as described in Section 4.3.2) were infused at 250 mbar. The composites were allowed to cure for 60 minutes before being demolded to make sure that the composites have reached both their final conversion and crystallinity.

8.2.3 Analysis methods

Degree of conversion (DOC)

Composite samples taken near the resin outlet (unless mentioned differently) were chopped into thin flakes (t < 0.5 mm), weighed (m_{tot}) and refluxed overnight in demineralized water. After drying, samples were weighed again. Whereas the monomer caprolactam dissolves easily in water, the polyamide-6 does not and the resulting reduction in mass can be attributed to the monomer (m_{mon}). Additionally, the fiber weight content was determined in a subsequent step by thermal cleaning at 565ºC followed by cooling in a dessicator prior to weighing (m_f). The degree of conversion (DOC) was determined according to Equation 8.1.

$$DOC = 100 - \frac{m_{mon}}{m_{tot} - m_f} \cdot 100\% \tag{8.1}$$

It has to be noted that together with the residual monomer also water-soluble low molecular weight PA-6 oligomers are washed out of the sample [151]. Although, as a consequence, the abovementioned method cannot be used to calculate the exact degree of conversion, it can determine the fraction of the polymer with load carrying capabilities, which is in fact more useful in the present research. The effect of the sizing (typically less than 0.2% of the fiber weight) on the degree of conversion was found to be negligible.

Differential Scanning Calorimetry (DSC)

A Perkin Elmer Differential Scanning Calorimeter (DSC-7) was used to measure the degree of crystallinity (X_c) and melting point (T_m) of disc shape specimens (∅5 mm, $m_{disc} \approx 50$ mg) that were punctured out of composite panels near the resin outlet

(unless mentioned differently) and dried overnight at 50°C in a vacuum oven. Samples were first held for 2 minutes at 25°C before being heated to 240°C at 10°C/min. Afterwards, the fiber content (m_f) of the disc shape specimen was determined in a Perkin Elmer Thermal Gravimetric Analyzer (TGA-7). Finally, X_c was calculated and corrected for the degree of conversion (DOC, see Equation 8.1) according to Equation 8.2.

$$X_c = \frac{\Delta H_m}{\Delta H_{100}} \cdot \frac{m_{disc}}{m_{disc} - m_f} \cdot \frac{1}{DOC/100} 100\% \tag{8.2}$$

In which ΔH_{100} is the melting enthalpy of fully crystalline PA-6: ΔH_{100} = 190 J/g [56].

Determination of density, void content and fiber content

First, the density of composite samples ($\rho_{c\_measured}$) was determined by displacement according to ASTM D792 (Test Method A) using a Mettler AG204 DeltaRange® microbalance. Prior to testing, all specimens were dried in a vacuum oven at 50 mbar and 70°C for at least 85 hours. Second, the fiber weight content (W_f) was determined by thermal cleaning at 565ºC followed by cooling in a dessicator prior to weighing. The density of the matrix (ρ_m) was calculated from the densities at 23ºC of the monomer (ρ_{mon} = 1.06 g/cm^3), the amorphous phase of the polymer (ρ_{am} = 1.08 g/cm^3) and crystalline phase (ρ_{cr} = 1.24 g/cm^3, α-phase) using the rule of mixtures and the results of previously conducted crystallinity (X_c) and conversion (DOC) measurements, see Equation 8.3 [146, 182]. After calculating the density of the composite ($\rho_{c\_calculated}$) in a similar way according to Equation 8.4, the void content (V_v) was determined with Equation 8.5. The density of the glass fabrics (ρ_f = 2.62 g/cm^3) was provided by the manufacturer.

$$\rho_m = (1 - DOC) \cdot \rho_{mon} + DOC \cdot X_c \cdot \rho_{cr} + DOC \cdot (1 - X_c) \cdot \rho_{am} \tag{8.3}$$

$$\rho_{c\_calculated} = W_f \cdot \rho_f + (1 - W_f) \cdot \rho_m \tag{8.4}$$

$$V_v = \frac{\rho_{c\_calculated} - \rho_{c\_measured}}{\rho_{c\_calculated}} \cdot 100\% \tag{8.5}$$

Short beam shear testing

The short beam shear tests were conducted on a Zwick-Roell Z250 25 ton force machine according to the ASTM D-2344 norm. A three point bending jig equipped with 3mm diameter supports and a 6mm diameter loading nose was adjusted to a span of 11mm to perform tests on rectangular shape specimens (16 x 5.5 x 2.7 mm). A schematic representation of the occurring shear stress distribution is presented in Figure 8.2. From the maximum force (F_m), the inter laminar shear strength (ILSS) was calculated according to Equation 8.6.

$$ILSS = \tau_3 = 0.75\frac{F_m}{w \cdot t} \tag{8.6}$$

in which w and t are the width and thickness of the test specimen. A minimum of 5 specimens (dried at 50ºC and 20mbar for at least 48 hours) was tested.

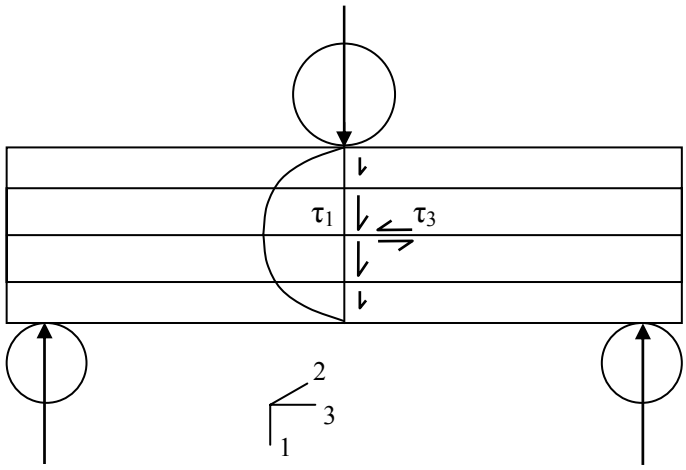

Fig. 8.2: Schematic representation of the shear stress distribution during short beam shear testing.

Microscopy

A Jeol JSM-840 scanning electron microscope (SEM) was used to analyze the fracture surface of composite specimen. Samples were gold covered by a Balzers Union SCD 040 gold sputter coater prior to analysis. For optical microscopy, a Leica DMLM system with CCD camera and Qwin color software was used.

Ultrasonic analysis

An automated Midas C-Scanner was used for ultrasonic single through transmission analysis of infused laminates using water as contact medium. An ultrasonic signal with a center frequency of 10 MHz was transmitted with a small (30%) bandwidth and amplitude with a dynamic range of 82 dB. Scans were performed at a speed of 352 mm/s to obtain images with a grid length of 0.5 mm and a width of 1 mm, which were analyzed using ALIS software.

8.3 Thermal interactions between the fibers and the matrix

In Chapter 6, the polymerization temperature was identified as the most important processing parameter. It was emphasized that this temperature is the accumulative effect of external heating sources (the mould) and the internal generation of heat caused by the exothermic nature of both polymerization and crystallization. One can imagine that the addition of 50 volume percent of glass fibers (≈ 70 wt%) has a significant effect on the heat transfer during infusion and processing, which is explained in this section.

8.3.1 Reduction of the infusion window

As described in Chapter 5, the combination of activator and initiator was specifically selected because it delays the onset of polymerization. Tests on the neat resin showed that depending on the mould temperature the exothermic peak temperature is reached after approximately 10 to 20 minutes, see Figure 5.9. For composites, however, these temperature peaks occur 3 to 5 minutes earlier, see Figure 8.3. Apparently the APA-6 resin reacts faster in the case of composites, which significantly reduces the allowable infusion time compared to processing of unreinforced APA-6 panels. This is explained by the fact that in between the fibers the infused resin heats up much faster, because:

- The fibers inside the mould are already pre-heated.
- The overall conductivity (as obtained by applying the rule of mixtures) of the infused fibers is much higher than of the neat resin, see Table 8.1.

The more fibers are added, the faster the infused resin heats up and the faster polymerization initiates. As a consequence, with increasing (pre-heated) fiber content the infusion window decreases.

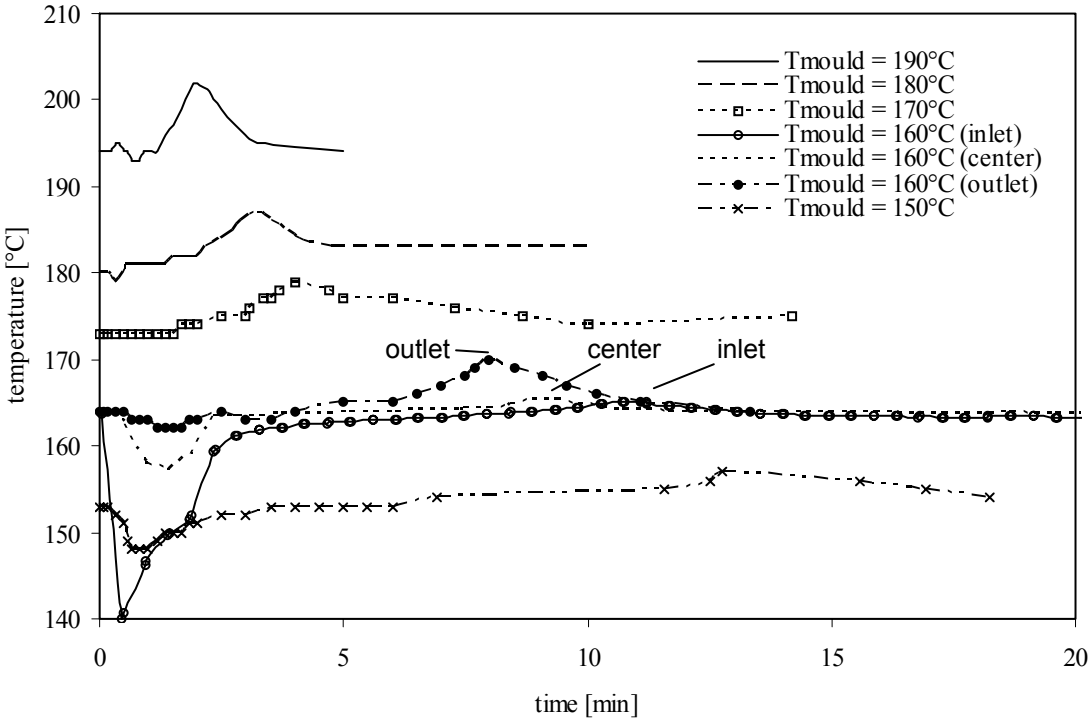

Fig. 8.3: Temperature progression during processing APA-6 composites for various initial mould temperatures. At the start of the infusion: t = 0 s.

Table 8.1: Thermal properties (Source: DSM Fibre Intermediates, The Netherlands and [55]).

Material	Density[1] [kg/m^3]	Conductivity[1] [J/(s· m·°C)]	Specific heat[1] [J/(kg·°C)]	ΔH_{pol} [J/g]	ΔH_{cryst} [J/g]
Caprolactam (l)	950	0.14	2500	-	-
Anionic polyamide-6[1]	1130	0.2	2250	166	144
Glass fiber	2525	1	840	-	-
Composite[2, 3]	1760-1912	0.57-0.6	1670-1545	47	41

[1] Measured at 150°C.
[2] Based on a final conversion of 100 wt% and a final crystallinity of 40 wt%.
[3] Based on a glass fiber volume content of 50 v%, values given for both unreacted and fully reacted matrix.

8.3.2 Occurrence of a temperature gradient in flow direction

Figure 8.3 also shows that a drop in temperature occurs in the laminate right after the infusion has started. This is caused by the fact that the relatively cold resin (110°C) initially cools down the pre-heated fibers. As the resin flows through the fibers it heats up until it has reached the mould temperature after which the temperature in flow direction remains constant. As a consequence, a temperature gradient (from cold to hot) in flow direction is established as can be clearly seen from the infusion conducted at 160°C during which three thermocouples were placed along the flow direction of the resin. Whether the inlet part of the laminate is heated up to the initial mould temperature before the polymerization initiates depends on parameters like the power of the heating system, the material of which the mould is made, the thickness of the laminate, and the type and amount of fibers. Figure 8.3 shows that for the infusion at 160°C the laminate has reached a homogeneous temperature after approximately five minutes. The overall resin temperature during the entire process, however, remains lowest near the inlet, which in combination with the fact that the resin at the outlet has the longest dwelling time in the mould causes polymerization to initiate first at the outlet. Next, a curing front will pass through the composite against the flow direction of the resin: at 160°C the exothermic temperature peak occurs at the outlet after 8 minutes, at the center after 9 minutes and at the inlet only after approximately 11 minutes.

8.3.3 Occurrence of a through-the-thickness temperature gradient

SEM micrographs of the surface of both sides of the composite are presented in Figure 8.4. Whereas the surface that is facing the metal plate is smooth, the surface in contact with the vacuum bag is covered with tiny pinholes, which indicates that a curing front also passes through the composite in thickness direction. Due to the use of spacers on the vacuum bag, see Figure 4.12, heating this side of the composite is less efficient. The surface facing the metal plate heats up more rapidly and consequently polymerization and crystallization initiate on this side. The resin will shrink towards the metal plate, leaving shrinkage holes behind on the opposite side.

The big difference with processing neat APA-6 parts through for instance casting or reaction injection molding (RIM) is the fact that without fiber reinforcement the resin can flow freely throughout the mould, which results in a more homogeneous temperature distribution.

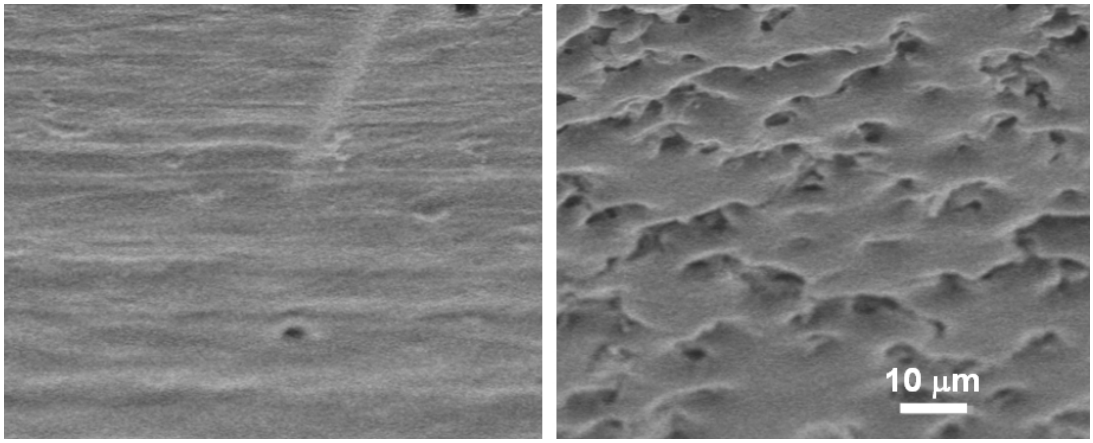

Fig. 8.4: SEM micrographs of the composite surfaces. Left: surface facing the metal plate (smooth), right: surface facing the vacuum bag (pinholes).

8.3.4 Flattening the exothermic peak temperature

Whereas for neat polymer samples the exothermic nature of the reaction causes a temperature rise in the order of 10 to 30°C (depending on the reaction rate and the thickness of the mould, see Section 5.4), Figure 8.3 shows that for the relatively thin composites this is typically less than 5°C. This is caused by the fact that the resin only occupies approximately 30 wt% of the mould cavity and that consequently the overall amount of internally produced heat per unit weight (of the composite) during polymerization (ΔH_{pol}) and crystallization (ΔH_{cryst}) is reduced to less than a third, see Table 8.1. Reduction of the exothermic peak temperature might proof convenient for manufacturing of thick laminates, which can suffer from exotherm-induced degradation of the core. Increasing the fiber content will further reduce the exothermic temperature rise. The reduction of internally produced heat, however, also has an effect on the APA-6 matrix properties as is discussed in the next paragraph.

8.3.5 Effect of the mould temperature on the matrix properties

As explained in Chapter 6, the rate of polymerization and crystallization are adversely affected by temperature, which has the following consequences: if the reaction temperature is too low, crystallization is too fast and reactive chain-ends and monomer are trapped inside crystals before they can polymerize, consequently reducing the final conversion in the APA-6 matrix. If the reaction temperature is too high a lower degree of crystallinity is obtained.
Figure 8.5 and 8.6 show the degree of crystallinity and degree of conversion for APA-6 composites manufactured at various mould temperatures using both sized and unsized fibers. Samples were taken near the outlet of the composites to minimize the effect of thermal gradient in flow direction as described in Section 8.3.2. The corresponding values for unreinforced APA-6 derived in Chapter 6 have been added for comparison.

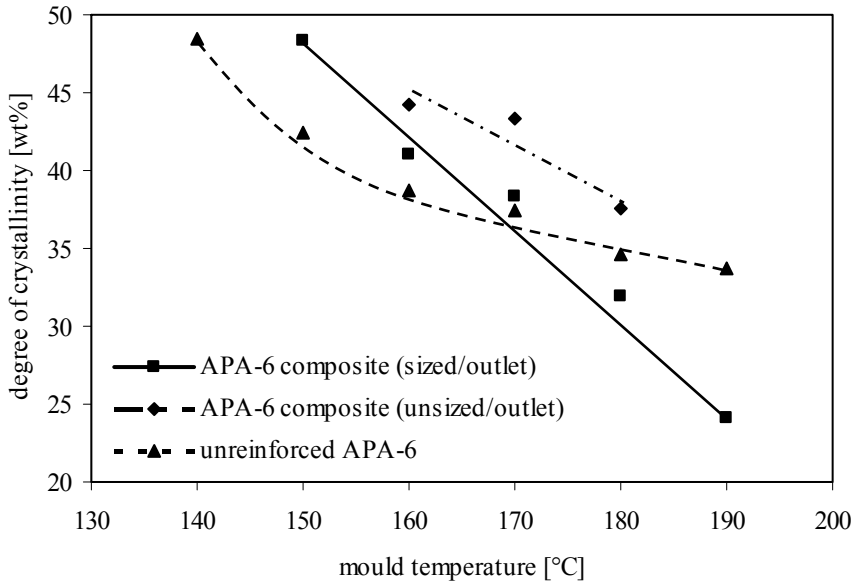

Fig. 8.5: Final degree of crystallinity for neat and reinforced APA-6 for various mould temperatures.

In order to get a polymer with high strength and stiffness, and a good chemical resistance, both a high degree of conversion and crystallinity are required. Because

the effect of the exotherm in the composites is less due to the presence of the fiber reinforcement it is necessary to compensate for the loss in internally produced heat by increasing the mould temperature to avoid entrapment of reactive end-groups in the rapidly growing crystals. It can indeed be seen in Figures 8.5 and 8.6 that the optimum mould temperature for processing of sized fiber composites seems to be 160ºC compared to 150ºC for manufacturing of the neat panels, see Chapter 6. The rather low degree of conversion of the unsized fibers is caused by deactivation of the initiator as is explained in Section 8.4.1.

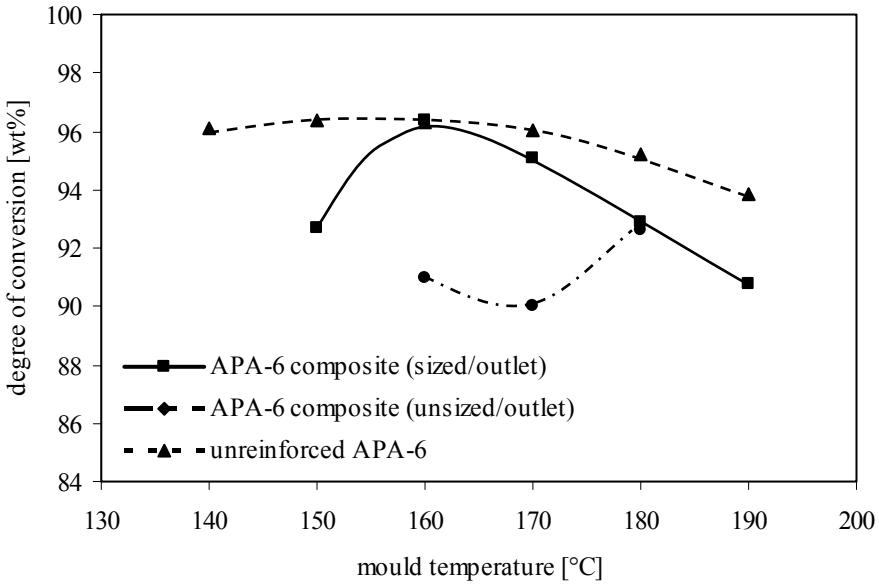

Fig. 8.6: Final degree of conversion for neat panels and reinforced APA-6 for various mould temperatures.

Because of the lower overall polymerization temperature (less internal heat generation), one would expect that at the same mould temperature the composites have a higher degree of crystallinity than the neat resin. Figure 8.5, however, shows that whereas this is true for the unsized composites, for sized composites this is only true for mould temperatures below 170ºC. At higher mould temperatures the crystallinity is significantly lower, which gives reason to believe that interaction of the matrix with the sized fibers makes the formation of crystals increasingly difficult. The much higher inter laminar shear strength (ILSS) of the composites with sized fibers, see Figure 8.7, forms a clear indication that this crystallization reducing interaction

could actually be the formation of fiber-to-matrix bonds, which is discussed in more detail in Chapter 9. The remark is made that due to their low conversion, samples taken from the outlet of the composites made with unsized fibers were unsuitable for mechanical testing. The ILSS values for the unsized fibers shown in Figure 8.7 therefore correspond to samples with a higher conversion, which were taken from the inlet, see also Figure 8.8.

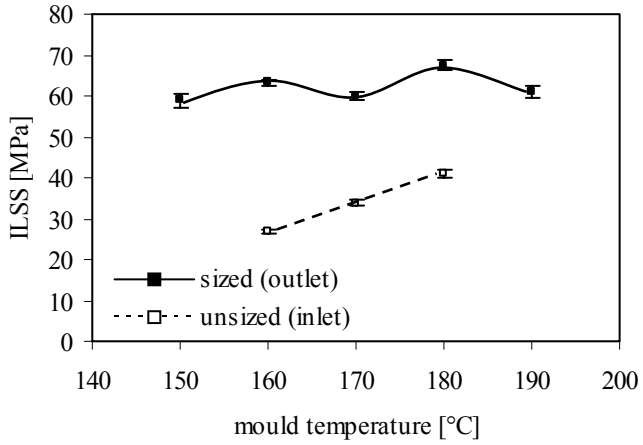

Fig. 8.7: The inter laminar shear strength (ILSS) of composites made with both sized and unsized fibers (dry as molded properties). The error bars indicate the standard deviations.

8.4 Partial deactivation of the initiator due to chemical interactions

Already during the initial experiments described in Section 4.2 it occurred that fibers with an incompatible sizing can deactivate the initiator, consequently reducing the conversion due to initiator depletion. A more detailed discussion on deactivation is presented in this section.

8.4.1 Protonation of anions by acidic siloxyl groups on the glass surface

Figure 8.8 shows that whereas the degree of conversion stays more or less constant for the sized fibers, the unsized fibers cause a strong reduction in flow direction, which is most likely caused by deactivation of the initiator by the acidic hydroxyl groups on

the bare fibers as is shown in Figure 8.9. During deactivation, anions turn into monomer leaving their positively charged cations behind in the vicinity of the (now negatively charged) glass surface. When a silane coupling agent is applied on the glass fibers, the siloxyl groups are partially masked (see Figure 8.1), consequently reducing their deactivating effect.

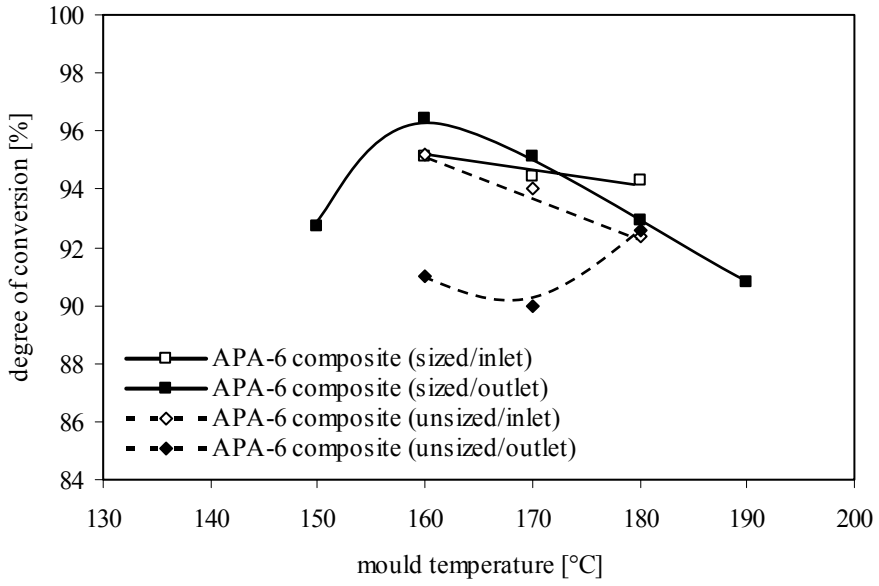

Fig. 8.8: The degree of conversion in flow direction for composites made with both sized and unsized fibers.

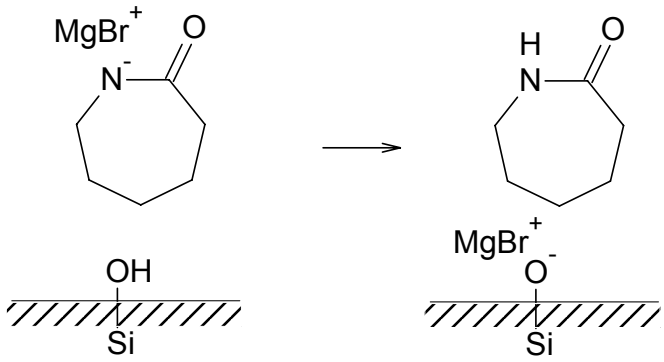

Fig. 8.9: Deactivation of anions by acidic siloxyl groups on the glass fibers.

8.4.2 Deactivation due to moisture on the glass surface

Water being a known source for deactivation of anionic initiators, the hygroscopic nature of the glass fibers (in this case both unsized and sized) is rather unfortunate. Bagged fibers were dried by placing them in between the hot press while already applying vacuum 30 minutes prior to infusion. Additionally, just before infusion, the bagged laminates were flushed with dry nitrogen to remove any residual traces of water. Comparison of laminates that were infused with and without flushing demonstrated that on average due to the nitrogen flush the amount of residual monomer decreases by 8% on average.

8.4.3 Deactivation due to impurities on the glass fabrics

During storage, handling and bagging of the fibers all sorts of organic dust particles from the workshop can get deposited on the fabrics. Depending on their nature they can locally disturb the anionic polymerization during composite processing, leaving a pocket of unreacted monomer behind as can be seen in Figure 8.10. Obviously, such pockets have a detrimental effect on the composite properties. By rinsing the fabrics prior to bagging in an acetone bath a decrease in monomer content of up to 30% on average has been encountered.

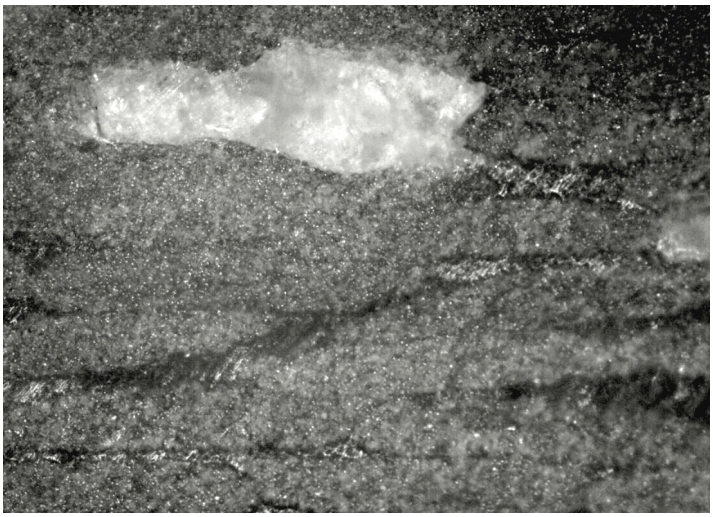

Fig. 8.10: Caprolactam pocket in between the fibers, which indicates local disturbance of the polymerization.

8.5 The effect of the dense fiber fabrics on various mass transport phenomena

Densely woven fabrics strongly restrict the flow of mass inside the mould cavity. In this section the effect on the resin flow and the transport of gasses (caprolactam vapor and nitrogen) during the vacuum infusion process is discussed.

8.5.1 Restriction on the resin flow

The flow of the liquid caprolactam resin through the porous fiber bed is described by Darcy's law [183]. For the case of a 1-dimensional flow this law is written as in Equation 8.7:

$$Q = \frac{A \cdot K \cdot \Delta P}{\eta \cdot L} \tag{8.7}$$

In which Q is the resin consumption rate [m^3/s], A is the cross-sectional area to flow [m^2], K the permeability of the fiber fabrics [m^2], η the viscosity of the resin [Pa·s], ΔP the pressure difference between the resin inlet and the outlet [Pa], and L the flow front progression [m].

Equation 8.7 indeed shows that a more densely woven fabric (lower K value) has a larger restricting effect on the resin flow rate. In contrast, a lower resin viscosity increases the flow rate and consequently reduces infusion times. Because the viscosity of caprolactam decreases at higher temperatures [85], one would expect that at higher mould temperatures the infusion times decrease when keeping all other parameters in Equation 8.7 the same. Figure 8.11, however, shows a different picture: the infusion times go up at higher temperatures, which is most likely caused by the higher reaction rate and the related slight increase in viscosity during the final stage of the infusion. Additionally, Figure 8.11 demonstrates the existence of a large amount of scatter in the infusion times. Homopolymerization of the contents of tank B seems a potential cause as is explained next.

The contents of tank B, which contains the initiator, can slowly start to polymerize without the presence of an activator, see Figure 8.12. Not only the viscosity of the resin increases, but also a layer of polyamide-6 oligomers is deposited on the inside of

tank B over time. Continuous stirring of the filled tanks can cause part of this layer to detach, which causes the caprolactam mixture to turn slightly cloudy during the day.

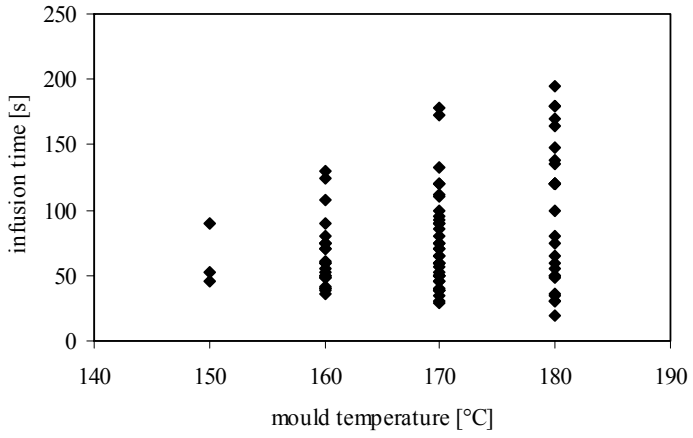

Fig. 8.11: Recorded infusion times at a pressure difference of 250 mbar for various mould temperatures.

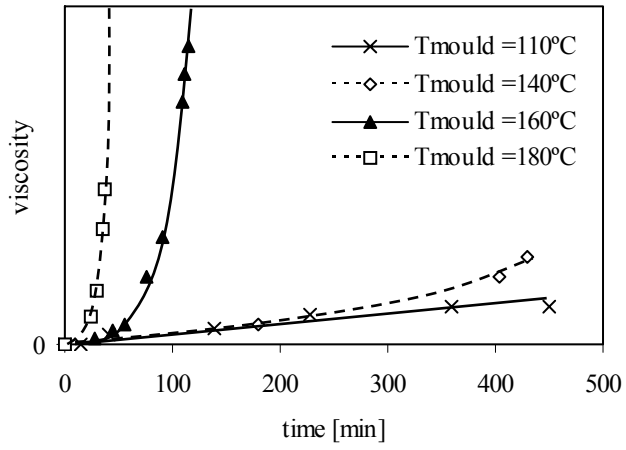

Fig. 8.12: Viscosity increase in tank B of the MMU due to homopolymerization at various temperatures.

Whereas these floating solid particles have only limited effect on cast products as they remain homogeneously distributed throughout the entire process, during vacuum infusion of composites their effect is significant:

1. The particles increase the viscosity of the resin.
2. The particles clog up the fabrics, consequently reducing their permeability.

According to Equation 8.7, homopolymerization should increase the infusion time, of which a clear proof is given by Figure 8.13: composites manufactured within 4 hours after preparing the material in the MMU have significantly shorter infusion times than composites that are infused with resin that has resided for prolonged time in the MMU.

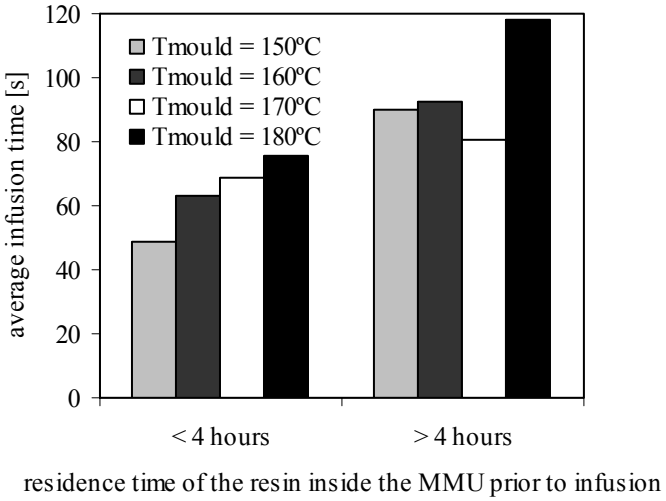

Fig. 8.13: The effect of the residence time of the resin inside the MMU on the infusion time of composites at various mould temperatures.

8.5.2 Restriction on in-mould degassing

In Chapter 6, it was demonstrated that degassing of the MMU tanks for 15 minutes at 100 mbar was sufficient for infusing a void free polymer panel. Table 8.2 shows that for composites the same degassing procedure leads to a void content of approximately 8 v%. As a consequence it is necessary to resort to an alternative degassing procedure, which was used to manufacture all composites discussed in this chapter: degassing in the resin buffer for 5 minutes at 10 mbar. The void content was consequently reduced to about 5 v%. The resulting improvements are clearly visible in the SEM micrographs (Figure 8.14) and the ILSS data presented in Figure 8.15.

Table 8.2: The effect of the degassing procedure on the composite properties.

	Degassed in MMU			Degassed in buffer vessel		
T_{mould} [°C]	Conversion [wt%]	Crystallinity [wt%]	Voids [v%]	Conversion [wt%]	Crystallinity [wt%]	Voids [v%]
150	92	49	9	92	48	2
160	93	44	8	96	41	6
170	92	39	8	95	38	7
180	92	30	8	93	32	2
190	91	23	6	91	24	8

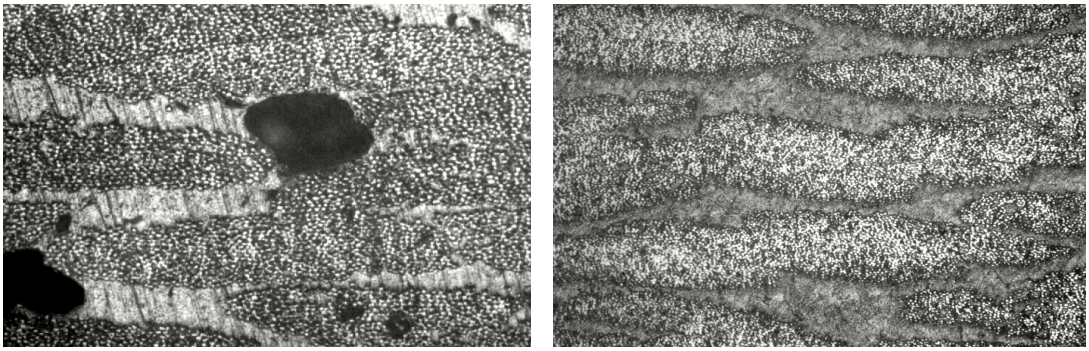

Fig. 8.14: SEM micrographs of composites after degassing in the MMU (left) and after degassing in the buffer vessel (right).

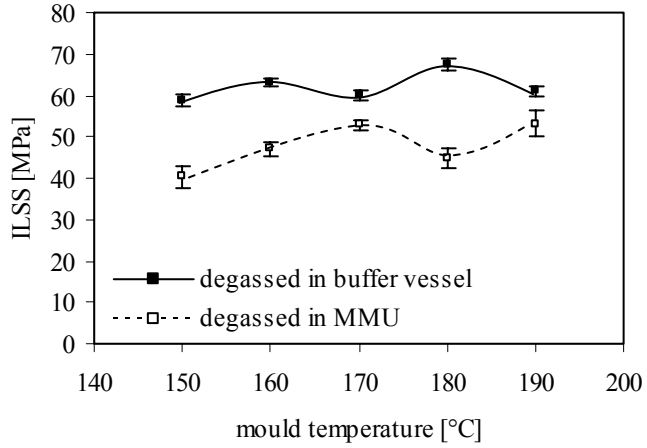

Fig. 8.15: The effect of the degassing procedure on the inter laminar shear strength (ILSS) of the composites. The error bars indicate the standard deviations.

Two explanations are given for the fact that although degassing in the MMU is sufficient for manufacturing void free neat polymer panels, it is insufficient for composite manufacturing:

1. The dense fiber fabrics make transport of gases like caprolactam vapor and nitrogen towards the outlet tube more difficult, significantly reducing so-called in-mould degassing as was explained in Section 6.5.2.
2. The fact that polymerization of infused composites progresses from the outlet towards the inlet, see Section 8.3, indicates that the connection between the mould and the vacuum pump is already blocked by polymer at the outlet, before polymerization initiates near the inlet. As a consequence, nitrogen that is released near the inlet has no means of escape and remains trapped inside the composite. The C-scan image presented in Figure 8.16 confirms that the void content increases towards the inlet.

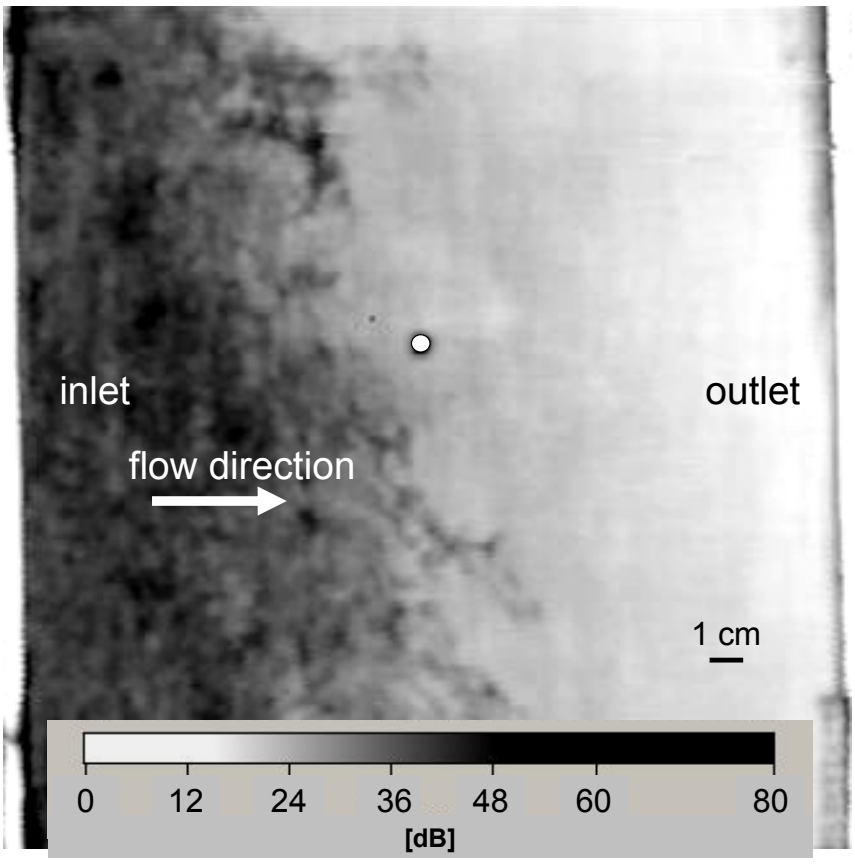

Fig. 8.16: Typical C-scan image of a vacuum infused APA-6 composite: Dark areas represent void-rich areas, whereas the white dot in the center is a reference point used during the scanning procedure.

Although degassing the resin in the buffer vessel yields a significant improvement, a void content of approximately 5 v% is still substantial. Because voids cause an enormous drop in composite properties and durability [184], 1 v% is commonly accepted as the maximum void content for structural applications. In addition to nitrogen-induced voids, literature mentions poor impregnation of the fibers by the extremely low viscosity monomer as a potential source for voids. For anionic polyamide-12 composites manufactured by resin transfer molding (RTM) the void content was reduced from 15 v% to less than 1 v% by balancing the hydrostatic (capillary) and hydrodynamic pressures during infusion, and by continuous resin bleeding through the infused fibers [100].
Because the two hot plates of the press prevent visual inspection of the infusion process, no study could be performed on the progression of the flow front. As a consequence, no attempts were made in improving the flow and impregnation behavior yet.

8.6 Conclusions

This chapter discussed the interactions between the fibers and the matrix during reactive processing of anionic polyamide-6 (APA-6) composites, which are summarized below:

- Due to the addition of pre-heated fibers with a relatively high thermal conductivity, the resin heats up much faster compared to processing of the neat resin, consequently reducing the infusion window.
- Due to infusing a relatively cold resin into the hot mould with pre-placed fibers and the restriction of convection flows by the dense fiber fabrics, a temperature gradient from cold to hot is established just after infusion. As a consequence, not only variations in curing time, but also in material properties exist in flow direction.
- Asymmetrical heating causes a similar through-the-thickness gradient, which results in a composite with a smooth surface on one side and a surface covered with tiny shrinkage holes on the other.
- The fibers significantly reduce the internal heat production due to the exothermic nature of both polymerization and crystallization.

- Interactions between the APA-6 matrix and the aminosilane sizing improves the inter laminar shear strength (ILSS) of the composites, which is further discussed in Chapter 9.
- Acidic siloxyl groups on the glass fiber surface have a deactivating effect on the initiator, as well as moisture and organic dust particles.
- Deposition of an oligomer layer on the tank walls introduces solid particles in the caprolactam resin, which clog up the fiber fabrics during infusion, consequently increasing the infusion time.
- The dense fiber fabrics and the fact that polymerization of infused composites starts at the outlet put severe restrictions on in-mould degassing of nitrogen that is released during polymerization.

Proper adjustment of the vacuum infusion process is necessary in order to anticipate to the abovementioned interactions. With respect to the various processing parameters the following conclusions are drawn:

- Addition of fibers reduces the exothermic heat production, which needs to be compensated for by a higher mould temperature to prevent confinement of reactive chain-ends in the rapidly growing crystals. Whereas for neat polymer panels the optimum mould temperature (for maximum conversion and crystallinity) is 150ºC, for composites this optimum is 160ºC.
- Only sized fibers should be used, as a sizing partially masks the deactivating siloxyl groups at the fiber surface. Additionally, fibers should be thoroughly dried before infusion and care should be taken to keep the fabrics clean during storage and handling.
- Periodic cleaning of the MMU tanks is necessary to prevent the formation of an oligomer layer on the tank walls.
- Because in-mould degassing is severely restricted in composites, it is necessary to subject the resin to a more rigorous degassing procedure prior to infusion. By degassing the caprolactam in the buffer vessel for 5 minutes at 10 mbar the average void content of the final composites was reduced from 8 to 5 v%.

CHAPTER 9

INTERFACIAL BOND FORMATION IN ANIONIC POLYAMIDE-6 GLASS FIBER COMPOSITES

9.1 Introduction

The formation of a chemical bond between the fibers and the APA-6 matrix was already briefly mentioned in Chapter 8 and is discussed in more detail in this chapter. It will be demonstrated that parallels exist with the formation of branch points in the neat APA-6 resin: de-blocking of the activator results in free isocyanate groups, which can form urea links with the aminosilanes on the glass surface, see Chapter 6. The temperature dependence of the interfacial bonding mechanism will be underlined and the effect of an activator with different de-blocking properties and mixtures of different activators is assessed. Finally, it is demonstrated that it is inevitable to compromise between maximizing the matrix properties and maximizing the interfacial bond strength by selecting the proper mould temperature. Also the consequences of this compromise are discussed briefly.

9.2 Experimental

9.2.1. Materials

The APA-6 resin material

The caprolactam monomer, hexamethylene-1,6-dicarbamoylcaprolactam activator (HDCL, Brüggolen C20) and caprolactam magnesium bromide initiator (MgBrCL, Brüggolen C1) are described in Section 5.2.1. The chemical structure of a second activator (toluylene-2,4-dicarbamoylcaprolactam, TDCL) is shown in Figure 9.1. Whereas the aliphatic HDCL activator has a de-blocking temperature of 160ºC, the aromatic TDCL already de-blocks above 125ºC [164]. A resin formulation containing

1.2mol% activator and 1.2mol% initiator relative to the amount of caprolactam was used, see Appendix I.

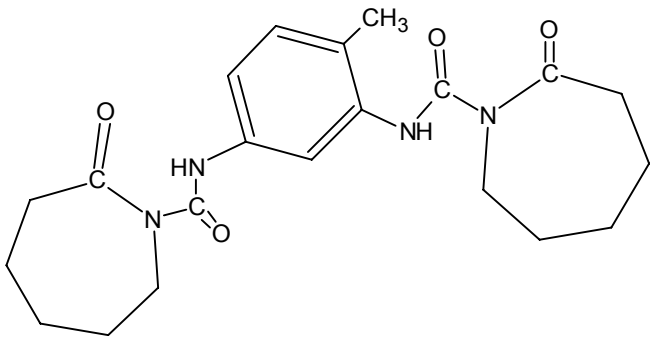

Fig. 9.1: The chemical structure of toluylene-2,4-dicarbamoylcaprolactam (TDCL).

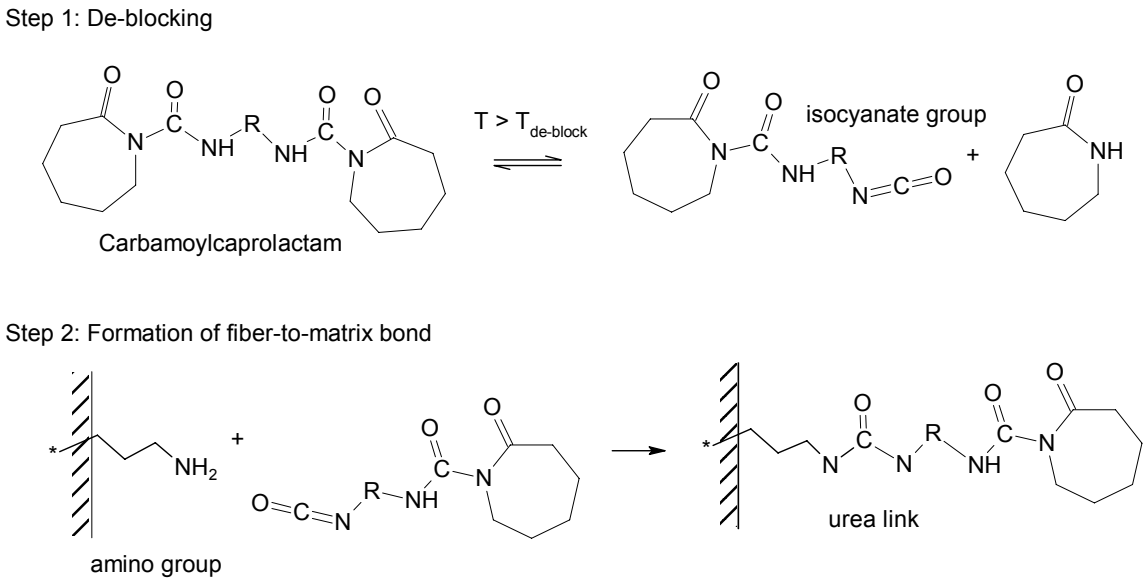

Fig. 9.2: De-blocking of carbamoylcaprolactam (step 1) and the subsequent formation of fiber-to-matrix bonds (step 2).

Glass fabrics

8-harness satin weave E-glass fabrics (SS 0303 050, weave style 7781, 300 gram/m^2, Ten Cate Advanced Composites, Nijverdal, The Netherlands) were used with an aminosilane coupling agent, see Figure 8.1. It is assumed that a chemical bond between the sizing and the APA-6 matrix is formed in a similar way as branching occurs in the neat resin, see Figure 6.4: de-blocking of the carbamoyl activator at temperatures in excess of its de-blocking temperature generates isocyanate groups, which can form urea linkages with the aminosilanes on the glass surface, see Figure 9.2. The fact that isocyanates already rapidly react with amines at temperatures as low as 60 to 80ºC [33], confirms that this reaction with the aminosilanes is likely to occur. Due to the di-functional nature of the activator, initiation of the anionic polymerization of caprolactam is still possible, which causes the polymer chains to grow from the fiber surface ultimately forming an interpenetrating network with the chains in the bulk matrix. In this chapter, the assumed bonding mechanism is verified.

9.2.2 Processing methods

Manufacturing of the APA-6 composites is described in Section 8.2.2.

9.2.3 Analysis methods

Rheology

The viscosity increase during polymerization was measured with a Bohlin V88 concentric cylinder viscometer (speed = 6, spindle type 6) for various resin formulations at various mould temperatures. An experimental setup with nitrogen supply provided a water and oxygen free environment for polymerization, see Figure 4.13. After injection, viscosities were measured continuously up to a value of 1 Pa·s. This value is generally regarded as the upper limit for the infusion window [27].

Degree of conversion

The method to determine the degree of conversion of the composites is described in Section 8.2.3.

Differential Scanning Calorimetry (DSC)

Determination of the degree of crystallinity and melting point of composites is explained in Section 8.2.3

Determination of density, void content and fiber content

Density measurement and subsequent calculation of the void content is described in Section 8.2.3.

Short beam shear testing

The short beam shear test, see Section 8.2.3, was conducted on samples dried in a vacuum oven at 50 mbar and 70°C for at least 85 hours before testing.

Microscopy

The scanning electron microscope (SEM) is described in Section 8.2.3.

9.3 Interfacial bonding with HDCL as activator

The composites manufactured in this section are infused with an APA-6 resin formulation containing a hexamethylene-1,6-dicarbamoylcaprolactam activator (HDCL).

9.3.1 The temperature dependence of the inter laminar shear strength

The inter laminar shear strength (ILSS) of composites (averaged over three laminates) manufactured at various mould temperatures is presented in Figure 9.3. The ILSS of a composite is determined by both mechanical locking and chemical bonding mechanisms between the matrix and the fibers. In the next paragraph, both bonding mechanisms are discussed separately.

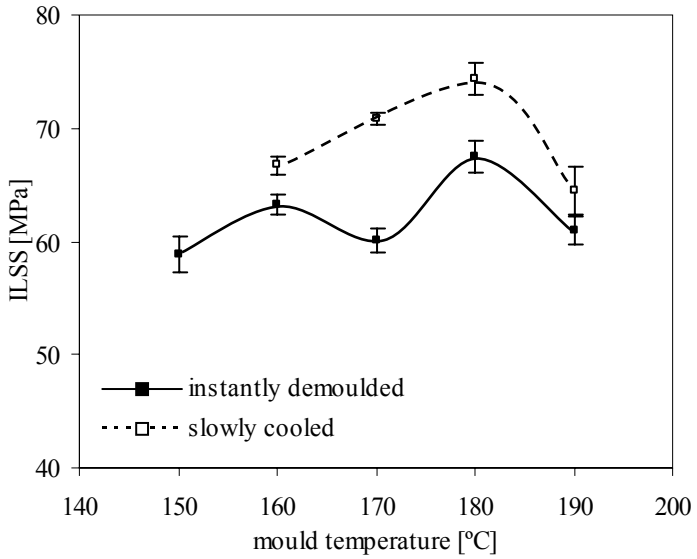

Fig. 9.3: The inter laminar shear strength (ILSS) of composites manufactured at various mould temperatures using HDCL as activator. The error bars indicate the standard deviations.

Mechanical locking

Mechanical locking depends amongst others on shrinkage of the matrix around the fibers and the matrix modulus and is therefore stronger at higher degrees of crystallinity and conversion. Figure 9.4 shows that in terms of conversion and crystallinity the matrix has the best mechanical properties at a mould temperature of 160°C (as is explained in Chapter 8 of this thesis).

Chemical bonding

According to the proposed chemical bonding mechanism in Figure 9.2, the fiber-to-matrix interface should improve at a higher mould temperature:

- Because the equilibrium (step 1, Figure 9.2) shifts to the right with increasing temperature, de-blocking of the activator occurs to a larger extend, which increases the chance of bond formation with the fibers.
- At higher temperatures the chains initiated at the fiber surface can reach longer lengths and interpenetrate with the bulk matrix at a higher level before crystallization 'freezes' the matrix.

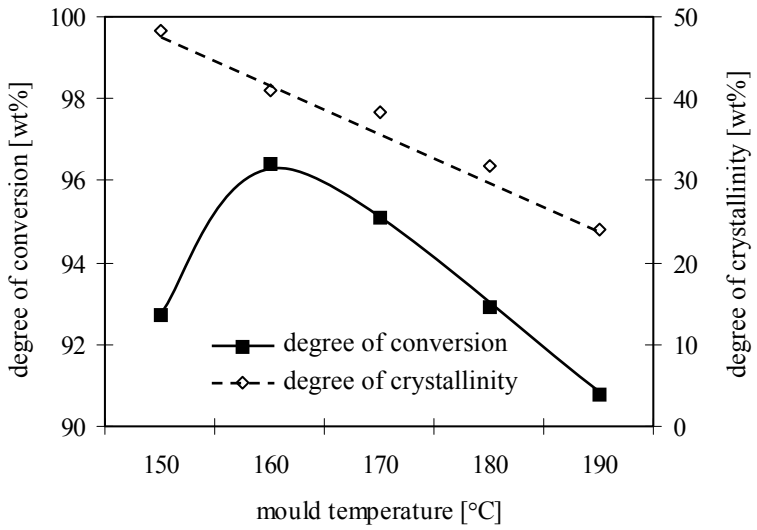

Fig. 9.4: The degree of conversion and crystallinity of the APA-6 composite matrix manufactured at various mould temperatures using HDCL as activator.

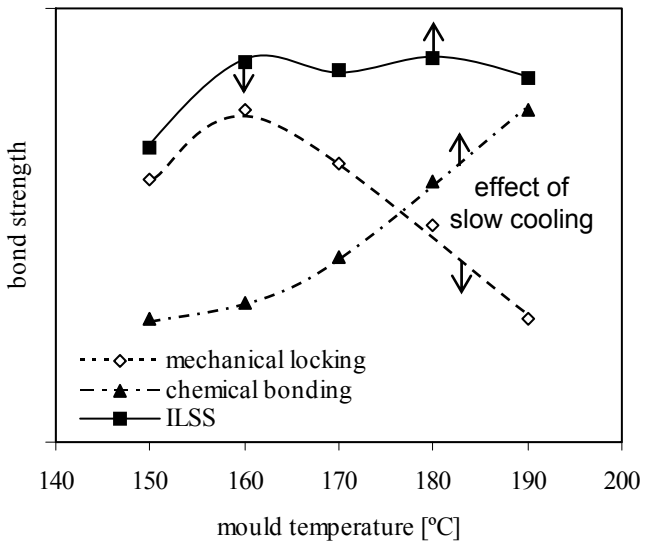

Fig. 9.5: Graphical representation of the assumption that the inter laminar shear strength is the combined effect of mechanical locking and chemical bonding. Arrows represent the effect of slow cooling of the laminates prior to demolding.

Figure 9.5 graphically depicts that when assuming that the ILSS is the combined effect of the mechanical locking strength (with a maximum at 160ºC) and the chemical bond strength (increasing with temperature) a result is obtained, which

corresponds to the experimentally determined values in Figure 9.3. Whereas at low processing temperatures a well-developed matrix is obtained, at higher processing temperatures the chemical bond with the fibers gets stronger, which is confirmed by the different failure modes that occurred during short beam shear testing, see Figure 9.6. The low temperature composite sheared of completely in between the center plies and subsequent surface analysis of the shear crack showed bare fibers, which confirms poor chemical bonding, see Figure 9.7. In the high temperature composites, on the other hand, extensive plastic deformation of the matrix demonstrates that not the interface but the matrix itself forms the weakest link. It seems that compromising between a strong matrix and a strong chemical interface is inevitable and that in the presented case an initial mould temperature of 180°C yields the best composite properties. Compromising, however, is not without consequences, which is further discussed in Section 9.6.

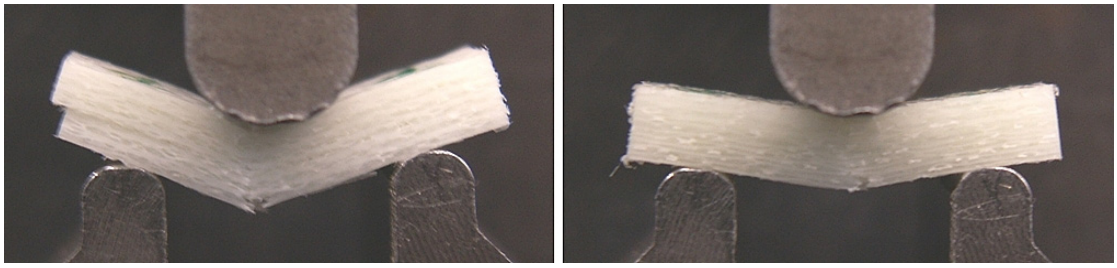

Fig. 9.6: Representative failure modes during short beam shear testing for composites manufactured at 150ºC (left) and manufactured between 160 an 180ºC (right).

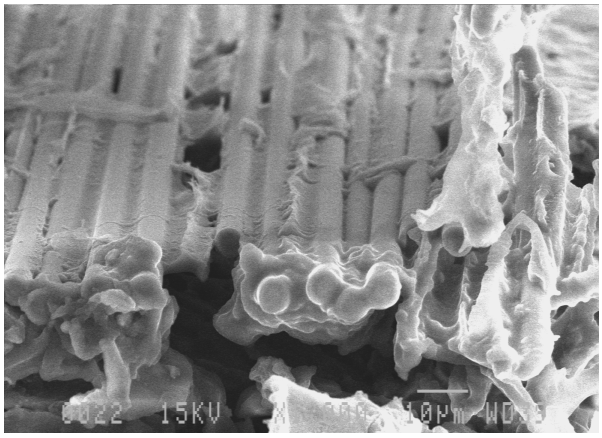

Fig. 9.7: SEM micrograph of the shear crack surface of the composite manufactured at 150°C.

9.3.2 The effect of the cooling rate

It was suggested in Chapter 8 that the formation of interfacial bonds might hinder the formation of crystals in the polymer matrix. To strengthen the mechanical locking of the matrix around the fibers, composites were infused and slowly cooled (-40ºC/hr) prior to demolding, which was expected result in a higher degree of crystallinity [65]. Although, the ILSS of these slowly cooled composites slightly improved, see Figure 9.3, an unexpected decrease in crystallinity was measured, see Table 9.1.
Due to the low cooling rate, the composites are longer subjected to high temperatures. It is assumed that while being exposed to these high temperatures, the number of interfacial bonds (and branch-points in the bulk matrix) keeps increasing. The mobility of the polymer chains is consequently further reduced, which results in a lower degree of crystallinity despite the low cooling rate.
Because the APA-6 matrix has already obtained a high conversion when cooling initiates, it is very unlikely that previously unreacted activator groups remain for bond formation through de-blocking as described earlier. Therefore, additional bond formation during the cooling step has to follow an alternative mechanism. Literature describes that at elevated temperature transamidation reactions occur during anionic polymerization of lactams [46, 48-50, 61]. When transamidation takes place between the polymer and the aminosilanes an interfacial bond is formed, see Figure 9.8, which is one of the commonly accepted mechanisms for interfacial bonding that occurs during melt processing of polyamide composites.
The effect of slow cooling on the ILSS of composites is graphically represented by the arrows in Figure 9.5: whereas the chemical bond strength increases, shrinkage-induced mechanical locking of the fibers decreases.

Table 9.1: Composite properties at various mould temperatures for different cooling rates.

	Degree of conversion [wt%]		Degree of crystallinity [wt%]	
T_{mould} [ºC]	Instantly demolded	Slowly cooled	Instantly demolded	Slowly cooled
150	92	-	48	-
160	96	96	41	41
170	95	92	38	34
180	93	93	32	28
190	91	93	24	27

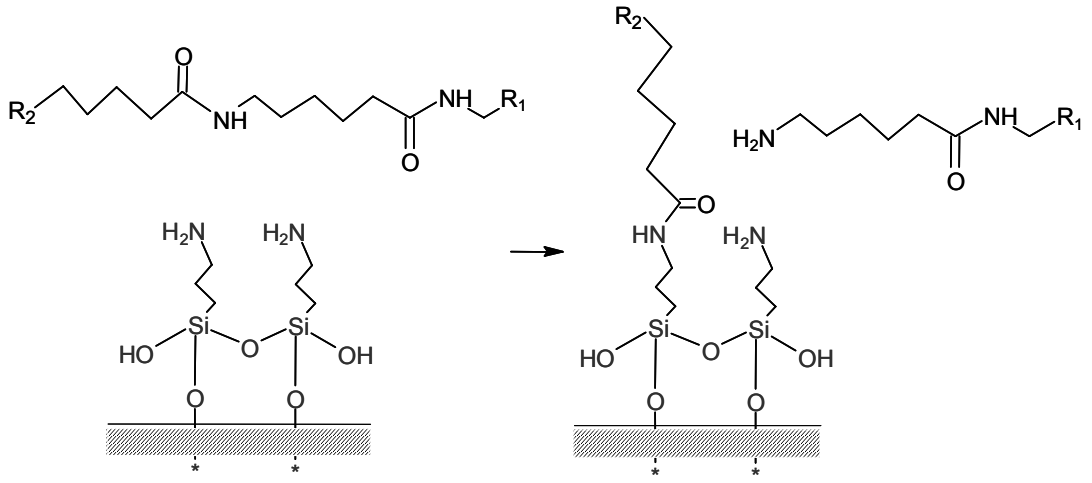

Fig. 9.8: Interaction between the aminosilanes on the glass surface and the APA-6 matrix through transamidation.

9.4 Interfacial bonding with TDCL as activator

In the previous section it was explained that above its de-blocking temperature, the HDCL activator is able to react with the aminosilane sizing on the glass fibers. In this section, the TDCL activator is introduced (toluylene-2,4-dicarbamoylcaprolactam, see Figure 9.1). Whereas the aliphatic HDCL activator has a de-blocking temperature of 160ºC, the aromatic TDCL already de-blocks above 125ºC [164]. It is expected that at the same mould temperature TDCL yields a higher interfacial strength. After comparing the reaction rates of both activators, the properties of composites made with different activators are discussed.

9.4.1 The effect of the TDCL activator on the reaction rate

The reaction rate of both activators was determined for various initial mould temperatures by measuring the rise in viscosity at the initial stage of the polymerization. Figure 9.9 shows that both carbamoyl caprolactam activators result in a long initiation time, which is desired for vacuum infusion as was explained in Chapter 5. It can also be seen that at the same mould temperature the reaction rate of HDCL is higher than of TDCL. This is explained using the following two facts:

1. Both carbamoylcaprolactam activators continuously shift from the blocked configuration into the de-blocked configuration and visa versa according to the equilibrium presented in Figure 9.2 (step 1). Whereas in the de-blocked configuration cross-linking and interfacial bonding can occur, only the blocked configuration can induce chain growth.
2. The larger the difference between the polymerization temperature and the de-blocking temperature of the activator, the further the equilibrium (Figure 9.2, step 1) shifts towards the de-blocked configuration.

The de-blocking temperature of TDCL (125ºC) is 35 degrees lower than of HDCL (160ºC). Therefore, at the same mould temperature, the formulation with the HDCL activator contains more blocked activator groups that can induce chain growth and consequently the reaction rate of HDCL is higher. It can be concluded that with TDCL a wider infusion window is obtained, which allows infusion of even larger composite parts.

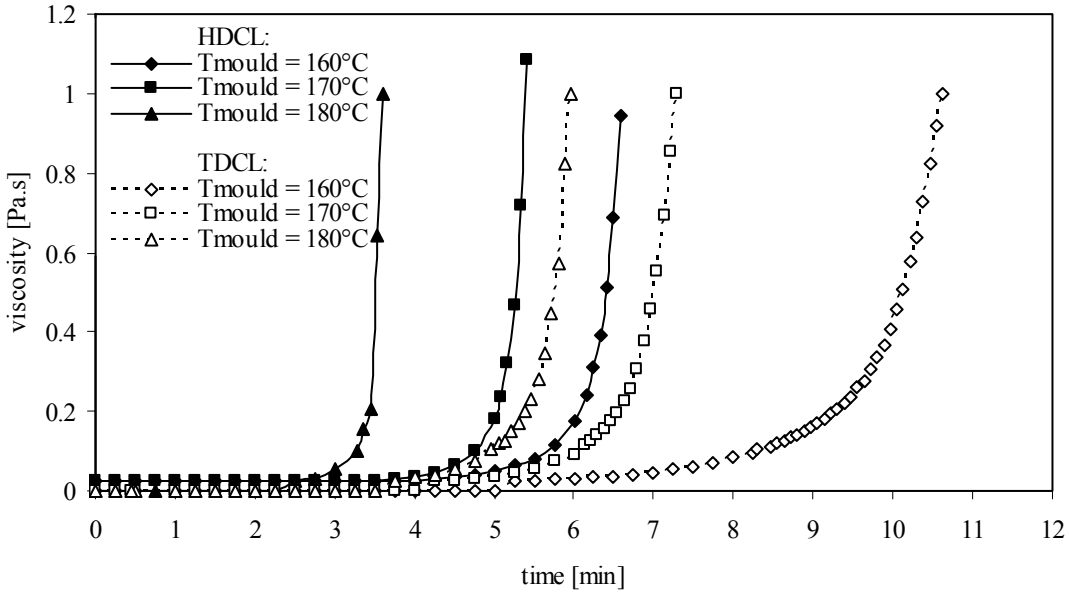

Fig. 9.9: Viscosity increase during polymerization at various mould temperatures for two types of activators: HDCL and TDCL. Both resin formulations contain 1.2 mol% activator and 1.2 mol% initiator.

9.4.2 The effect of the TDCL activator on the composite properties

Two types of infusion strategies are discussed:

- Non-isothermal infusion: the relatively cold reactive mixture (110ºC) is infused in a preheated fiber pre-form (150-190ºC).
- Isothermal infusion: the reactive mixture is infused in a fiber pre-form of equal temperature (110ºC) after which the fibers and the infused resin are jointly heated to the final polymerization temperature (160-180ºC).

9.4.2.1 Non-isothermal infusion

Whereas the composites infused with the HDCL activator have a homogeneous appearance, a gradient in flow direction is visible in the ones made with TDCL: at the inlet the matrix seems more transparent and glossy, whereas towards the resin outlet the matrix becomes increasingly matte white. In addition to this visual gradient a remarkable difference in inter laminar shear strength (ILSS) was found between the inlet region and the outlet region of the laminate (up to 27% at a mould temperature of 170ºC), see Figure 9.10. In Chapter 8, a thermal gradient from cold to hot in flow direction was identified. Based on the fact that the previously discussed de-blocking mechanism leads to a higher interfacial strength at higher temperatures, this thermal gradient cannot explain the decrease in ILSS in flow direction. Alternatively, it is assumed that the fibers filter out the TDCL activator groups during infusion: despite the relative cold temperature of the resin prior to infusion (110ºC), the preheated fibers prevent the temperature in the laminate during infusion from dropping below 140ºC (see Figure 8.3), which is above the de-blocking temperature of the TDCL activator ($T_{de\text{-}block}$=125ºC). It is plausible that de-blocked TDCL already bonds to the amino groups on the glass surface during infusion, hence causing a gradual reduction in activator concentration in flow direction. Not only the number of bonds that can be formed reduces in flow direction, also the reaction rate decreases due to activator depletion. Whereas the former causes a drop in ILSS, the latter results in an increasingly white appearance of the composites near the resin outlet due to the formation of caprolactam infested crystals, see Section 6.3.5. Whereas the lack of activator results in a low conversion near the outlet, the surplus in activator causes the same near the inlet due to extensive oligomer formation [151], see Figure 9.11.

The potential of TDCL for improving the interfacial bond strength of APA-6 composites becomes clear from the fact that at 170 and 180ºC the ILSS at the inlet is significantly higher than of composites made with HDCL at a lower degree of conversion and almost equal degree of crystallinity (31 vs. 32 wt%). Unfortunately, non-isothermal infusion leads to a strong decay in properties in flow direction due to filtration of the activator. Isothermal infusion is discussed as an alternative processing method in the next section.

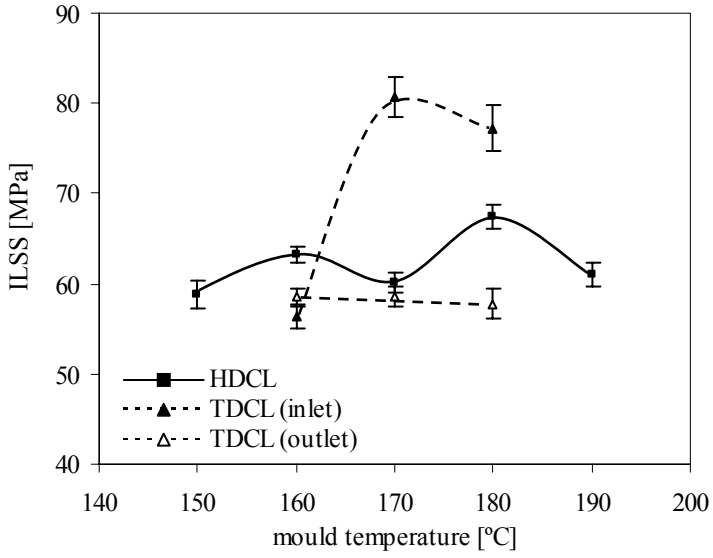

Fig. 9.10: Inter laminar shear strength (dry as molded) for different activators at various mould temperatures. The error bars indicate the standard deviations.

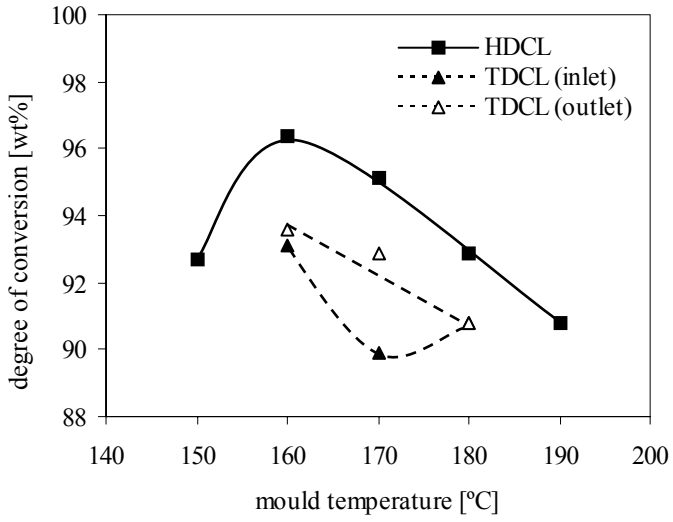

Fig. 9.11: Degree of conversion for different activators at various mould temperatures.

9.4.2.2 Isothermal infusion

In order to prevent the occurrence of a gradient in flow direction due to bond formation between the de-blocked activator and the fibers during infusion, the mould temperature is reduced to 110ºC, which keeps the temperature during the entire infusion well below the de-blocking temperature of both activators. After infusion, the temperature of the mould is increased by 10ºC per minute to the final polymerization temperature (160-180ºC). The additional advantage of this infusion strategy is that without initiation of polymerization the infusion window at 110ºC is more or less infinite, which allows manufacturing of infinitely large composite parts.

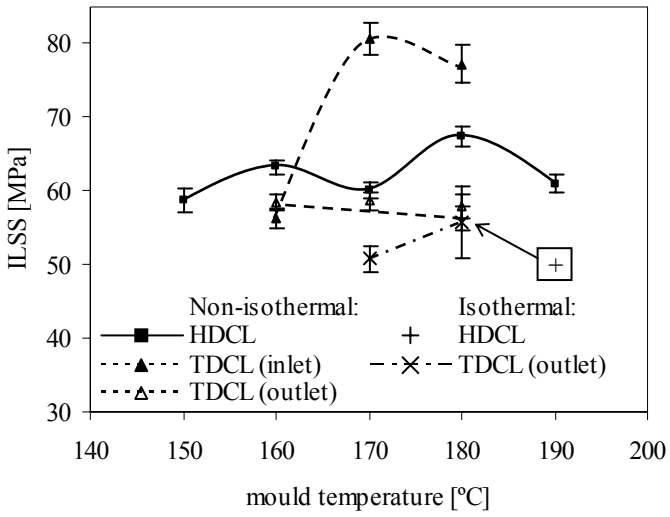

Fig. 9.12: Inter laminar shear strength (dry as molded) for different activators at various mould temperatures: isothermal vs. non-isothermal infusion. The error bars indicate the standard deviations.

Although gradients were indeed no longer visible, the ILSS of the isothermally infused composites is disappointingly low for both activators, see Figure 9.12. It is feared that the heating rate after infusion is not sufficiently high to shift the de-blocking equilibrium (Figure 9.2, step 1) to the de-blocked side before the first anions react with the activator. Surely, after a single monomer addition, continued polymerization is inevitable consequently eliminating the possibility of linking to one of the amino groups on the fiber surface. The higher conversion of the isothermally infused composites underlines this hypothesis given the fact that without bonding to

the fibers the polymerization suffers less from activator depletion, see Figure 9.13. Due to the limited heating rate of the equipment, isothermal infusion of composites is currently not feasible.

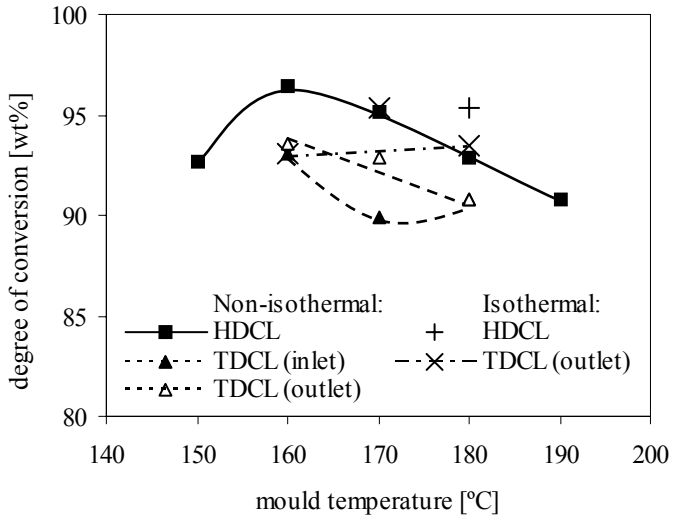

Fig. 9.13: Degree of conversion for different activators at various mould temperatures: isothermal vs. non-isothermal infusion.

9.5 Interfacial bonding with resin formulations containing both activators

Despite its potential of easier bonding to the glass surface, the previous section demonstrated that using only TDCL as activator for reactive processing of APA-6 composites does not lead to desirable results yet. Therefore, this section explores the option of mixing the HDCL and TDCL activators in a single resin formulation. The idea is to add a small amount of TDCL (0.3mol% or 0.6 mol% with respect to the monomer) as 'bonding agent' to a HDCL resin formulation (1.2 mol% with respect to the monomer, together with 1.2mol% initiator).
Figure 9.14, however, shows that the addition of the 'bonding agent' has an adverse effect: the more TDCL is added, the lower the ILSS values. Figure 9.9 provides a quick explanation: compared to HDCL, TDCL initiates polymerization approximately 2 to 4 minutes later. When mixing activators, the first chains will grow from the

HDCL activator and given the fast rate of polymerization, all monomer will be consumed before TDCL becomes an active site for chain growth. Therefore in composites, TDCL will bond with the amino groups on the fiber surface without contributing to the formation of an interpenetrating network, see Figure 9.15. Only HDCL that is capable of reacting with an amino group not yet blocked by a TDCL molecule can initiate chain growth from the fiber surface. When adding more TDCL, less amino groups remain available for bond formation with the HDCL activator and consequently the ILSS reduces.

It is concluded that mixing of activators with different initiation times (de-blocking temperatures) has a negative effect on the ILSS of APA-6 composites.

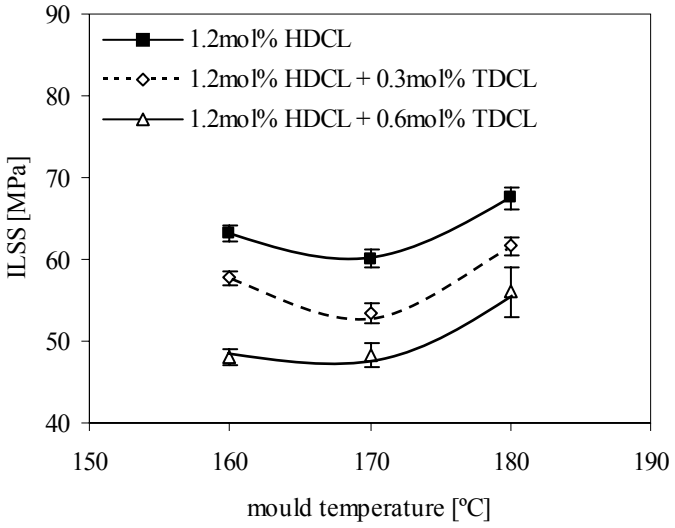

Fig. 9.14: Inter laminar shear strength (dry as molded) for different activator mixtures at various mould temperatures. The error bars indicate the standard deviations.

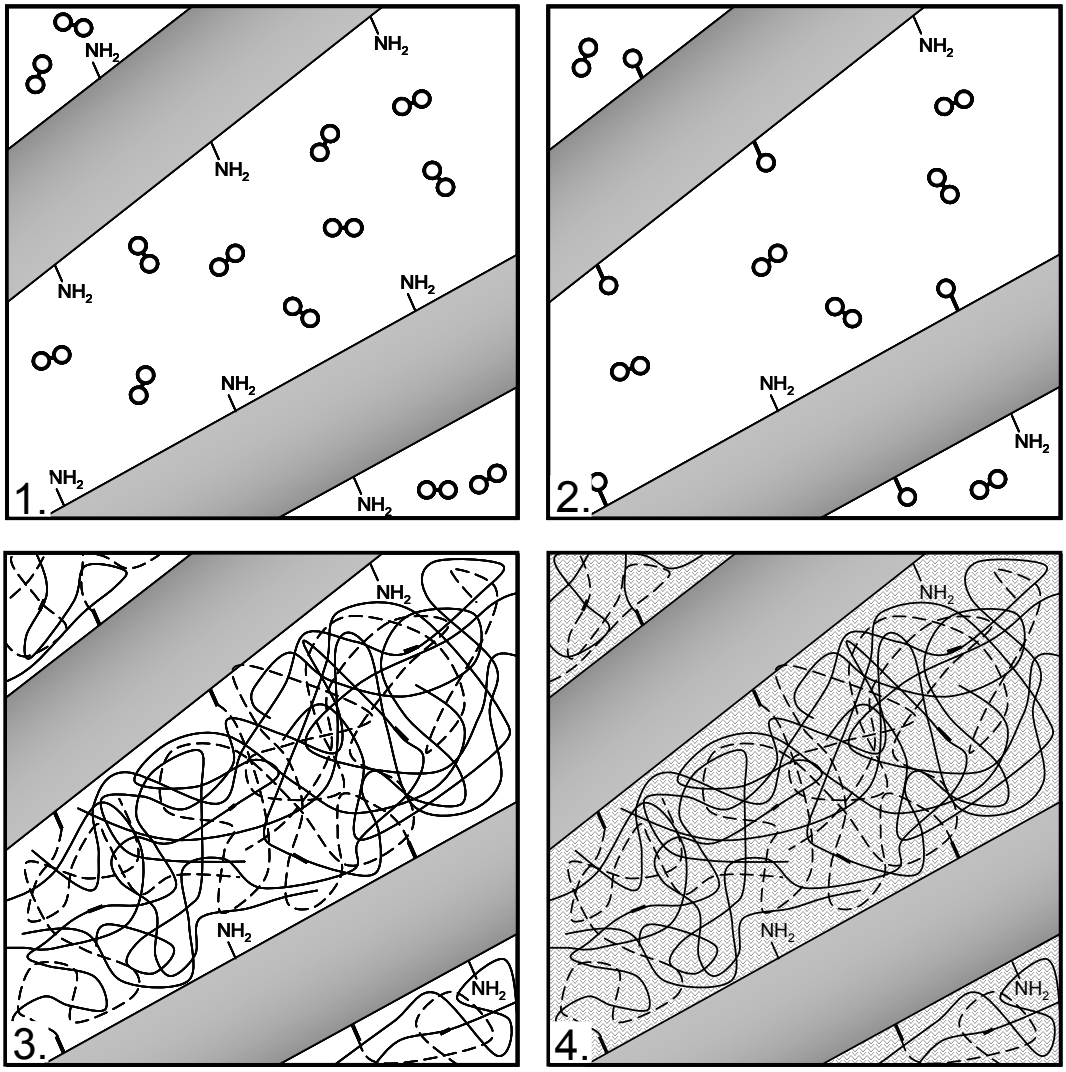

Formation of a strong interpenetrating network when using a single type of activator.

(Figure continued on the next page)

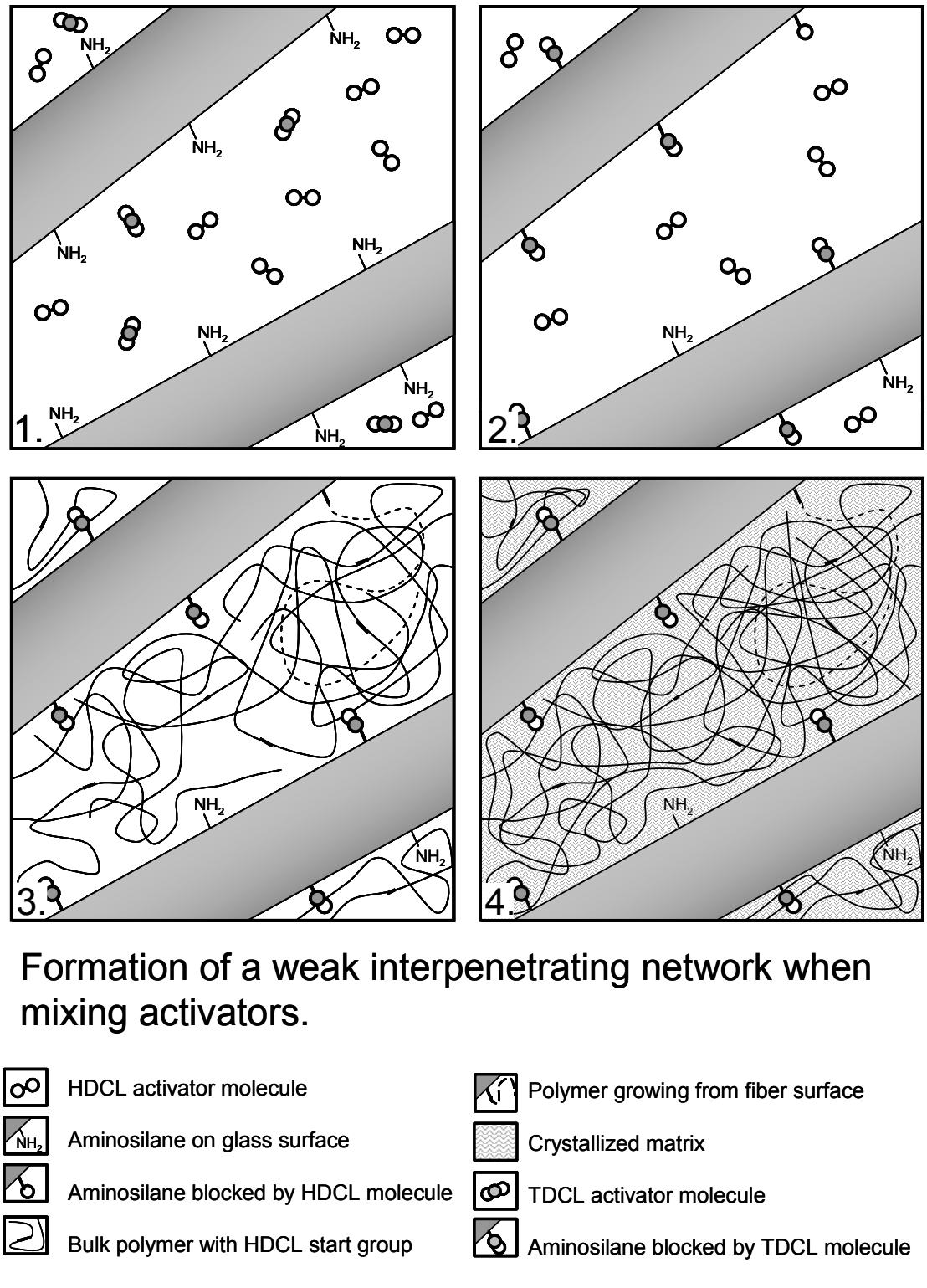

(Figure continued on the previous page)

Fig. 9.15: The effect of mixing activators on the formation of an interpenetrating polymer network: 1 – the situation just after infusion, 2 – interfacial bonding, 3 – polymerization, 4 – crystallization.

9.6 The effect of interfacial bond formation on the bulk matrix

As was mentioned earlier, the formation of interfacial bonds seems to put a restriction on the mobility of the polymer chains, which disturbs the crystallization process in such way that it reduces the degree of crystallinity of the composites. This interaction has a significant effect on the void content and the composite properties when moisture conditioned as will be discussed next.

9.6.1 The void content of composites

Because the crystalline phase has a higher density than the amorphous phase (1.24 vs. 1.08 g/cm^3 [146, 182]), crystallization-induced resin shrinkage is inevitable, which is a common source for voids in composites. Therefore, a stronger interface not only reduces the degree of crystallinity but also the void content. Figure 9.16 indeed shows that a linear relation exists between the ILSS of the composites (which was previously linked to the formation of interfacial bonds) and the void content.

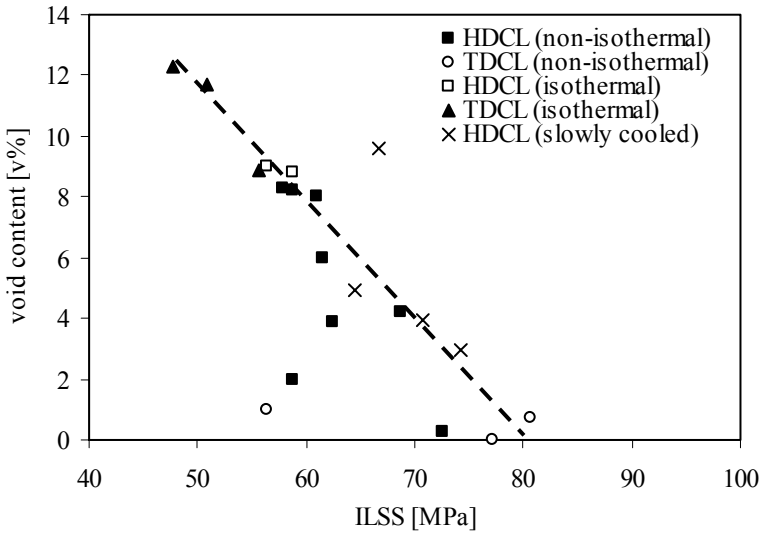

Fig. 9.16: The linear relation between the inter laminar shear strength (ILSS) and the void content of composites.

As was explained in Chapter 8, the existence of a thermal gradient during infusion causes the number of interfacial bonds to increase in flow direction. The C-scan image presented in Figure 8.16 shows that also the void content decreases in flow direction, which confirms the previously explained relation between interfacial bonding and the void content of composites.

9.6.2 The moisture conditioned properties of composites

Whereas the amorphous phase of APA-6 is capable of absorbing a vast amount of water, the crystalline phase cannot and, therefore, a higher the degree of crystallinity reduces the total amount of moisture that is absorbed by the matrix. Because water acts as a plasticizer for PA-6, a high degree of crystallinity is beneficial for retaining strength and stiffness in humid conditions, see Section 7.5.

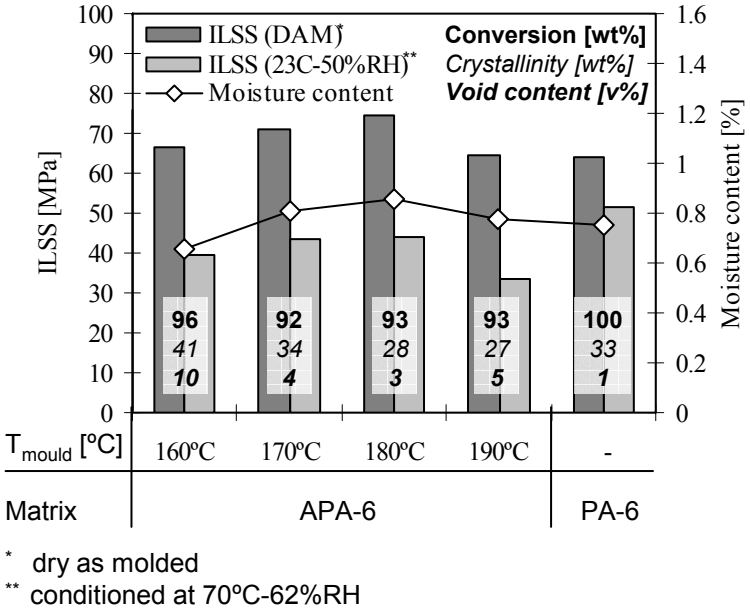

Fig. 9.17: The effect of moisture conditioning on the inter laminar shear stress (ILSS) of reactively processed APA-6 composites and melt processed PA-6 composites.

Figure 9.17 shows that when tested in dry conditions reactively processed APA-6 composites have a higher ILSS than their melt processed PA-6 counterpart (same thickness, same fiber fabrics, same fiber content, see Chapter 10) due to their strong interface. Because the formation of interfacial bonds significantly reduces the crystallinity of the APA-6 matrix, the matrix becomes more susceptible to moisture absorption, which causes a steep drop in ILSS. Also the lower void content of the melt-processed PA-6 composites contributes positively to retention of properties when moisture conditioned. The same conclusions are drawn in Chapter 10, in which APA-6 composites are subjected to a more detailed mechanical testing program.

9.7 Conclusions

The interaction between the carbamoylcaprolactam activator and the aminosilane sized fibers is summarized as follows:

- The assumed mechanism for bond formation between APA-6 and aminosilanes is similar to the branching mechanism in the neat polymer: de-blocking of the activator generates isocyanate groups that can subsequently react with amino groups on the fiber surface.
- According to the de-blocking equilibrium, the activators continuously shift between their blocked configuration, which induces polymerization, and their de-blocked configuration, which can cause branching or interfacial bond formation.
- At increasing temperature relative to the de-blocking temperature, the activator tends to exist more in a de-blocked configuration, which increases the chance of interfacial bond formation. Whether bond formation actually occurs, however, remains time dependent and can still be prevented if the activator reacts with a monomer when it briefly shifts back into its blocked configuration.
- With every interfacial bond that is made, the total number of activator groups is reduced by one. As a consequence, the activator concentrations before and after infusion differ. It is expected that fine-tuning of the formulation in order to obtain the optimum activator concentration after infusion can further improve the composite properties. The same is applicable for the initiator, which is partially deactivated by the fibers as was discussed in Section 8.4.

- When an interfacial bond is made between the activator and the amino surface group, it will only contribute positively to the inter laminar shear strength (ILSS) of the composite if a sufficiently long polymer chain grows from the same activator consequently forming an interpenetrating network with the bulk matrix.
- When mixing multiple activators with different de-blocking temperatures, it is possible that the activator with the highest de-blocking temperature consumes all monomer before the other activators get a chance to initiate polymerization.

The formation of interfacial bonds affects the crystallization process in the bulk matrix, which has the following consequences:

- A compromise between maximizing the matrix properties and maximizing the interfacial strength is inevitable in order to maximize the properties of the entire composite. In this case, the highest inter laminar shear strength is obtained at a mould temperature of 180ºC, whereas in terms of conversion and crystallinity the optimum matrix is obtained at a mould temperature of 160ºC, see Chapter 8.3.5.
- Interfacial bond formation contributes to a reduction of void content by limiting the crystallization-induced shrinkage of the matrix, which further increases the performance of the composites.
- The reduction in crystallinity that is caused by interfacial bond formation makes the composites more susceptible to moisture absorption. As a consequence, the ILSS of reactively processed APA-6 is higher than of its melt-processed PA-6 counterpart in dry conditions, but lower when moisture conditioned.

CHAPTER 10

STATIC AND DYNAMIC PROPERTIES OF FABRIC REINFORCED ANIONIC POLYAMIDE-6 COMPOSITES: A COMPARATIVE STUDY

10.1 Introduction

In the previous two chapters the manufacturing of anionic polyamide-6 (APA-6) was discussed as well as fiber-to-matrix bond formation. In this chapter, the static and dynamic mechanical properties of APA-6 composites are determined and compared with values of a melt-processed HPA-6 composite and a vacuum infused epoxy composite. Given the importance of dynamic testing for typical fatigue-driven structures such as wind turbine blades [185], the remark is made that only preliminary conclusion can be drawn from the limited number of fatigue tests conducted in this research. It will be demonstrated that the fiber-to-matrix interface of both thermoplastic composites appears to behave differently to static and dynamic loads. In agreement with the test results from the previous chapter, a huge difference in performance of APA-6 composites is found in dry and moist conditions. Attempts to reduce the negative effect of moisture absorption are discussed in Chapter 11.

10.2 Experimental

10.2.1 Materials and processing methods

The composites analyzed in this chapter are all balanced and symmetrical laminates consisting of 12 plies of 8-harness satin weave E-glass fabrics (SS 0303 050, weave style 7781, 300 gram/m^2, Ten Cate Advanced Composites, Nijverdal, The Netherlands). The fabric selected is coated with aminosilanes (finish 8702), commonly known to be compatible with both epoxy and PA-6 matrices. Special care

was taken to maintain a constant fiber volume content in order to make comparison of the following three composites possible:

I - Vacuum infused APA-6 composites (APA-6/GF)

The manufacturing process of APA-6 composites is extensively documented in Section 8.2.2. Although it was shown in Chapters 8 and 9 that a mould temperature of 180ºC yields the highest inter laminar shear strength (ILSS) and that the highest conversion and crystallinity are obtained at a mould temperature of 160ºC, a mould temperature of 170ºC was selected to manufacture APA-6 composites for static mechanical testing, which is explained as follows:

- At the moment of conducting this comparative study, optimization of the APA-6 composites was focused more on optimization of the matrix in terms of conversion and crystallinity than on fiber-to-matrix bonding.
- Lacking exothermic heat build-up, the edges of the infused composites are exposed to a relatively lower processing temperature compared to their center. The composites processed at 160ºC have poorly polymerized edges that are not suitable for testing or gluing tabs. The edges of composites infused at 170ºC on the other hand are suitable for gluing tabs, which increases the area of test material per infused panel and significantly reduces the number of panels that needs to be manufactured for the entire test program.

For dynamic mechanical testing, APA-6 composites were infused at mould temperatures ranging from 160 to 180°C. Table 10.1 provides an overview of the processing parameters for APA-6 composites used for either static or dynamic testing.

Table 10.1: Summary of processing parameters for manufacturing APA-6 composites.

Processing parameter	Static testing	Dynamic testing
Resin formulation	1.2mol% HDCL activator – 1.2mol% MgBrCL initiator	
Degassing procedure	in MMU (15 minutes at 100 mbar)	in buffer vessel (5 minutes at 10 mbar)
Mould temperature	170ºC	160-180ºC
Infusion pressure	250 mbar	
Curing pressure	250 mbar	
Polymerization time	60 minutes	
Cooling rate	-40ºC/hr (Instant demolding)	

II - Thermoformed HPA-6 composites (HPA-6/GF)

Hydrolytic polyamide-6 composites (HPA-6/GF) were produced by thermoforming a stack of alternating layers of glass fabrics and dried PA-6 films (Akulon F132-E, DSM, The Netherlands) in a hot flat platen press (LAP 100, Gottfried Joos Maschinenfabrik GmbH & Co, Germany). The laminate was heated up from room temperature to 275ºC at a rate of 9°C/min and kept at that temperature for 10 minutes before being cooled down to room temperature at a rate of 20°C/min.

III - Vacuum infused epoxy composites (epoxy/GF)

Epoxy composites were manufactured with a classic thermoset vacuum infusion process as is shown in Figure 1.11, using a Prime20LV epoxy resin with a slow hardener (Spsystems, UK). The laminates were infused (50 mbar) and cured (500 mbar) at room temperature for 16 hours and then post-cured at 65°C for 7 hours (ambient pressure).

Various properties of the three matrix materials are summarized in Table 10.2

Table 10.2: Neat resin properties of the various matrices used.

Mechanical property	APA-6	HPA-6[*]	Epoxy[**]
Viscosity during processing [Pa·s]	0.01	200	0.31
Shrinkage during processing [%]	4.9[+]	4.7[+]	1.8
Tensile strength [MPa]	85[++]	65	66
Young's modulus [GPa]	3.7[++]	2.3	3.3
Strain at failure [%]	19[++]	10	3.2
Shear strength [MPa]	-	59	73
Shear modulus [GPa]	-	1.0	1.2

[*] Taken from Akulon F132-E datasheet
[**] Taken from Prime20LV datasheet
[+] Calculation based on the measured crystallinity of the composite (Table 10.3) and the densities of the amorphous phase (1.08 g/cm^3) and the crystalline phase (1.24 g/cm^3).
[++] Extrapolated data from Chapter 6 based on the measured crystallinity of the composite (Table 10.3).

10.2.2 Analysis methods

Degree of conversion

The degree of conversion of both PA-6 composites was determined according to the method described in Section 8.2.3. The conversion of the epoxy matrix was not measured, but assumed to be 100%.

Differential Scanning Calorimetry (DSC)

The degree of crystallinity and the melting points of both PA-6 composites were determined according to the method described in Section 8.2.3.

Determination of density, fiber content and void content

The method to determine the composition of the three composites is described in Section 8.2.3.

Tensile testing

Tensile tests were conducted on a Zwick-Roell Z250 25 ton force machine equipped with extensometers according to ISO 527. Rectangular specimens (Type 3, 250 x 25 x 2.7 mm) with a 0°/90° fiber orientation were used with bonded end tabs. A minimum of 5 specimens was tested at a crosshead speed of 2 mm/min. When failure occurred within 10 mm of the grips the test results were discarded.

Compressive testing

Compression tests were conducted on a Zwick-Roell Z250 25 ton force machine equipped with extensometers according to ISO 14126 (Method 2) and ASTM D695. Rectangular specimens (75 x 15 x 2.7 mm) with a 0°/90° fiber orientation were used with bonded end tabs. Special care was taken to obtain specimens with parallel end surfaces. A maximum gage length of 10 mm was determined at which Euler buckling was prevented. A minimum of 5 specimens was tested at a crosshead speed of 1 mm/min. When failure occurred outside the gage length the test results were discarded.

In-plane shear testing

Shear tests were conducted on a Zwick-Roell Z250 25 ton force machine equipped with extensometers according to ISO 14129. Rectangular specimens (250 x 25 x 2.7 mm) with a ±45° fiber orientation were used with bonded end tabs. A minimum of 5 specimens was tested at a crosshead speed of 2 mm/min. When failure occurred within the grips the test results were discarded.

Short beam shear testing

The inter laminar shear properties of composites was determined by short beam shear test as is described in Section 8.2.3

Fatigue testing

Tension-tension fatigue testing (R = 0.1) was conducted on a MTS 831 Elastomer Test System with 647 Hydraulic Wedge Gips (1 MPa clamping force) according to ASTM D3479/D3479M. A minimum of 5 samples (75 x 10 x 2.9 mm, with end tabs, gage length: 10 mm) was tested per amplitude at 10 Hz (sinusoidal). This frequency was selected for the following two reasons:

- At this frequency, the sample temperature during testing remained below 31ºC for all composites, which is well below the glass transition point of all matrices in dry as molded conditions.
- At this frequency, the maximum duration of a single test remains below 3 days. In this time interval the maximum moisture absorption remains below 0.3 wt% for all composite matrices and all test results can therefore be regarded as dry as molded values.

Although the fatigue spectrum of a wind turbine blade is much more complex than a tension-tension fatigue test [185], this type of testing was selected because it is one of the easier fatigue tests to perform and because it already makes an initial comparison of the fatigue properties possible.

Moisture conditioning

The static mechanical tests were conducted on samples conditioned in two different ways before testing:

- Dry as molded (DAM) samples were dried in a vacuum oven at 20 mbar and 50°C for at least 48 hours before testing.
- Moisture treated samples were conditioned, according to ISO 1110, in a climate chamber (Weiss SB11/300-40) at 70°C and 62% RH (relative humidity) until a constant weight was obtained as was measured using a Mettler AG204 DeltaRange® microbalance. According to the ISO 1110 standard, these conditions lead to an equivalent moisture content as when conditioned at 23°C and 50% RH but in a shorter time period.

Fatigue testing was only conducted on dry as molded samples.

10.3 Physical composite properties

The physical properties of all three composites are summarized in Table 10.3. It can be seen that tailoring the processing parameters indeed resulted in three composites with more or less equal fiber volume content. The relatively high void content and crystallinity of the APA-6 composites form an indication of a weak fiber-to-matrix bond, which was correlated in Section 9.6.1 to the relatively low mould temperature. The void contents of the HPA-6 and epoxy composites on the other hand are much lower, which is a direct result of the fact that processing of these two composites is more or less common practice. The lower melting point of the APA-6 composites compared to its melt processed counterpart is a direct result of the occurrence of branching in the bulk matrix and the presence of 5 wt% residual monomer as is explained in Section 6.3.4.

Table 10.3: Physical properties of the various glass fiber composites. Values between brackets represent the standard deviation.

Physical property	APA-6/GF	HPA-6/GF	Epoxy/GF
Thickness [mm]	2.8	2.7	2.9
Density [g/cm^3]	1.8	1.9	1.8
Fiber volume content [v%]	50	51	48
Void content [v%]	3.0 (1.6)	1.3 (0.5)	2.1 (0.8)
Melting point [ºC]	217	220	-
Degree of conversion [wt%]	95	100	100
Degree of crystallinity [wt%]	35	33	-
Matrix moisture content (23ºC-50%RH) [wt%]	2.7	2.5	0.8

10.4 Mechanical properties: dry as molded values

For dry as molded conditions, the static mechanical properties of the composites are presented in Table 10.4, whereas the S-n curves, or Wöhler curves, for tension-tension fatigue are shown in Figure 10.1. The equal density of the three composites, see Table 10.3, makes a material comparison based on the mechanical properties 'as measured' possible and does not require the so-called specific properties (properties per unit weight).

Table 10.4: Static mechanical properties of the various glass fiber composites (Dry as molded values). The standard deviation is given by the values between brackets.

Mechanical property	APA-6/GF	HPA-6/GF	Epoxy/GF
Compressive strength [MPa]	473 (21)	390 (26)	392 (34)
Compressive modulus [GPa]	26 (1.8)	25 (1.8)	25 (1.3)
Compressive strain [%]	1.9 (0.1)	1.5 (0.1)	1.7 (0.2)
Tensile strength [MPa]	495 (24)	456 (41)	476 (14)
Tensile modulus [GPa]	26 (0.3)	26 (0.5)	26 (0.3)
Tensile strain [%]	2.4 (0.1)	2.5 (0.4)	2.3
In-plane shear strength [MPa]	127 (0.1)	117 (9.0)	94 (1.7)
In-plane shear modulus [GPa]	4.1 (0.2)	3.7 (0.1)	3.5 (0.1)
Inter laminar shear strength [MPa]	69 (1.8)	65 (0.9)	59 (1.1)

10.4.1 Static properties

Table 10.4 shows that the tensile strength of the composites, which is a typical fiber dominated property, differs for the various matrices. Because the tensile strength decreases with the viscosity of the matrix during processing, see Table 10.2, it is assumed that the decrease in tensile strength is related to fiber waviness: the higher the viscosity of the matrix, the more the fibers are pushed aside during impregnation and the higher the degree of misalignment of the fibers in the final composites, which is obviously detrimental for the tensile properties. Misalignment of fibers should have the same effect on the compressive properties and indeed a similar viscosity-related trend is found in the compressive strength. The remark is made that in general the

influence of the matrix modulus on the compressive strength is much larger than on the tensile strength. In this case, the higher the matrix modulus, see Table 10.2, the higher indeed the compressive strength of the composite.
Both thermoplastic composites have higher shear properties (both in-plane and inter laminar) than the thermoset one despite the lower shear properties of the neat matrix itself, see Table 10.2. Therefore, the higher shear properties of the thermoplastic composites are expected to be related to the fiber-to-matrix interface and most likely originate from strong mechanical locking of the matrix around the fibers, which is caused by crystallization-induced shrinkage, see Table 10.2.

10.4.2 Dynamic properties

From the previous section, it can be concluded that in dry as molded conditions, a high degree of crystallinity is of paramount importance for the static mechanical performance of both thermoplastic composites as it results in a high matrix modulus and shrinkage-induced mechanical locking of the fibers by the matrix. Due to its high crystallinity, APA-6/GF outperformed both reference materials in all tests conducted.

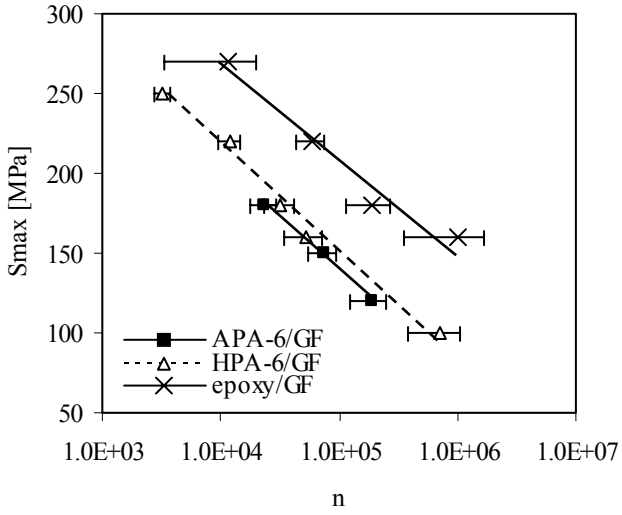

Fig. 10.1: S-n curves of the various glass fiber composites. The standard deviations are represented by the error bars.

Dynamic testing, however, shows a different ranking as is shown in Figure 10.1. The epoxy composite has a higher fatigue resistance compared to the thermoplastic composites, whose performance is equally poor. Three explanations for this different behavior are given:

- APA-6/GF has substantially more initial defects (voids, unreacted monomer), which is beneficial for crack initiation and leads to a reduction in fatigue life [186].
- The brittle nature of the epoxy matrix results in stress concentrations, which during static testing determine the moment failure, but which can be leveled of by cyclic loading during dynamic tests. Clearly, this stress-relieve during fatigue analysis results in a huge improvement in performance of the epoxy composite. The tougher PA matrix leads to substantially less stress concentrations, which implies that no significant difference regarding trhis matter is encountered between static and dynamic testing.
- The nature of the fiber-to-matrix interface of both thermoplastic composites (a combination of mechanical locking and chemical bonding) substantially differs from the interface of the thermoset one (purely chemical bonding). It could well be possible that whereas mechanical locking contributes positively to the static properties, its contribution to the dynamic properties is far less. In the following paragraphs this assumption is verified.

During testing of epoxy/GF, growth of multiple small cracks perpendicular to the load direction is visible throughout the entire specimen, see Figure 10.2. Combined with crack surface analysis by SEM, which shows no fiber-to-matrix debonding, the following failure mechanism is deducted: matrix cracks start growing in the 90º direction until a fiber is reached. The strong fiber-to-matrix interface (as is evident from the absence of matrix debonding) prevents the cracks from following the interface and forces growth to continue in the same direction. The fiber-bridged cracks continue to grow until finally failure occurs. This type of failure is typical for thermoset composites with a strong chemical fiber-to-matrix bond and has been extensively described in literature [26, 186].

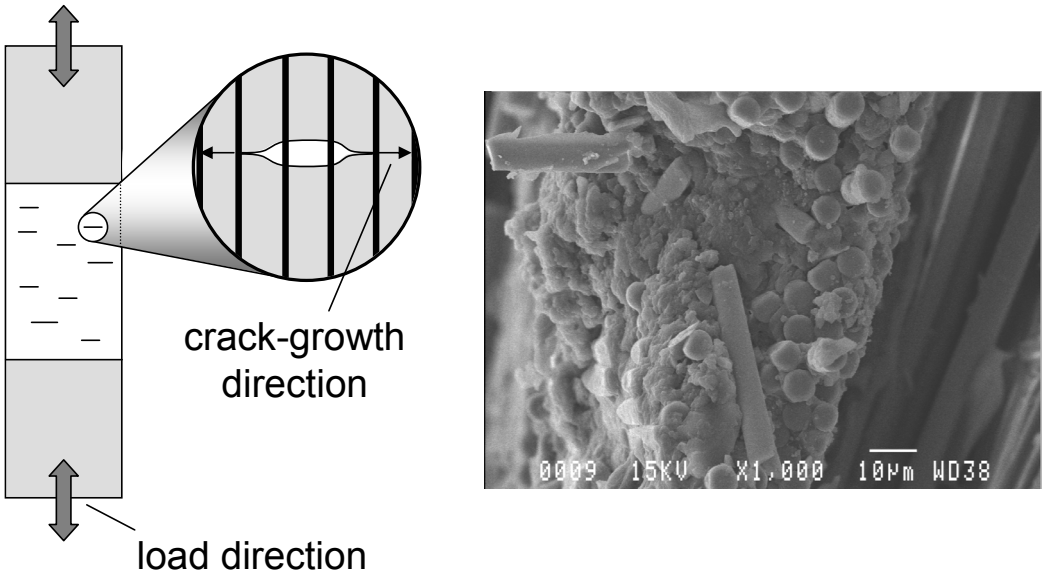

Fig. 10.2: Fatigue failure in epoxy/GF: crack growth perpendicular to direction of load (left), fiber-bridging (center), absence of fiber-to-matrix debonding (right).

For both thermoplastic composites a different failure behavior is encountered. Although the white matrix prevents visual inspection of crack-growth during testing of both thermoplastic composites, subsequent crack surface analysis revealed bare fibers and extensive fiber pull-out, see Figure 10.3, which indicates a poor fiber-to-matrix interface. Most likely cracks grow along this interface until failure occurs.

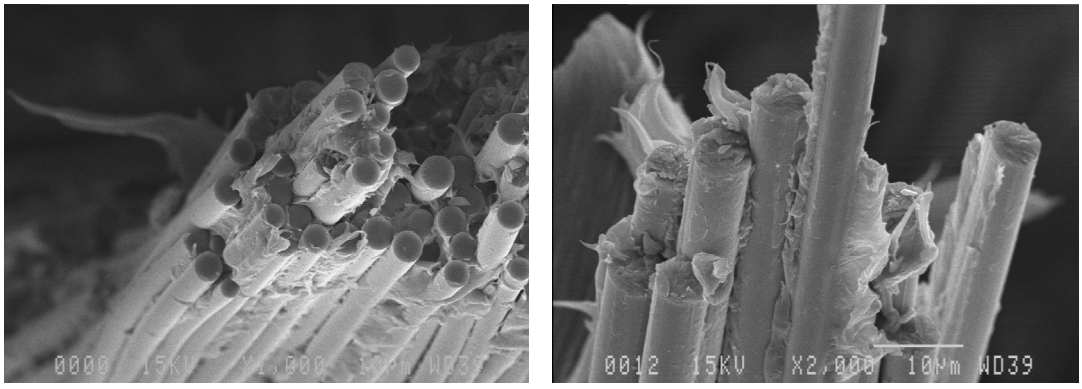

Fig. 10.3 SEM micrographs of the fracture surface of APA-6/GF (left) and HPA-6/GF (right) after fatigue testing.

The previously made assumption seems to hold: dynamic failure seems to follow a fiber-to-matrix debonding mechanism and as a consequence mechanical locking does not appear to contribute substantially to the resistance against fatigue. As a final test, two additional APA-6 composites were included in the dynamic test program:

- APA-6/GF manufactured at 160°C: higher conversion and crystallinity compared to the one manufactured at 170°C, which results in stronger mechanical locking of the fibers, see Figure 9.5.
- APA-6/GF manufactured at 180°C: less mechanical locking of the fibers, but more chemical bonding, see Figure 9.5.

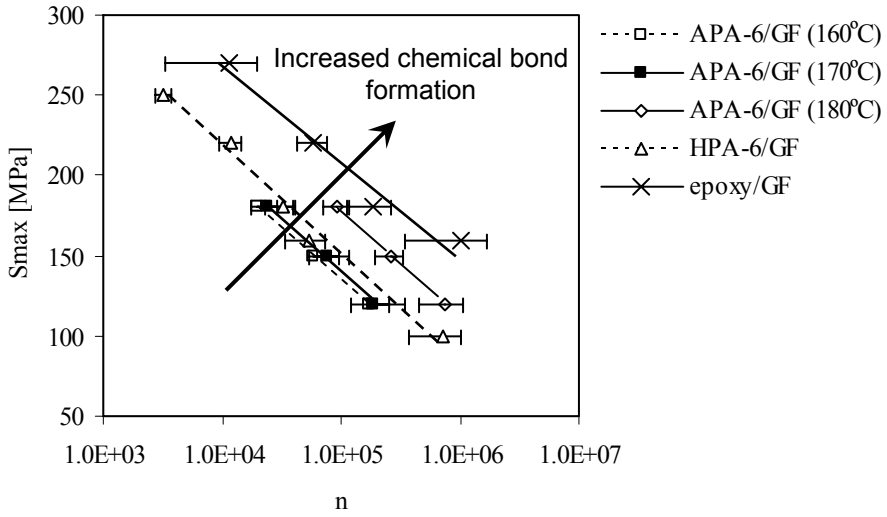

Fig. 10.4: S-n curves of various glass fiber composites, showing the importance of chemical bond formation on the fatigue life. The standard deviations are represented by the error bars.

The results of all composites tested in fatigue are shown in Figure 10.4. The coincidence of the S-n curves of HPA-6/GF and APA-6/GF manufactured at 160°C and 170°C, shows that increased mechanical locking does not increase the fatigue life of the polyamide composites. On the other hand, the significant increase in performance of APA-6/GF manufactured at 180°C shows the importance of the formation of interfacial bonds. This is especially true for APA-6 composites as

chemical bond formation also reduces the void content, see Section 9.6.1. Chemical bond formation also has an effect on the failure mode as is shown in Figure 10.5: after failure, the fibers are still covered by matrix, which indicates that instead of following the interface, the cracks are forced to progress through the ductile matrix. The appearance of striations confirms this as these form the classic fingerprint of ductile materials when failed under cyclic loading [187].

Figure 10.4 also proofs that with respect to fatigue resistance, reactively processed thermoplastic composites can bridge the gap between their melt processed counterparts and reactively processed thermoset composites. An interesting detail is the fact that although the fatigue performance of the epoxy composite is still better than of all thermoplastic composites tested, the average relative standard deviation of the thermoset composite is also 20% higher (50% compared to 30% on average for the thermoplastic composites), see also the error bars in Figure 10.1 and 10.4. The higher toughness of the thermoplastic matrix most likely causes the reduction in scatter, which should lead to more accurate fatigue life predictions and potentially lower safety factors when designing fatigue driven structures.

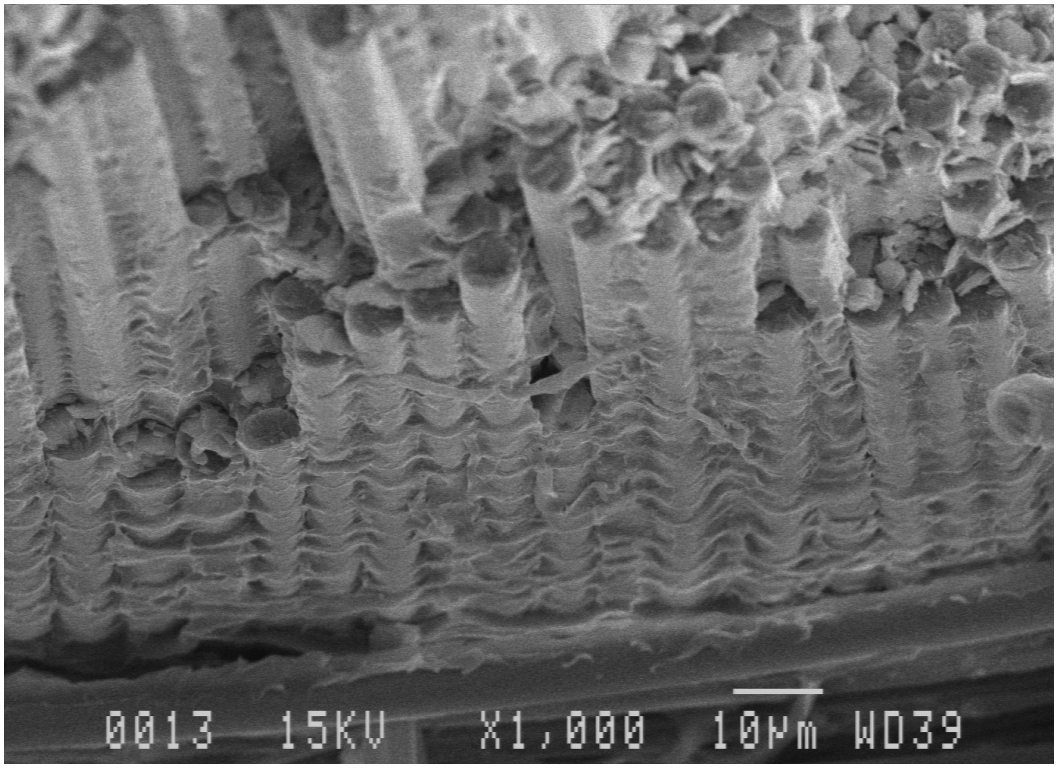

Fig. 10.5: SEM micrograph of the fatigue fracture surface of APA-6/GF manufactured at 180°C.

10.5 Mechanical properties: the effect of moisture conditioning

In addition to dry as molded values presented in the previous section, static mechanical tests were performed on moisture conditioned samples of which the results are summarized in Table 10.5.

Table 10.5: Static mechanical properties of the various glass fiber composites (Moisture conditioned values: 23ºC-50%RH*). The standard deviation is given by the values between brackets.

Mechanical property	APA-6/GF	HPA-6/GF	Epoxy/GF
Compressive strength [MPa]	290 (10)	314 (17)	376 (40)
Compressive modulus [GPa]	23 (0.8)	23 (0.9)	24 (1.4)
Compressive strain [%]	1.3 (0.01)	0.9 (0.1)	0.8 (0.3)
Tensile strength [MPa]	430 (19)	450 (16)	458 (13)
Tensile modulus [GPa]	23 (0.2)	24 (0.4)	25 (0.2)
Tensile strain [%]	2.0 (0.2)	2.0 (0.2)	2.3 (0.1)
In-plane shear strength [MPa]	105 (2.8)	100 (2.3)	85 (1.4)
In-plane shear modulus [GPa]	1.9 (0.001)	1.7 (0.1)	3.0 (0.1)
Inter laminar shear strength [MPa]	59 (0.7)	51 (0.5)	54 (0.7)

* Conditioned at 70°C-62%RH

Table 10.6: Wet retention values at 23ºC-50%RH* of the static mechanical properties of the various glass fiber composites.

Mechanical property	APA-6/GF	HPA-6/GF	Epoxy/GF
Compressive strength	61%	91%	96%
Compressive modulus	88%	82%	96%
Compressive strain	68%	60%	47%
Tensile strength	87%	99%	96%
Tensile modulus	88%	92%	96%
Tensile strain	83%	80%	100%
In-plane shear strength	83%	85%	90%
In-plane shear modulus	46%	46%	86%
Inter laminar shear strength	85%	78%	91%

* Conditioned at 70°C-62%RH

Table 10.6 shows that the polyamide-6 composites are much more affected by the absorbed moisture than the epoxy one. On average, retention levels for the modulus and strength of 76%, 82% and 93% are found for respectively the APA-6, HPA-6 and epoxy composite. The poor performance of both thermoplastic composites is explained as follows:

- The polyamide-6 matrices absorb more water, see Table 10.3.
- Moisture significantly reduces the modulus and strength of the polyamide-6 matrices as was explained in Chapter 7. As a consequence, typically the matrix-dominated properties are affected most by moisture: compressive strength and the in-plane shear modulus.
- Moisture causes the polyamide matrices to swell and consequently the mechanical locking of the matrix around the fibers is compromised. What remains is the chemical interface strength, which is highest for the epoxy composite as was explained in Section 10.4.2.

The APA-6 composites have a much lower retention level than their HPA-6 counterpart, which is mainly caused by a weaker chemical bond between the fibers and the matrix as becomes clear from the SEM micrographs in Figure 10.6, which were taken after moisture conditioning and subsequent testing. Whereas the fracture surface of the HPA-6 composites show that some matrix material remains attached to the fibers, the fibers of the APA-6 composites are completely clean.

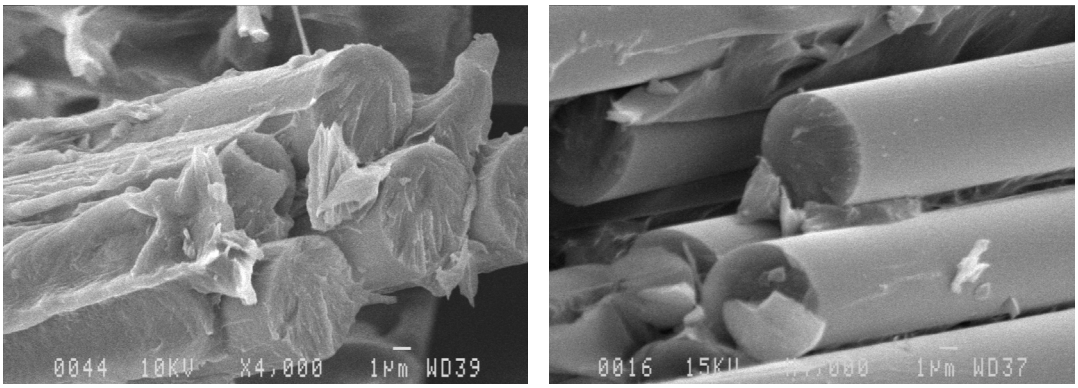

Fig. 10.6: SEM micrographs of fracture surfaces of composites taken after moisture conditioning and subsequent testing. Left: HPA-6/GF, right: APA-6/GF.

For the following reasons, the chemical interface of the APA-6 composites is lower:

- At a mould temperature of 170ºC, fiber-to-matrix bond formation according to the mechanism based on de-blocking of the activator is very limited, see Figure 9.2.
- Fiber-to-matrix bonding due to transamidation reactions, see Figure 9.8, is more extensive at higher processing temperatures. Therefore transamidation is more likely to occur during thermoforming of the HPA-6 composite.

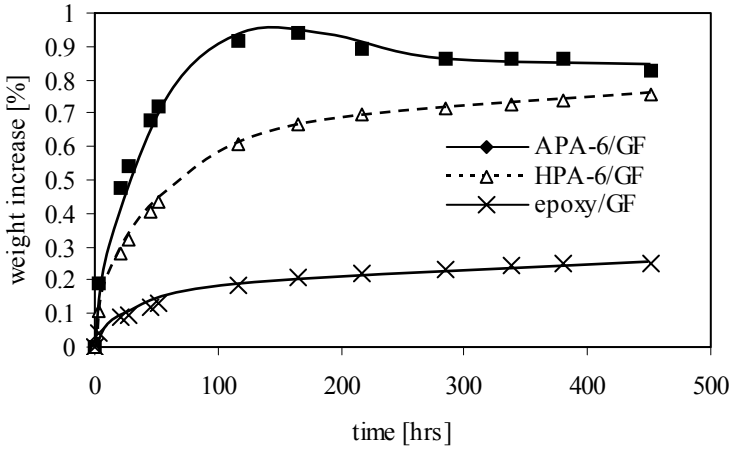

Fig. 10.7: Moisture absorption curves of the various glass fiber composites (70°C-62%RH).

- The higher void content and the presence of residual monomer in the APA-6 composites make moisture absorption much faster, see Figure 10.7. As a consequence, more time is available to reduce the number of fiber-to-matrix bonds by hydrolysis of the siloxane bonds that connect the aminosilane coupling agents to the glass surface, see Figure 10.8 [178, 188]. The reduction in weight of the APA-6 composites is caused by extraction of unreacted monomer during conditioning as was also encountered during conditioning of neat resin samples, see Figure 7.6 and 7.7.

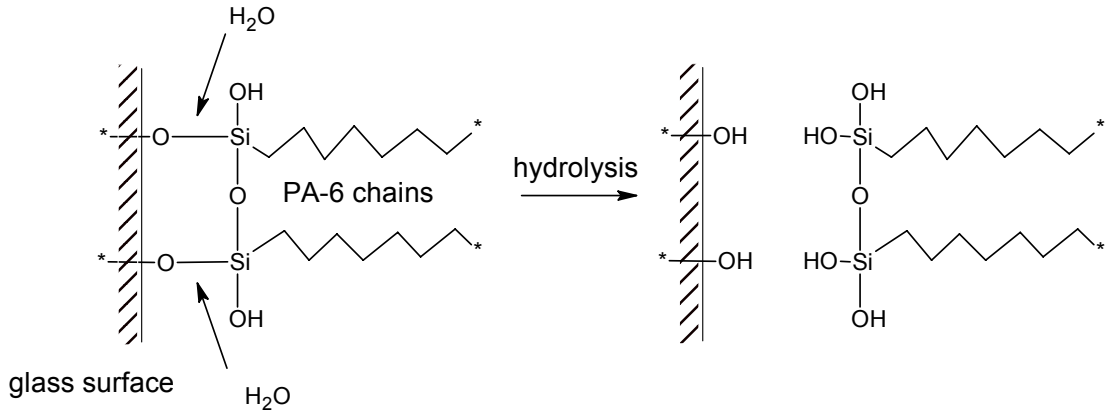

Fig. 10.8: Reduction of fiber-to-matrix bonds by hydrolysis of siloxane bonds.

10.6 Conclusions

The static mechanical properties of APA-6 composites manufactured at 170°C were compared to HPA-6 and epoxy composites in dry and moist conditions. Also, a preliminary fatigue analysis was conducted. The following conclusions are drawn:

- The high degree of crystallinity causes the polyamide matrices to firmly shrink around the fibers, which results in superior static properties in dry conditions compared the epoxy one. Moisture absorption, however, degrades the mechanical properties of the matrix itself and causes the matrix to swell, which reduces the mechanical locking strength. As a consequence, moisture absorption significantly reduces the overall static mechanical performance of both polyamide thermoplastic composites.
- In fatigue tests, chemical bonding is preferred over mechanical locking of the fibers as it prevents fiber-to-matrix debonding and results in fiber-bridged cracks perpendicular to the load direction instead, which increases the fatigue life.
- It was demonstrated that by increasing the chemical bond strength (simultaneously decreasing the void content), reactively processed thermoplastic composites can bridge the gap between their melt processed counterparts and reactively processed thermoset composites with respect to fatigue resistance.
- Although at the moment the epoxy composite still has the highest fatigue resistance, it also has a significantly higher relative standard deviation due to its brittle nature, which is not beneficial for making accurate fatigue life predictions.

CHAPTER 11

THE USE OF ADDITIVES TO INCREASE THE CRYSTALLINITY AND CONVERSION OF ANIONIC POLYAMIDE-6 COMPOSITES

11.1 Introduction

In Chapter 7 it was shown that reactive processing of anionic polyamide-6 leads to a high degree of crystallinity, which gives the neat polymer an extraordinary modulus and strength up to relatively high temperatures and humidity levels. Unfortunately, it was demonstrated in Chapter 8 and 9 that in composites the inevitable need for forming interfacial bonds between the matrix and the fibers influences the crystallization process and that as a consequence the crystallinity of the composite matrix reduces significantly and with it the conversion and the resistance against both temperature and humidity. In this chapter, the effect of two additives on the neat APA-6 resin and its composites is assessed: (i) a nucleating agent to increase the degree of crystallinity and (ii) a co-catalyst to increase the degree of conversion.

11.2 Experimental

11.2.1. Materials

The APA-6 resin material

The caprolactam monomer, hexamethylene-1,6-dicarbamoylcaprolactam activator (HDCL, "Brüggolen C20") and caprolactam magnesium bromide initiator (MgBrCL, "Brüggolen C1") are described in Section 5.2.1.

The Microtuff nucleating agent

Microtuff AG 609 (Barrets Minerals Inc, USA), is an inorganic microtalc, which is a commonly used nucleating agent for melt processing of polyamide-6. As suggested by the supplier, 0.07wt% of Microtuff was added to the APA-6 resin (1.2mol% activator and 1.2mol% initiator) equally divided over both tanks of the mini mixing unit, see Figure 4.6 and 4.7.

The 2-Pyrrolidinone co-catalyst

According to literature, 2-Pyrrolidinone (2P or γ-butyrolactam, see Figure 11.1) increases the reactivity of the particular activator-initiator combination that is used in this study to manufacture composites [189]. Being incorporated in the APA-6 backbone [190, 191], 2P can be regarded as a co-catalyst. In this chapter, 2P is added to the APA-6 resin in order to reduce the initiator concentration without changing the reactivity of the system. As was already explained in Section 5.3.3, every initiator molecule added reduces the maximum achievable conversion and therefore, the less initiator that is added, the higher the final degree of conversion. Relative to caprolactam, 0.075 mol% 2-Pyrrolidinone was used to replace 0.6mol% of the caprolactam magnesium bromide initiator. In the so-called 'boosted' resin formulations 0.075mol% 2P was added together with the activator (0.6mol% for the neat polymer panels and 1.2mol% for the composites) to tank A of the mini mixing unit (Figure 4.6 and 4.7), whereas 0.6mol% C1 initiator was added to the caprolactam in tank B.

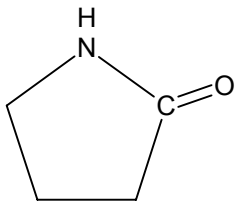

Fig. 11.1: The chemical structure of the 2-Pyrrolidinone co-catalyst.

Glass fabrics

8-harness satin weave E-glass fabrics (SS 0303 050, weave style 7781, 300 gram/m^2, Ten Cate Advanced Composites, Nijverdal, The Netherlands) were used with an

aminosilane coupling agent, see Figure 8.1. The formation of interfacial bonds with the APA-6 resin is extensively discussed in Chapter 9.

11.2.2 Processing methods

Manufacturing of neat APA-6 panels is described in Section 6.2.2, whereas infusion of composites is described in Section 8.2.2.

11.2.3 Analysis methods

Reaction rate

Due to the exothermic nature of polymerization and crystallization, the exothermic temperature increase can be used to monitor the progression of the reaction. To obtain the necessary temperature profiles, polymerizations were conducted using test tubes (Schott-Duran, 20 x 150 mm) as casting mould, see Figure 11.2. A thermocouple was placed in the center of the test tubes, which were heated in an oil reservoir (Rhodorsil 47v100 oil) that could be placed in the heated press, see Figure 4.9.

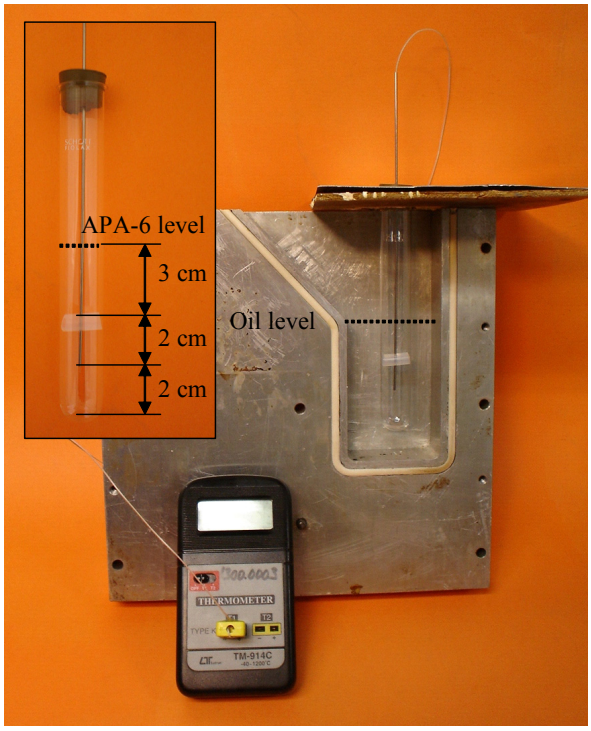

Fig. 11.2: Setup to measure the temperature progression during the reaction. Insert: Thermocouple with silicon spacer inside the test tube.

Rheology

The viscosity increase at the initial stage of polymerization was measured by rheology as explained in Section 9.2.3.

Differential Scanning Calorimetry (DSC)

Determination of the crystallinity of the neat APA-6 resin is described in Section 5.2.3, whereas for composites this method is described in Section 8.2.3. To determine the crystallization temperature (T_c) of the neat resin, samples were held at 230°C for 2 minutes before being cooled down to room temperature at 10°C/min.

Degree of conversion

The method to determine the degree of conversion of the neat resin is explained in Section 5.2.3, for composites in Section 8.2.3.

Tensile testing of the neat polymer

Tensile testing is described in Section 6.2.3.

Short beam shear testing

The short beam shear test is described in Section 8.2.3.

11.3 The effect of the Microtuff nucleating agent

The effect of the nucleating agent on the neat resin and composites will be discussed consecutively.

11.3.1 The effect of the nucleating agent on neat APA-6

Figure 11.3 shows that the nucleating agent only has an effect on the degree of crystallinity at higher mould temperatures. To understand this, it is important to recall that crystallization during anionic polymerization of APA-6 occurs in two distinct stages, see Figure 6.10: primary crystallization during the early stage of the reaction and secondary crystallization towards the end.

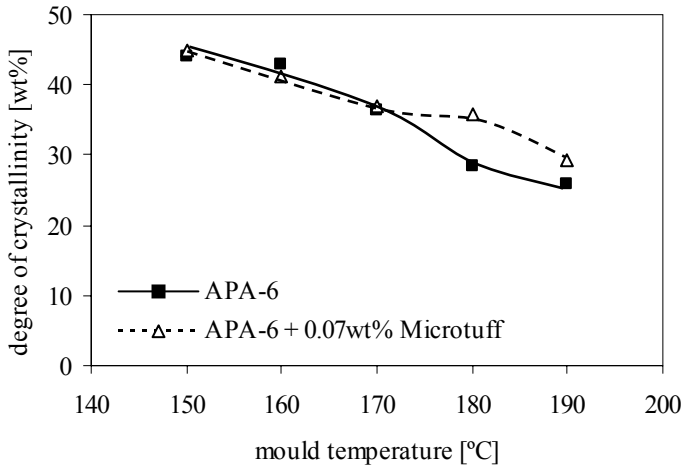

Fig. 11.3: The effect of the nucleating agent on the degree of crystallinity of the neat polymer.

At low mould temperatures, circumstances are such that nucleation points for primary crystallization are plenty and the growth rate of crystals is high even without a nucleating agent [32]: (i) the temperature at the initial stage of the reaction is relatively low, (ii) the molecular weight of the growing polymer chains is still low, and (iii) the abundant monomer, being a solvent for PA-6, increases the mobility of the crystallizing chains. Apparently, the addition of a nucleating agent offers no additional benefits and is therefore seemingly without effect. The nucleating agents, being already incorporated in the primary crystals, are consequently also ineffective in the secondary crystallization stage during which crystals continue to grow from the surface of the primary crystals.

At high mould temperatures, however, the nucleating agent clearly seems to have an effect, for which three explanations can be given:

1. At higher temperatures nucleating points are less abundant and consequently the addition of a nucleating agent makes a big difference.
2. The rise in crystallization temperature, see Figure 11.4, shows that the tendency to crystallize increases due to the presence of the nucleating agent. When during polymerization the polymer chains crystallize more rapidly, the dwell time in the amorphous phase is significantly shortened and with it the time during which branches can be formed as described in Section 6.3.1. As described in the same

chapter, a reduction in branch-points is beneficial for obtaining a higher degree of crystallinity. Because branching only occurs above the de-blocking temperature of the activator (160ºC), a nucleating agent is only effective at higher mould temperatures.

3. Only at higher initial mould temperatures the maximum temperature encountered during processing is sufficiently high to re-melt the primary crystals, hence setting free the nucleating agents. When this happens, the nucleating agents can influence secondary crystallization in the subsequent cooling phase. Given the high molecular weight of the polymer chains and the low monomer concentration, secondary crystallization closely resembles crystallization from the melt for which the Microtuff nucleating agent is commonly used.

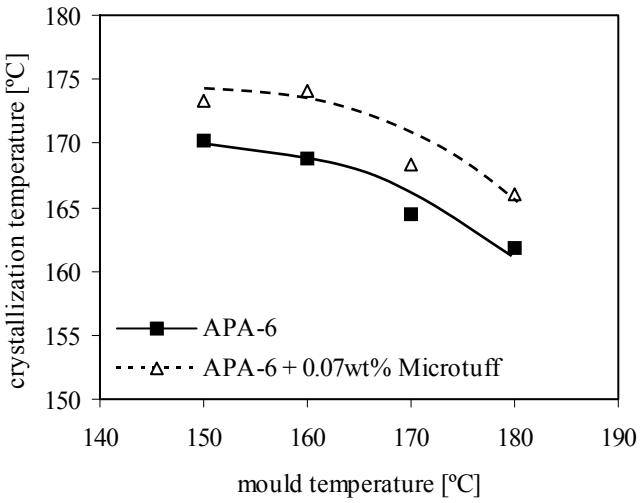

Fig. 11.4: The effect of the nucleating agent on the crystallization temperature of the neat polymer.

Although the effect of the nucleating agent on the degree of crystallinity is very limited, the conversion increases by 1.5 wt% on average over the entire range of mould temperatures, see Table 11.1. The change in mechanical properties, however, is in contradiction with the higher conversion and crystallinty: the modulus and strength decrease, whereas the strain at failure increases. Entrapment of reactive chain-ends in rapidly growing crystals could cause the odd effects of the nucleating agent as is explained in the next paragraph.

Table 11.1: Tensile properties of neat and nucleated APA-6 (1.2mol% activator and 1.2mol% initiator).

	Degree of conversion [wt%]		Young's Modulus [GPa]		Maximum strength [MPa]		Strain at failure** [%]	
T_{mould} [°C]	neat	MT*	neat	MT*	neat	MT*	neat	MT*
150	96	97	4.9	4.7	90	90	6	21
160	95	97	4.3	4.3	93	86	19	23
170	96	97	4.1	3.8	85	82	30	36
180	93	97	3.8	3.8	79	79	36	43
190	93	94	3.4	2.6	70	62	32	50

* MT – Microtuff nucleating agent
** Stopped at a maximum of 50% strain

As was explained in Chapter 5.3.3, a too high activator concentration results in extensive oligomer formation, which causes the conversion to drop [85, 151]. In this study, an activator concentration of 1.2 mol% was specifically selected for the manufacturing of fiber composites during which interfacial bond formation reduces the number of activator groups before polymerization commences, see Section 9.2.1. Clearly, this activator concentration is too high for manufacturing of neat polymer panels as it leads to low conversions. As proposed earlier, the addition of a nucleating agent explains the increase in conversion when assuming that entrapment of reactive chain-ends in rapidly growing nucleated crystals reduces the number of activator groups and with it the final oligomer content. Just like interfacial bond formation in composites, the nucleating agent might neutralize the 'activator overdose'.
To verify whether entrapment of reactive chain-ends occurs, the reaction rate was measured by monitoring the temperature during the polymerization, see Figure 11.5. It can indeed be seen that for temperatures up to 170°C the nucleating agent slows down the reaction, which indicates that entrapment reduces the number of reactive chain-ends that can participate in the reaction. Although the reduction in reaction rate seems only marginal, it is significant considering that crystallization would normally increase the reaction rate due to the crystallization induced autocatalytic effect, which is explained in Section 5.5.2.

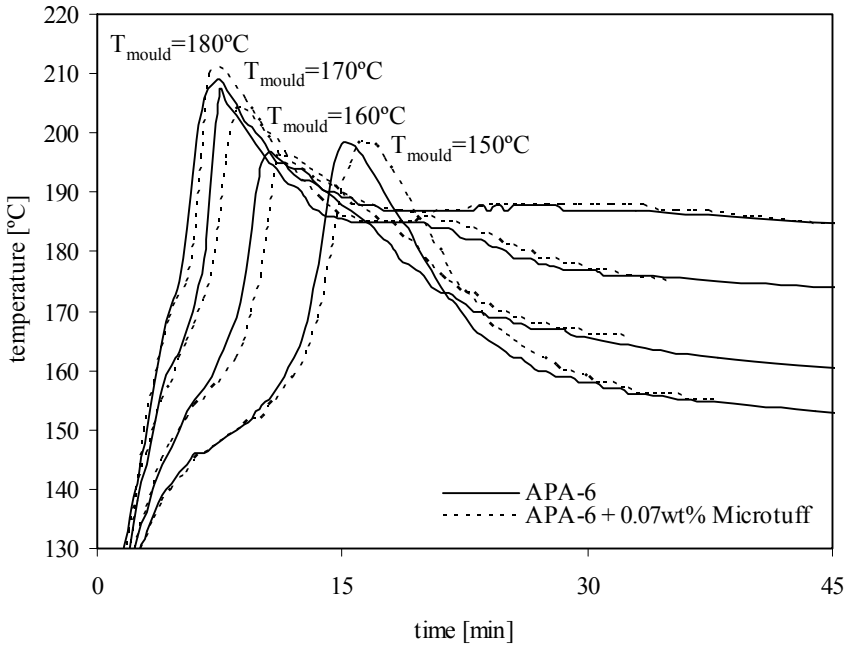

Fig. 11.5: Temperature progression at various initial mould temperatures during anionic polymerization of caprolactam with and without nucleating agent.

Entrapment also explains the change in mechanical properties as it either prevents the formation of branch-points or limits the length of the growing branches. As a consequence, the number of polymer chains that form a connection between the various crystals is reduced significantly. Normally, these tie-molecules form a network, which in combination with the high degree of crystallinity results in an extraordinary modulus and strength, and a rather low strain at failure, see Chapter 6 and 7.

Although the effect of the higher conversions and crystallinity on the mechanical properties of the neat polymer is counteracted by the abovementioned phenomena, composites were infused with the addition of a nucleating agent, which is discussed in the next section.

11.3.2 The effect of the nucleating agent on APA-6 composites

Table 11.2 shows the conversion and crystallinity of composites manufactured with and without nucleating agent. Although at higher mould temperatures the nucleating

agent was effectively applied for increasing the crystallinity of the neat polymer, see Figure 11.3, no effect is encountered for the composites. Due to the high fiber content, the exothermic temperature rise in the composites is very limited, see Figure 8.3 and the processing temperature never gets sufficiently high to re-melt the primary crystals in order to make the nucleating agent effective during the secondary crystallization stage. In addition, it is very likely that the fibers itself already act as a nucleating agent, consequently making the Microtuff nucleating agent seemingly ineffective [56].

Whereas for the neat polymer the overdose of activator is reduced by entrapment of reactive chain-ends, fiber-to-matrix bonding already does the same for the composites and no increase in conversion is obtained.

Table 11.2: Physical properties of APA-6 composites with and without nucleating agent.

	Degree of crystallinity [wt%]		Degree of conversion [wt%]	
T_{mould} [ºC]	APA-6	APA-6 + MT*	APA-6	APA-6 + MT*
160	41	43	96	96
170	38	38	95	95
180	32	32	93	94

* MT – Microtuff nucleating agent

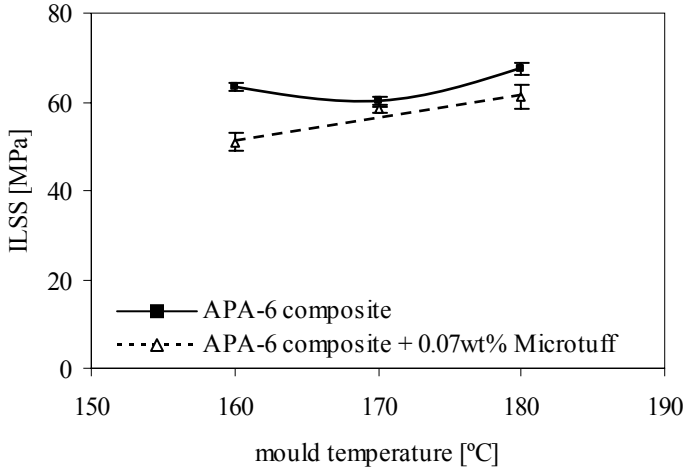

Fig. 11.6: The effect of the nucleating agent on the inter laminar shear strength (ILSS) of APA-6 composites. The error bars indicate the standard deviations.

Finally, the nucleating agent causes a notable reduction (10% on average) in the ILSS of the APA-6 composites, see Figure 11.6. In addition to matrix weakening due to a reduction in tie-molecules, which was discussed previously, one can imagine that the ILSS drops because premature crystallization prevents proper development of the interpenetrating network of chains growing from the fiber surface and chains growing in the bulk matrix.

11.4 The effect of the 2-Pyrrolidinone co-catalyst

After discussing the effect of the co-catalyst on the neat polymer properties, the effect on APA-6 composites is discussed. As mentioned in the experimental section, 0.075mol% 2-Pyrrolidinone was used to replace 0.6mol% initiator. Figure 11.7 shows that this so-called 'boosted' formulation has an equal or higher reactivity than the normal formulation at mould temperatures that are typically used for infusion of composites.

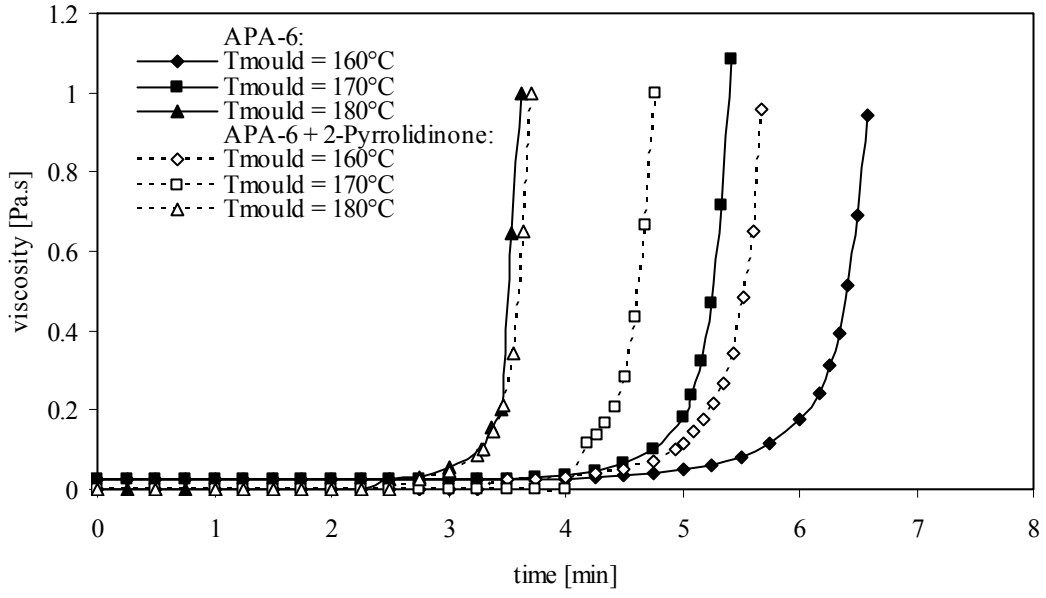

Fig. 11.7: Viscosity increase during polymerization at various mould temperatures for APA-6 and 'boosted' APA-6, which contains the 2-Pyrrolidinone co-catalyst (1.2mol% activator, 0.6mol% initiator, 0.075mol% 2P).

11.4.1 The effect of the co-catalyst on neat APA-6

Figure 11.8 shows that on average 2-Pyrrolidinone increases the conversion of the APA-6 polymer by 1.2 wt%, which corresponds to a reduction in residual monomer content of 29%. The higher modulus at lower mould temperatures directly shows the benefit of obtaining a higher conversion, see Figure 11.9. The effect of 2-Pyrrolidinone on the modulus, however, decreases sharply at higher mould temperatures following the decrease in crystallinity, whereas the modulus of APA-6 without 2P increases again due to the formation of branch-points as was explicated in Section 6.3.6. As was explained in Section 6.3.1, the HDCL activator can either polymerize (in its blocked configuration) or form branch-points (in its de-blocked configuration). The fact that 2P increases the tendency of HDCL to polymerize, see Figure 11.7, implies that at the same time the tendency to branch decreases. As was discussed in Chapter 6 and 7, a slight degree of branching is beneficial for the strength and stiffness of the polymer at higher mould temperatures. Just like the nucleating agent described in the previous section, the 2P co-catalyst seems to reduce the integrity of the network of tie-molecules, which leads to a reduction in strength and stiffness and an increase in crystallinity and strain at failure, see Table 11.3. In addition, literature mentions that the tendency of 2P to co-polymerize with caprolactam decreases with increasing temperature [190]. Therefore, at higher mould temperatures more 2P remains as unreacted residue, which has an effect on the conversion and the mechanical properties.

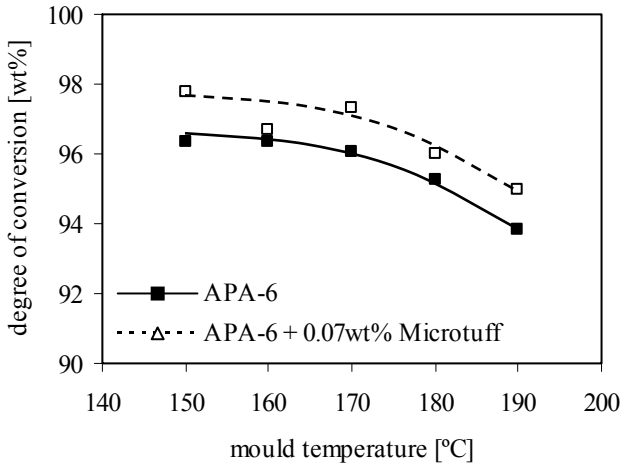

Fig. 11.8: Degree of conversion of neat APA-6 with and without 2P for various mould temperatures (0.6mol% activator, 0.6mol% initiator, 0.075mol% 2P).

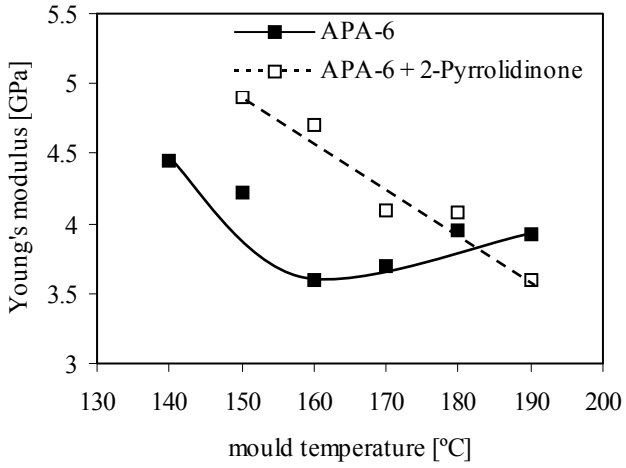

Fig. 11.9: Young's modulus of neat APA-6 with and without 2P for various mould temperatures (0.6mol% activator, 0.6mol% initiator, 0.075mol% 2P).

Table 11.3: Properties of neat APA-6 with and without 2-Pyrrolidinone (0.6mol% activator, 0.6mol% initiator, 0.075mol% 2P).

	Degree of crystallinity [wt%]		Maximum strength [MPa]		Strain at failure** [%]	
T_{mould} [ºC]	neat	2P*	neat	2P*	neat	2P*
150	42	43	96	92	8	17
160	39	43	88	92	19	23
170	37	37	82	85	19	32
180	35	36	81	84	43	30
190	34	31	76	73	40	50

* 2P – 2-Pyrrolidinone co-catalyst
** Stopped at a maximum of 50% strain, see paragraph 6.2.3.

11.4.1 The effect of the co-catalyst on APA-6 composites

Figure 11.10 shows that also in composites 2-Pyrrolidinone increases the conversion. Unfortunately, the inter laminar shear strength (ILSS) of the composites drops with 23% on average, see Figure 11.11. The higher crystallinity and void content (Figures 11.12 and 11.13) indicate that the resin can shrink freely and that it is not restricted by interfacial bond formation as is explained in Section 9.6.1. Just like 2P prevents the

formation of branches in the neat APA-6 polymer, it is proposed that 2P prevents the formation of urea linkages between the HDCL activator and the amino groups on the glass surface (see Figure 9.2), consequently weakening the fiber-to-matrix interface.

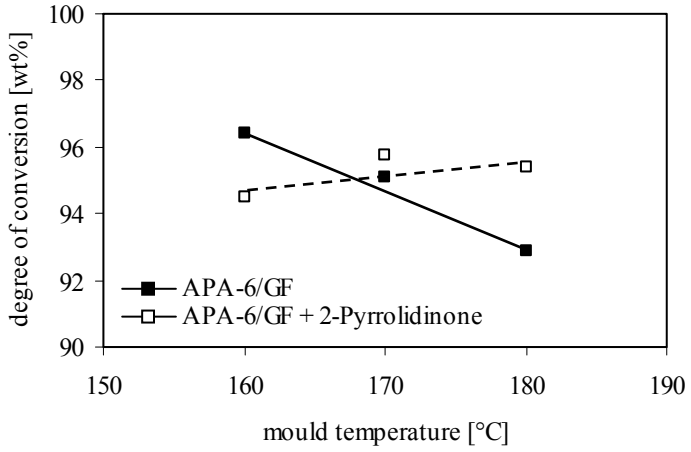

Fig. 11.10: The effect of 2-Pyrrolidinone on degree of conversion of APA-6 composites.

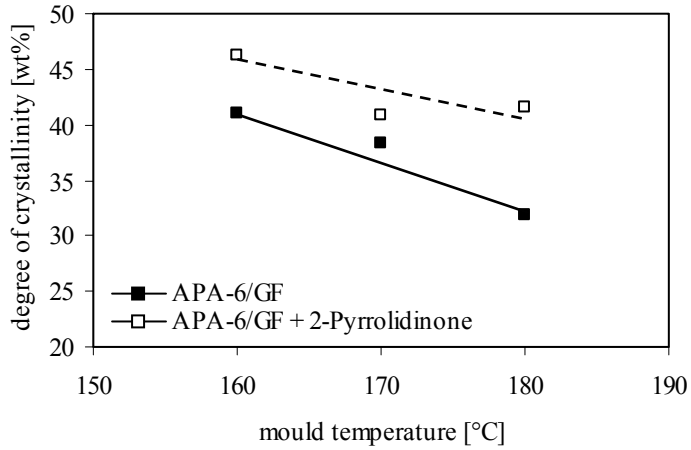

Fig. 11.11: The effect of 2-Pyrrolidinone on degree of crystallinity of APA-6 composites.

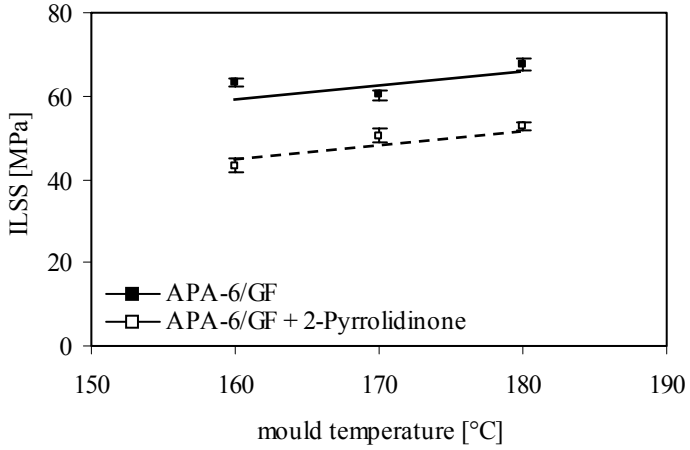

Fig. 11.12: The effect of 2-Pyrrolidinone on the inter laminar shear strength (ILSS) of APA-6 composites. The error bars indicate the standard deviations.

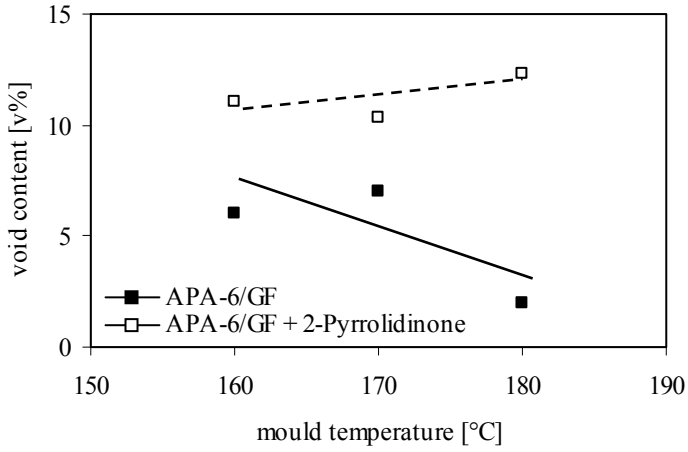

Fig. 11.13: The effect of 2-Pyrrolidinone on the void content of APA-6 composites.

11.5 Conclusions

The effect of the Microtuff nucleating agent on the properties of neat APA-6 and APA-6 composites is summarized as follows:

- The nucleating agent influences the reaction rate: the crystallization-induced autocatalytic effect increases the reaction rate, whereas entrapment of reactive species in rapidly growing crystals renders a decrease.

- During primary crystallization at the early stages of the reaction, the circumstances for crystallization are favorable and the addition of a nucleating agent does not yield an increase in crystallinity. Only when the processing temperature gets sufficiently high to re-melt the primary crystals the nucleating agent is set free and can consequently increase the degree of crystallization during the secondary crystallization stage at the end of the reaction.
- Because fibers act as a heat sink, the exothermic temperature rise during cure of composites is not as high as during the cure of the neat resin. For the thin composites that were studied the temperature never gets high enough for a nucleating agent to have an effect on the degree of crystallinity.
- Early entrapment of reactive chain-ends inside rapidly growing crystals reduces the number of tie-molecules between the various crystals, which leads to a polymer with a lower modulus and strength and a higher strain at failure even when the crystallinity is higher.
- For composites, early crystallization prevents the proper development of an interpenetrating network of polymer chains in the bulk matrix and polymer chains growing from the fiber surface, consequently reducing the inter laminar shear strength.

The effect of the 2-Pyrrolidinone co-catalyst on the properties of neat APA-6 and APA-6 composites is summarized as follows:

- 2-Pyrrolidinone increases the reactivity of the activator-initiator combination that is used in this study and can therefore be successfully used to partially substitute the initiator without changing the reactivity of the APA-6 resin. In this study, 0.075mol% 2-Pyrrolidinone was used to replace 0.6mol% initiator. Decreasing the initiator concentration results in a higher conversion of both neat APA-6 and its composites.
- The increasing tendency to polymerize is accompanied by a reducing tendency to form branches in the neat resin. Severe weakening of the tie-molecular network results in a polymer with a lower modulus and higher strain at failure when polymerized above the de-blocking temperature of the HDCL activator.

- For composites, the addition of 2-Pyrrolidinone reduces the tendency to form interfacial bonds between the APA-6 matrix and the fibers, which is disastrous for the composite properties in general.

The overall conclusion of this chapter is that both the Microtuff nucleating agent and the 2-Pyrrolidinone co-catalyst are not suitable for improving the properties of APA-6 composites as they both significantly weaken the interphase region between the fibers and the bulk matrix.

CHAPTER 12

CONCLUSIONS AND RECOMMENDATIONS

The main goal of this thesis is to develop reactive processing technology for manufacturing of thermoplastic composite wind turbine blades. This chapter presents the outcome of the thesis by grouping various results and issues mentioned in the individual chapters into thematic conclusions. In Section 12.1 conclusions with respect to the reactive processing technology itself are discussed, whereas Section 12.2 elaborates specifically on the use of the presented technology for manufacturing of wind turbine blades. Recommendations for further improvement of the technology and continued research at the Delft University of Technology are presented in Section 12.3 and 12.4.

12.1 Conclusions: reactive processing of thermoplastic composites

12.1.1 Reactive processing of thermoplastic composites

Reactive processing was introduced as alternative to melt processing in order to manufacture thicker, larger and more integrated thermoplastic composite parts, directly from the monomer without the need of expensive intermediate processing steps (Chapter 1). As is clearly pointed out in this thesis, development of this technology involves more than replacement of a classic thermoset resin by a thermoplastic one: dedicated processing equipment and tooling is necessary; insight in the substantially different curing processes (involving both polymerization and crystallization) is essential for process and material optimization; and surface and sizing chemistry needs to be applied for engineering a proper fiber-to-matrix interface (Chapters 4, 5, 6, 8 and 9). Suitable thermoplastic resin systems range from commercially available engineering plastics to experimental high-performance plastics. In general, reactive processing of high-performance plastics is more complicated due to their stiff polymer backbone combined with outstanding chemical

resistance and thermal properties (Chapter 2). For manufacturing of wind turbine blades, an anionic polyamide-6 (APA-6) casting resin was selected in combination with a vacuum infusion process.

12.1.2 The temperature as most important processing parameter

Because the processing temperature is below the crystallization temperature of the final APA-6 polymer, polymerization and crystallization occur simultaneously (Chapter 5). As it affects the rates of polymerization and crystallization in an opposite manner, the temperature is the most important processing parameter and determines largely the conversion and crystallinity of the final polymer. If the overall temperature during cure is too low, crystallization is too fast and reactive chain-ends and monomer are trapped inside crystals before they can polymerize, which results in a rather brittle polymer. If the reaction temperature is too high, branching limits the formation of crystals, which reduces the modulus of the polymer together with its chemical and thermal resistance (Chapter 6 and 7). The fact that the temperature is determined by both external (the mould) and internal heat sources (exothermic nature) makes the part geometry and the fiber content important parameters for the manufacturing of composites (Chapter 8).

12.1.3 Controlling the reaction rate

In order to allow filling of large moulds with dense fiber pre-forms, it was necessary to reduce the reaction rate of the APA-6 casting resin. It was pointed out that reducing the reaction rate once polymerization has been initiated is not only difficult due to the exothermic and crystallization-induced autocatalytic nature of the reaction, but that also the potential danger exists of confinement of reactive species, which strongly degrades the final polymer properties. Alternatively, an activator-initiator combination was selected specifically for the vacuum infusion process: Initially both reactive species cannot form a complex, which delays the onset of polymerization. Once polymerization has started, however, complex formation becomes possible, which increases the polymerization rate, consequently preventing confinement of reactive species (Chapter 5).

12.1.4 The neat APA-6 properties: a unique polymer morphology

At the optimum processing temperature, initial crystallization takes place well below the crystallization temperature of the APA-6 polymer. As a consequence, crystal nuclei are plentiful and the final size of the crystals is relatively small. In combination with the high molecular weight and a slight degree of branching, this leads to a polymer morphology in which small crystals are connected by a well-developed network of tie-molecules (Chapter 7). Due to this unique morphology that can only be obtained through reactive processing, the modulus of APA-6 is 41% higher in dry conditions, 59% higher in moist conditions and 65% higher at elevated temperatures compared to common injection-molded PA-6. Although the strain at failure of APA-6 is significantly less, it is still sufficiently high for a matrix material for composites.

12.1.5 The de-blocking equilibrium of the activator: compromising

To further complicate matters, the temperature not only governs the polymerization and crystallization processes, but also influences the de-blocking equilibrium of the caprolactam-blocked isocyanate activators used in this thesis. At lower temperatures, the activators tend to exist more in a de-blocked configuration, which is capable of polymerizing into APA-6. At higher temperatures, the activators tend to de-block more and more, generating free isocyanate groups that are capable of forming branch-points in the neat resin (Chapter 6) or interfacial bonds with the aminosilanes on the glass fiber surface (Chapter 9). Due to their di-functional nature, one side of the activator can still induce chain growth, ultimately forming an interpenetrating network with other polymer chains. Whereas for composites interfacial bond formation is desirable for obtaining a strong fiber-to-matrix interface, branching is not as it reduces the crystallinity of the matrix. Also at higher temperatures, the small crystal size, previously linked to outstanding mechanical properties (Chapter 7), is no longer maintained. A compromise between an extremely strong interface on one hand and a high degree of crystallinity and a small crystal size on the other seems inevitable for optimizing the overall composite properties (Chapter 9).

12.1.6 The APA-6 composite properties: consequences of compromising

The properties of fabric reinforced APA-6 composites are excellent in dry conditions, which is mainly caused by a strong fiber-to-matrix interface: (i) due to the high degree of crystallization induced shrinkage, the APA-6 matrix firmly locks itself around the fibers and (ii) due to the simultaneous formation of urea linkages between the de-blocked activator and the aminosilane groups on the glass fibers, a level of chemical bonding is obtained that can normally not be achieved during common melt processing (Chapter 9). As a consequence, the APA-6 composite outperforms the reference materials (a melt processed PA-6 composite and an infused epoxy one with the same fiber reinforcement) in static tensile, compression, in-plane shear and inter laminar shear tests, whereas in tension-tension fatigue tests the APA-6 composites bridge the gap between the two reference materials (Chapter 10). The consequences of the previously mentioned compromise between maximizing the matrix properties and the interfacial properties become clear when repeating the tests after moisture conditioning. Due to the reduced crystallinity, the presence of unreacted monomer and the relatively high void content, the APA-6 composites absorb more water and consequently display a stronger degradation in static properties than both reference materials.

12.1.7 Improving APA-6 composites: attempts to work around the compromise

None of the attempts made to improve the properties of APA-6 composites were successful: improvements to the interface weakened the bulk matrix, whereas improvements of the bulk matrix lead to a weaker interface:

- Mixing an activator with a low de-blocking temperature (the ‘bonding agent’) with an activator with a high de-blocking temperature (the ‘polymerization agent’) to combine a highly crystalline matrix (initiated by the polymerization agent) with a strong interfacial bond (initiated by the bonding agent) failed. Due to the higher reaction rate of the ‘polymerization agent’ it consumed all monomer before the ‘bonding agent’ could initiate chain growth from the fiber surface to become part of the interpenetrating network (Chapter 9).

- A nucleating agent proved to be little effective in increasing the crystallinity because the circumstances for crystal formation during the cure of APA-6 are already favorable. Instead, early crystallization prevents the proper development of an interpenetrating network of polymer chains in the bulk matrix and polymer chains growing from the fiber surface, consequently degrading the interface (Chapter 11).
- Finally, a co-catalyst (2-pyrrolidinone) was successfully applied to increase the conversion of the APA-6 composites. However, at the same time this co-catalyst reduced the tendency of the activator to bond to the fibers, consequently degrading the composite properties (Chapter 11).

12.1.8 The APA-6 composite properties: fluctuations in quality

Substantial fluctuations in the properties of APA-6 composites were encountered not only between different laminates but also within the same laminate. Ageing of chemicals (loss in reactivity due to moisture absorption) during storage and processing can cause day-to-day property fluctuations that are related to for instance the humidity level in the laboratory, whereas homopolymerization and the introduction of solid particles in the tanks of the MMU cause property fluctuations between laminates produced at the same day (Chapter 8). Finally, thermal and chemical interactions (deactivation and interfacial bond formation) between the resin and the fibers cause property fluctuations in flow direction within a composite (Chapter 8 and 9).

12.1.9 Voids at the interface: the chicken or the egg?

It is commonly accepted that voids at the interface between the fiber surface and the matrix is detrimental for the interfacial strength, which has an obvious negative effect on the overall composite properties. In other words, voids result in a poor interface. In this thesis it was shown, however, that a poor interface can actually result in a high void content as it allows the unbound matrix to shrink freely, consequently generating voids (Chapter 9). In other words, a poor interface results in voids. Without giving the answer to this chicken-and-the-egg type of question, it is expected that awareness of

its existence alone is sufficient to improve the interface/reduce the void content of APA-6 composites in future.

12.2 Conclusions: reactive processing of thermoplastic composite wind turbine blades

In this section, the applicability of APA-6 composite infusion technology for manufacturing of large wind turbine blades is discussed. Economical and technological advantages and disadvantages of a few key aspects are presented.

12.2.1 APA-6 composite properties

The high modulus of the APA-6 matrix in combination with the strong fiber-to-matrix bond (mechanical locking combined with chemical bonding) provide APA-6 composites with excellent tensile, compression and shear properties in dry as molded conditions (Chapter 10). Preliminary fatigue analysis demonstrated that although APA-6 composites already bridge the gap between the classic thermoplastic and thermoset composites, further improvements are essential in order to become truly competitive with the currently used blade materials. The main drawback of APA-6 composites, however, is without doubt the strong decay in properties due to moisture absorption, which is caused by the high void content, the low conversions and the fact that a compromise needs to be made between a high degree of crystallinity and a large number of fiber-to-matrix bonds (Chapter 9). Being exposed to the offshore environment makes the moisture conditioned situation the relevant operational condition for wind turbine blade composites and although the ingress depth of moisture and the related property degradation of thick APA-6 composites is currently unknown, it is emphasized to direct future research on improving moisture resistance of APA-6 composites, as is further discussed in Section 12.3.

12.2.2 Manufacturing of thick APA-6 laminates

Whereas melt processing sets a limit to the maximum size and thickness of thermoplastic composite parts that can be manufactured, vacuum infusion with the

low viscosity APA-6 resin allows manufacturing of parts of virtually infinite size and thickness, which is essential for blade manufacturing. As Figure 12.1 shows, 25 mm thick composites with 50% glass fibers by volume were successfully infused with the technology described in this thesis. The to the formation of crystals related self-braking mechanism that is incorporated in the exothermic cure of APA-6 has important consequences for manufacturing of thick composites as it will prevent the occurrence of excessive core temperatures and will allow the use of fast curing APA-6 systems. It is emphasized that the sensitivity of the polymerization reaction to moisture and oxidation requires a clean and controlled production process and a certain skill-level.

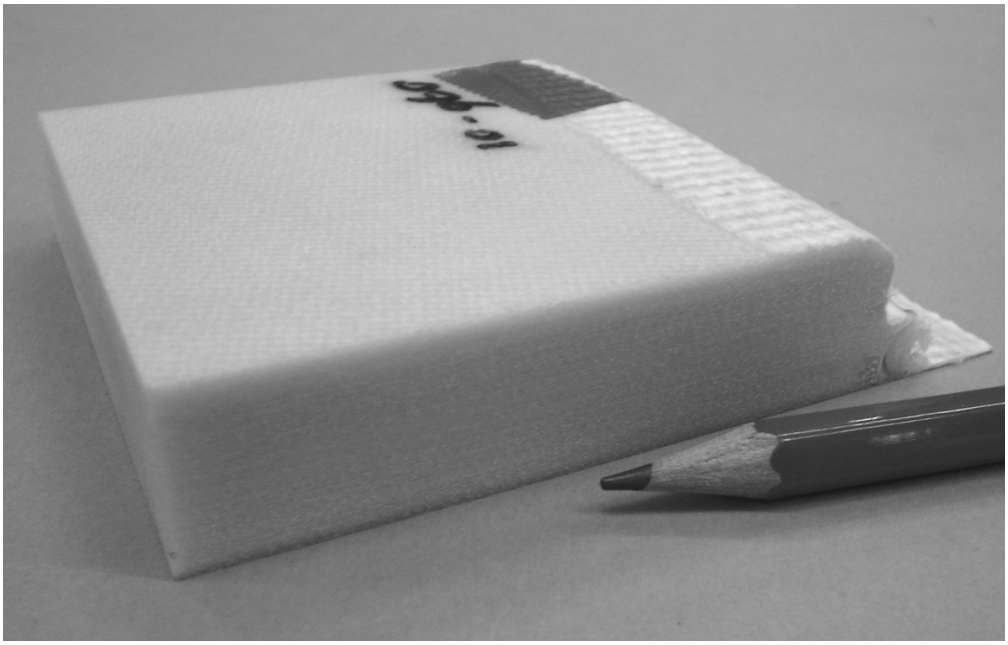

Fig. 12.1: A 25 mm thick APA-6 composite.

12.2.3 Economy of manufacturing

Using the same monomer as for hydrolytic polymerization of PA-6, guarantees not only world-wide availability, but also a low resin price (±3 €/kg). Also the compatibility with common aminosilane sized glass fibers is beneficial for keeping material costs low. In addition, fast infusion (caused by the low resin viscosity) and short curing times (minutes instead of hours as is common for most thermoset resins)

contribute positively to a reduction in cycle times, which is essential for rapid manufacturing of a large number of blades. Although a process temperature of 180ºC is unusually high for blade manufacturing, the related cost increase (energy consumption, high-temperature tooling and equipment) is expected to stay limited, because of current research efforts made by the aerospace and automotive industries on cost-efficient manufacturing of composites at high temperatures (up to 400ºC).

12.2.4 Recycling of APA-6 composites

In addition to the common way of recycling thermoplastic composites through mechanical grinding and subsequent melt processing into new parts, technology developed by DSM offers the possibility to depolymerize APA-6 back into its caprolactam monomer [43]. The Evergreen polyamide-6 recycling plant (Augusta, USA) for instance recycles PA-6 carpets during which the recycled caprolactam is separated from the non-PA-6 backing material. This process seems easily adaptable for recycling of APA-6 composites, resulting in recycling of both caprolactam and fibers. Although the 'Evergreen process' itself has proven to be economically sound, identification and separation of the PA-6 carpets from the waste streams formed an economical bottleneck, which is highly unlikely to occur for large wind turbine blades.

12.3 Recommendations

12.3.1 More moisture resistant composites: a high crystallinity and a strong interface

The thesis mentions the inevitable compromise between a highly crystalline APA-6 matrix and a large number of interfacial bonds, which is caused by the fact that formation of interfacial bonds occurs at the same time as branching in the bulk matrix. To work around this compromise to obtain a more moisture resistant composite with a highly crystalline matrix and a strong chemical interface, it is recommended to use a mixture of activators: a mono-functional aliphatic carbamoylcaprolactam and a mixed aliphatic-aromatic di-functional carbamoylcaprolactam, see Figure 12.2. The lower

de-blocking temperature of the aromatic group will cause the di-functional activator to bond to the fibers, whereas the aliphatic groups will simultaneously polymerize to form an interpenetrating network without generating a lot of branches, which otherwise decrease the crystallinity of the bulk matrix. In addition, a reduction in void content should be pursued to reduce the ingress of moisture, which is discussed next.

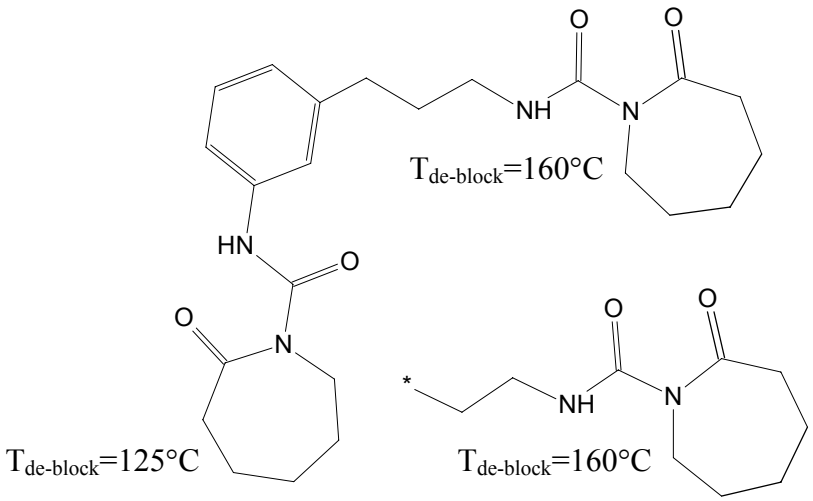

Fig. 12.2: Proposed activator combination to obtain a composite with a highly crystalline matrix and a strong chemical interface.

12.3.2 Reducing the void content of APA-6 composites

In order to reduce the void content of APA-6 composites, three recommendations are given:

- The number of voids caused by dissolving of nitrogen can be reduced by placement of floaters inside the tanks of the mini mixing unit, which, after degassing, reduce the contact area of the reactive mixture with the nitrogen atmosphere.
- Voids caused by shrinkage of the APA-6 resin during cure can be reduced by using an elastomer modified APA-6 grade called Nyrim® [81]. By incorporating elastomeric parts in the polymer backbone, APA-6 is capable of compensating the

resin shrinkage internally by stretching the elastomeric part. This way resin shrinkage will reduce the density of the polymer matrix without introducing voids. According to literature on processing of neat Nyrim, mould shrinkage reduces significantly without affecting the polymer modulus that much.

- A study on the impregnation and wetting behavior of APA-6 resin should be conducted as it can lead to a significant void reduction as is described in literature for APA-12 composites [100].

12.3.3 Increasing the homogeneity of APA-6 composites

Due to thermal and chemical interactions between the APA-6 resin and the fibers during infusion, gradients in temperature and resin composition are established in flow direction, which results in inhomogeneous composites. It is recommended to switch to isothermal infusion ($T_{mould} = T_{MMU} = T_{buffer\ vessel}$) at a temperature just above the melting point of caprolactam ($T_m = 69ºC$). Whereas isothermal processing omits the thermal gradient, the low temperature reduces the chemical interactions between the fibers and the resin during infusion, hence omitting the gradient in resin composition. Subsequent heating to the desired polymerization temperature must be sufficiently fast to establish fiber-to-matrix bonds before polymerization initiates, see Section 9.4.2. To achieve a more homogeneous temperature distribution and higher heating rates, it is recommended to put effort in investigating alternative heating methods and mould materials. Because of the relevance for blade manufacturing, not only thin laminates, but also thick laminates up to 100 mm should be taken into account as through-the-thickness temperature and property gradients are likely to occur.

12.3.4 The use of fabrics made of different fibers and weave styles

Only glass fibers have been investigated in the present research for use in APA-6 composites as it is the most widely used fiber for manufacturing of wind turbine blades. It is recommended, however, to investigate the use of other types of reinforcement such as the stiffer carbon fibers, the cheaper basalt fibers and the more impact resistant aramide fibers. Also the use of different weave styles should receive attention: blade manufacturers commonly use coarser fabrics than the 8-harness satin

weave fabrics used in the present research. Coarser fabrics generally result in composites with larger resin pockets, which due to the exothermic nature of the APA-6 resin will have a strong local effect on the temperature distribution.

12.3.5 Improved monitoring of the curing process

Insight in the simultaneous occurrence of polymerization and crystallization proved to be essential for development of APA-6 composite technology. It is recommended to further increase this insight by development of sensing technology that is capable of independent monitoring of the polymerization and crystallization processes. Independent polymerization and crystallization data can be used to develop a cure model for numerical simulation and optimization tools. Dielectric sensing [192] and simultaneous measurement of temperature and shrinkage with fiber Bragg grating technology [193] are mentioned as potential sensing methods.

12.3.6 Fatigue driven optimization of APA-6 composites

Fatigue resistance is one of the main requirements for wind turbine blade composites. In Chapter 10 the conclusion was drawn that the fiber-to-matrix interface plays a dominant role in the accumulation of damage during cyclic loading. Because reactive processing offers the possibility to chemically engineer the fiber-to-matrix interface, it is recommended to exploit this opportunity to further increase the fatigue characteristics of APA-6 wind turbine blade composites. Additionally, it is recommended to investigate other fatigue spectra (frequencies, R values) and also the effect of different testing conditions (temperature, humidity).

12.3.7 Reactively processed composites for melt processing

Although one of the benefits of reactive processing is that thermoplastic composites can be manufactured directly from the monomer, it is recommended to explore the possibility of using infused APA-6 composites as sheet material for subsequent melt processing through for instance rubber forming, see Figure 1.7. It is expected that in this additional processing step the current drawbacks of the APA-6 composites disappear (voids will be compressed, residual monomer will evaporate), while the

benefit of having a strong fiber-to-matrix bond remains. This way, infused flat laminates can be used for instance rubber forming of composite ribs with improved fatigue characteristics for use in wind turbine blades.

12.4 Continued research at the Delft University of Technology

The overall conclusion of this thesis is that APA-6 composites have a great potential for manufacturing of wind turbine blades (and for instance pressure vessels and aerospace components), but that still a lot of research remains to be done. The Delft University of Technology will continue the research on APA-6 composite technology and it is planned to build the first full-scale demonstrator (a 2x3 m cross-section of a wind turbine blade, with a spar-rib-skin structure) before the end of 2009. For more info on the progress of the APA-6 composite research one can visit the website (www.dpcs.lr.tudelft.nl) or contact Dr.ir. H.E.N. Bersee (H.E.N.Bersee@TUDelft.nl).

APPENDIX I

CALCULATION OF THE RESIN FORMULATION

Throughout the research the resin formulations were calculated using a method provided by Brüggemann Chemical as described in this appendix. This method calculates the amount of activator and initiator relative to the total amount of caprolactam, which includes the caprolactam part of the activator, but does not include the caprolactam part of the initiator.

I.1 Resin formulations containing one type of activator

First, the mass (M [g]) of the desired formulation is calculated based on 100 mol of caprolactam according to Equation I.1.

$$M = X_a \cdot M_a + X_i \cdot M_i + 100 \cdot M_{CL} \tag{I.1}$$

in which

X_a = desired activator concentration [mol%]

M_a = molar mass of the non-caprolactam part of the activator

X_i = desired initiator concentration [mol%]

M_i = molar mass of the initiator

M_{CL} = molar mass of caprolactam

Next, the mass of the activator (A [g]) to be inserted in tank A of the MMU and the mass of the initiator (I [g]) that needs to be added to the B tank are calculated according to Equation I.2 and I.3.

$$A = \frac{X_a}{F_a / S_a} \cdot 1000 \cdot \frac{M_t}{M} \tag{I.2}$$

$$I = \frac{X_i}{S_i} \cdot 1000 \cdot \frac{M_t}{M} \tag{I.3}$$

in which

F_a = functionality of the activator

S_a = concentration of the activator [mol/kg]

S_i = concentration of the initiator [mol/kg]

M_t = total mass of the resin that needs to be prepared [g]

Finally, the mass of caprolactam that needs to be added to both tanks is calculated according to Equation I.4 and I.5. The caprolactam is divided of both tanks of the MMU in such way that the weight of the material in both tanks is the same.

$$CL_A = \tfrac{1}{2} \cdot \left(M_t - A - I\right) + \tfrac{1}{2}\left(I - A\right) \tag{I.4}$$

$$CL_B = \tfrac{1}{2} \cdot \left(M_t - A - I\right) - \tfrac{1}{2}\left(I - A\right) \tag{I.5}$$

in which

CL_A = is the mass of caprolactam in tank A of the MMU

CL_B = is the mass of caprolactam in tank B of the MMU

Table I.1 provides the characteristics of the various chemical compounds necessary to calculate the formulations used throughout the research.

Table I.1: Characteristics of various chemical compounds.

Compound	Chemical name	Chemical formula	M_w	F_a	S [mol/kg]
AP-Caprolactam	caprolactam	$C_6H_{11}NO$	113.2	-	8.837
2P booster	2-pyrrolidinone	C_4H_7NO	85.1	1	11.75
HDCL activator	hexamethylene-1,6-dicarbamoylcaprolactam	$C_{30}H_{34}N_4O_4$	394.5	2	2
Activator0	N-acetylcaprolactam	$C_8H1_3N_2O_1$	155.2	1	6.45
TDCL activator	toluylene-2,4-dicarbamoylcaprolactam	$C_{21}H_{28}N_4O_4$	400.5	2	2.5
MgBrCL initiator	caprolactam magnesium bromide	$C_6H_{10}NOMgBr$	216.4	-	1
NaCL initiator	sodium caprolactamate	$C_6H_{10}NONa$	135.1	-	1.4

I.2 Resin formulations containing two types of activators

When mixing two types of activators, first a formulation is calculated based on the total amount of activator as described above, using the characteristics of the primary activator (the one that is added in the highest concentration). Next, part of this activator is substituted by the secondary activator. For instance, when preparing a formulation containing 1.2mol% C20 and 0.3mol% TDCL, first a formulation containing 1.5 mol% C20 is calculated after which 20% of the mass of C20 is substituted by TDCL according to Equation I.6 and I.7. The subscript 'p' refers to the primary activator, whereas the subscript 's' refers to the secondary one.

$$A_p = A \cdot (1 - sc) \tag{I.6}$$

$$A_s = A \cdot sc \cdot \frac{M_{as} \cdot F_{ap} \cdot S_{ap}}{M_{ap} \cdot F_{as} \cdot S_{as}} \tag{I.7}$$

in which

sc = substitution coefficient $\in$ [0,1>

After that, the mass of the caprolactam in both tanks needs to be recalculated according to Equations I.8 and I.9.

$$CL_A = \tfrac{1}{2} \cdot M_t - A_p - A_s \tag{I.8}$$

$$CL_B = \tfrac{1}{2} \cdot M_t - I \tag{I.9}$$

I.3 Resin formulations containing 2-pyrrolidinone

For formulations with 2-pyrrolidinone, this catalyst is treated in the calculations as a secondary activator and the method described in the previous paragraph is followed.

REFERENCES

1. European Wind Energy Association (2003): *WINDFORCE 12: A Blueprint to Achieve 12% of the World's Electricity from Wind Power by 2020*.
2. Rasmussen, F., P.H. Madsen (2004): *Current Direction of Danish Wind Energy Research*. Journal of Solar Energy Engineering 126:1105-1109.
3. De Vries, E. (2005): *Thinking Bigger*. Renewable Energy World May-June:42-55.
4. Joosse, P.A., D.R.V. Van Delft, C. Kensche, F. Hahn, T.K. Jacobsen, R.M. Van den Berg (2000): *Economic Use of Carbon Fibers in Large Wind Turbine Blades?* 19th ASME Wind Energy Symposium: Reno, 10-13 January.
5. Brøndsted, P., H. Lilholt, A. Lystrup (2005): *Composite Materials for Wind Power Turbine Blades*. Annual Review of Materials Research 35:505-538.
6. www.duwind.tudelft.nl.
7. www.dpcs.lr.tudelft.nl.
8. Beukers, A., E. Van Hinte (1998): *Lightness: The Inevitable Renaissance of Minimum Energy Structures*. Rotterdam, 010 Publishers.
9. Berenberg, B. in High-Performance Composites (2002): *Redesigning Wind Blades*. July: 27-32.
10. Zingraff, L., P.-E. Bourban, M.D. Wakeman, M. Kohler, J.-A.E. Månson (2002): *Reactive Processing and Forming of Polyamide 12 Thermoplastic Composites*. 23rd SAMPE Europe International Conference: Paris, France, 9-11 April.
11. Joncas, S., M. De Ruiter, F. Van Keulen (2004): *Preliminary Design of Large Wind Turbine Blades Using Topology Optimization Techniques*. 10th AIAA/ISSMO Multidisciplinary Analysis and Optimization Conference: Albany, NY, USA, 30 August - 1 September.
12. Putnam, P.C. (1948): *Power from the Wind*.
13. Joncas, S., O.K. Bergsma, A. Beukers (2005): *Power Regulation and Optimization of Offshore Wind Turbines through Trailing Edge Flap Control*. ASME Wind Energy Symposium: Reno, 10-13 January.
14. Marrant, B.A.H., T. Van Holten (2003): *Smart Dynamic Rotor Control on Large Offshore Wind Turbines*. European Seminar Offshore Wind Energy in Mediterranean and other European Seas (OWEMES): Naples, Italy, 10-12 April.
15. National Renewable Energy Laboratory of Denmark (1999): *Structural Health Monitoring Test of a Wind Turbine Blade*.
16. Krebber, K., W. Habel, T. Gutmann, C. Schram (2005): *Fiber Bragg Grating Sensors for Monitoring of Wind Turbine Blades*. 17th International Conference on Optical Fibre Sensors: Bruges, Belgium, 23-27 May.
17. Stavrov, D., H.E.N. Bersee (2005): *Resistance Welding of Thermoplastic Composites - an Overview*. Composites Part A: Applied Science and Manufacturing 36:39-54.
18. Mallon, P.J., C.M. Ó Brádaigh (2001): *Compliant Mold Techniques for Thermoplastic Composites*. *Polymer Matrix Composites*. Talreja, R. and J.-A.E. Månson. Amsterdam, Elzevier: 873-914.
19. Boogh, L., R. Mezzenga (2001): *Processing Principles for Thermoset Composites*. *Polymer Matrix Composites*. Talreja, R. and J.-A.E. Månson. Amsterdam, Elsevier: 671-700.

20. Ahmed, T.J., D. Stavrov, H.E.N. Bersee, A. Beukers (2006): *Induction Welding of Thermoplastic Composites - an Overview*. Composites Part A: Applied Science and Manufacturing 37(10):1638-1651.
21. Foley, M., E. Bernardon (1990): *Thermoplastic Composite Manufacturing Cost Analysis for the Design of Cost Effective Automated Systems*. SAMPE Journal 26(4):67-74.
22. Lambing, C.L.T., R.C. Don, S.M. Andersen, S.T. Holmes, B.S. Leach, J.W. Gillespie Jr. (1991): *Design and Manufacturing of an Automated Resistance Welder for Thermoplastic Composites*. ANTEC: Montreal, Quebec, 5-9 May.
23. Iversen, F.S. *A New Use for Old Turbines*, www.vestas.com/pdf/forsideartikler/ n_a_v_230204/n_a_v_UK190204.pdf.
24. Risø National Laboratory (1999): *Material Research Department Annual Report*.
25. Risø National Laboratory (1998): *Hybrid Yarns for Thermoplastic Fiber Composites - Final Report MUP2 Framework Program*.
26. Gamstedt, E.K., R. Talreja (1999): *Fatigue Damage Mechanisms in Unidirectional Carbon-Fibre-Reinforced Plastics*. Journal of Materials Science 34:2535-2546.
27. Hoebergen, A., J.A. Holmberg (2001): *Vacuum Infusion*. *ASM Handbook 21*: 501-515.
28. Wang, Y.-F., A.S. Hay (1997): *Macrocyclic Arylene Ether Ether Sulfide Oligomers: New Intermediates for the Synthesis of High-Performance Poly(arylene ether ether sulfide)s*. Macromolecules 30(2):182 - 193.
29. Qi, Y., T. Chen, J. Xu (1999): *Synthesis of Cyclic Precursor of Poly(ether ether ketone)*. Polymer Bulletin 42:245-249.
30. Brunelle, D.J. (1995): *Solvent-Resistant Polycarbonates*. Trends in Polymer Science 3(5):154-158.
31. Hodge, P., H.M. Colquhoun, D.J. Williams (1998): *From Macrocycles to Macromolecules - and Back*. Chemistry & Industry:162-167.
32. Young, R.J., P.A. Lovell (1991): *Introduction to Polymers, second edition*. London, Chapman & Hall.
33. Randall, D., S. Lee (2002): *The Polyurethanes Book*. NY, John Wiley & Sons, Ltd.
34. Dubé, M.G., G.L. Batch, J.H. Vogel, C.W. Macosko (1995): *Reaction Injection Pultrusion of Thermoplastic and Thermoset Composites*. Polymer Composites 16(5):378-385.
35. d'Hooghe, E.L., C.M. Edwards (2000): *Thermoplastic Composite Technology; Tougher Than You Think*. Advanced Materials 12(23):1865-1868.
36. DowFulcrum in Reinforced Plastics (2001): *Thermoplastic Pultrusion Promises New Synergies*. 45: 34-38.
37. Edwards, C.M. (2004): *Personal Communication*.
38. d'Hooghe, E.L., B. Hoek, C.M. Edwards (2000): *Applications for Fulcrum Thermoplastic Composite Technology*. www.DowFulcrum.com.
39. FME-NIL (1976): *Materiaalomschrijving van Thermoplastische Kunststoffen: PVC, PMMA, PE en PP*. Culemborg, Stam Technische Boeken B.V.
40. Delft University of Technology (2003): *Composite Applications using Coir Fibres in Sri Lanka*.
41. Ma, C.-C.M., C.-H. Chen (1991): *Pultruded Fiber Reinforced Thermoplastic Poly(Methyl Methacrylate) Composites. Part I. Correlation of Processing Parameters for Optimizing the Process*. Polymer Engineering and Science 31(15):1086-1093.

42. Ma, C.-C.M., C.-H. Chen (1991): *Pultruded Fiber Reinforced Thermoplastic Poly(Methyl Methacrylate) Composites. Part II: Mechanical and Thermal Properties*. Polymer Engineering and Science 31(15):1094-1100.
43. Booij, M. (2000): *Polyamide-6 Recycling to Caprolactam - DSM Closes the Loop*. Polyamide 2000 World Congress: Zurich, Switzerland, 14-16 March.
44. Hedrick, R.M., W.R. Richard Jr., Monsanto Company (1968): *Reinforced Polyamides and Process of Preparation Thereof.* US 3,419,517: Dec. 31, 1968.
45. Bolgov, S.A., V.P. Begishev, A.Y. Malkin, V.G. Frolov (1981): *Role of the Functionality of Activators during Isothermal Crystallization Accompanying the Activated Anionic Polymerization of ε-Caprolactam*. Polymer Science U.S.S.R. 23(6):1485-1492.
46. Udipi, K., R.S. Davé, R.L. Kruse, L.R. Stebbins (1997): *Polyamides from Lactams via Anionic Ring-Opening Polymerization: 1. Chemistry and Some Recent Findings*. Polymer 38(4):927-938.
47. Ueda, K., K. Yamada, M. Nakai, T. Matsuda, M. Hosoda, K. Tai (1996): *Synthesis of High Molecular Weight Nylon 6 by Anionic Polymerization of ε-Caprolactam*. Polymer Journal 28(5):446-451.
48. Russo, S., A. Imperato, A. Mariani, F. Parodi (1995): *The Fast Activation of ε–Caprolactam Polymerization in Quasi-Adiabatic Conditions*. Macromolecular Chemistry & Physics 196:3297-3303.
49. Ricco, L., S. Russo, G. Orefice, F. Riva (1999): *Anionic Poly(ε-caprolactam): Relationships among Condition of Synthesis, Chain Regularity, Reticular Order, and Polymorphism*. Macromolecules 32:7726-7731.
50. Mateva, R., P. Petrov, S. Rousseva, R. Dimitrov, G. Zolova (2000): *On the Structure of Poly-ε-caprolactams, Obtained with Bifunctional N-Carbamyl Derivatives of Lactams*. European Polymer Journal 36:813-821.
51. Scelia, R.P., S.E. Schonfeld, L.G. Donaruma (1967): *Some Effects of Cocatalyst Structure on the Anionic Polymerization of ε-Caprolactam. II.* Journal of Applied Polymer Science 11:1299-1313.
52. Hornsby, P.R., J.F. Tung (1994): *Characterization of Polyamide 6 Made by Reactive Extrusion. II. Analysis of Microstructure*. Journal of Applied Polymer Science 54:899-907.
53. Mateva, R., O. Delev, E. Kaschcieva (1995): *Structure of Poly(ε-caprolactam) Obtained in Anionic Bulk Polymerization*. Journal of Applied Polymer Science 58:2333-2343.
54. Frunze, T.M., R.B. Shleifman, V.I. Zaitsev, V.V. Kurashev, T.M. Babchinitser, V.V. Korshak (1972): *Effect of the Cooling Conditions Upon the Structure and Mechanical Properties of Poly-ε–caproamide Prepared by Anionic Polymerization of ε–Caprolactam*. Polymer Science U.S.S.R. 14(4):1071-1079.
55. Rigo, A., G. Fabbri, G. Talamini (1975): *Kinetic Study of Anionic Polymerization of 6-Caprolactam by Differential Calorimetry*. Polymer Letters Edition 13:469-477.
56. Cartledge, H., C.A. Baillie (1999): *Studies of Microstructural and Mechanical Properties of Nylon/Glass Composites. Part I: The Effect of Thermal Processing on Crystallinity, Transcrystallinity and Crystal Phases*. Journal of Materials Science 34(20):5099-5111.

57. Malkin, A.Y., V.G. Frolov, A.N. Ivanova, Z.S. Andrianova (1979): *The Nonisothermal Anionic Polymerization of Caprolactam*. Polymer Science U.S.S.R. 21:691-700.
58. Malkin, A.Y., S.L. Ivanova, V.G. Frolov, A.N. Ivanova, Z.S. Andrianova (1982): *Kinetics of Anionic Polymerization of Lactams. (Solution of Non-Isothermal Kinetic Problems by the Inverse Method)*. Polymer 23:1791-1800.
59. Greenley, R.Z., J.C. Stauffer, J.E. Kurz (1969): *The Kinetic Equation for the Initiated, Anionic Polymerization of ε-Caprolactam*. Macromolecules 2(6):561-567.
60. Stratula-Vahnoveanu, B., C. Vasiliu-Oprea (2002): *Anionic Polymerization of Lactams in Microdispersion. I. Kinetic Aspects of the Process of Caprolactam Polymerization*. Polymer-Plastics Technology and Engineering 41(5):981-995.
61. Davé, R.S., R.L. Kruse, L.R. Stebbins, K. Udipi (1997): *Polyamides from Lactams via Anionic Ring-Opening Polymerization: 2. Kinetics*. Polymer 38(4):939-947.
62. Davé, R.S., R.L. Kruse, K. Udipi, D.E. Williams (1997): *Polyamides from Lactams via Anionic Ring-Opening Polymerization: 3. Rheology*. Polymer 38(4):949-954.
63. Ueda, K., M. Nakai, M. Hosoda, K. Tai (1997): *Synthesis of High Molecular Weight Nylon 6 by Anionic Polymerization of ε-Caprolactam. Mechanism and Kinetics*. Polymer Journal 29(7):568-573.
64. Qu, X., H. Ding, J. Lu, Y. Wang, L. Zhang (2004): *Isothermal and Nonisothermal Crystallization Kinetics of MC Nylon and Polyazomethine/MC Nylon Composites*. Journal of Applied Polymer Science 93:2844-2855.
65. Miscevic, M., I. Catic, M. Sercer (1993): *Production of Nylon-6 Castings by Anionic Polymerisation of ε-Caprolactam*. International Polymer Science and Technology 20(11):90-98.
66. Rusu, M., C. Ibanescu, M. Murariu, A. Bordeianu, S. Balint, E. Andrei (1998): *Centrifugal Casting of Polyamide 6. I. Influence of Thermal Treatment*. Polymers & Polymer Composites 6(3):143-146.
67. Schaaf, S. (1986): *Monomergussverfahren und Nylon-RIM-Verfahren*. Kunststoffe-Plastics 3:24-26.
68. Vass, J.A. (1994): *Taking Advantage of Cast Nylon*. Machine Design:70-74.
69. Worthington, M. (1996): *The Many Wonders of Cast Nylon*. IAPD Magazine June:32-33.
70. Hedrick, R.M., J.D. Gabbert, M.H. Wohl (1985): *Nylon 6 RIM*, American Chemical Society: 135-162.
71. Long, S.D., I. Dawood, P.D. Coates, A.F. Johnson (1995): *Influence of Reaction Injection Moulding (RIM) Processing Variables on the Mechanical Properties of a Commercial Linear Segmented Polyamide*. Plastics, Rubber and Composites Processing and Applications 23(3):161-174.
72. Lee, K.H., S.C. Kim (1988): *Engineering Analysis of Reaction Injection Moulding Process of Nylon 6*. Polymer Engineering and Science 28(7):477-484.
73. Mateva, R., O. Ishtinakova, R.N. Nikolov, C. Djambova (1998): *Kinetics of Polymerization of ε-Caprolactam in the Presence of Inorganic Dispersed Additives*. European Polymer Journal 34(8):1061-1067.
74. Te Nijenhuis, K., R. Addink, A.K. Van der Vegt (1989): *A Study on Composites of Nylon-6 with Hollow Glass Microspheres*. Polymer Bulletin 21:467-474.

75. Karger-Kocsis, J. (1992): *Fracture and Failure Behavior of Glass Fiber Mat-Reinforced Structural Nylon RIM Composites*. Journal of Polymer Engineering 11(1-2):153-173.
76. Pillay, S., H. Ning, U.K. Vaidya, G.M. Janowski (2004): *Liquid Molding of Carbon Fabric Reinforced Nylon Matrix Composite Laminates*. 7th International Conference on Flow Processes in Composite Materials: Newark, USA, 7-9 July.
77. Pillay, S., U.K. Vaidya, G.M. Janowski (2005): *Liquid Molding of Carbon Fabric-Reinforced Nylon Matrix Composite Laminates*. Journal of Thermoplastic Composite Materials 18:509-527.
78. Cho, B.G., S.P. McCarthy, J.P. Fanucci, S.C. Nolet (1996): *Fiber Reinforced Nylon-6 Composites Produced by the Reaction Injection Pultrusion Process*. Polymer Composites 17(5):673-681.
79. Ning, X., H. Ishida (1991): *RIM-Pultrusion of Nylon-6 and Rubber-Toughened Nylon-6 Composites*. Polymer Engineering and Science 31(9):632-637.
80. Gardlund, Z.G., M.A. Bator (1990): *In Situ Polymerization of Nylon-Polyurea Block Copolymers. I. Synthesis and Characterization*. Journal of Applied Polymer Science 40:2027-2035.
81. Gabbert, J.D., R.M. Hedrick (1986): *Advances in Systems Utilizing Nyrim Nylon Block Copolymer for Reaction Injection Molding*. Polymer Process Engineering 4(2-4):359-373.
82. Harkin-Jones, E., R.J. Crawford (1995): *Rotational Moulding of Liquid Nyrim in Biaxially Rotating Heated Moulds*. Plastics, Rubber and Composites Processing and Applications 24(1):1-6.
83. Harkin-Jones, E., R.J. Crawford (1995): *An Investigation of the Flow Behaviour of Rotationally Moulded NYRIM*. Plastics, Rubber and Composites Processing and Applications 23(4):211-220.
84. Harkin-Jones, E., R.J. Crawford (1996): *Mechanical Properties of Rotationally Molded Nyrim*. Polymer Engineering and Science 36(5):615-625.
85. Van Rijswijk, K., H.E.N. Bersee, W.F. Jager, S.J. Picken (2005): *Optimisation of Anionic Polyamide-6 for Vacuum Infusion of Thermoplastic Composites: Choice of Activator and Initiator*. Composites Part A: Applied Science and Manufacturing 37:949-956.
86. Kotel'nikov, V.A., N.N. Surin, S.G. Cherepanov, I.E. Persits, L.B. Danilevskaya, I.O. Konova, V.V. Gavrilenko, L.A. Chekulaeva (1995): *Synthesis of Cross-Linked Nylon RIM Block Copolyamides*. Polymer Science, Series A 37(12):1198-1205.
87. Mathias, L.J., A.M. Sikes (1987): *Star-Branched Nylon 6: The Effects of Branching and Crosslinking on Polymer Properties*. Polymer Preprints, American Chemical Society, Division Polymer Chemistry:87-90.
88. Van Rijswijk, K., H.E.N. Bersee, A. Beukers, S.J. Picken, A.A. Van Geenen (2005): *Optimisation of Anionic Polyamide-6 for Vacuum Infusion of Thermoplastic Composites: Influence of Polymerisation Temperature on Matrix Properties*. Polymer Testing 25:392-404.
89. Van Rijswijk, K., S. Joncas, H.E.N. Bersee, O.K. Bergsma, A. Beukers (2005): *Sustainable Vacuum-Infused Thermoplastic Composites for MW-Size Wind Turbine Blades-Preliminary Design and Manufacturing Issues*. Journal of Solar Energy Engineering 127:570-580.
90. Van Rijswijk, K., K. Koppes, H.E.N. Bersee, A. Beukers (2004): *Processing Window for Vacuum Infusion of Fiber-Reinforced Anionic Polyamide-6*. 7th

International Conference on Flow Processes in Composite Materials (FPCM-7): Newark, USA, 7-9 July.
91. Van Rijswijk, K., D.P.N. Vlasveld, H.E.N. Bersee, S.J. Picken (2003): *Vacuum Injection of Anionic Polyamide 6*. 4th International Conference on Composite Structures and Technology (ICCST-4): Durban, South Africa, 21-23 January.
92. Van Rijswijk, K., D.P.N. Vlasveld, P. Van Rhijn, H.E.N. Bersee, A. Beukers, S.J. Picken (2003): *Process Considerations for Liquid Molding of Composites based on Anionic Polyamide 6*. 14th International Conference on Composite Materials (ICCM-14): San Diego, USA, 14-18 July.
93. Luisier, A., P.-E. Bourban, J.-A.E. Månson (2002): *Initiation Mechanisms of an Anionic Ring-Opening Polymerization of Lactam-12*. Journal of Polymer Science: Part A: Polymer Chemistry 40:3406-3415.
94. Luisier, A., P.-E. Bourban, J.-A.E. Månson (1999): *In-Situ Polymerisation of Polyamide 12 for Thermoplastic Composites*. 12th International Conference on Composite Materials (ICCM-12): Paris, France.
95. Michaud, V., L. Zingraff, J. Verrey, P.-E. Bourban, J.-A.E. Månson (2003): *Resin Transfer Molding of Anionically Polymerized Polyamide 12*. 7th International Conference on Flow Processes in Composite Materials (FPCM-7): San Diego, USA, 7-9 July.
96. Zingraff, L., P.-E. Bourban, V. Michaud, J.-A.E. Månson (2003): *Liquid Composite Moulding of Anionically Polymerised Polyamide 12*. 14th International Conference on Composite Materials (ICCM-14): San Diego, USA, 14-18 July.
97. Luisier, A., P.-E. Bourban, J.-A.E. Månson (2003): *Reaction Injection Pultrusion of PA12 Composites: Process and Modelling*. Composites Part A: Applied Science and Manufacturing 34A(7):583-595.
98. Verrey, J., V. Michaud, J.-A.E. Månson (2003): *Processing of Complex Parts with Thermoplastic RTM Techniques*. 24th International SAMPE Europe Conference: Paris, France, 1-3 April.
99. Máirtín, P.Ó., P. McDonnel, M.T. Connor, R. Eder, C.M. Ó Brádaigh (2001): *Process Investigation of a Liquid PA-12/Carbon Fibre Moulding System*. Composites Part A: Applied Science and Manufacturing 32(7):915-923.
100. Zingraff, L., V. Michaud, P.-E. Bourban, J.A. Månson (2005): *Resin Transfer Moulding of Anionically Polymerised Polyamide 12*. Composites Part A: Applied Science and Manufacturing 36:1675-1686.
101. Rosso, P., K. Friedrich, A. Wollny, R. Mulhaupt (2005): *A Novel Polyamide 12 Polymerization System and its Use for a LCM-process to Produce CFRP*. Journal of Thermoplastic Composite Materials 18:77-90.
102. Greaney, M., C.M. Ó Brádaigh (2004): *Development of a Polyamide Copolymer Resin Transfer Molding System for Thermoplastic Composites*. 7th International Conference on Flow Processes in Composite Materials (FPCM-7): Newark, Delaware, USA, 7-9 July.
103. Kubota, H., J.B. Nowell (1975): *Changes in Morphology of Cast Nylon 6 Through Copolymerization*. Journal of Applied Polymer Science 19:1521-1538.
104. Ricco, L., S. Russo, G. Orefice, F. Riva (2001): *Caprolactam-Laurolactam Copolymers: Fast Activated Anionic Synthesis, Thermal Properties and Structural Investigations*. Macromolecular Chemistry & Physics 202:2114-2121.

105. Brunelle, D.J., J.E. Bradt, J. Serth-Guzzo, T. Takekoshi, T.L. Evans, E.J. Pearce, P.R. Wilson (1998): *Semicrystalline Polymers via Ring-Opening Polymerization: Preparation and Polymerization of Alkylene Phthalate Cyclic Oligomers*. Macromolecules 31:4782-4790.
106. Ciovacco, J., S.J. Winckler (2000): *Cyclic Thermoplastic Properties and Processing*. 45th International SAMPE Symposium: Long Beach, CA, USA.
107. Winckler, S.J. (2002): *CBT Resin Wordt Thermoharder met Thermoplastische Eigenschappen*. Kunststof & Rubber(10):22-23.
108. Youk, J.H., R.P. Kambour, W.J. MacKnight (2000): *Polymerization of Ethylene Terephthalate Cyclic Oligomers with Antimony Trioxide*. Macromolecules 33(10):35-94-3599.
109. Youk, J.H., A. Boulares, R.P. Kambour, W.J. MacKnight (2000): *Polymerization of Ethylene Terephthalate Cyclic Oligomers with a Cyclic Dibutyltin Initiator*. Macromolecules 33(10):3600-3605.
110. Nagahata, R., J.-I. Sugiyama, M. Goyal, M. Goto, K. Honda, M. Asai, M. Ueda, K. Takeuchi (2001): *Thermal Polymerization of Uniform Macrocyclic Ethylene Terephthalate Dimer*. Polymer 42:1275-1279.
111. Nagahata, R., J.-I. Sugiyama, M. Goyal, M. Asai, M. Ueda, K. Takeuchi (2000): *Solid-Phase Thermal Polymerization of Macrocyclic Ethylene Terephthalate Dimer Using Various Transesterification Catalysts*. Journal of Polymer Science: Part A: Polymer Chemistry 38:3360-3368.
112. Brunelle, D.J., J. Serth-Guzzo (1999): *Titanate-Catalyzed Ring-Opening Polymerization of Cyclic Phthalate Ester Oligomers*. Polymer Preprints, American Chemical Society, Division Polymer Chemistry 40(1):566-567.
113. Brunelle, D.J., J.E. Bradt, J. Serth-Guzzo, T. Takekoshi, R.A. Evans, E.J. Pearce, P.R. Wilson (1998): *Semicrystalline Polymers via Ring-Opening Polymerization: Preparation and Polymerization of Alkylene Phthalate Cyclic Oligomers*. Macromolecules 31(15):4782-4790.
114. Eder, R.H.J., S.J. Winckler (2001): *Processing of Advanced Thermoplastic Composites using Cyclic Thermoplastic Polyesters*. 22nd SAMPE Europe Conference: Paris, France, 27-29 March.
115. Parton, H., J. Baets, P. Lipnik, J. Devaux, I. Verpoest (2004): *Liquid Moulding of Textile Reinforced Thermoplastics*. 11th European Conference on Composite Materials (ECCM-11): Rhodos, Greece, 31 May - 3 June.
116. Steenkamer, D.A., J.L. Sullivan (1998): *On the Recyclability of a Cyclic Thermoplastic Composite Material*. Composites Part B: Engineering 29B:745-752.
117. Parton, H., I. Verpoest (2003): *Reactive Processing of Textile Reinforced Thermoplastics*. 14th International Conference on Composite Materials (ICCM-14): San Diego, USA, 14-18 July.
118. Parton, H., I. Verpoest (2004): *Thermoplastic Liquid Composite Molding: Production and Characterization of Composites based on Cyclic Oligomers*. 7th International Conference on Flow Processes in Composite Materials: Newark, Delaware, USA, 7-9 July.
119. Parton, H., I. Verpoest (2005): *In Situ Polymerization of Thermoplastic Composites Based on Cyclic Oligomers*. Polymer Composites 26(1):60-65.
120. Chatterjee, A., P.J. Mallon, M.A. Dweib, S. Saied, J.W. Gillespie Jr, D. Heider (2002): *Development of an Elevated Temperature Vacuum Assisted Resin Transfer Molding System for Thermoplastic Composites*. 34th International SAMPE Technical Conference: Baltimore, MD, USA, 4 November.

121. Coll, S.M., A.M. Murtagh, C.M. Ó Brádaigh (2004): *Resin Film Infusion of Cyclic PBT Composites: A Fundamental Study*. 25th SAMPE Europe International Jubilee Conference: Paris, France, 30 March - 1 April.
122. Coll, S.M., A.M. Murtagh, C.M. Ó Brádaigh (2004): *Resin Film Infusion of Cyclic PBT Composites: Consolidation Analysis*. 7th International Conference on Flow Processes in Composite Materials (FPCM-7): Newark, Delaware, USA, 7-9 February.
123. www.eirecomposites.com.
124. Stewart, K.R. (1989): *Melt Polymerization of BPA Cyclic Polycarbonate Oligomers: Rheokinetics of Polymerization Relevant to Reactive Processing*. Polymer Preprints, American Chemical Society, Division Polymer Chemistry 30(2):575-576.
125. Brunelle, D.J., T.L. Evans, T.G. Shannon, E.P. Boden, K.R. Stewart, L.P. Fontana, D.K. Bonauto (1989): *Preparation and Polymerization of Cyclic Oligomeric Carbonates: New Route to Super-High Molecular Weight Polycarbonate: An Overview*. Polymer Preprints, American Chemical Society, Division Polymer Chemistry 30(2):569-570.
126. Brunelle, D.J., H.O. Krabbenhoft, D.K. Bonauto (1993): *Preparation of Crystalline and Solvent Resistant Polycarbonates via Ring-Opening Polymerization of Cyclic Oligomers*. Polymer Preprints, American Chemical Society, Division Polymer Chemistry 34(1):73-74.
127. Rosenquist, N.R., L.P. Fontana (1989): *Formation of Crosslinked Networks via Polymerization of Oligomeric Cyclic Carbonates in the Presence of Polyfunctional Co-Reactants*. Polymer Preprints, American Chemical Society, Division Polymer Chemistry 30(2):577-578.
128. Evans, T.L., J.C. Carpenter (1990): *Use of Cyclic Carbonate Oligomers in the Synthesis of Bisphenol-A Polycarbonate/Polydimethylsiloxane Copolymers*. Polymer Preprints, American Chemical Society, Division Polymer Chemistry 31(1):18-19.
129. Salem, A.J., K.R. Stewart, S.K. Gifford, A.M. Berenbaum (1991): *Fabrication of Thermoplastic Matrix Structural Composites by Resin Transfer Molding of Cyclic Bisphenol-A Polycarbonate Oligomers*. SAMPE Journal 27(1):17-22.
130. Baxter, I., H.M. Colquhoun, P. Hodge, F.H. Kohnke, D.F. Lewis, D.J. Williams (2000): *Macrocyclic Oligomers of the Aromatic Polyetherketone "PK99": Synthesis, Fractionation, Structural Characterisation and Ring-Opening Polymerisation*. Journal of Material Chemistry 10:309-314.
131. Hall, A.J., P. Hodge (1999): *Recent Research on the Synthesis and Application of Cyclic Oligomers*. Reactive & Functional Polymers 41(1-3):133-139.
132. Chen, M., H.W. Gibson (1996): *Large-Sized Macrocyclic Monomeric Precursors of Poly(ether ether ketone): Synthesis and Polymerization*. Macromolecules 29(16):5502-5504.
133. Jiang, H., T. Chen, S. Bo, J. Xu (1997): *Novel Macrocyclic Precursors of Phenolphthalein Poly(arylene ether ketone) and Poly(arylene ether sulfone): Synthesis and Polymerization*. Macromolecules 30(23):7345-7347.
134. Chen, C., H. Zhou, Z. Wu, W.J. Zhang (1998): *Macrocyclic Oligomers of the Phenolphthalein Poly Aryl Ether Ketones: Synthesis and Characterization*. Polymer Preprints, American Chemical Society, Division Polymer Chemistry 39(2):531.
135. Jiang, H., T. Chen, Y. Qi, J. Xu (1998): *Ring-Opening Polymerization of Polyarylates*. Indian Journal of Chemical Technology 5:146-150.

136. Jiang, H.-Y., Y.-H. Qi, T.-L. Chen, Y. Xing, Y.-H. Lin, J.-P. Xu (1997): *Isolation, Spectra, Structure, and Ring-Opening Polymerization of Strained Macrocyclic Aryl(ether ketone) Dimer*. Journal of Polymer Science: Part A: Polymer Chemistry 35(9):1753-1761.
137. Wang, Y.-F., K.P. Chan, A.S. Hay (1996): *Rheological and Chemorheological Studies of Cyclic Aryl Ether Ketone and Aryl Ether Thioether Ketone Oligomers Containing the 1,2-Dibenzoylbenzene Moiety*. Journal of Applied Polymer Science 59:831-843.
138. Chan, K.P., Y.-F. Wang, A.S. Hay, X.L. Hronowski, R.J. Cotter (1995): *Synthesis and Characterization of Novel Cyclic (Aryl Ether Ketone)s, Cyclic (Aryl Ether Phthalazine)s, and Cyclic (Aryl Ether Isoquinoline)s*. Macromolecules 28(20):6705-6717.
139. Ben-Haida, A., H.M. Colquhoun, P. Hodge, D.J. Williams (2000): *Cyclic Oligomers of Poly(ether ketone) (PEK): Synthesis, Extraction from Polymer, Fractionation, and Characterisation of the Cyclic Trimer, Tetramer and Pentamer*. Journal of Material Chemistry 10:2011-2016.
140. Mullins, M.J., E.P. Woo, C.C. Chen, D.J. Murray, M.T. Bishop, K.E. Balon (1991): *Synthesis and Polymerization of Aryl Ether Cyclooligomers*. Polymer Preprints, American Chemical Society, Division Polymer Chemistry 32(2):174-175.
141. Ganguly, S., H.W. Gibson (1993): *Synthesis of a Novel Macrocyclic Arylene Ether Sulfone*. Macromolecules 26(10):2408-2412.
142. Gibson, H.W., S. Ganguly, N. Yamaguchi, D. Xie, M. Chen, M. Bheda, P. Miller (1993): *Macrocyclic Monomers for High Performance Polymers*. Polymer Preprints, American Chemical Society, Division Polymer Chemistry 34(1):576-577.
143. Miyatake, K., Y. Yokoi, K. Yamamoto, E. Tsuchida (1997): *Selective and Efficient Synthesis of Cyclic Hexakis(thio-1,4-phenylene) through Oxidative Polymerization of Diphenyl Disulfide*. Macromolecules 30(15):4502-4503.
144. Wang, Y.-F., K.P. Chan, A.S. Hay (1995): *Synthesis and Novel Free-Radical Ring-Opening Polymerization of Macrocyclic Oligomers Containing Sulfide Linkage*. Macromolecules 28(18):6371-6374.
145. Hubbard, P., W.J. Brittain, W.J. Simonsick Jr, C.W. Ross III (1996): *Synthesis and Ring-Opening Polymerization of Poly(alkylene-2,6-naphthalenedicarboxylate) Cyclic Oligomers*. Macromolecules 29(26):8304-8307.
146. Kohan, M.I. (1995): *Nylon Plastics Handbook*. Munich, Hanser Publishers.
147. Puffr, R., V. Kubanek (1991): *Lactam-Based Polyamides. Volume I: Polymerization, Structure, and Properties*. Boca Raton, CRC Press.
148. Strobl, G. (1996): *The Physics of Polymers, 2nd Edition*. Berlin, Springer.
149. Ueda, K., M. Nakai, K. Hattori, K. Yamada, K. Tai (1997): *Synthesis of High Molecular Weight Nylon 6 by Anionic Polymerization of ε-Caprolactam: Evaluation of Molecular Weight and Molecular Weight Distribution*. Kobunshi Ronbunshu 54(6):401-406.
150. DSM Research (1990-2000): *Anionic Polyamide - Chemistry and Processing*.
151. Ueda, K., M. Hosoda, T. Matsuda, K. Tai (1998): *Synthesis of High Molecular Weight Nylon 6 by Anionic Polymerization of ε-Caprolactam. Formation of Cyclic Oligomers*. Polymer Journal 30(3):186-191.

152. Kvarda, J., I. Prokopova (1998): *Polymerization of Lactams, 93. Formation of 6-Hexanelactam Oligomers*. Macromolecular Chemistry & Physics 199:971-975.
153. Brooks, R. (2001): *Injection Molding Based Techniques*. *Polymer Matrix Composites*. Talreja, R. and J.-A.E. Månson. Amsterdam, Elsevier: 999-1028.
154. Wakeman, M.D., C.D. Rudd (2001): *Compression Molding of Thermoplastic Composites*. *Polymer Matrix Composites*. Talreja, R. and J.-A.E. Månson. Amsterdam, Elsevier: 915-964.
155. Gibson, A.G. (2001): *Continuous Molding of Thermoplastic Composites*. *Polymer Matrix Composites*. Talreja, R. and J.-A.E. Månson. Amsterdam, Elsevier: 979-998.
156. Kotel'nikov, V.A., L.B. Danilevskaya, V.V. Kurashev, M.N. Il'ina, V.S. Papkov, V.V. Gavrilenko, L.A. Chekulaeva (1993): *The Effect of the Catalyst Used in the Anionic Polymerization of Lactams on the Thermal Stability of Polyamides*. Polymer Science 35(8):1040-1043.
157. Jaroslav, K., J. Dybal, D. Kurkova, P. Arnoldova, I. Prokopova, J. Brozek, Z. Hroch (2001): *Molecular Structure of the Complex of Hexano-6-Lactam with Magnesium Bromide*. Macromolecular Chemistry & Physics 202:1194-1199.
158. Kotel'nikov, V.A., V.V. Kurashev, L.B. Danilevskaya, I.O. Konova, V.V. Gavrilenko, L.A. Chekulaeva, I.A. Garbuzova, I.E. Persits (1992): *Active Centers of Anionic Polymerization for ε-Caprolactam Initiated by Magnesium Lactamates and Some Pecularities of the Polymerization Process*. Polymer Science U.S.S.R. 34(1):66-71.
159. Rusu, G., K. Ueda, E. Rusu, M. Rusu (2001): *Polyamides from Lactams by Centrifugal Molding via Anionic Ring-Opening Polymerization*. Polymer 42:5669-5678.
160. Sittler, E., J. Sebenda (1967): *Alkaline Polymerization of Caprolactam. XXI. Dissociation of Alkali Metal Salts of 6-Caprolactam in the Polymerization of 6-Caprolactam*. Journal of Polymer Science: Part C(16):67-77.
161. Kulicke, W.M., C. Clasen (2004): *Viscosimetry of Polymers and Polyelectrolytes*. Berlin, Springer.
162. Chien, J.J., H. Shih, K.I. Shih (1955): Acta Chemica Sinica 21:50.
163. Biernacki, P., M. Wlodarcyk (1984): *A Study of the Chemical and Physical Structure of Polycaproamide obtained in Anionic Polymerization of Caprolactam in Solvent*. European Polymer Journal 20(6):635-643.
164. Wicks Jr., Z.W. (1975): *Blocked Isocyanates*. Progress in Organic Coatings 3:733-739.
165. Cawthon, T.M., E.C. Smith (1960): Polymer Preprints 1:98.
166. Iobst, S.A. (1985): *Polymerization and Crystallization Behavior of Anionic Nylon 6*. Polymer Engineering and Science 25(7):425-430.
167. Risch, B.G., G.L. Wilkes, J.M. Warakomski (1993): *Crystallization Kinetics and Morphological Features of Star-Branched Nylon-6: Effect of Branch-Point Functionality*. Polymer 34(11):2330-2343.
168. Flory, P.J. (1949): *Thermodynamics of Crystallization in High Polymers. IV. A Theory of Crystalline States and Fusion in Polymers, Copolymers, and Their Mixtures with Diluents*. The Journal of Chemical Physics 17:223-350.
169. Olsen, E., F. Nielsen (2001): *Predicting Vapour Pressures of Organic Compounds from Their Chemical Structure for Classification According to the VOC-Directive and Risk Assessment in General*. Molecules 6:370-389.

170. Shinoda, K. (1978): *Principles of Solution and Solubility*. New York, Marcel Dekker.
171. Ben Naim, A., S. Baer (1963): *Method for Measuring Solubilities of Slightly Soluble Gasses in Liquids*. Transfaraday Society 59:2735-2738.
172. Vlasveld, D.P.N., S.G. Vaidya, H.E.N. Bersee, S.J. Picken (2005): *A Comparison of the Temperature Dependence of the Modulus, Yield Stress and Ductility of Nanocomposites based on High and Low MW PA6 and PA66*. Polymer 46:3452-3461.
173. Vlasveld, D.P.N. *Fibre Reinforced Polymer Nanocomposites*. Delft University of Technology: Delft, 2005.
174. Chen, F., S. Bazhenov, A. Hiltner, E. Baer (1994): *Flexural Failure Mechanisms in Unidirectional Glass-Fiber-Reinforced Thermoplastics*. Composites 25(1):11-20.
175. Marissen, R., H.R. Brouwer (1999): *The Significance of Fibre Microbuckling for the Flexural Strength of a Composite*. Composite Science and Technology 59(3):327-330.
176. Hahn, H., J. Williams (1986): *Compression Failure Mechanisms in Unidirectional Composites*. *American Society for Testing and Materials*. Whitney, J.M.: 115-139.
177. Vlasveld, D.P.N., H.E.N. Bersee, S.J. Picken (2005): *Nanocomposite Matrix for Increased Fibre Composite Strength*. Polymer 46:10269-10278.
178. Plueddemann, E.P. (1982): *Silane Coupling Agents*. New York, Plenum.
179. Loewenstein, K.L. (1993): *The Manufacturing Technology of Continuous Glass Fibres*. Amsterdam, Elsevier.
180. Naviroj, S., J.L. Koenig, H. Ishida (1983): *Molecular Structure of an Aminosilane Coupling Agent as Influenced by Carbon Dioxide in Air, pH, and Drying Conditions*. Journal of Macromolecular Science and Physics B22(2):291-304.
181. Naviroj, S., S.R. Culler, J.L. Koenig, H. Ishida (1983): *Structure and Adsorption Characteristics of Silane Coupling Agents on Silica and E-Glass Fiber; Dependence on pH*. Journal of Colloid and Interface Science 97(2):308-317.
182. Vlasveld, D.P.N., J. Groenewold, H.E.N. Bersee, E. Mendes, S.J. Picken (2006): *Analysis of the Modulus of Polyamide-6 Silicate Nanocomposites using Moisture Controlled Variation of the Matrix Properties*. Polymer 46:6102-6113.
183. Hoebergen, A., J.A. Holmberg (2001): *Vacuum Infusion*. *ASM Handbook*. 21: 501-515.
184. Judd, N.C.W., W.W. Wright (1978): *Voids and Their Effects on the Mechanical Properties of Composites - An Appraisal*. SAMPE Journal 14(1):10-14.
185. Nijssen, R.P.L. *Fatigue Life Prediction and Strength Degradation of Wind Turbine Rotor Blade Composites*. Delft University of Technology: Delft, 2006.
186. Talreja, R. (1990): *Fatigue of Composite Materials: Analysis, Testing and Design*. Lancaster, Technomic.
187. Carlson, R.L., G.A. Kardomateas (1996): *Introduction to Fatigue in Metals and Composites*. London, Chapman and Hall.
188. Plueddemann, E.P. (1974): *Interfaces in Polymer Matrix Composites*. New York, Academic Press.

189. Gabbert, J.D., R.M. Hedrick, Monsanto Company (1986): *Promotion of ε-Caprolactam Polymerization with Lactam Magnesium Halide Catalyst and 2-Oxo-Pyrrolidinyl Groups*. US 4,595,746: 17 June.
190. Schirawski, G. (1972): *Untersuchungen zur Copolymerisation von Pyrrolidon und Caprolactam*. Die Makromolekulare Chemie 161:69-83.
191. Kobayashi, F., K. Matsuya (1963): *Copolymerization of α-Pyrrolidone and ε-Caprolactam*. Journal of Polymer Science: Part A 1:111-123.
192. Willems, C.R.J. *A Dielectric Study of Melting and Crystallization of Semi-Rigid and Flexible-Chain Polymers*. Delft University of Technology: Delft, 1995.
193. Webb, D. (2002): *Optical-Fiber Sensors - An Overview*. MRS Bulletin 27(5):365-369.

ACKNOWLEDGEMENTS

A South African rugby shirt formed the start of a conversation back in 2002, which ultimately lead to the question whether I wanted to do a PhD at the disciplinary group Production Technology, nowadays called Design and Production of Composite Structures (DPCS). Therefore, I'd like to thank first of all Harald Bersee for being the fanatic rugby fan that he is, and for being the initiator of a fantastic 4-year period here at TU Delft, during which I not only obtained my doctorate but also the unofficial title of 'travel-pope'. I also like to thank Ab van Geenen, for the many interesting discussions, which significantly raised the quality of the research and Gijs van Kuik for keeping me and my research in touch with reality. Furthermore, I'd like to thank my promotors Adriaan Beukers and Stephen Picken, and the other members of the promotion committee for their time, effort and valuable advice.

This research project could not have been accomplished without the financial support of SenterNovem who funded my research (BSIK 03041) and without participation of companies like DSM, Brüggemann Chemical, Ten Cate Advanced Composites and Bronk Industrial, which kindly supplied the research materials and supported the development of the equipment. Most of all, however, I value the advice and assistance of a few people working for these companies: Arno Kerssemakers, Marco Houben, Jos Bongers and Willy Moons (all DSM Fibre Intermediates), who familiarized me with the APA-6 material and gave the project its swift take-off; Klaus Titzschkau (Brüggemann Chemical), who modified the APA-6 material according to my specifications, which greatly improved my understanding of APA-6 composites; Robert Lenferink (Ten Cate Advanced Composites), who introduced me to the world of fiber sizings and who assisted in selecting the proper type of reinforcement; and Joost and Johan Bronk (Bronk Industrial), for always being available for support and assistance.

Despite the initial fear that research on APA-6 composites would not yield sufficient results to obtain a PhD, after the complexity and potential of the technology had become clear, the APA-6 team at DPCS gradually increased. This team clearly showed that effort, fun and teamwork lead to great results. I owe this team a lot of gratitude: Simon 'El mustachio' Joncas, thanks for your help on characterizing the

APA-6 composites and the many discussions on why engineers should rule the world. I hope that soon you will be able to escape the long teaching hours in order to finish your PhD. I miss the running and the hours in the gym, thanks buddy!; my roommate and 'fellow-cottonball' Patricia Parlevliet, good luck with finishing your PhD, which partially deals with thick APA-6 composites; my Surfnician Sebastiaan Lindstedt, thanks for being the diesel engine of the research project, your contribution was gigantic. Good luck to Julie, Ab, Witchuda and Teun in bringing APA-6 technology to the next level in the next years, I hope you will enjoy your PhDs as much as I did. I'd also like to thank the many talented student members of the team who I was fortunate enough to supervise: Marcel, Karst, Arthur, Bart, Olivier, Julie, Eelco and Jac (TU Delft); Paul, Kris, Robert and Robert (INHOLLAND); Oanh and Phan (Hanoi University of Technology, Vietnam); Jean-Francois and Karine (École de Technologie Supérieure, Canada).

The 4-years at TU Delft could not have been as fun and successful without my colleagues and friends at university. We had great fun in the lab and also on the many conferences/holidays in for instance the USA and South Africa. Thanks to Darko, Tai, Giovanni, Marc, Bert, Fred, Rogier, Rogier, Bas and last but not least François for the fantastic time; the DPCS staff members Adriaan Beukers, Otto Bergsma, Sotiris Koussios, Coen Vermeeren; our secretaries Gemma and Lisette; the foundation of the Structures and Materials Laboratory: Dylan, Serge, Frans, Michel, Hans, Niels, Berthil, Kees and Rob; the guys from the metal workshop Ed, Bertus, Peter and Herman: goud waard!

Many hours were spent analyzing APA-6 samples at the section Nano-Structured Materials (NSM) at DelftChemTech. Daniel, thanks for introducing me to the APA-6 material and for all the struggling in the pioneering phase of my project. Man, we produced a lot of rubbish back then, fun it was, though. Thanks as well for making your data available for the neat resin comparison. A special thanks to Ben Norder for familiarizing me with polymer analysis and all the 'gezellige' hours and coffee in the lab. Thanks also to Wolter Jager, Eduardo Mendes and Gerard de Vos.

Although I always enjoyed working at TU Delft, I have never forgotten that the real life takes place outside office hours. I have to admit that I am spoiled rotten with the fact that I could spend these hours with great friends like Vinny and Margreet, Arjan and Lianne, Rino and Lineke, Jeroen and Rush, Kim and Esther, and my 'bru' Ali.

Vanka, thanks for being the little sister from who I learned so much about family and family life. When it comes to these things, I am miles behind you (but, I am catching up). I am really proud that you, Jimmy and your son Daim form part of my family. Daim's birth was one of the best events in the past years and has helped me to put things into perspective, which was extremely useful for making the decision that the research was finished and that it was time to start writing this thesis. Although I know Daim the least of all the people that I've mentioned, I know that I am going to miss him the most when I am moving to South Africa.

No parents, no PhD. Gerro and Hetty, imagine the consequences if you guys hadn't exist. Thanks for always helping out, thanks for always supporting me, thanks for always giving good advice. All these things no longer surprise me, because I know by now that you will always be there for me. Thank you so much and keep the granny cottage in mind.

Bedankt O&O voor alle wijze lessen: "Beleef aan alles wat je doet plezier" en "Wie bescheiden leeft komt bescheten uit". Opoe, ook heel veel sterkte, we zullen opa missen.

There's one final thing about doing a PhD, which needs to be said. Within 4-years a PhD project can turn you from a "party animal" into a "married man". I sincerely believe that four years is the absolute maximum for doing a PhD, who knows what else it can do to you. It is time now for this married man to thank the most important person in his life, his fantastic all inclusive total package of a wife Fiona. Thanks babe for your support and your overseas supervision. My PhD has ended and finally we can start a life together…

Thanks everyone,

Kjelt van Rijswijk

Den Haag, February 2007

ABOUT THE AUTHOR

Kjelt van Rijswijk was born on 17th November 1976 in Gouda, The Netherlands. At the age of four he moved to Apeldoorn where he graduated from the Stedelijk Gymnasium in 1995. Having developed a clear interest in technology and the exact sciences, he enrolled at the Faculty of Aerospace Engineering at the Delft University of Technology (TU Delft) the next year. Throughout his studies he developed himself into a "lightweight engineer" at the disciplinary group Design and Production of Composite Structures (DPCS), focusing on composite and polymer technology. Participating as an intern in the development of a micro-satellite at the Stellenbosch University at the end of the millennium formed a first introduction to South Africa for which a passion started to develop. After graduating in July 2001 on the design and manufacturing of a filament wound pressure vessel, he became project coordinator at TU Delft on the development of natural fiber-based composite technology in cooperation with the Hanoi University of Technology (Vietnam). A switch to glass fibers in 2002 indicates the start of his PhD research at DPCS on the development of vacuum infused thermoplastic composites of which the results are described in this thesis. After finishing his PhD, he moved to South Africa to continue his career in composite technology.

PUBLICATIONS

Journal articles

1. K. van Rijswijk and H.E.N. Bersee (2007): *Reactive processing of Textile Fiber-Reinforced Thermoplastic Composites – An Overview*. Composites Part A 38: 666-681.

2. K. van Rijswijk, S. Lindstedt, D.P.N. Vlasveld, H.E.N. Bersee and A. Beukers (2006): *Reactive Processing of Anionic Polyamide-6 for Application in Fibre Composites: a Comparative Study with Melt Processed Polyamides and Nanocomposites.* Polymer Testing 25: 873-887.

3. K. van Rijswijk, H.E.N. Bersee, A. Beukers, S.J. Picken and A.A. van Geenen (2006): *Optimisation of Anionic Polyamide-6 for Vacuum Infusion of Thermoplastic Composites: Influence of Polymerisation Temperature on Matrix Properties.* Polymer Testing 25:392-404.

4. K. van Rijswijk, H.E.N. Bersee, W.F. Jager and S.J. Picken (2006): *Optimisation of Anionic Polyamide-6 for Vacuum Infusion of Thermoplastic Composites: Choice of Activator and Initiator*. Composites Part A 37:949-956.

5. K. van Rijswijk, S. Joncas, H.E.N. Bersee and O.K. Bergsma (2005): *Sustainable Vacuum-Infused Thermoplastic Composites for MW-Size Wind Turbine Blades – Preliminary Design and Manufacturing Issues*. Journal of Solar Energy Engineering 127:570-580.

6. K. van Rijswijk, S. Koussios and O. Bergsma (2004): *Filament Wound Container made of Natural Fibers and –Rubber*. Journal of Materials: Design & Applications 217(4):277-286.

7. K. van Rijswijk, J.J.E. Teuwen and H.E.N. Bersee (2007): *Textile Fiber-Reinforced Anionic Polyamide-6 Composites. Part I: The Vacuum Infusion Process*. Manuscript to be submitted to Composites Part A.

8. K. van Rijswijk, A.A. van Geenen and H.E.N. Bersee (2007): *Textile Fiber-Reinforced Anionic Polyamide-6 Composites. Part II: Interfacial Bond Formation.* Manuscript to be submitted to Composites Part A.

9. K. van Rijswijk, J.J.E. Teuwen and H.E.N. Bersee (2007): *The Effect of a Nucleating Agent on the Properties of Anionic Polyamide-6 and its Composites.* Manuscript to be submitted to Composites Part A.

Conference proceedings

1. K. van Rijswijk, S. Lindstedt, H.E.N. Bersee, K.F. Gleich, K. Titzschkau and E.J. McDade (2006): *Reactively Processed Polyamide-Structural Composites for Automotive Applications*. 6th Annual Automotive Conference and Exhibition: Troy, Michigan, USA: 12-14 September.

2. K. van Rijswijk, S. Joncas, O.J.A. Malek, H.E.N. Bersee and A. Beukers (2006): *Vacuum Infused Thermoplastic Composites for Wind Turbine Blades*. 27th Risø International Symposium on Materials Science: Polymer Composite Materials for Wind Power Turbines: Roskilde, Denmark, 4-7 September.

3. S. Joncas, K. van Rijswijk, J.-F. Charron, H.E.N. Bersee and A. Beukers (2006): *Interfacial Shear Strength Properties of Vacuum-infused Anionic Polyamide-6 Glass-fiber Composites*. 47th AIAA/ASME/ASCE/AHS/ASC Structures, Structural Dynamics, and Materials Conference: Newport, Rhode Island, USA, 1-4 May.

4. K. van Rijswijk, E. Mendes and H.E.N. Bersee (2006): *On the Simultaneous Occurrence of Polymerization and Crystallization during Cure of Anionic Polyamide-6 Composites*. SAMPE Europe Conference: Paris, France, 27-29 March.

5. S. Joncas, K. van Rijswijk, K. Thibault-Liboiron, H.E.N. Bersee and A. Beukers (2006): *Mechanical Properties of Vacuum Infused Anionic Polyamide-6 (APA-6) Glass Fiber Composites: A Benchmark Study*. SAMPE Europe Conference: Paris, France, 27-29 March.

6. K. van Rijswijk, H.E.N. Bersee, A. Beukers, W.F. Jager and S.J. Picken (2005): *Choice of Activator and Initiator for Vacuum Infusion of Anionic Polyamide-6 Composites*. 15th International Conference on Composite Materials (ICCM-15): Durban, South Africa, 27 June – 1 July.

7. K. van Rijswijk, S. Joncas, H.E.N. Bersee and O.K. Bergsma (2005): *Vacuum Infused Fiber Reinforced Thermoplastic MW-Size Turbine Blades: A Cost-Effective Innovation?* AIAA 2005 Wind Energy Symposium: Reno, USA, 10-13 January.

8. K. van Rijswijk, K. Koppes, H.E.N. Bersee and A. Beukers (2004): *Processing Window for Vacuum Infusion of Fiber Reinforced Anionic Polyamide-6*. 7th International Conference on Flow Processes in Composite Materials (FPCM-7): Newark, Delaware, USA, 1-3 July.

9. K. van Rijswijk, K.H. Boonstra, D.P.N. Vlasveld, H.E.N. Bersee and S.J. Picken (2004): *Creep in Thermoplastic /Nano- and Fibercomposites*. SAMPE Europe Conference: Paris, France, 7-11 April.

10. K. van Rijswijk, D.P.N. Vlasveld, P. van Rhijn, H.E.N. Bersee, A. Beukers and S.J.Picken (2003): *Process Considerations for Liquid Moulding of Composites based on Anionic Polyamide-6*. 14th International Conference on Composite Materials (ICCM-14): San Diego, California, USA, 14-18 July.

11. K. van Rijswijk, B. Parixatranond, H.E.N. Bersee and R. Brouwer (2003): *Latex Impregnation for Natural Fiber Reinforced Plastics*. 14th International Conference on Composite Materials (ICCM-14): San Diego, California, USA, 14-18 July.

12. K. van Rijswijk (2003): *The Future of Natural Fiber Reinforced Plastics*. 4th International Conference on Composite Structures and Technology (ICCST-4): Durban, South Africa, 21-23 January.

13. K. van Rijswijk, D.P.N. Vlasveld, H.E.N. Bersee and S.J. Picken (2003): *Vacuum Injection of Anionic Polyamide-6*. 4th International Conference on Composite Structures and Technology (ICCST-4): Durban, South Africa, 21-23 January.

14. K. van Rijswijk and R. Brouwer (2002): *Cost Effectiveness of Composites with Natural Materials*. SAMPE Europe Conference: Paris, France, 7-11 April.

15. K. van Rijswijk, S. Koussios and O.K. Bergsma (2002): *Filament Wound Container made of Natural Fibers and –Rubber*. 10th European Conference on Composite Materials: Brugge, Belgium, 3-7 June.

16. K. van Rijswijk, S. Koussios and O.K. Bergsma (2001): *Fibre Thickness Distribution of a Filament Wound Rotational Symmetric Pressure Vessel*. 3rd European Conference on Launcher Technology: Strasbourg, France, 11-14 December.

NOMENCLATURE

Symbols

A	cross-sectional area to flow [m^2]
a	Mark-Houwink constant [-]
c	concentration [g/dl]
C_g	concentration of a dissolved gas [$m^{-3}bar^{-1}$]
E_{am}	modulus of the amorphous phase [GPa]
E_{cr}	modulus of the crystalline phase [GPa]
E_{pol}	modulus of the polymer [GPa]
H	Henry's coefficient [$m^{-3}bar^{-1}$]
K	permeability of the fiber fabrics [m^2]
K'	Mark-Houwink constant [dl/g]
K_d	dissociation constant [mole/l]
L	lamellar thickness [m]
L	flow front progression [m]
M_n	number average molecular weight [-]
M_v	viscosity average molar mass [-]
M_w	molecular weight [-]
m_{disc}	mass of disc-shaped composite specimen [g]
m_f	mass of fibers [g]
m_{pol}	polymer mass [g]
m_{tot}	total mass [g]
n	amount of gas [mole] / number of cycles [-]
p	pressure [Pa]
p_{vap}	vapor pressure [Pa]
Q	resin consumption rate [m^3/s]
R	universal gas constant [8.3143 J· K^{-1}·$mole^{-1}$]
S_{max}	amplitude of the sinusoidal stress signal during fatigue testing [MPa]
t_0	flow time of pure solvent [s]
t_{pol}	polymerization time [min]
T	temperature [K]

T_b	boiling point at atmospheric pressure [K]
T_c	crystallization point [°C]
$T_{de\text{-}block}$	de-blocking temperature of the activator [°C]
T_g	glass transition temperature [°C]
T_m	melting point [°C]
T_m^0	melting point of a perfect crystal/polymer [°C]
T_{max}	maximum temperature [°C]
T_{mould}	mould temperature [°C]
T_{pol}	polymerization temperature [°C]
v	volume [m^3]
V_c	volume of the crystalline phase [v%]
V_v	void content [v%]
W_f	fiber weight fraction [wt%]
X_B	molar fraction of imperfections in a polymer
X_c	degree of crystallinity [wt%]

Greek symbols

γ_e	fold surface energy of the lamellae
δ	solubility coefficient [-]
ΔH_{100}	melting enthalpy of a fully crystalline polymer [J/g]
ΔH_{cryst}	crystallization enthalpy [J/g]
ΔH_m	melting enthalpy [J/g]
ΔH_{pol}	polymerization enthalpy [J/g]
ΔH_{pol}	molar evaporation enthalpy [J/mole]
ΔH_v	volumetric enthalpy of fusion [J/m^3]
ΔP	pressure difference over the mould [mbar]
Δw	weight increase [wt%]
ε	strain [%]
ε_f	strain at failure [%]
η	viscosity [Pa·s]
η_{inh}	inherent viscosity [-]

η_{int}	intrinsic viscosity [-]
ρ_{am}	density of the amorphous phase [g/cm^3]
$\rho_{c\_calculated}$	calculated density of the composite [g/cm^3]
$\rho_{c\_measured}$	measured density of the composite [g/cm^3]
ρ_{cr}	density of the crystalline phase [g/cm^3]
ρ_f	density of the fibers [g/cm^3]
ρ_m	density of the matrix [g/m^3]
ρ_{mon}	density of the monomer [g/cm^3]
σ	stress [Mpa]
σ_1	stress at 0.1% strain [MPa]
σ_2	stress at 0.2% strain [MPa]
σ_{max}	maximum strength [MPa]

Abbreviations

2P	2-pyrrolidinone
ABS	acrylonitrilebutadienestyrene
act	activator
ALIS	Advanced Laminate Inspection Software
AP	anionic polymerization
APA-6	anionic polyamide-6
APA-12	anionic polyamide-12
ASTM	American Society for Testing and Materials
CCCL	cyclohexylcarbamoylcaprolactam
CL	caprolactam
CsF	Caesium fluoride
D	degassed
DAM	dry as molded
DMA	dynamic mechanical analysis
DOC	degree of conversion [wt%]
DPCS	Design and Production of Composite Structures (disciplinary group)
DPRP	depolymerization-repolymerization

DSC	differential scanning calorimetry
DUWIND	Delft University Wind Energy Research Institute
FEP	fluorinatedethylenepropylene
GF	glass fiber
GMT	glass matt thermoplastic
HDCL	hexamethylene-1,6-dicarbamoylcaprolactam
HDPE	high-density polyethylene
HDT	heat distortion temperature
HPA-6	hydrolytically polymerized polyamide-6
hr	hour
ini	initiator
ILSS	inter laminar shear strength
ISO	International Standards Organization
LDPE	low-density polyethylene
mc	moisture content
Me	metal
MgBrCL	caprolactam magnesium bromide
min	minute
MMA	methylmethacrylate
MMU	mini mixing unit
mol%	molar percentage
MT	Microtuff nucleating agent
Mw	molecular weight
MW	megawatt
N-ACL	N-acetylcaprolactam
NaCL	sodium caprolactamate
ND	non-degassed
PA	polyamide
PA-4	polyamide-4
PA-4,6	polyamide-4,6
PA-6	polyamide-6
PA-6,6	polyamide-6,6
PA-12	polyamide-12
PBI	polybenzimidazole

PBN	polybuthylenenapthalate
PBT	polybuthyleneteraphthalate
PC	polycarbonate
PEEK	poleetheretherketone
PEI	polyetherimide
PEN	polyethylenenaphthalate
PEK	polyetherketone
PES	polyethersulfon
PET	polyethyleneteraphthalate
PMMA	polymethylmethacrylate
PP	polypropylene
ppm	parts per million
PPS	polyphenylenesulfide
PS	polystyrene
PU	polyurethane
PVC	polyvinylchloride
Rel.St.Dev.	relative standard deviation
RH	relative humidity
RIM	reaction injection molding
RIP	reactive injection pultrusion
ROMP	ring-opening metathesis polymerization
ROP	ring-opening polymerization
RRIM	reinforced reaction injection molding
RTM	resin transfer molding
SEM	scanning electron microscope
SRIM	structural reaction injection molding
TDCL	toluylene-2,4-dicarbamoylcaprolactam
TGA	thermal gravimetric analysis
TPI	thermoplastic polyimide
TPU	thermoplastic polyurethanes
UV	ultra violet
v%	volume percentage
WAXS	wide angle x-ray scattering
wt%	weight percentage